ZfK – 584

ANNUAL REPORT 1985 ON NUCLEAR PHYSICS ACTIVITIES AND APPLICATIONS

Zentralinstitut für Kernforschung, Rossendorf
Technische Universität, Dresden
Karl-Marx-Universität, Leipzig
Humboldt-Universität, Berlin
Friedrich-Schiller-Universität, Jena
Bergakademie Freiberg

Edited by K. Hennig

Editorial staff: H. W Barz, F. Dönau, R. Flagmeyer, M. Friedrich, W. D. Fromm, K. Möller, J. Mösner, F. Naehring, D. Schmidt, S. Unterricker, W. Wesch, G. Winter

April 1986

Postanschrift: Akademie der Wissenschaften der DDR
Zentralinstitut für Kernforschung Rossendorf
Postschließfach 19
Dresden
8051
Deutsche Demokratische Republik

Diese Publikation wurde in der Abteilung Information des Zentralinstitutes für Kernforschung hergestellt

III-12-12 J 1110/86

AKADEMIE DER WISSENSCHAFTEN DER DDR

Z E N T R A L I N S T I T U T F Ü R K E R N F O R S C H U N G
R O S S E N D O R F B E I D R E S D E N

ZfK - 584

ANNUAL REPORT 1985
ON NUCLEAR PHYSICS ACTIVITIES AND APPLICATIONS

Zentralinstitut für Kernforschung, Rossendorf

Technische Universität, Dresden

Karl-Marx-Universität, Leipzig

Humboldt-Universität, Berlin

Friedrich-Schiller-Universität, Jena

Bergakademie Freiberg

Edited by K. Hennig

Editorial staff: H.W. Barz, F. Dönau, R. Flagmeyer, M. Friedrich, W.D. Fromm, K. Möller, J. Mösner, F. Naehring, D. Schmidt, S. Unterricker, W. Wesch, G. Winter

April 1986

Contents page

Nuclear Reactions 1

Nuclear Spectroscopy 20

Theory 25

Applied Methods of Nuclear Physics 45

Accelerators 85

Nuclear Electronics and Methods 87

Computational methods and codes 128

List of publications, academic promotions, lectures and conference contributions, scientific meetings and awards of honour 138

Inhaltsverzeichnis Seite

Arbeiten auf dem Gebiet der Kernreaktionen 1

Arbeiten auf dem Gebiet der Kernspektroskopie 20

Arbeiten auf den Gebieten der Kern- und Festkörpertheorie 25

Anwendung kernphysikalischer Methoden 45

Berichte zu den Beschleunigern 85

Apparative und methodische Arbeiten 87

Zentrale Rechentechnik und Rechenprogramme 128

Liste der Veröffentlichungen, Diplomarbeiten, Promotionen, Vorträge, Veranstaltungen, wissenschaftlichen Preise und Auszeichnungen 138

Содержание стр.

Ядерные реакции I

Ядерная спектроскопия 20

Теория 25

Прикладные методы ядерной физики 45

Ускорители 85

Ядерная электроника и методы измерения 87

Вычислительный центр и программное обеспечение I28

Список публикаций и докладов I38

CONTRIBUTIONS

NUCLEAR REACTIONS

page

TKE vs. mass distributions obtained by investigation of the collision system $^{40}Ar + ^{232}Th$

P. Gippner, K.D. Schilling, W. Seidel, F. Stary, E. Will, H. Sodan, S.M. Lukyanov, G.G. Chubarian, V.S. Salamatin, Yu.E. Penionzhkevich 1

TKE vs. mass distributions obtained by investigation of the systems $^{22}Ne + ^{249}Cf$ and $^{56}Fe + ^{208}Pb$

P. Gippner, K.D. Schilling, W. Seidel, F. Stary, E. Will, H. Sodan, S.M. Lukyanov, G.G. Chubarian, V.S. Salamatin, Yu.E. Penionzhkevich 2

In-beam investigations of ternary fission at the Rossendorf cyclotron U-120

R. Rotte, H.-G. Ortlepp, H.-J. Keller, F. Stary, E. Hentschel, J. Fiedler 3

Results of absolute fission cross-section measurements of Pu-239 at 4.8, 8.65 and 18.8 MeV neutron energy using the TCAPM

C.-M. Herbach, K. Merla, G. Musiol, H.-G. Ortlepp, G. Pausch, I.D. Alkhazov, L.V. Drapchinsky, E.A. Ganza, S.S. Kovalenko, O.I. Kostochkin, S.M. Solovjev, V.I. Shpakov 4

Absolute measurement of the U-238 fission cross-section at 18.8 MeV neutron energy using the TCAPM

C.-M. Herbach, K. Merla, G. Musiol, H.-G. Ortlepp, G. Pausch, L.W. Drapchinsky, E.A. Ganza, V.I. Shpakov, S.M. Solovjev 5

Theoretical study of fission neutron emission during fragment acceleration

H. Märten 6

About the mean-square radii of the 236-U nucleus in excited states with different fission widths

A. Meister, S. Mittag, W. Pilz, D. Seeliger, K. Seidel, L.B. Pikelner 7

Angular correlations and mass loss in 1 GeV proton-nucleus collisions

L.N. Andronenko, M.N. Andronenko, A.A. Kotov, L.A. Vaishnene, W. Neubert 8

Hadron and fragment emission in cluster excitation processes at medium energies

H. Müller, C. Schneidereit, Zs. Kovacs 9

A measurement of the total cross section of the capture reaction $^{2}H(n,t)\gamma$ at E_p = 25 MeV

J. Mösner, K. Möller, W. Pilz, J. Schmidt, T. Stiehler 10

Off-shell sensitivity of the M1-contribution to the capture reaction $n + p \rightarrow d + \gamma$

K. Möller 11

Phenomenology of angular distributions of 14-MeV-neutron-inelastic scattering: systematics and theoretical approaches

D. Hermsdorf, H. Kalka 12

Phenomenology of angular distributions of 14-MeV-neutron-inelastic scattering: comparison of experimental and theoretical results

D. Hermsdorf, H. Kalka, U. Steiniger 13

About the possibility of a bound ^{12}C-^{12}C quasimolecular band in ^{24}Mg

H.U. Gersch, V. Goldberg, V. Rudakov 14

Application of K^+-interferometry for the investigation of the early stage in heavy ion collisions at relativistic energies

H.U. Gersch 15

Quenching of the correlation function at the Hanbury brown-twiss effect

H.U. Gersch 17

page

MAT 1402 and MAT 8201 - Two revised versions of evaluated neutron nuclear data files for silicon and lead for BROND
D. Hermsdorf, A.V. Klokhin, A.V. Ignatyuk 18

On the use of nuclear data libraries in CDR - Updating and Extension of data bases and nuclear data service
S. Eckstein, D. Hermsdorf, D. Saeliger, K. Friedrich, L. Jankowski, B. Letz 19

NUCLEAR SPECTROSCOPY

Mean lifetimes of positive-parity states in ^{79}Br
R. Schwengner, G. Winter, J. Döring, L. Funke, H. Rotter 20

New ps - lifetimes and electromagnetic transition probabilities in ^{79}Kr
G. Winter, R. Schwengner, L. Funke, J. Döring 21

Subnanosecond isomers in ^{97}Y
L.K. Kostov, W. Andrejtscheff, L.G. Kostova, P. Petkov, H. Prade, H. Rotter, L. Käubler, F. Stary 22

Lifetime measurements in ^{123,125}I
L.K. Kostova, W. Andrejtscheff, L.K. Kostov, P. Petkov, L. Käubler, H. Prade, H. Rotter, F. Stary 23

The magnetic moment of the 10^+ isomer in ^{140}Ce and temperature dependence of the paramagnetism for Ce ions in BaO
L. Käubler, H. Prade, W. Engherdt, F. Stary, P. Carlé, L.O. Norlin, K.-G. Rensfelt, U. Rosengard 24

THEORY

Hadron yields from the decaying quark gluon plasma
B. Kämpfer, H.W. Barz, B. Lukács 25

Cascade-model studies of lambda-particle production in the carbon on tantalum reaction at dubna energies
H.W. Barz, H. Iwe 26

Population of hypernuclear states via nucleon decay channels
R. Wünsch, L. Majling, J. Žofka 27

Electromagnetic radiation of rotating nuclei
F. Dönau 28

Critical behaviour of collective fluctuations
A. Pfitzner 29

Target-mass dependence of preequilibrium neutron yields in heavy ion collisions
P. Mädler 30

Incident-energy and projectile-mass dependence of preequilibrium neutron yields in heavy ion reactions
M. Biedermann, P. Mädler 31

Coupling between energy- and mass-equilibration in HIC
R. Schmidt 32

A simple model to approximate TDHF results on fast particle emission
M. Biedermann, P. Mädler 33

Azimuthal correlations between two fast particles within the two-stage model
M. Biedermann, P. Mädler 34

page

Comparison of the two-stage model for fast particle emission with hot-source parametrizations
M. Biedermann, P. Mädler 35

Polar particle emission in spontaneous fission
B. Milek, R. Reif, J. Revai 36

Angular distributions from Gamow states in $^{17}O + ^{16}O$
J. Fandrich, B. Milek, R. Reif 37

Model investigations on nitrogen implantation in silicon
E. Sobeslavsky, K. Wollschläger 38

Modelling of the oxygen redistribution during formation of buried SiO_2 layers by high dose oxygen implantation
H.U. Jäger 39

On the choice of the electronic stopping formula for range profile calculations in the MeV region
M. Posselt, W. Skorupa, A. Beyer, W. Markgraf 40

Influence of the energy transport by recoils on energy-loss profiles
M. Posselt 41

Computer simulation of the evolution of low-angle grain boundary networks during zone-melting of SOI-layers
K.-H. Heinig, H.-J. Müller, G. Otto 42

Computersimulation versus analytical formulae: a critical discussion of theories of transformation
H.-J. Müller, K.-H. Heinig 43

Computer simulation of the primary crystallization a-Si to poly-Si
H.-J. Müller, K.-H. Heinig 44

APPLIED METHODS OF NUCLEAR PHYSICS

High energy (0.99 MeV) phosphorus implantation into silicon
W. Skorupa, E. Wieser, R. Grötzschel, M. Posselt, A. Armigliato, A. Garulli 45

Formation of buried silicon nitride layers in silicon by ion implantation-new results
W. Skorupa, K. Wollschläger, H. Oertel, R. Grötzschel, H. Bartsch 46

Anodic oxidation as sectioning technique for the determination of high dose B^+ and As^+ implantation profiles in Si
G. Mende 47

Diffusion enhancement and electrical activation during rapid isothermal annealing (RIA) of B and As implanted Si
R. Kögler, E. Wieser 48

Electrical activation of implanted GaAs by short-time annealing
D. Panknin, C. Döring, J. Hüller, C. Weise, E. Wieser 49

Formation of Schottky barriers and deep levels
H. Morgenstern 50

Minority carrier lifetime improvement of high resistivity NTD-silicon and its application for counting detectors
L. Bischoff 51

page

Two-step-annealing of high resistivity NTD-silicon
L. Bischoff 52

Fundamental studies to sensors made by silicon-on-insulator technology
D. Schubert, U. Lorenz, W. Jenschke, T. Uhlig 53

Construction and performance of a large area ΔE-E silicon detector telescope
M. Deutscher, R. Förster, G. Mende, H.-G. Ortlepp, W. Seidel 54

Capacity model of a silicon strip detector
M. Teichfuß, L. Bischoff 55

Performance of silicon nuclear radiation detectors
J. von Borany, L. Bischoff, B. Schmidt 56

Two-dimensional position-sensitive photodetectors
B. Schmidt, H. Schott 57

One-dimensional position-sensitive photodetectors
B. Schmidt, H. Schott 58

Methods of producing grain boundary free silicon stripes on insulating substrates
J. Matthäi, M. Voelskow, K. Höppner, W. Scharff, D. Gerisch, K.-H. Stegemann 59

Electrical properties of MOS-structures fabricated in lamp recrystallized Si film on oxid
N. Sieber, M. Voelskow, H. Oertel 60

Characterization of PECVD nitride layers
C. Bauer, D. Grambole, C. Heiser, F. Herrmann, W. Rudolph 61

Boron depth profiling by the $^{11}B(d, \alpha_0)^9Be$ reaction
W. Rudolph, C. Bauer, C. Heiser, P. Urwank 62

Characterization of boron doped silicon oxide layers by helium backscattering and prompt nuclear reactions
W. Rudolph, C. Bauer, C. Döring, D. Grambole, R. Groetzschel, C. Heiser, F. Herrmann, P. Urwank 62

Plastic foils as primary hydrogen standards for nuclear reaction analysis
W. Rudolph, C. Bauer, K. Brankoff, D. Grambole, R. Groetzschel, C. Heiser, F. Herrmann 63

50 kV fine focused ion beam apparatus
A. Hoffmann, A. Kahn, U. Kreißig, F.K. Naehring 64

On geometrical aberrations of third and higher order in tube lenses of finite length
R.R. Bartl 65

The magnetic form factor of iron in amorphous $Fe_{75}B_{25}$
W. Matz 66

Methodical investigations via texture of rock salt
M. Betzl, W. Voitus, A. Ertel 67

Neutronographic texture investigations of Halit
M. Betzl, W. Voitus, A. Ertel, P. Bankwitz, H. Kämpf 68

Texture development in pass-rolling of FCC metals
P. Klimanek, K. Cyrener, A. Mücklich, U. Scholz 69

page

Texture development during cold rolling of ($\alpha + \beta$)-brass
P. Klimanek, A. Kühl, A. Mücklich, U. Scholz 70

Small-angle neutron scattering on hydrating cement paste
F. Eichhorn, F. Häußler, U. Miehe 71

Depth distribution of F, Na, and P in tooth enamel measured by means of nuclear reactions
H.-E. Zschau, J. Vogt, G. Otto 72

Investigation of epitaxial $(Ca,Sr)F_2$/GaAs heterostructures by RBS/channeling technique
R. Flagmeyer, B. Schumann 73

Microhardness of proton bombarded GaP single crystals
C. Ascheron, H. Neumann, G. Dlubek, R. Krause 74

Hydrogen depth profiling in implanted GaP using elastic recoil detection
D. Lehmann, C. Ascheron 75

Depth resolution in differential hall-effect measurements for shallow implantation profiles
B. Lukasch 76

The use of secondary ion mass spectrometry for steel analysis
S. Mechahougui, G. Lehmann, U. Müller-Jahreis 77

A method of quantification of mass spectra in secondary ion mass spectrometry (SIMS)
H. Düsterhöft, A. Lüders 78

Deep levels in n-Si caused by low energy ion implantation
J. Bollmann, H.A. Klose, A. Mertens 79

Structure dependence of quadrupole coupling constants in $A^{II}B^{IV}C_2^{V}$ chalcopyrite compounds
S. Unterricker 80

Mössbauer study of Fe^{2+}-Fe^{3+} ordering in natural chromites
C. Pietzsch 81

Rare earth element and Yttrium contents in fluorite samples
D. Degering, S. Unterricker, W. Stolz, O. Leeder, G. Wendebaum 82

Defects in laser annealed ion implanted GaAs layers
W. Wesch, P. Ressel, E. Wendler 83

RBS investigations of defects in weakly damaged GaAs
W. Wesch, K. Gärtner, E. Wendler 84

ACCELERATORS

Operation of the cyclotron U-120
B. Anders, W. Guratzsch 85

Operation of the electrostatic accelerators in 1985
W. Bürger, S. Turuc 86

NUCLEAR ELECTRONICS AND METHODS

First investigations with a stationary positron camera
P. Manfraß, W.D. Fromm, M. Sobiella, D. Wohlfarth 87

page

The converter-MWPC in the multi-step avalanche mode
P. Manfraß, W.D. Fromm, M. Sobiella, D. Wohlfarth 88

A microprocessor controlled Mössbauer spectrometer
P. Reichel, W. Matz, W. Boede 89

A nuclear micro-beam probe for the investigation of surfaces
W.D. Fromm, D. Grambole, F. Herrmann, F. Schwarzenberg 90

Investigation of scintillation materials
J. Rüdiger 91

Development and test of a ΔE-E annular detector telescope
P. Kleinwächter, J. Rüdiger, J. Döring, L. Funke, M. Freitag, H. Rotter, Th. Scholz, W. Schulze, R. Schwengner, E. Will, G. Winter 92

Construction of a plunger for coincidence experiments
G. Winter, M. Freitag, W. Schulze 93

Double grid avalanche counter with large dynamic range
W. Seidel, H.-G. Ortlepp, J. Fiedler 94

Timing with fast particle detectors
H.-G. Ortlepp 95

A bragg curve ionization chamber
R. Kotte 96

Test measurement with a bragg ionization chamber at the Rossendorf tandem accelerator
R. Kotte, H.-G. Ortlepp, H.-J. Keller, F. Stary 97

Shaping amplifier for bragg curve spectroscopy
H.-G. Ortlepp 98

An axial ionization chamber for fragment detection
L.N. Andronenko, V.V. Janofsky, A.A. Kotov, L.A. Vaishnene, W. Neubert 99

A fast discriminator with low-level threshold
A.I. Iljin, W. Neubert 100

Preamplifier for silicon particle detectors
H.-G. Ortlepp, E. Schuster 101

Suppression of low-multiplicity γ-radiation in plunger experiments by means of coincidence technique
G. Winter, W. Schulze, E. Will 102

Majority coincidence unit
E. Will 103

Electronic developments of the KFM group
H. Angermann, W.D. Fromm, F. Schwarzenberg 104

Hard- and software supplements for the computer Z 9001
F. Schwarzenberg 105

Soft- and hardcopy for homecomputers
H.-J. Müller, F. Schwarzenberg, W.D. Fromm 106

page

The data-link- and physical-layer in the lan GDP-NET
W.-J. Linnemann 107

A variant for on-line rapid extraction in nuclear-chemical experiments with crown ethers
E.J. Langrock, K. Eichhorn, K. Gloe, P. Mühl 108

Optimization of the associated particle (AP) detection system used for TCAPM fission cross-section measurements in the 4.5 and 8.5 MeV neutron energy range
C.-M. Herbach, G. Musiol, G. Pausch, E.A. Ganza 109

Analysis of associated particle spectra in TCAPM fission cross-section measurements at ~19 MeV neutron energy
C.-M. Herbach, K. Merla, G. Musiol, G. Pausch, L.V. Drapchinsky 110

Experimental determination of the $^{3}H(d,p)^{4}He$ background portion in TCAPM-measurements of about 19 MeV neutron energy
C.-M. Herbach, K. Merla, G. Musiol, G. Pausch, L.V. Drapchinsky, E.A. Ganza 111

Cone broadening in TCAPM fission cross-section measurements
C.-M. Herbach, G. Musiol, G. Pausch 112

Consideration of the $^{12}C(n,n')3\alpha$-reaction as a background source within a methan filled fission chamber for neutrons of ~19 MeV
C.-M. Herbach, K. Merla, G. Musiol, G. Pausch 113

A correlation between fission fragment absorption losses and the plateau height in fission chamber spectra
C.-M. Herbach, G. Pausch 114

Determination of the areal density of the Pu-239 fission-foils
K. Merla, C.-M. Herbach, R. Perez, O.I. Kostochkin, S.M. Solovjev 115

Determination of the inhomogeneity of U-238 fission-foils by RBS-measurements
K. Merla, R. Groetzschel 116

Separation of outer-shell satellite X-ray lines at sources of highly ionized atoms
W. Wagner, G. Zschornack 117

Temperature control of analyzer crystals in crystal diffraction spectrometers with discontinuous optimized controllers
D. Kreiseler, G. Zschornack 118

A two-beam laser angle interferometer for bragg crystal diffraction spectrometers
G. Zschornack, G. Müller, G. Karrasch, W. Schulze, W. Wagner 119

Investigations with the aim of installation a low-level γ-spectrometer
J.H. Kim, S. Unterricker, W. Stolz, D. Degering and D. Hebert, D. Simon 120

Fast trigger for neutron time-of-flight measurement
P. Eckstein, A. Meister, U. Gohs 121

Gradually evaporated foils for aberration correction of fission fragment time-of-flight in a direction-sensitive arrangement
H. Märten, D. Richter, W. Neubert, I. Probst 122

Experimental arrangement for the measurement of correlations between fission products and neutrons
H. Märten, D. Richter, D. Seeliger, W.D. Fromm, W. Neubert 123

Implementation of serial multi-master bus controller using single-chip microcomputer
W. Meiling, R. Krause 124

page

Mass spectrometry of liquid metal ion sources
R. Mühle, F. Machalett 125

Basic characteristics of an Au-Si-liquid metal ion source
R. Mühle, F. Machalett 127

COMPUTATIONAL METHODS AND CODES

Fortran programmes for the calculation of single-particle quantities in heavy-ion collisions in a two-center basis
B. Milek 128

PEP - A Fortran program for calculation of fast nucleon emission in heavy-ion reactions
M. Biedermann, P. Mädler 129

HOT - A Fortran program for calculation of fast nucleon emission from a hot zone
M. Biedermann, P. Mädler 130

Fortran code for the calculation of "realistic" distributions of neutrons produced in hydrogene-isotope reactions
H. Märten, A. Ruben 131

The implementation of an universal stopping power code to the ES 1055 computer
W. Enghardt, J. Henniger 132

The Fortran programs KASSAMBA and STRIDEM
H.-J. Keller 133

ISOPLOT 2 - A program for graphic representation of functions Z = F(X,Y)
H. Böttger, P. Gippner 134

The evaluation of $\gamma\gamma$-coincidence matrices
W. Enghardt 135

On-line programs for multi-parameter measurements
W.D. Fromm 136

Bit-map graphics with EC 1055 programs
U. Fromm, W.D. Fromm, K.-H. Heinig, G. Otto 137

NUCLEAR REACTIONS

TKE v.s. MASS DISTRIBUTIONS OBTAINED BY INVESTIGATION OF THE COLLISION SYSTEM $^{40}Ar + ^{232}Th$

P. Gippner, K.D. Schilling, W. Seidel, F. Stary and E. Will
Zentralinstitut für Kernforschung, Rossendorf, Bereich KF
H. Sodan, S.M. Lukyanov, G.G. Chubarian, V.S. Salamatin and Yu.E. Penionzhkevich
Joint Institute for Nuclear Research, Dubna

In reactions between heavy ions the total cross section is generally composed of several components, which are due to contributions of different reaction mechanisms. In order to study these contributions one has to measure the mass and energy distributions of the correlated reaction products as well as their angular correlations in a broad range of entrance channel parameters. For this purpose, the double-arm time-of-flight spectrometer DEMAS described in detail elsewhere /1/ has been developed. Preliminary results obtained by investigation of the reactions $^{22}Ne + ^{249}Cf$, $^{32}S + ^{238}U$, $^{40}Ar + ^{232}Th$ and $^{56}Fe + ^{208}Pb$ have already been published in /2-4/. These projectile-target combinations were chosen with regard to the formation of composite systems with an identical nuclear charge number $Z = 108$.

In the case of $^{40}Ar + ^{232}Th$, studied at a projectile energy $E_1 = 301$ MeV, we found a Gaussian-shaped fragment mass distribution with a value $\Gamma_{FWHM} = 88$ amu lying beyond the width obtained in /5/ for the fusion of heavy collision systems. The conclusion drawn from this picture is that the system $^{40}Ar(301\ MeV) + ^{232}Th$ undergoes fast fission, fully in accordance with calculations of the driving potential /4/. For $E_1 = 220$ MeV and 206 MeV, respectively, the mass distributions tend to broaden and the intensity maximum at $M = (M_1+M_2)/2$ vanishes. Relative maxima appear in the region of $M \approx 205$ and of the complementary masses $M \approx 65$. The enhanced yield of fragments near the doubly magic nucleus ^{208}Pb is interpreted here as due to shell effects, which generate and/or stabilize components with closed nuclear shells during the drift process /4/. This is supported by the TKE vs. mass distributions shown in fig. 1, where the dashed lines represent the expected release of total kinetic energy for fully relaxed events. These TKE values are scaled by the expression $kM_3M_4/(M_3^{1/3} + M_4^{1/3})$ and normalized to the centroids of the TKE release for symmetric fragmentation /5/. Generally, the dashed parabolas follow the ridges of mass drift except the regions of $M \approx 205$ and $M \approx 65$. We suppose the emerging shells near the nucleus ^{208}Pb to be responsible for the formation of fission products, which are less deformed. Such more compact configurations result in a higher Coulomb energy (larger TKE release) than predicted by the Viola systematics, which for asymmetric fragmentation refers to highly deformed liquid-drop configurations /6/.

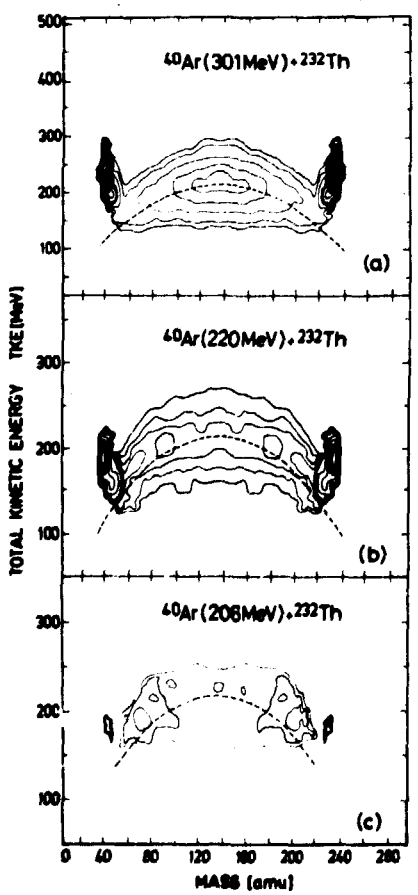

Fig. 1

References

/1/ Will, E. et al., Report JINR 13-85-754, Dubna (1985)
Schilling, K.D. et al., to be published

/2/ Sodan, H. et al., JINR Rapid Comm. (Dubna) N4-84 (1984) 15

/3/ Lukyanov, S.M. et al., Proc. Int. Worksh. on Gross Prop. of Nuclei and Nucl. Excitations XIII, Hirschegg (1985) 123

/4/ Gippner, P. et al., to be published

/5/ Töke, J. et al., Nucl. Phys. A440 (1985) 327

/6/ Hulet, E.K. et al., Preprint UCRL 93218 (1985)

TKE vs. MASS DISTRIBUTIONS OBTAINED BY INVESTIGATION OF THE SYSTEMS $^{22}Ne + ^{249}Cf$ AND $^{56}Fe + ^{208}Pb$

P. Gippner, K.D. Schilling, W. Seidel, F. Stary and E. Will
Zentralinstitut für Kernforschung, Rossendorf, Bereich KF
H. Sodan, S.M. Lukyanov, G.G. Chubarian, V.S. Salamatin and Yu.E. Penionzhkevich
Joint Institute for Nuclear Research, Dubna, USSR

Energy and mass distributions of binary fragments formed in the collision systems $^{22}Ne + ^{249}Cf$, $^{40}Ar + ^{232}Th$, $^{32}S + ^{238}U$ and $^{56}Fe + ^{208}Pb$ were measured by means of the correlation spectrometer DEMAS /1/. Preliminary results of these investigations were already published elsewhere /2/. In order to draw some conclusions on the mechanisms dominating the studied reactions the static driving potentials have been calculated in dependence on the mass asymmetry $\eta = (M_t - M_p)/(M_p + M_t)$ and the different angular momenta l /3/. According to these calculations the system $^{22}Ne + ^{249}Cf$ is the most interesting one, since its starting point for the mass drift is just at the maximum of the potential curve. Hence, the system should be able either to move towards increasing η values (fusion-fission) or towards decreasing η values (fast fission). A distinction between these reaction mechanisms should be possible by taking into account the half-widths of the measured TKE distributions of the correlated fragments. In ref. /4/ the heavy collision systems $^{238}U + ^{16}O$ (Z=100) and $^{238}U + ^{27}Al$ (Z=105) were studied at an icidence energy of 6 MeV/amu. The results of /4/ allow to predict the quantity Γ_{FWHM} of the mass distribution of fusion-fission fragments to be in the order of 70 amu for Z = 108. Contrary to this one expects a broader mass distribution for fast fission /4/. Considering the value Γ_{FWHM} = 90 amu obtained in our experiments /3/ we conclude that the system $^{22}Ne + ^{249}Cf$ undergoes fast fission.

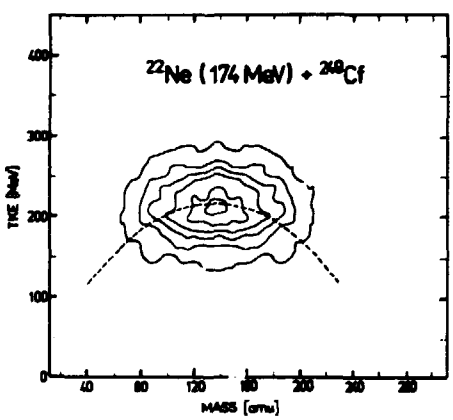

Fig. 1

Fig. 1 shows the TKE vs. mass distribution of the measured fragments. The contour lines form a ridge, which demonstrates the mass drift to symmetry when the reaction partners are in contact. The dashed parabola drawn in fig. 1 exhibits the expected TKE release for fully relaxed events, as already described in /5/. The elastic peaks could not be observed for kinematical reasons at the chosen experimental geometry /3/.

The TKE vs. mass distribution of the correlated fragments obtained in the reaction ^{56}Fe(354 MeV) + ^{208}Pb is shown in fig. 2. The plot reveals mainly asymmetric fragmentation with a very low yield of symmetric fragments. More detailed considerations show that for the system $^{56}Fe + ^{208}Pb$ the shape at the conditional saddle is more compact than two nuclear spheres in contact /6/. Hence, already for central collisions (l = 0) an extra-push energy $E_x \approx 30$ MeV is needed to overcome this saddle and to form a stable neck. We suppose for higher l-values the formation of a neck to be suppressed for energetical reasons ($\bar{E} - V_{CB}$ = 54 MeV), what prevents the mass drift. The high yield of fragments near the elastic peaks is therefore interpreted as due to deep inelastic collisions.

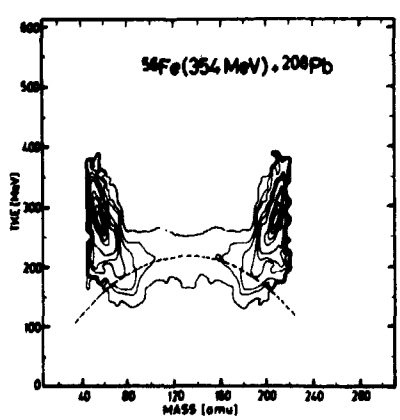

Fig. 2

References

/1/ Will, E. et al., Report JINR 13-85-754, Dubna (1985)
Schilling, K.D. et al., to be published
/2/ Sodan, H. et al., JINR Rapid Comm. (Dubna) N4-84 (1984) 15
/3/ Gippner, P. et al., to be published
/4/ Töke, J. et al., Nucl. Phys. A440 (1985) 327
/5/ Gippner, P. et al., this annual report p. 1
/6/ Bock, R. et al., Nucl. Phys. A388 (1982) 334

IN-BEAM INVESTIGATIONS OF TERNARY FISSION AT THE ROSSENDORF CYCLOTRON U-120

R. Kotte, H.-G. Ortlepp, H.-J. Keller, F. Stary, E. Hentschel and J. Fiedler
Zentralinstitut für Kernforschung, Rossendorf, Bereich KF

The in-beam investigation of charged particle induced ternary fission was probed at the Rossendorf Cyclotron U-120. A 4 nA beam of 13.5 MeV deuterons was focused on a 1.3 mg cm^{-2} target of nat.UO_2 electroplated on a 1.5 mg·cm^{-2} nickel backing. Two parallel plate avalanche counters (PPAC) with an active area of 2 x 4 cm^2 (2 mm gap) were installed both 2 cm apart from the target (fig. 1). These PPACs were operated such ($-U_{det}$ = 345 V) that only fission fragments (ff) generated fast signals for triple coincidences with the light charged particle (lcp).

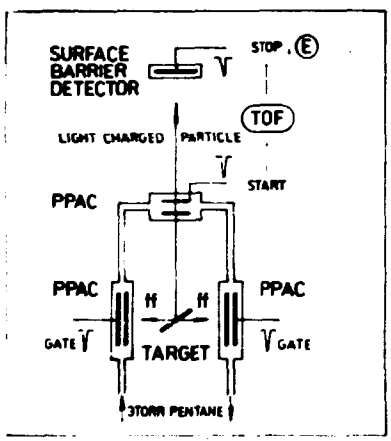

Fig. 1
Experimental set up

A third PPAC (lcp-PPAC) with an active area of 1.5 cm in diameter (4.5 mm gap) was installed 11 cm apart from the target perpendicular to both the fission-axis and the beam direction. It was operated at a higher reduced field E/p ($-U_{det}$ = 530 V) allowing an effective triggering on lcp. It's fast pulses were used as START signals for a time-of-flight measurement (TOF). The corresponding STOP signal and the energy (E) information were derived from a large area surface barrier detector (Ø = 3.2 cm, U_{det} = 180 V) installed at a flight distance L = 15 cm from the lcp-PPAC (solid angle $\Delta\Omega$ = 12 msr). The mass resolving power $m/\Delta m \sim 4$ (at E/A = 4 MeV/amu) was mainly determined by the time resolution Δt = 0.7 ns (FWHM). The three PPACs were commonly supplied with 3 torr n-pentane by a gas flowing-through system. TOF-E-distributions were recorded into a twodimensional analyzer with colour display. Fig. 2 shows an ungated spectrum, and fig. 3 a spectrum gated by a fission fragment coincidence. In order to obtain the energy distribution of the alpha particles accompanying fission the following procedure was done:

(1) The alpha energy spectra were deduced from the twodimensional TOF-E-distributions (fig. 4).

(2) The contribution of random triple coincidences was subtracted from the gated alpha energy distribution by using the ratio ($9 \cdot 10^{-4}$) of ff-events in both the twodimensional plots multiplied with the ungated alpha energy spectrum.

Despite the bad statistics the determined large range alpha (lra) energy distribution from deuteron induced fission of ^{238}U is in good agreement with the corresponding ones from $^{252}Cf(sf)$, $^{235}U(n_{th},f)$ or $^{239}Pu(n_{th},f)$ /1/, i.e. ternary fission was observed indeed.

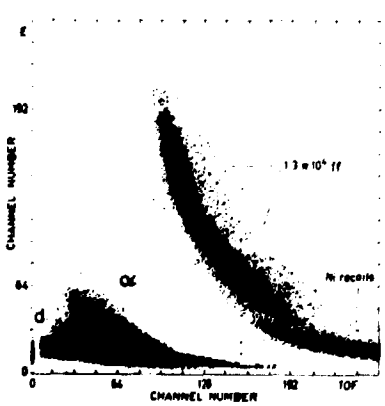

Fig. 2
Ungated TOF-E-distribution

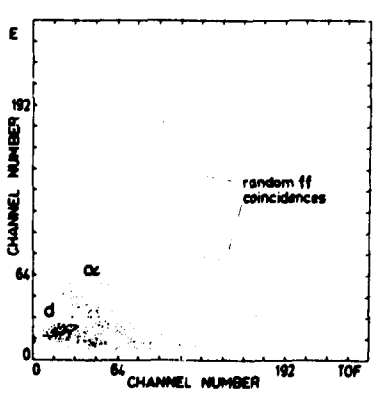

ig. 3
Gated TOF-E-distribution

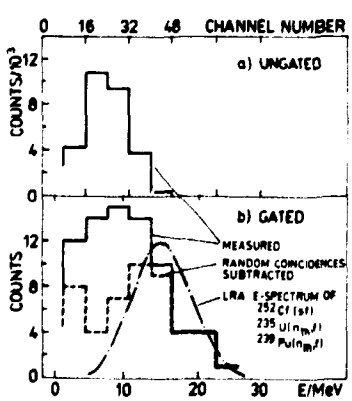

Fig. 4
Alpha energy spectra

References

/1/ Kondurov, I.A. et al., IAEA, INDC(CCP)-162/GJ

RESULTS OF ABSOLUTE FISSION CROSS-SECTION MEASUREMENTS OF Pu-239 AT 4.8, 8.65 AND 18.8 MeV NEUTRON ENERGY USING THE TCAPM

C.-M. Herbach, K. Merla, G. Musiol, H.-G. Ortlepp+), G. Pausch
Technische Universität Dresden, Sektion Physik, WB Angewandte Kernphysik
+)Zentralinstitut für Kernforschung Rossendorf, Bereich KF
I.D. Alkhazov, L.V.Drapchinsky, E.A. Ganza, S.S. Kovalenko, O.I. Kostochkin, S.M. Solovjev, V.I. Shpakov
Khlopin Radium Institute Leningrad

Absolute measurements of the Pu-239 fast neutron fission cross-section were finished at three different energy spot points. By using the Time-Correlated Associated Particle Method (TCAPM) at the 5 MV tandem accelerator of the CINR Rossendorf (GDR) accuracies of ≤ 1 % were achieved for the neutron flux determination (see Tab. 1). The produced averaged flux within the neutron cone of ~ 3600 s^{-1} /1,2/ was much higher than in earlier measurements at U-235 /3,4/. Fissions were detected by placing thin targets ≤ 300 $\mu g/cm^2$ inside a parallel plate ionization chamber filled with methane /1/.

New measurements of the target areal densities by α-counting at the TUD confirm the used RIL data within the error limits. The results at 8.65 MeV and 18.8 MeV neutron energy represent a summary of independent measurements (Fig. 1).

The comparision with data evaluations indicates a significant discrepancy at 8.65 MeV especially for the ENDF/B-V data (Tab. 2). Final results will be represented after checking the isotopic composition of the targets by means of mass-spectrometry and the experimental prove of the absorption correction, which was still calculated by assuming a range of (7.5 ± 2) mg/cm^2 of the fragments within the fission foils.

Mean neutron energy (MeV)	4.8±0.20		8.65±0.20		18.8±0.20	
FWHM of energy distr. (MeV)	0.25		0.45		0.60	
	Corr. (%)	Error contr. (%)	Corr. (%)	Error contr. (%)	Corr. (%)	Error contr. (%)
Counting of coincidences						
- Statistics of effect	-	1.27	-	1.08	-	1.51
- Random coincidences	0.64	0.11	1.86	0.17	4.69	0.41
Fission chamber efficiency						
- Correlated background	-	-	-	-	0.24	0.11
- Extrapolation to zero	1.50	0.34	1.04	0.24	2.69	0.36
- Fragment absorption	1.21	0.46	1.20	0.43	1.30	0.39
AP counting						
- Background	2.30	0.36	1.62	0.32	5.34	1.00
Neutron cone						
- Neutron scattering	0.25	0.40	0.36	0.40	0.34	0.40
- Effective fission foil thickness due to the cone aperture	0.08	0.05	0.07	0.05	0.12	0.08
- Cone neutrons outside the angular extent of the fission foils	not corrected					
Fissile layers						
- Areal density	-	1.00	-	1.00	-	1.00
- Inhomogeneity	-	0.88	-	0.85	-	0.88
Standard deviation (%) of error	2.00		1.85		2.39	

Tab. 1: Corrections and error contributions

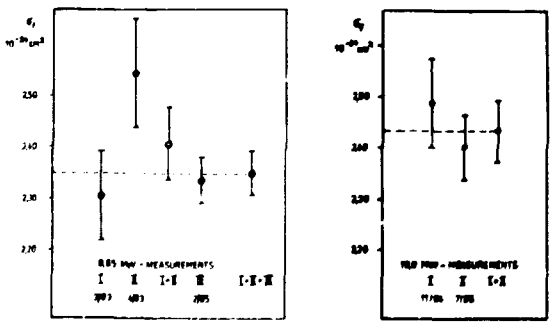

Fig.1a and 1b: Results of the independent measurements at 8.65 and 18.8 MeV

Neutron energy (MeV)	Presented TCAPM-measurements		Discrepancies to data files	
	Result ($10^{-24}cm^2$)	Error (%)	ENDF/B-V (%)	Antsipov/5/ (%)
4.8	1.740	2.00	+ 2.90	+ 0.40
8.65	2.350	1.85	+ 4.26	+ 2.89
18.8	2.431	2.39	- 1.10	-

Tab. 2: Comparision of the presented results with actual data evaluations

REFERENCES

/1/ C.M. Herbach et al.; report 05-06-85, TU Dresden, 1985
/2/ C.M. Herbach et al.; XV. Internat.Symp. on Nucl.Phys."Nuclear Fission", Gaussig, GDR, Nov. 1985,Proc.to be publ. as a *ZfK-report*
/3/ R. Arlt et al.; Proc.X.Internat.Symp. on Selected Topics of the Interaction of Fast Neutron and Heavy Ions with Atomic Nuclei, Gaussig, GDR, Nov.1980, ZfK-459 (1981), p. 27
/4/ R. Arlt et al.; Proc of an Advisory Group Meeting on Nuclear Standard Reference Data, Geel, Belgium, 1984 IAEA-TECDOC-335, p. 18, (1985)
/5/ G.V. Antsipov et.al., IAEA-report INDC (CCP)-166/GHJ (1981)

ABSOLUTE MEASUREMENT OF THE U-238 FISSION CROSS-SECTION AT 18.8 MeV NEUTRON ENERGY USING THE TCAPM

C.-M. Herbach, K. Merla, G. Musiol, H.-G. Ortlepp[+], G. Pausch
Technische Universität Dresden, Sektion Physik, WB Angewandte Kernphysik
[+] since 1984 ZfK Rossendorf
L.W. Drapchinsky, E.A. Ganza, V.I. Shpakov, S.M. Solovjev
Khlopin Radium Institute Leningrad

The joint measurements program of the Khlopin Radium Institute Leningrad and the Technical University of Dresden [1] was continued with a series of measurements of the U-238 fission cross-section, started by a measurement at 18.8 MeV neutron energy. The main experimental features in neutron production and monitoring correspond to those in the U-235 measurement [2], but in contrary to [2] a selfsupporting Ti-T target without Al-layer (thickness 3.1 mg/cm^2, inventory 62.3 GBq/cm^2) was used. The absence of the Al(d,α) background component reduced the error contribution of the background correction in the associated particle channel (see fig. 1) from 1.35 % to 0.60 %. Employing a roteting target holder system the use of beam-currents to about 500 nA was possible without noticeable T-escape out of the target.

E_n = (18.8 ± 0.2) MeV	Corr.	Error contr.
Counting coincidences		
- Statistics of effect	-	1.81 %
- Random coincidences	1.07 %	0.21 %
Fission chamber efficiency		
- Correlated background	6.01 %	0.04 %
- Extrapolation to zero	0.81 %	0.20 %
- Fragment absorption	1.99 %	0.84 %
AP counting		
- Background	5.65 %	0.60 %
Neutron cone		
- Neutron scattering	0.54 %	0.40 %
- Effective fission foil thickness due to the cone aperture	0.12 %	0.08 %
Fissile layers		
- Areal density	-	1.00 %
- Inhomogenity	-	1.51 %
Result (10^{-24} cm^2)	1.337 ±	0.038
Standard deviation		2.81 %

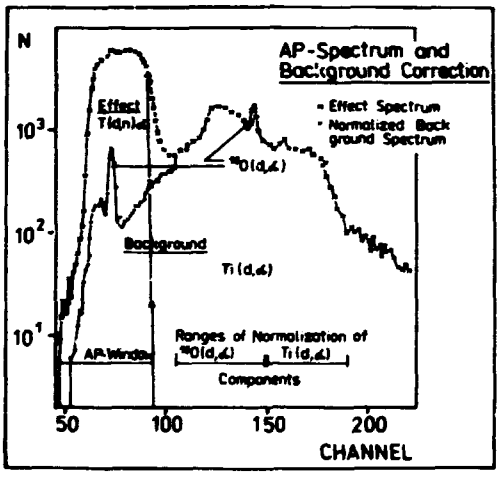

Fig. 1: AP-spectrum of the Ti-T target foil and background correction

Tab. 1: Summary of the corrections and error contributions of the presented measurement

The used 5 fission-foils (Σm_s = 1.909 mg/cm^2) were prepared by HF-sputtering and separation out of an metal-organic compound. The areal densities were measured by 2/3π α-counting and calculated by using $T_{1/2}$ = 4.468 . 10^9 y ± 0.11 % [3]. The inhomogeneity was determined by RBS [4] and the used fission chamber configuration optimised as described in ref. [5] to get a minimum total inhomogeneity. To improve the accuracy further efforts have to be directed especially to the preparation of foils with better inhomogeneity.
The preliminary result ((1.337 ± 0.038) . 10^{-24} cm^2) agrees within the error limits with the ENDF-BV-compilation (1.326 . 10^{-24} cm^2).

REFERENCES

[1] R. Arlt et.al., Kernenergie 24 (1981), p. 48
[2] C.-M. Herbach et.al., preprint TUD 05-07-85 (1985)
[3] A. Lorenz (Ed), INDC(NDS)-149/NE, Vienna, Dec. 1985
[4] K. Merla, R. Groetschel, this report, p. 116
[5] C.-M. Herbach et.al., preprint TUD 05-06-85 (1985)

THEORETICAL STUDY OF FISSION NEUTRON EMISSION DURING FRAGMENT ACCELERATION

H. Märten
Technische Universität Dresden, Sektion Physik, WB Kernphysik

Based on dynamical calculations of post-scission processes /1/ we introduced the time-dependence of fragment excitation energy $E^x(t)$ and kinetic energy $E_k(t)$ into the cascade evaporation model /2/ to estimate the influence of neutrons emitted during fragment acceleration on total double-differential emission probabilities $N(E,\Theta)$ (E,Θ - neutron energy and emission angle with reference to the light fragment direction, lab. frame coordinates). The considered emission mechanism was assumed to be significant in different fission reactions /3,4,5/, but earlie studies involved arbitrary approximations like the reduction of the problem to a single intermediate emission time.

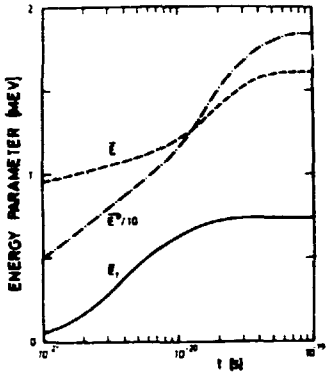

Fig. 1
Fragment kinetik energy per nucleon Ef, the average excitation energy E , and the average cms emission energy as a function of time t after scission for symmetric fission of ^{252}Cf

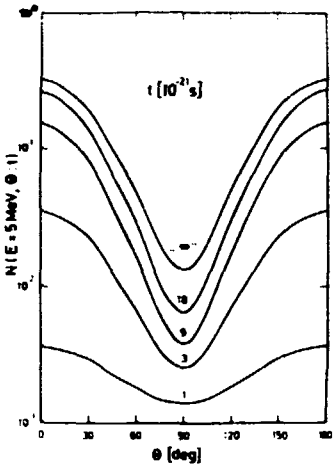

Fig. 2
The angular distribution of fission neutrons for a fixed emission energy (2 MeV) in dependence of t for ^{252}Cf(sf)(symmetric).

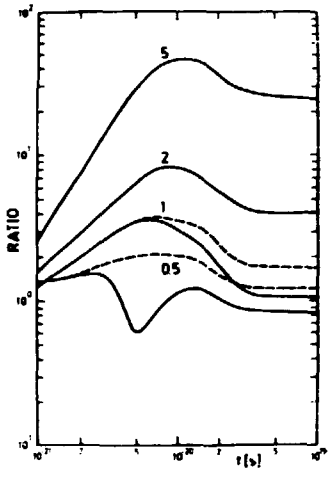

Fig. 3
0°/90°-anisotropy of ^{252}Cf (sf) neutron emission versus t for fixed emission energies (parameter in MeV). The structure at low energy appears due to kinematics.

The calculation of the cms emission distribution $\mathcal{P}_0(\mathcal{E})$ of the first cascade step was carried out as a function of t, i.e.

$$\mathcal{P}_0(\mathcal{E} : E_k(t),t)dt = W(t)\cdot \int_0^\infty dE^x \cdot P_0(E^x;t)\cdot \mathcal{P}(\mathcal{E} : \mathcal{E}^*)dt, \qquad (1)$$

where $P_0(E^x;t)$ - excitation energy distribution. The emission probability per time unit $W(t)$ is deduced according to statistical assumptions /3/. The corresponding $N(E,\Theta)$ data (Fig.2) show a time-dependent $0^0/90^0$-anisotropy (Fig. 3) which can be approximated by $\sinh(3 \cdot \sqrt{E\cdot E_k(t)/A} \,/\, \bar{\mathcal{E}}(t))$ (A-fragment mass number). Hence, the relative behaviour of $E_k(t)$ and $E^x(t)$ as well as $W(t)$ determine $N(E,\Theta;t)$. The used input data /1/ give rise to an unexpected anisotropy maximum close to 10^{-20}s (Fig. 3) for a symmetric mass split in ^{252}Cf(sf). A remarkable enhancement of neutron emission in equatorial direction can only be deduced for unreasonably short neutron life times, i.e. simulation of non-equilibrium emission.

References

/1/ B.C. Samanta et al., Phys. Lett. 108 B (1982) 83
/2/ H. Märten et al., J. Phys. G 10 (1984) 349
/3/ G.A. Pik-Pitchak, Yad. Fiz. 10 (1969) 321
/4/ P. Riehs, Acta Phys. Austr. 53 (1981) 271
/5/ D.J. Hin e et al., Phys. Rev. Lett. 52 (1984) 986

ABOUT THE MEAN-SQUARE RADII OF THE 236-U NUCLEUS IN EXCITED STATES WITH DIFFERENT FISSION WIDTHS

A. Meister, S. Mittag, W. Pilz, D. Seeliger, K. Seidel
Technische Universität Dresden, Sektion Physik, WB Kernphysik
L.B. Pikelner
Joint Institute for Nuclear Research, Dubna, USSR

Experimentally determined mean-square charge radii of ^{236}U compound-nucleus states excited by neutron resonance absorption in ^{235}U s ow on average a weak diminution as compared with the ground state data, and a correlation of these $\langle r^2 \rangle_n$ with the fission widths of the compound-nucleus states seems to appear /1,2/. In Ref. /3/ an attempt was made to discuss this correlation in the frame of the double-humped fission barrier model. This model is successfully used to describe subthreshold fission processes, whereas in the present case states are excited lying about 1 MeV above the barrier. But investigations of the fission cross section of $^{235}U+n$ showed intermediate structures which could also be interpreted with the same model that has been used to describe structure in subthreshold fission /4/.

With the $\langle r^2 \rangle_n$ -data, the fraction α^2_{II} of configurations with deformation corresponding to the second well of the fission barrier was estimated for each excited compound-nucleus state. Using the value α^2_{II} of the 4.8 eV-resonance, which has a fission width of only 4 meV, as a reference (j) the fractions α^2_{II} of the other states are of the order of 10% (Fig. 1). In the frame of the model the α^2_{II} may be related to the transition rates between the wells. This yields a fission, width $\Gamma_{IIf} \simeq 1...5$ eV for the second well states responsible for fission of compound-nucleus states excited by low energy neutrons. The value is very small in comparison to an estimate of the statistical average $\bar{\Gamma}_{If} \approx 50...120$eV obtained by the Bohr-Wheeler formula. In priciple, large statistical fluctuations of Γ_{If} are possible, but it can not be excluded that the observed correlation of the $\langle r^2 \rangle_n$ with Γ_f is connected with any other phenomena not included in the model used.

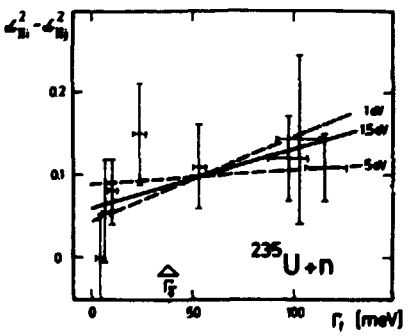

Fig. 1:
Differences of fractions of second well configurations in 236-U compound-nucleus states in dependence on their fission widths (+) and estimated dependences with indicated Γ_{IIf} (---)

References:

/1/ Mittag, S., et al., Nucl. Phys. A 435 (1985) 97
/2/ Meister, A., et al., Gemeinsamer Jahresbericht 1983, ZfK-530 (1984) 12
/3/ Meister, A., et al., XV. Int. Symp. Nuclear Physics, Gaußig 1985
/4/ Moore, M.S., et al., Phys. Rev. C 30 (1984) 214

ANGULAR CORRELATIONS AND MASS LOSS IN 1 GeV PROTON-NUCLEUS COLLISIONS

L.N. Andronenko, M.N. Andronenko, A.A. Kotov, L.A. Vaishnene
Leningrad Nuclear Physics Institute, Gatchina, U.S.S.R.
W. Neubert
Zentralinstitut für Kernforschung Rossendorf, Bereich KF

The experiment was performed at the Gatchina synchrocyclotron using the 1 GeV external proton beam. Coincident heavy fragments were detected in the two arms of the TOF spectrometer. The emission angle of one fragment was measured by a position sensitive PPAC (18 x 3.5 cm^2). A double-grid avalanche counter mounted at a distance of 3 cm from the target provided the common start signal for the TOF measurements. Two silicon detectors at $\Theta_1 = 90°$ to the beam axis supplied the stop signal and energy information. In this way it was possible to measure two angular correlations simultaneously and to check the reliability of the data. The mass distributions of the fragments were determined from the measured TOF's and kinetic energies. The mean value of the single mass distribution $\langle A_1 \rangle$ was found to be less than the half of the target mass A_T.
The corresponding mean mass loss $\langle \Delta A \rangle$ carried away by the undetected particle was obtained from the relation $\langle \Delta A \rangle = (A_T + 1) - 2 \langle A_1 \rangle$.
Figures 1, 2 and 3 show the mean mass-loss for targets of uranium, bismuth and samarium in dependence on the folding angle $\Theta_1 + \Theta_2$ of the fragments. The mass loss increases in forward direction ($\Theta_1 + \Theta_2 < 180°$) and the r.m.s. variances $\langle \sigma_{A1} \rangle$ of the corresponding mass distributions become broader. The same tendency was observed in backward direction. This behaviour could not yet be understood.
In a first approximation, we used the two-body kinematics to estimate the transferred forward momentum p_w for several folding angles. A least square fit (solid line in fig. 4) shows that p_w increases approximately linearly with the mass loss $\langle \Delta A \rangle$ in agreement with the data of ref. /1/. Furthermore, a comparison at given $\langle \Delta A \rangle$ of our data with recent measurements /1/ shows that p_w varies inversely with the proton incidence energy.

Fig. 3 ▶

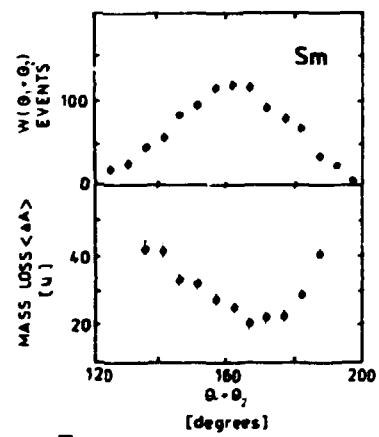

References

/1/ S.B. Kaufman et al., Phys. Rev. C26 (1982) 2694

Fig. 1 ▼

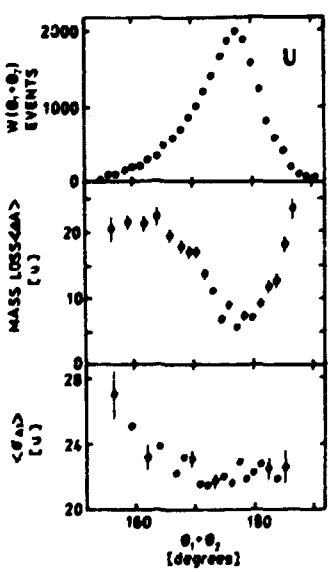

Fig. 2 ▼

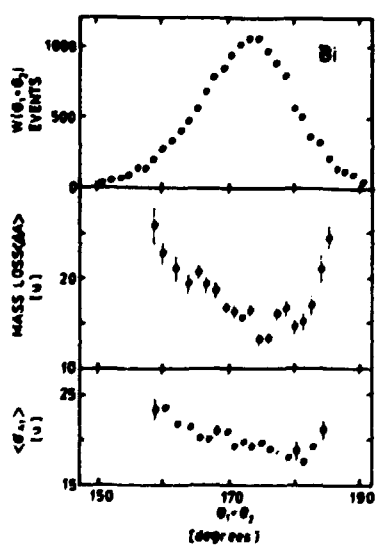

Fig. 4 ▼

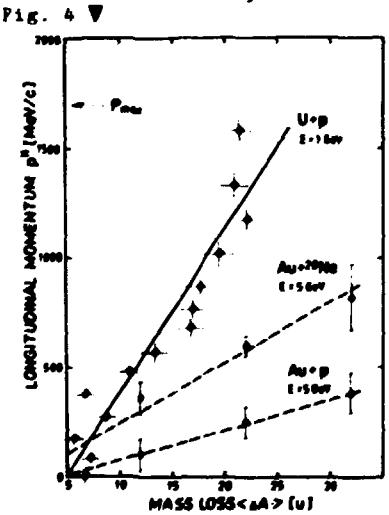

HADRON AND FRAGMENT EMISSION IN CLUSTER EXCITATION PROCESSES AT MEDIUM ENERGIES

H. Müller and C. Schneidereit, Zentralinstitut für Kernforschung, Rossendorf, Bereich KF
Zs. Kovacs, Central Research Institute for Physics, Budapest, Hungary

An extended version of the cluster excitation model /1/ is proposed to describe the inclusive spectra of various particle types in a consistent way. The emission of particles in hadron-nucleus interactions is assumed to be caused by a sequence of quasi-free binary collisions between the projectile and clusters of k ($1 \leq k \leq A$) target nucleons. These interactions are connected with the conversion of kinetic energy into excitation energy of the colliding systems. The subsequent decay of an excited system is described according to the statistical model /2/, i. e. the decay probability $P^{\alpha}(M)$ into a certain channel α is assumed to be proportional to the number $d\mathcal{A}^{\alpha}(M)$ of quantum states per energy interval accessible at the given invariant mass M of the system

$$d\mathcal{A}^{\alpha}(M) \sim (\Omega/(2\pi\hbar)^3)^{n-1} \cdot g \cdot \prod_{i=1}^{n} 2m_i \, dR_n^{\alpha}(M)$$

with the masses m_i of the final particles. Spin- and isospin states are counted by the factor g, the Lorentz-invariant phase space is denoted by $dR_n^{\alpha}(M)$, and Ω means the volume from which the particles are emitted. The decay probability is normalized according to

$$P^{\alpha}(M) = \mathcal{A}^{\alpha}(M)/\sum_{\alpha} \mathcal{A}^{\alpha}(M).$$

These probabilities are employed in the model /1/ for the description of the whole interaction process. In this way all possible decay channelc are taken into consideration. In fig. 1 the calculated spectra of protons, deuterons, tritons and pions from the interaction of neutrons with carbon at 545 MeV /3/ are compared with model calculations. With the parameters of ref. /1/ a fair description of the whole data set has been achieved.

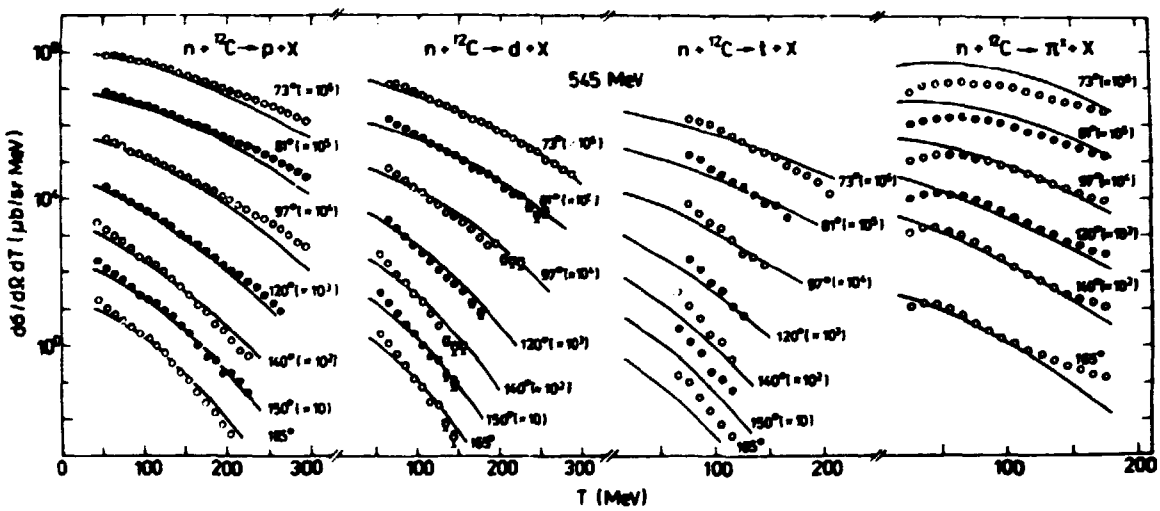

Fig. 1
Energy spectra of protons, deuterons, tritons and charged pions at different angles /3/. Data and curves are multiplied by the factors given in parentheses.

/1/ Komarov, V.I., H. Müller and S. Tesch, Fortschr. Phys. 33 (1985) 595
/2/ Fermi, E., Progr. of Theor. Phys. 5 (1950) 570
/3/ Rössle, E. Proceedings of the 6 th Balaton Conference on Nuclear Physics, 1983, ed. J. Erö (KFKI, Budapest) p. 141; Franz, J., et al., Phys. Lett. 153B (1985) 382

A MEASUREMENT OF THE TOTAL CROSS SECTION OF THE CAPTURE REACTION $^2H(n,t)_\gamma$ AT E_n = 25 MeV

J. Mösner, K. Möller, W. Pilz, G. Schmidt and T. Stiehler
Zentralinstitut für Kernforschung, Rossendorf, Bereich KF

Photodisintegration of ^3H and its inverse, the radiative n-d capture, are a tool to investigate the three-body wave function in its more general aspect and can provide basic information on the properties of the nuclear forces.

The present paper represents the first measurement of the total cross section of the capture reaction $^2H(n,t)_\gamma$. We used an experimental set-up similar to that described in ref. /1/. The 25 MeV neutrons are produced at a Ti-T target bombarded by the 8 MeV pulsed deuteron beam of the Rossendorf tandem accelerator. After collimation the neutrons are incident on a 10 mg/cm^2 gaseous deuterium target containing two MWPC's. The capture tritons, recoil deuterons and break-up protons produced within the deuterium gas volume are detected simultaneously by a charged-particles spectrometer which allows to separate these kinds of particles. Fig. 1 shows the result of about 440 hours measuring time.

The total capture cross section is determined from the ratio of the number of measured tritons to the number of recoil deuterons with the help of a Monte-Carlo simulation using the known differential cross section of the elastic n-d scattering /2/. The resulting capture cross section amounts to σ_{capt} = (7.6 ± 0.8) µb. Using detailed balance this value corresponds to σ_{dis} = (453 ± 48) µb for the photodisintegration cross section at E_γ = 25 MeV.

A comparison with existing photodisintegration data and four different theoretical calculations is given in fig. 2.

The present value confirms the data points measured by Skopik et al. /3/ (open circles in fig. 2). It should be noted here that in the case of photodisintegration measurements the absolute normalisation of the cross section is a difficult experimental task and, therefore, systematic errors can be underestimated easily.

Obviously, this also is the reason of the discrepancies between the data of the measurements of the different groups.

Whith this respect our measurement serves as a kind of calibration of the photodisintegration data.

A more detailed description of the experiment and a discussion of the conclusions will be published in /4/.

Fig. 1: A plot of the measured events

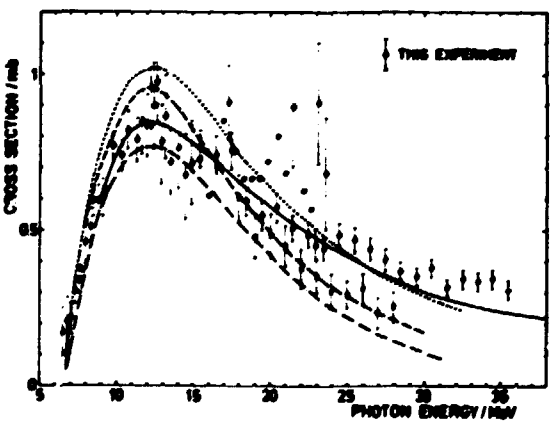

Fig. 2: Total cross sections for the two-body photodisintegration of ^3H

References:

/1/ Stiehler, T., et al.; Nucl. Instrum. Methods A 236 (1985) 343
/2/ Doll, P., et al. (Karlsruhe); private communication
/3/ Skopik, D.M., et al.; Phys. Rev. C 24 (1981) 1791
/4/ Mösner, J., et al.; to be published in Few-Body Systems

OFF-SHELL SENSITIVITY OF THE M1-CONTRIBUTION TO THE CAPTURE REACTION $n + p \rightarrow d + \gamma$

K. Möller
Zentralinstitut für Kernforschung, Rossendorf, Bereich KF

In connection with a measurement of the capture reaction $n + p \rightarrow d + \gamma$ with 25 MeV neutrons at the Rossendorf tandem accelerator /1/ a theoretical investigation was started to study the influence of off-shell changes in the nucleon-nucleon potential on the capture cross section.

In the neutron energy range from 0 to 50 MeV the cross section of the $n + p \rightarrow d + \gamma$ capture reaction is dominated by M1 and E1 transitions according to the matrix elements

$$T_{M1} = \langle d(^3S_1) | M1 | np(^1S_0) \rangle,$$
$$T_{E1} = \langle d(^3S_1) | E1 | np(^3P) \rangle.$$

To study the influence of off-shell changes on these matrix elements sets of phase equivalent rank-2 separable potentials were generated using a method proposed by Fiedeldey /2/. In an earlier paper /3/ off-shell changes in the E1 transitions were investigated which are due to changes in the triplet np-potential.

To study the influence of off-shell changes in the singlet np-interaction in the present paper the M1 transitions were investigated. Off-shell changes were generated by using different wave functions u_d^* for the singlet virtual deuteron d^* (Fig. 1). The corresponding changes in the M1 photodisintegration cross section are shown in Fig. 2. From this figure one can conclude that there are practically no off-shell changes in the capture cross section if one passes from curve 2 to curve 3. Up to now it is not yet clear whether there exists a simple argument to explain this strong cancellation.

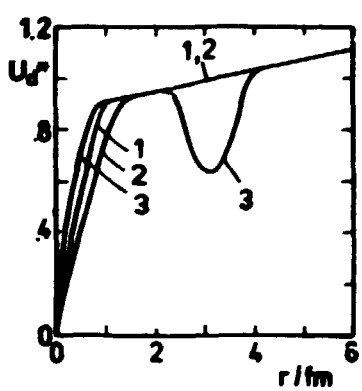

Fig. 1 Wave functions of the virtual deuteron state d^*

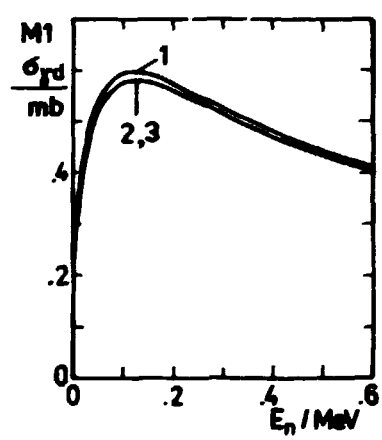

Fig. 2 Off-shell changes of the total $\gamma + d$ disintegration cross section due to the wave functions d^* in Fig. 1

References

/1/ Stiehler, T. et al. Phys. Lett. 151B (1985) 185
/2/ Fiedeldey, H. Nucl. Phys. A135 (1969) 353
/3/ Möller, K. Proc. of the X. European Symp. on the Dynamics of Few-Body Systems, Balatonfüred 1985

PHENOMENOLOGY OF ANGULAR DISTRIBUTIONS OF 14-MEV-NEUTRON-INELASTIC SCATTERING: SYSTEMATICS AND THEORETICAL APPROACHES

D. Hermsdorf and H. Kalka

Technische Universität Dresden, Sektion Physik, WB Kernphysik

Generally, the energy and angular dependence of neutron emission cross sections $\sigma_{nM}(E,E',\vartheta)$ is favourable represented in terms of Legendre polynomials according to

$$\sigma_{nM}(E,E',\vartheta) = \frac{\sigma_{nM}(E)}{2\pi} \sum_{l=0}^{L} \left(\frac{2l+1}{2}\right) f_l(E')\, P_l(\cos\vartheta) \qquad (1)$$

introducing reduced coefficients f_l by the normalization condition

$$f_0(E,E') = \sigma_{nM}(E,E')/\sigma_{nM}(E). \qquad (2)$$

The systematics of higher-order coefficients f_l $(l \geq 1)$ carried out by Briseño et al. /1/ yields following results:

i) independence on the target nucleus mass number in the range $30 \lesssim A \lesssim 200$;
ii) independence on the incidence energy in the energy range $5 \lesssim E \lesssim 26$ MeV;
iii) independence on the kind of incidence and emerging particle (at least for neutrons and protons).

At present, two different approaches exist for an interpretation of this systematical behaviour of f_l :

i) the "Leading-Particle-Model" developed by Mantzouranis et al. /2/ which has been implemented into the Generalized Exciton Model (GEM) by Akkermans et al. /3/.
ii) the semi-empirical formalism of Kalbach and Mann /4/ which has been derived from (p,n) and (p,p') experiments at high energies ($E \approx 50$ MeV). Assuming the correspondence of the transmission of a particle with angular momentum l through a nucleus' potential well and the moment f_l it has been found

$$f_l(E') = 1/(1 + \exp(A_l(B_l - E'))) \qquad (3)$$

with parameters

$$\left.\begin{aligned} A_l &= (0{,}036 + 0.0039\, l\,(l+1))/\text{MeV} \\ B_l &= (92. \quad - 90/\sqrt{l(l+1)}\ )\text{MeV} \end{aligned}\right\} \quad \text{for } l = 1\ldots6 \qquad (4)$$

This formalism also reflects all independencies of f_l stated above. But, any application at 14 MeV has to be investigated carefully /5/.

References:

/1/ Briseño-Galvez, J., Hermsdorf, D. and Kalka, H., Jahresbericht ZfK-559 (1985) 45
/2/ Mantzouranis, G. et al., Phys. Lett. 57B (1975) 220
/3/ Akkermans, J.M., Gruppelaar, H. and Reffo, G., Phys. Rev. C22 (1980) 73
/4/ Kalbach, C. and Mann, F.M., Phys. Rev. C23 (1981) 112
/5/ Hermsdorf, D., Kalka, H. and Steininger, U., this report p. 13

PHENOMENOLOGY OF ANGULAR DISTRIBUTIONS OF 14-MEV-NEUTRON-INELASTIC SCATTERING: COMPARISON OF EXPERIMENTAL AND THEORETICAL RESULTS

D. Hermsdorf, H. Kalka and U. Steiniger
Technische Universität Dresden, Sektion Physik, WB Kernphysik

In a preceding contribution two phenomenological models for the calculation of double-differential cross sections (DDX) are described /1/. Both formalisms have been applied to interpret experimental data for Lead obtained by several authors.

i) The "Leading-Particle-Model" is realized in the computer code AMAPRE /2/ which supplies all Legendre moments f_l inclusively f_o.

ii) The application of Kalbach-Mann's formalism necessarily requires to account for contributions by compound processes (MSCR) by a reduction factor r(E) defined as the relative contribution of direct reactions (DI) to the total emission cross section

$$r(E') = \sigma_{nM}(E')^{DI} / \sigma_{nM}(E')^{exp} \qquad (1)$$

to yield Legendre' moments

$$f_l(E') = \sigma(E') - f_l^{KM}(E') \quad \text{for } l = 1,\dots,6 \qquad (2)$$

Usually, $\sigma_{nM}(E')^{DI}$ is approximated by $\sigma_{nM}(E')^{DWBA}$.

Comparing reduced coefficients extracted from experiments and calculated results following conclusions can be drawn:

i) the theoretically predicted f_l in both formalisms agree very well within the experimental uncertainties /3/ (and fig. 1)

ii) the predicted absolute angular distributions $\sigma_{nM}(E,E',\vartheta)$ are also in quite good agreement if the normalization factor $f_o(E,E')$ can be correctly determined by theory or experiment. At high emission energies DI components have to be superimposed to the results of AMAPRE /3,4/.

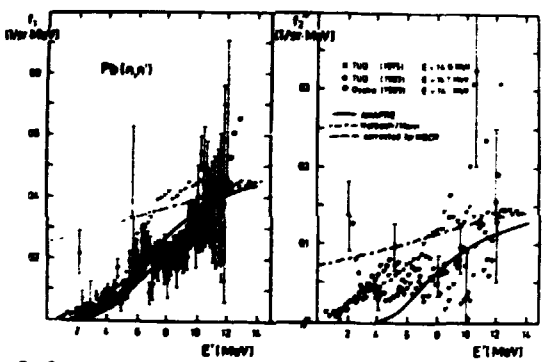

Fig. 1:
f_l as function of energy E .

References:

/1/ Hermsdorf, D. and Kalka, H., this report, p. 12

/2/ Hermsdorf, D., Kalka, H. and Seeliger, D., Jahresbericht ZfK-530 (1984) 16, Jahresbericht ZfK-559 (1985) 44

/3/ Hermsdorf, D. et al., Proc. Conf. on Neutron Physics, Kiev, 1983, Vol. I, p. 131, 1984

/4/ Elfruth, T. et al., Proc. Int. Symp. on Fast Neutron Physics, Chiang Mai, Thailand, 1985, to be published

ABOUT THE POSSIBILITY OF A BOUND ^{12}C-^{12}C QUASIMOLECULAR BAND IN ^{24}Mg

M.U. Gersch
Zentralinstitut für Kernforschung, Rossendorf, Bereich KF
V. Goldberg and V. Rudakov
Institute of Atomic Energy, Moscow

Recently we presented as a result of our Moscov - Rossendorf collaboration the direct evidence of a ^{12}C transfer in the $^{12}C(^{14}N,d)$-reaction, populating the (13.450 $\pm$ 0.015)MeV 6^+ level in ^{24}Mg /1/. This statement is based on

- the agreement of the (d,α_0) correlation function with the squared Legendre polynom for an orbital momentum l=6 and
- the disagreement of the deuteron angular distribution with a Hauser-Feshbach calculation.

The quoted level has been found and investigated already in different reaction channels (e.g. /2,3,4/). Assuming a rather large spectroscopic factor for the cluster component ^{12}C-^{12}C (both in the groundstate), we suggest:

1) The level could be a member of a rotational band with an anomal large momentum of inertia. Using $\frac{2\theta}{\hbar^2} \cong$ 10 MeV^{-1}, as found for the quasimolecular resonances in ^{12}C-^{12}C collisions, the next members of the band should be situated at $E^*(4^+) \cong 11.3$ MeV and $E^*(8^+) \cong 16.5$ MeV, respectively.

2) The expected members of the rotational band should have similar intrinsic structure. Taking into account the spectroscopic factors of the 6^+ level /2/ and the energy dependence of the penetrability we get the following α-particle widths (table 1). From this point of view it is worth while to investigate the 4^+(?)-level at 11.30 MeV /3,4/ and the three 8^+ levels /5/ at about 16.5 MeV more in detail.

Table I

I^π	E^* /MeV/	Γ_{α_0} /eV/	Γ_{α_1} /eV/
4^+	11.3	3.5 meV	-
6^+	13.45	1.6	4.1
8^+	16.5	0.7	15

3) The special method of distinction of a direct transfer from a compound process in heavy ion reactions is described in /1/, according to which following conditions must be fulfilled:
   - angular momentum matching for a periphere collision
   - fragment (here the deuteron) with spin $\neq$ 0 as a spectator
   - final state (here ^{20}Ne) of the angular correlation measurement with spin = 0.

   As shown in table 1 the last of these conditions is hard to fulfill for the expected 4^+ and 8^+ members. However it should be possible to investigate the mechanism in a more complicated experiment, using for example the d-α_1-γ coincidence.

4) A rotational band is characterized by collective intraband γ-transitions. However the known γ-transition /2/ from the 6^+ level leading to the 4^+ level at 4.107 MeV competes seriously with an expected intraband transition even in the case of strong collectivity. Thus, an identification in a dγ-coincidence experiment seems to be hopeless. The $^{12}C(^{16}O,\alpha\gamma)$- or $^{20}Ne(\alpha,\gamma)$-reaction has probably a better chance.

5) The 6^+ level at 13.45 MeV in ^{24}Mg is situated about 9 MeV below the well known 6^+ resonances of the quasimolecular band. This fact suggests an interpretation of the quasimolecular resonances in the frame of the double resonance mechanism /6/, in which resonances with excited relative motion (n$\neq$0) are coupled to molecular configurations, containing two excited carbon clusters.

   The generally used nucleus-nucleus potentials do not permit bound ^{12}C-^{12}C states. However, the parameters of these potentials are gained by fitting to the experimental quasimolecular band. Some deep potentials, independently determined /7/ have bound nucleus-nucleus states and permit the interpretation of the found 13.45 MeV 6^+ level as a quasimolecular state.

References

/1/ Artemov, K.P. et al., Phys. Lett. 149B (1984) 325
/2/ Fifield, L.K. et al., Nucl. Phys. A309 (1978) 77
/3/ Greenwood, L.R. et al., Phys. rev. C6 (1972) 2112
/4/ Szanto de Toledo, A. et al., Nucl. Phys. A315 (1979) 500
/5/ Fifield, L.K. et al., Phys. Rev. C8 (1973) 2217
/6/ Scheid, W. et al., Phys. Rev. Lett. 25 (1970) 176
/7/ Baye, D., N. Pecher, Nucl. Phys. A379 (1982) 330: Satchler, G.R., Nucl. Phys. A409 (1983) 3c

APPLICATION OF K^+-INTERFEROMETRY FOR THE INVESTIGATION OF THE EARLY STAGE IN HEAVY ION COLLISIONS AT RELATIVISTIC ENERGIES

Proposal for an experimental arrangement at the Dubna Synchrophasotron

H.U. Gersch

Zentralinstitut für Kernforschung, Rossendorf, Bereich KF

Collisions of relativistic heavy ions (RHI) are the unique possibility to study nuclear matter under extreme conditions. One of the fundamental problems is the existence of the quark-gluon plasma (QGP). In some theoretical models the transition to the QGP seems to be possible already at Dubna energies /1/.

The aim of the proposed experiment are informations about the evolution of a RHI collision in the stopping region of energy. Pions and nucleons emitted during the collision reflect only the thermal freeze out in a later stage of the reaction. From the study of strange particles we expect informations of the early hot and dense stage of the collision and about the phase transition into the QGP. The inclusive K^+-spectra can be used for measuring of the temperature parameter T. The density ρ of the nuclear matter in an early stage of the collision can be determined from the size of the kaon source and the number of participating nucleons. The space-time behaviour of the K^+-emitting source can be investigated with help of the intensity interferometry /2/.

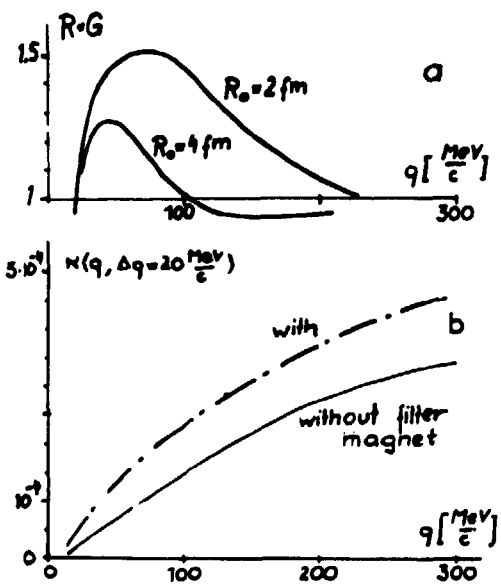

Fig. 1

Expected correlation function for K^+ pairs at different sizes of the emitting source (a) and phase space factor for the proposed experimental setup (b)

In fig. 1a the expected correlation function is presented for two different source dimensions R_0. Here, the Coulomb repulsion between identical kaons was taken into account by the so called Gamow-factor G /3/. The life time of the source and the effect of coherence between the kaons is assumed to be sufficiently small. Fig. 1a shows, that in a practical measurement the events of 2-particle coincidences can be cumulated in bins of the parameter $q = |\vec{p}_1 - \vec{p}_2|$ of $\Delta q \leq 30$ MeV/c ($\vec{p}$: momentum of K^+ in the rest frame of the source).

Only very scarce rates of K^+-coincidences are expected. Therefore it is necessary to use a filmless detector system. The proposed experiment can be realized in principle by the magnetic spectrometer of the device GIBS at the Dubna Synchrophasotron, consisting of the dipol magnet SP 57 and three systems of multiwire proportional chambers (MWPC). The spectrometer has to guarantee

- the identification of kaons in the background of pions and protons
- the measurement of the kaon momenta
- the selection of central collisions by a suitable trigger.

The yield of K^+-coincidences has been estimated on the basis of the following conditions:

- beam: Si or heavier, 4.2 A GeV/c(lab), 10^6 particles/pulse
- target: Si or heavier, 3 g/cm^2
- two-kaon production cross section σ(2 K^+, b $\leq$ 2 fm) $\approx$ 10 mb (b: collision parameter)
- survival of K^+-pairs in the spectrometer with the length L = 3.3 m : 50 %
- phase space factor κ (fig. 1b), calculated by simulation with a Monte-Carlo code, taking into account
  - the source of K^+ with a temperature T $\approx$ 140 MeV, isotrope
  - the spectrometer geometry with an acceptance of $\Omega \approx$ 75 msr, spectrometer axis $\approx$ 15° out of the beam axis
  - the momentum acceptance p(lab) = 0.5...2 GeV/c.

For the second bin (q_{CM} = 30...50 MeV/c) we got $\kappa \approx 3 \cdot 10^{-5}$ and a yield of N $\approx$ 0.02 K^+-pairs per accelerator cycle. Thus, a correlation function can be gained with sufficient statistics during a few hundred hours beam time.

The identification of kaons is based on the particle momentum (from the reconstructed trajectory in the magnetic dipol field) and the time of flight (TOF). For the length of the spectrometer of L = 3.3 m the TOF has to be measured with 0.2 ns accuracy. Therefore behind the last MWPC a wall of scintillation stop detectors sectionated

in about 100 modules has to be installed. The start detector eventually must be placed into the primary beam, which needs a large counting capability.
Additionaly a beam detector determines the trajectory at the position of the target. A filter magnet at the first part of the spectrometer can help to select the interesting particles from the primary beam and enlarges the efficiency of the device by about a factor 2 (fig. 1b).

A similar experimental setup is under construction in the Brookhaven National Laboratory for the investigation of RHI collisions at 15 A GeV/c(lab) /5/.

References

/1/ 7. High Energy Heavy Ion Study, GSI-85-10 (1985)
/2/ Yano, F.B., S. Koonin, Phys. Lett. 78B (1978) 556
/3/ Beavis, D. et al., Phys. Rev. C28 (1983) 2561
/4/ Kulakow, B.A., Project GIBS, Dubna 1976
/5/ Nagamiya, S., Int. School of Nuclear Physics, Erice, 1985

QUENCHING OF THE CORRELATION FUNCTION AT THE HANBURY BROWN-TWISS EFFECT

H.U. Gersch

Zentralinstitut für Kernforschung, Rossendorf, Bereich KF

Using the HBT-effect it is possible to get information about the space-time structure of the radiating source /1/. If Boson pairs (e.g. K^+) /2/ are emitted with a Gaussian-like manner regarding the source distribution R_0 and the time behaviour τ the correlation function has the form /3/

$$R(q,q_0) = 1 + \lambda e^{-\frac{q^2 R_0^2}{2}} e^{-\frac{q_0^2 \tau^2}{2}} \tag{1}$$

$q = |\vec{p}_1 - \vec{p}_2|$, $q_0 = |E_1 - E_2|$, λ: degree of coherence, where $\lambda = 1$, if no coherence between the particles exists /4/.

In the experiment the product of $R(q,q_0)$ and the phase space function $W(q,q_0)$ will be measured. $R(q,q_0)$ is gained in praxis by normalization to a function without correlation behaviour, which can be determined experimentally by using surely not correlated particles or by simulation, taking into account the parameters of the source (fireball) and the geometry of the spectrometer /2/. In general however because of small coincidence rates the correlation function can be measured only in dependence of q (e.g. 5,6). In this case the measured function R(q) is interpreted as

$$R(q) = 1 + \lambda_{eff} e^{-\frac{q^2 R_{eff}^2}{2}} \tag{2}$$

Realy this function is gained by integration over q_0

$$R(q) = 1 + \lambda \cdot e^{-\frac{q^2 R_0^2}{2}} \cdot T(q) \tag{3}$$

with the quenching factor T

$$T = \frac{\int e^{-\frac{q_0^2 \tau^2}{2}} W(q,q_0)\, dq_0}{\int W(q,q_0)\, dq_0} \tag{4}$$

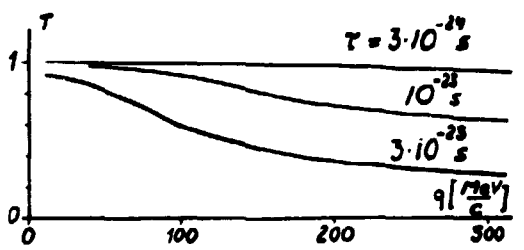

Fig. 1

Quenching factor for different life times of the emitting source (fireball)

Using the model of the source and the spectrometer geometry in /2/ for kaons we calculated the quenching factor T shown in fig. 1.

In the simple interpretation (2) the size of the source R_0 will be overestimated or λ can be underestimated for lifetimes of the fireball $\tau \gtrsim 10^{-23}$ s, respectively.

In the case of kaon interferometry this quenching effect probably may be neglected because of the short period of predominant kaon production (highly compressed stage). However, it must be taken into account, that protons and pions are emitted during the expansion of the fireball, which should last some 10^{-23} s.

References

/1/ Hanbury-Brown, R., R.Q. Twiss, Nature 10 (1965) 1046

/2/ Gersch, H.U., this report p. 15

/3/ Yano, F.B., S.E. Koonin, Phys. Lett. 78B (1978) 556

/4/ Guylassy, M. et al., Phys. Rev. C20 (1979) 2267

/5/ Nagamiya, S., Hyperfine Interactions 21 (1985) 219

/6/ Zarbakhsh, F. et al., Phys. Rev. Lett. 46 (1981) 1268

MAT 1402 AND MAT 8201 -
TWO REVISED VERSIONS OF EVALUATED NEUTRON NUCLEAR DATA FILES FOR SILICON AND LEAD FOR BROND

D. Hermsdorf
Technische Universität Dresden, Sektion Physik, WB Kernphysik

A.V. Blokhin and A.V. Ignatyuk
Fisiko - Energeticheskij Institut Obninsk, Centre po yadernim dannim (CJD)

Starting in 1985 the library BROND (Biblioteka Rekomendovanikh Otsenenikh Neutronnikh Dannikh) has been initiated and designed for general purpose in the CMEA-region. This library (formerly SOKRATOR) is established and will be maintained and disseminated by the CJD Obninsk whereas all responsibilities concerning correctness of any included data file are committed to originators or evaluators respectively.
In this year two files most recently evaluated at TU Dresden have been contributed to BROND. Basing on earlier version (MAT 2015 for Silicon /1/ and MAT 1502 for Lead /2/ both files have been improved or extended in various quantities (files MF, data types MT).

Silicon:

i) re-evaluation of resolved resonances parameters in Multi-Level-Breit-Wigner representation (MLBW) (MF2, MT151)

ii) re-evaluation of capture cross sections in the fast neutron energy range (MF3, MT102)

Lead:

i) inclusion of resolved resonances parameters in MLBW representation (MF2, MT151)

ii) re-formulation of neutron production cross sections by inclusion of neutron multiplicities (MF6, MT10)

iii) inclusion of γ-ray production cross sections (MF13, MF14, MF15, MT3 and MT102)

iv) inclusion of covariance matrices (MF33, MT's 1,2,4,10,16,17,91,102,103,107)

All improvements and extensions had been stimulated by customers' requests or internal data checks by comparison with integral experiments. Both new versions will be documented in the next future as separate publications in the INDC(GDR)-report series.

References

/1/ Hermsdorf, D. et al., Jahresberichte ZfK-408 (1979) 39, ZfK-443 (1980) 22, ZfK-488 (1981) 28 and 30, Hermsdorf, D., Reports INDC(GDR)-20/L and 22/L, 1983

/2/ Hermsdorf, D. et al., Jahresbericht ZfK-559 (1984) 16

ON THE USE OF NUCLEAR DATA LIBRARIES IN GDR - UPDATING AND EXTENSION OF DATA BASES AND NUCLEAR DATA SERVICE

S. Eckstein, D. Hermsdorf and D. Seeliger
Technische Universität Dresden, Sektion Physik, WB Kernphysik
K. Friedrich, L. Jankowski and B. Letz
Zentralinstitut für Isotopen- und Strahlenforschung Leipzig, Informations- und Rechenzentrum

In 1985 the data base of the Neutron Nuclear Data Library maintained at TU Dresden has been extended by adopting

i) the Japanese Evaluated Nuclear Data Library JENDL-2 in both versions (point-wise and resolved-resonances representation)
ii) the Evaluated Nuclear Data Library ENDL-84 (an ENDF/B-V formatted version of ENDL-82)
iii) the International Nuclear Data Library INDL/V-85
iv) the 2nd revised version of ENDF/B-V Dosimetry Library
v) the ENDF/B-III scattering Law Library
vi) the ECN Neutron Dosimetry Cross Section Library DOSCROS
vii) the ECN Radiation Damage Cross Section Library DAMSIG

Within the Nuclear Data Service 20 requests ordered by 5 customers have been fulfilled by preparation of 28 data sets on magnetic tapes and 30 data sets in printed listings inclusively informative materials.
In 1985 a computer EC 1055 M could be put into operation at TU Dresden providing for further improvements of the technical basis for data storage, maintainance and updating as well as for data dissemination by the GDR internal data network in the nearest future.

The data base "Non Neutron Nuclear Data" at ZfI Leipzig had to serve 35 user request in 1985. The main progress is the installation of a modern information retrieval system ISIS (Unesco) for the storage and retrieval of charged particle nuclear data in the EXFOR - Format. The first experiences show, that ISIS allowes a fast and comfortable search. A special index file of all stored reactions (Charged Particle Data Index - CPDI) gives the possibility for choosing reactions according to target, incident particle or product. Reaction parameters and energy range are also included. This system is ready for a use via remote terminals. First tests will start in 1986.

NUCLEAR SPECTROSCOPY

MEAN LIFETIMES OF POSITIVE-PARITY STATES IN ^{79}Br

R. Schwengner, G. Winter, J. Döring, L. Funke and H. Rotter
Zentralinstitut für Kernforschung Rossendorf, Bereich KF

The in-beam study of ^{79}Br performed at the Rossendorf cyclotron revealed a sequence of positive-parity states on top of the $9/2^+$ isomeric state at 207.4 keV /1/.
The mean lifetimes of the $13/2^+$, $17/2^+$ and $21/2^+$ states have been determined by recoil-distance Doppler shift (RDDS) and Doppler shift attenuation (DSA) measurements performed in the (α,pn) reaction at a bombarding energy of 27 MeV. The target used in the RDDS measurement consisted of a 0.21 mg cm^{-2} layer of enriched ^{77}Se evaporated on a 0.5 mg cm^{-2} backing of aluminized polyesther. The stopper was made from the same material as the backing, and target-stopper distances from 0.016 to 5.0 mm were used in the experiment. Gamma-ray spectra were recorded by a Ge(Li) detector located at 25° with respect to the beam direction. In the DSA measurement a 5.0 mg cm^{-2} self-supporting foil of ^{77}Se was used as target and the gamma-rays were registered at angles of 25° and 155°.
The lifetimes were derived from a comparison of experimental with calculated lineshapes of the gamma-rays. The velocity distribution of the emitting nuclei was calculated by a Monte Carlo code that takes into account reactions in different depths of the target, the kinematics of the reaction as well as the slowing down and deflection of the recoils /2/. Examples of the lineshape analysis in the RDDS method are shown in figure 1. The lifetimes obtained from the present experiments are listed in table 1, which includes also the E2 transition probabilities derived. The B(E2) values indicate rather strong collectivity and prove the rotational character of the band built on the $g_{9/2}$ proton excitation.

References

/1/ Schwengner, R. et al., Gemeinsamer Jahresbericht 1984, ZfK-559 (1985) 28
/2/ Winter, G., ZfK Rossendorf report ZfK-497 (1983), Nucl. Instr. 214 (1983) 537

Table 1. Mean lifetimes and E2 transition probabilities

E_x/keV	I^π	E_γ/keV	τ/ps[1)]	Method	B(E2)/W.u.[2)]
797.0	$13/2^+$	589.4	17(3)	RDDS	34(6)
1732.4	$17/2^+$	935.4	2.5(5)	DSA	23(5)
2866.7	$21/2^+$	1133.3	0.8(2)	DSA	27(7)

[1)] The errors are given in units of the last decimal in parentheses. They include statistical errors, uncertainties of the nuclear and electronic stopping power and of the feeding times and intensities. Furthermore, uncertainties of the target thickness and the flight distance are taken into account in the RDDS method.
[2)] 1 W.u. = 20 e^2fm^4

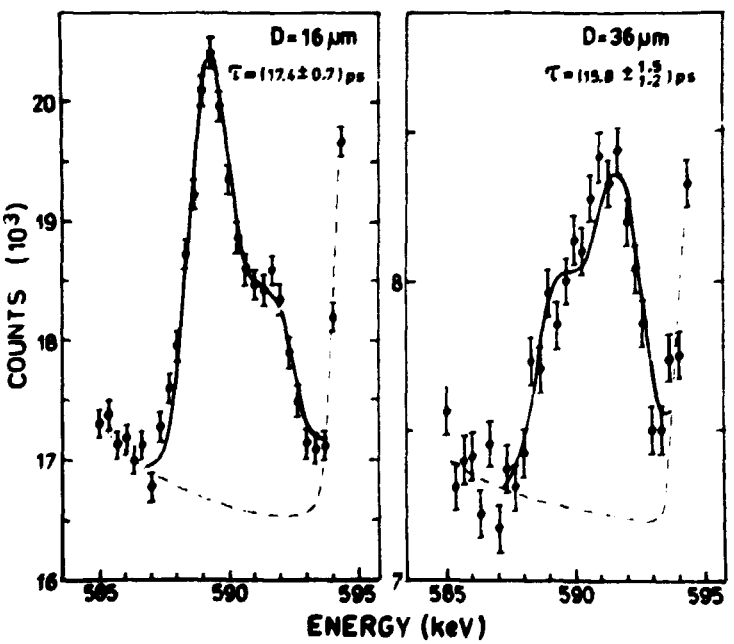

Figure 1. Lineshape analysis of the peak at 589.4 keV in the RDDS method for two different flight distances. The errors given are due to the fitting procedure only.

NEW ps - LIFETIMES AND ELECTROMAGNETIC TRANSITION PROBABILITIES IN ^{79}Kr

G. Winter, R. Schwengner, L. Funke and J. Döring
Zentralinstitut für Kernforschung Rossendorf Bereich KF

The investigation of yrast states in ^{79}Kr has been the subject of several experimental works (see the recent paper of Kajrys et al. /1/). Nevertheless, electromagnetic transition probabilities have only been determined /2/ for three E2 transitions connecting members of the positive-parity sequence and, very recently /3/, for some high-lying states of negative parity. In this laboratory a new in-beam study of ^{79}Kr was initiated in order to extend our knowledge on band crossing phenomena in the Kr isotopes to the nucleus ^{79}Kr. Preliminary results have been published previously /4/. An other important aim was to study the electromagnetic transition probabilities between members of the negative-parity level sequences.

Lifetime measurements have been carried out using the plunger method in connection with the (α,2n) reaction on ^{77}Se at a bombarding energy of 27 MeV. The experiments for the target to plunger distances D = 0, 21 and 42 μm have been performed in the $\gamma\gamma$-coincidence mode /5/ with the help of a new plunger chamber. Since the target backing and the plunger are made from the same material the distance D = 0 is obtained when the orientation of the plunger arrangement with respect to the beam direction is reversed.

Preliminary values for the lifetimes as deduced from these measurements are presented in table 1. The lifetimes were found by lineshape analysis of the spectra recorded at an observation angle of 24 $\pm$ 8 degrees /6/. Up to now, the cascade feeding was only approximately taken into account by assuming constant B(E2) values for the transitions within the two level sequences. An inspection of the reduced transition probabilities (table 1) reveals B(M1) values of about 40 or 10 W.U. for the transitions within the $1/2^-$ or $5/2^-$ sequence, respectively. These values are in accordance with the assignment of the $p_{1/2}$ or $f_{5/2}$ configurations to these sequences. The B(E2) values in the negative-parity sequences are of similar magnitude as found in the positive-parity sequence ($\approx$ 40 W.U.) where the values in the $1/2^-$ sequence might be slightly greater than in the $5/2^-$ sequence.

Table 1. Lifetimes and transition probabilities for transitions in ^{79}Kr.

E_{level} keV	E_γ keV	Branching %	Distance μm	$\tau_{eff.}$ ps	τ_{level} ps	$\tau_{adopted}$ ps	$\tau_{partial}$ ps	Multipolarity $\sigma\lambda$	$B(\sigma\lambda)$ [b] W.U.
402	402	52	42	57(6)	43(6)	42(6)	81(11)	E2	47(8/5)
	219	48	42	46(6)	40(6)		87(13)	M1	39(7/5) 10^{-3}
450	267	4.7					2130(350)	E2	14(3/3)
	302	67	42	120(20)	100(20)	100(20)	150(30)	M1	9(2/2) 10^{-3}
	320	28	42	100(15)	90(15)		360(70)	E1	5(1/1) 10^{-5}
695	293	33	21	12(3)	9(3)	9(3)	27(9)	M1	52(24/14) 10^{-3}
	512	66					13(5)	E2	88(40/16)
815	667	91	21	10(2)	8(2)	8(2)	9(2)	E2	34(10/6)
			42	10(2)	8(2)				
	365	9					89(13)	M1	8(2/1) 10^{-3}
1063	661	82	21	3(2/1)[a]	3(2/1)	3(2/1)	4(2/1)	E2	80(27/25)
	368	18					16(11/5)	M1	44(20/18) 10^{-3}
1172	722	94	21	5(1)	4(1)	4(1)	4(1)	E2	52(16/11)
	356	6					66(17)	M1	12(4/3) 10^{-3}

[a]) Lower limit estimated from DSAM. [b]) Errors are given in parenthesis in units of the last decimal. When asymmetric, the notation is (upper/lower) uncertainty.

References:

/1/ Kajrys, G., et al.; Phys. Rev. C27 (1983) 983
/2/ Panqueva, J., et al.; Nucl. Phys. A389 (1982) 424
/3/ Shovliev, U.Ju., et al.; Tesisi dokladov , Leningrad (1985) 66
/4/ Schwengner, R., et al.; Gemeinsamer Jahresbericht 1984 ZfK - 559 (1985) 29
/5/ Winter, G., Schulze, W., and Will, E.; this report p. 102
/6/ Winter, G., Freitag, M., and Schulze, W.; this report p. 93

SUBNANOSECOND ISOMERS IN ^{87}Y

L.K. Kostov, W. Andrejtscheff, L.G. Kostova and P. Petkov
Institute for Nuclear Research and Nuclear Energy Sofia Bulgaria

H. Prade, H. Rotter, L. Käubler and F. Stary
Zentralinstitut für Kernforschung Rossendorf Bereich KF

The level scheme of ^{87}Y has been studied in (p,2n) and (α,2n) reactions /1/. The γ-rays observed in the (α,2n) reaction are grouped into two distinct cascades with opposite parity and different decay patterns. The negative-parity states, which are interpreted /1/ as coupling of one $2p_{1/2}$ proton to $\nu(g_{9/2})^{-2}$ ^{86}Sr core levels, decay through dipole transitions. In the positive-parity cascade arising from the $\pi(g_{9/2})\ \nu(g_{9/2})^{-2}$ configuration the E2 transitions prevail. This fact has been expleined /1/ with a possible small quedrupole deformation at higher excitations of the $\pi(g_{9/2})\ \nu(g_{9/2})^{-2}$ configuration.

We have performed lifetime measurements in the $^{85}Rb(\alpha,2n)^{87}Y$ reaction with the γ - r.f. method /2/. For the first time the half-lives of the $17/2^-$ and $21/2^+$ levels have been measured:

$$T_{1/2}(17/2^-,\ 2675.9\ \text{keV}) = 0.2 \pm 0.1\ \text{ns},$$
$$T_{1/2}(21/2^+,\ 2827.1\ \text{keV}) = 0.8 \pm 0.2\ \text{ns}.$$

Further, the half-life of the 5^- state at 232.1 keV in ^{88}Y has been determined as $T_{1/2} = 0.8 \pm 0.2$ ns, in accordance with the value $T_{1/2} = 0.6\ ^{+0.3}_{-0.2}$ ns, obtained by Doppler shift measurements /3/.

For the 399.1 keV E2 transition, deexciting the $21/2^+$ level at 2827.1 keV we have derived the reduced transition rate $B(E2,\ 21/2^+ \rightarrow 17/2^+) = 7.1\times10^{-3}\ e^2b^2$ (3.1 W.u.). This value is of the same order of magnitude as the transition probability for the $21/2^+ \rightarrow 17/2^+$ transition in ^{91}Nb ($10.6\times10^{-3}\ e^2b^2$) and in ^{91}Zr ($11.1\times10^{-3}\ e^2b^2$) where the $21/2^+$ states are conconsidered as spherical configurations /4,5/. This analogy is an indication, that the positive-parity levels in ^{87}Y at least up to 21/2 can be considered as spherical shell-model states.

References:

/1/ Fields, C.A., et al.; Z. Phys. A295 (1980) 365
/2/ Schilling, K.D., et al.; Nucl. Phys. A265 (1976) 59
/3/ Brenner, M., et al.; USIP Report 74-17, may 1974
/4/ Fields, C.A., et al.;Nucl. Phys. A326 (1979) 55
/5/ Brown, R.A., et al.; Phys. Rev, C13 (1976) 1900

LIFETIME MEASUREMENTS IN $^{123,125}I$

L.G. Kostova, W. Andrejtscheff, L.K. Kostov and P. Petkov
Institute for Nuclear Research and Nuclear Energy Sofia Bulgaria

L. Käubler, H. Prade, H. Rotter and F. Stary
Zentralinstitut für Kernforschung Rossendorf Bereich KF

In-beam γ-ray investigations of the odd-mass I nuclei /1,2,3/ have revealed two collective features: $\Delta J=2$ bands, built on the $5/2^+$, $7/2^+$ and $11/2^-$ quasiproton states and $\Delta J=1$ bands, built on the $9/2^+$ proton-hole states. These features have been related with a different degree of deformation of the proton-hole and proton-particle configurations.

Excited states in $^{123,125}I$ have been populated using the α-beam of the Rossendorf cyclotron. Applying the generalized centroid shift method /4/ subnanosecond lifetimes have been measured. We have determined for the first time the half-lives of the $9/2^+$ and $11/2^-$ bandheads:

$$^{123}I: \quad T_{1/2}(9/2^+, 641.3 \text{ keV}) = 0.4 \pm 0.1 \text{ ns},$$
$$T_{1/2}(11/2^-, 943.5 \text{ keV}) = 0.2 \pm 0.1 \text{ ns};$$
$$^{125}I: \quad T_{1/2}(9/2^+, 935.8 \text{ keV}) = 0.2 \pm 0.1 \text{ ns},$$
$$T_{1/2}(11/2^-, 1084.9 \text{ keV}) \lesssim 0.2 \text{ ns}.$$

The $9/2^+$ bandheads in the lighter iodine isotopes are known to be also nanosecond isomers /1,2/.

Further results from our investigations are the half-lives of the states at 2350.6 keV and 2791.0 keV in ^{125}I, which amount to

$$T_{1/2} = 1.6 \pm 0.3 \text{ ns and}$$
$$T_{1/2} = 0.4 \pm 0.1 \text{ ns},$$

respectively. Spin and parity for these states have been only tentatively assigned /3/. The isomeric character of the states under discussion is an indication, that they are probably of three-quasiparticle type.

References:

/1/ Shroy, R.E., et al.; Phys. Rev. C26 (1982) 1089
/2/ Gai, M., et al.; Phys. Rev. C26 (1982) 1101
/3/ Hagemann, U., et al.; Nucl. Phys. A289 (1977) 292
/4/ Schilling, K.D., et al.; Nucl. Phys. A265 (1976) 59

THE MAGNETIC MOMENT OF THE 10^+ ISOMER IN ^{140}Ce AND TEMPERATURE DEPENDENCE OF THE PARAMAGNETISM FOR Ce IONS IN BaO

L. Käubler, H. Prade, W. Engehardt and F. Stary
Zentralinstitut für Kernforschung, Rossendorf, Bereich KF
P. Carlé, L.O. Norlin, K.-G. Rensfelt and U. Rosengard
Research Institute of Physics, Stockholm, Sweden

In the course of our investigations on N=82 nuclei the magnetic moment of the $J^{\pi} = 10^+$ isomer /1/ in ^{140}Ce has been measured with the (α,2n) reaction at the Rossendorf cyclotron (E_{α} = 27.0 MeV) and the Stockholm 225 cm cyclotron (E_{α} = 32.5 MeV). Some experimental details are given in table 1. The experimental arrangements are described in refs. /2,3/.

Both the assumption of the calculated paramagnetic correction Θ (T = 300 K) = 1.42 (ref. /4/) for Ce^{3+} ions used in experiment 1 (ref. /5/) and the extrapolation for T to infinity for experiments 1,2,3 (ref. /6/) resulted in uncorrect preliminary g-factors. Learning of the reduced paramagnetism in cerium /7/ we evaluated in experiments 4 and 5 the g-factor with an internal field calibration (table 1). Thus, the g-factor amounts to the averaged value $g_{exp}(10_1^+, {}^{140}Ce) = +1.03(4)$ and the magnetic moment to $\mu(10_1^+, {}^{140}Ce) = 10.3(4)\mu_N$.

The excellent agreement of the experimental value with the result of our shell model calculations /1/ $g_{th} = 1.01$ ($g_s^{eff} = 0.6\, g_s^{free}$) supports strongly the interpretation of the 10^+ isomer as a $(g_{7/2}^2, d_{5/2}^2)$-proton state. On the other hand the strong E1 transition $10_1^+ \rightarrow 9_1^-$ suggests small contributions of configurations outside the shell model approach used.

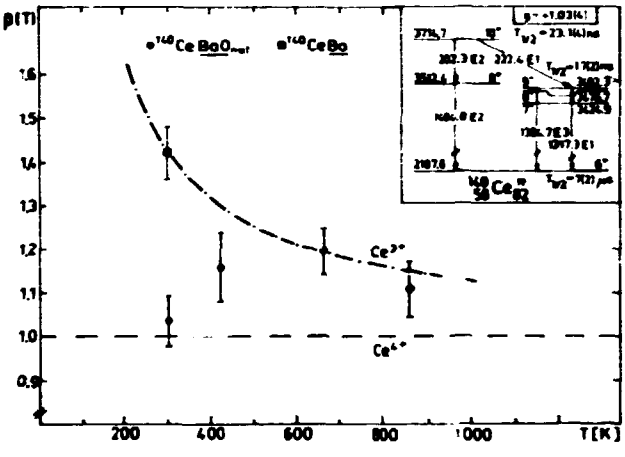

Fig. 1

Temperature dependence $\Theta(T)$ for ^{140}CeBaO and ^{140}CeBa. Dashed: Θ for the nonmagnetic Ce^{4+} ions, dashed-dotted: $\Theta(T)$ calculated /4/ for Ce^{3+} ions. The insert shows the relevant part of the level scheme /1/.

Table 1

Experimental results of the TDPAD-experiments

No.	Target	B_{ext}(T)	T(K)	ω_L (MHz)	$\Theta(T)$ [a]
1	BaO	2.527(4)	300	129(5)	1.04(6)
2	BaO	2.525(4)	423	144(8)	1.16(8)
3	BaO	2.526(4)	663	149(3)	1.20(5)
4[b]	BaO	2.234(1)	857	122(5)	1.11(6) 1.18(3)[c]
5	Ba	2.522(4)	300	177(3)	1.42(6) 1.34(4)[c]

[a] Calculated with $g(10^+) = 1.03(4)$, [b] Measured in Stockholm, [c] Field calibration by means of $g(19/2^-, {}^{139}Ce) = 0.420(6)$, ref. /8/

The measured value Θ (T = 300 K) for the system CeBa is in exact agreement with the calculation /4/ for Ce^{3+} ions. However, the temperature dependence $\Theta(T)$ for CeBaO exhibits a strange behaviour (fig. 1). Assuming the idea of mixed valence as in ref. /7/ the Ce ions might be at room temperature in a nonmagnetic tetravalent state, i.e. possibly at a Ba site. For $T \gtrsim 650$ K the $\Theta(T)$ values follow the temperature dependence of Ce^{3+} ions which possibly come to rest at an oxygen site. At 423 K a noninteger valence V(423 K) = 3.5(3) may be deduced giving rise to the suggestion of an interstitial.

References

/1/ Engehardt, W. et al., Nucl. Phys. A449 (1986) 417

/2/ Käubler, L. et al., ZfK-455 (1981) 1

/3/ Rensfelt, K.-G. et al., Phys. Scr. 14 (1976) 95

/4/ Günther, G., I. Lindgren: Perturbed Angular Correlations. Eds. E. Karlsson et al. Amsterdam: North-Holland 1964, p. 356

/5/ Käubler, L. et al., Book of Abstract of the Sixth Int. Conf. on Hyperfine Interactions, Groningen, The Netherlands, 1983, p. NP17

/6/ Käubler, L. et al., Gemeinsamer Jahresbericht 1984, ZfK-559 (1985) 31

/7/ Bertschat, H.H. et al., Solid State Commun. 47 (1983) 525

/8/ Barth, H.J. et al., Phys. Rev. Lett. 45 (1980) 1015

THEORY

HADRON YIELDS FROM THE DECAYING QUARK GLUON PLASMA

B. Kämpfer, H.W. Barz
Zentralinstitut für Kernforschung Rossendorf, Bereich KP
B. Lukács
Central Research Institute for Physics, Budapest, Hungary

One of the most intriguing prospects of relativistic heavy ion collisions is the possibility of exciting transiently a quark gluon plasma. The proposals of identifying this novel matter state concern pecularities in the ignition process, direct probes and final products of the decaying plasma. In the present note we analyse whether the final hadron yields might carry, via the chemical composition, some message being characteristic for the plasma source.

The redistribution of quarks into hadrons is obviously a complex process. One may expect that the final yields depend on three kinds of data: characteristics of the initial plasma state, those of the final hadronic state and the history of the phase transition. A relatively simple model is the combinatoric model [1] where the yields depend only on initial state characteristics (i.e. the corresponding quark-quark collisions), but not on the phase transition dynamics. Now, we propose a modified model, which takes into account the thermodynamical properties of the final state too. The old combinatoric model is proportional to all the number of quark constituents (collision probability) and to a channel factor too (distinguishing between e.g. meson and baryon formation). The quark numbers are given, and the channel factors can be determined from balance equations expressing, for example, the assumption that there is no annihilation or splitting of gluons into quark pairs. Then there are four such equations:

$$Q = K + \pi + 2Y + \Xi + 3N; \quad S = \bar{K} + \eta + Y + 2\Xi + 3\Omega \qquad (1)$$

+ conjugate equations for antiparticles,

where the letters stand for particle numbers of the indicated particles, and Y is a common name for Λ and Σ. These four equations can be satisfied by four channel factors in the generic case (here we choose a distinction between formation of mesons containing and not containing S quarks, and the same for baryons); because of symmetries in the original combinatoric model the number of different channel factors reduces to 2.

Now, one can assume that the probability of the appearance of a particular hadron as final state is proportional both to the initial probability (given by e.g. the combinatoric model) and to the number of microstates belonging to the particular hadronic final state. These statistical weight factors f_i can be calculated from thermodynamics [2], and in lowest order one finds

$$f_i = e^{-\frac{m_i}{T}}, \qquad (2)$$

where m_i stands for particle masses and T denotes the final temperature. Results for an isothermal transition are displayed in fig. 1 for two values of the temperature T. The relative yields of the dominant components are similar to the predictions of Ref. [1], however, the rare hadrons are now suppressed due to their large masses. Our predictions for the ratios $\bar{Y}/Y$ and $\bar{K}/K$ are in the same order of the magnitude as in the nuclear fireball model, thus these ratios are not useful as plasma signals. A possible extension of our present model should take into account another possibilities of the freez-out regime, the redistribution of energy stored in the gluons and the vacuum by creating quark pairs.

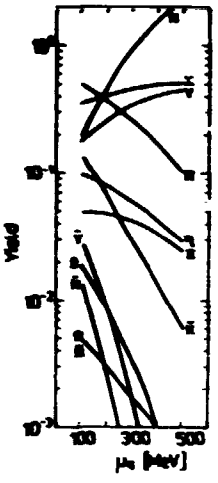

Fig.1. Unnormalized hadron yields versus plasma chemical potential at freeze-out, for a hadronic temperature of 150 MeV.

References

[1] T.S. Biró and J. Zimányi, Nucl.Phys. A395(1983)525
[2] B. Kämpfer et al., KFKI-report KFKI-1985-65

CASCADE-MODEL STUDIES OF LAMBDA-PARTICLE PRODUCTION IN THE CARBON ON TANTALUM REACTION AT DUBNA ENERGIES

H. W. Barz and H. Iwe
Zentralinstitut für Kernforschung Rossendorf, Bereich KF

At the Dubna synchrophasotron the production of Λ particles was investigated in the reaction C on Ta at a bomberding energy of E/A=3.36 GeV[1]. We have analysed this experiment using our intranuclear cascade code CASIMIR. This code models the interaction process of heavy ions as a sequence of binary collisions of freely moving hadrons. The production of Λ particles proceeds via either direct nucleon-nucleon encounters or else via secondary pion-nucleon encounters. Mean field effects are neglected. In fig.1 we show the contour lines for the invariant differential cross section $d^2\sigma/dy\,dp_\perp$ in the rapidity(y)- $p_\perp$ plane together with the rapidity distribution $d\sigma/dy$ and the $p_\perp$ distribution $d\sigma/dp_\perp$. A satisfactory agreement with the measurements is attained, although the average rapidity ($\langle y\rangle$ =0.7, $\langle y_{exp}\rangle$ =0.58±0.07) and transverse momentum($\langle p_\perp\rangle$ =0.50, $\langle p_{\perp exp}\rangle$ =0.43±0.05 GeV) are slightly overestimated. The analysis reveals further that the NN as well as the πN encounters give an important contribution to the Λ production and one third of the Λ's stem from the Σ^0 decay.

All in all, we have found that the mechanism of strange particle production in hadron-hadron cascades is equally well applicable in the energy domain of 3-4 GeV per nucleon. Obvious hints for a possible occurence of a new phenomenon could not be found.

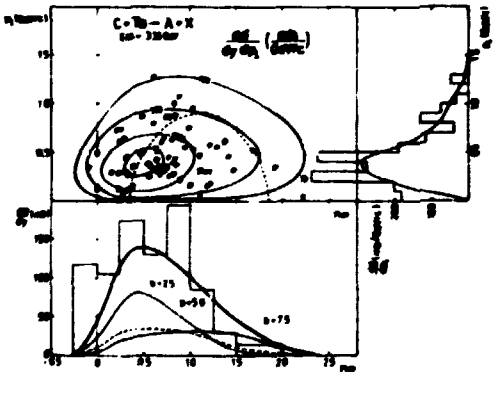

Fig.1. Invariant cross sections for Λ production compared to experiment [1](dots and histograms)

Reference

[1] K.Iovchev et al., Dubna report P1-84-279 (1984)

POPULATION OF HYPERNUCLEAR STATES VIA NUCLEON DECAY CHANNELS

R. Wünsch
Zentralinstitut für Kernforschung Rossendorf, Bereich KF

L. Majling and J. Žofka
Institute for Nuclear Research Řež near Prague, ČSSR

Using our continuum shell-model code we have calculated the emission probability of baryons (nucleons and Λ hyperons) from hypernuclear substitutional states produced in (K^-,π^-) strangeness transfer reactions at small momentum transfer. The calculated appreciable probability for reaching a hyperfragment with mass number A-1 offers a new possibility of producing hypernuclei in non-substitutional configurations which are of great interest for hypernuclear spectroscopy.

Fig. 1 shows the calculated /1/ relative partial decay widths of the $^{14}_{\Lambda}C$ substitutional states which dominate the $^{14}C(K^-,\pi^-)$ excitation spectrum. The two lower states populate mainly the low-lying hypernuclear states of $^{13}_{\Lambda}C$. The hyperon emission probability of the second state amounts to only 23 per cent, while the first state lies below the corresponding threshold. The state at 25 MeV populates high-lying states of $^{13}_{\Lambda}C$ and the ground state of $^{13}_{\Lambda}B$ with isospin T=1. The decay to the low-lying T=0 hypernuclear states of $^{13}_{\Lambda}C$ and to the T=1/2 states of ^{13}C is isospin forbidden. The small decay probability of 0.1 per cent to the ground state of ^{13}C demonstrates the accuracy of the isospin selection rule in light hypernuclei.

All the hypernuclear levels populated in fig. 1 are not accessible in the (K^-,π^-) reaction on the corresponding A=13 target.

A similar calculation has been performed for the $^{14}_{\Lambda}N$ hypernucleus.

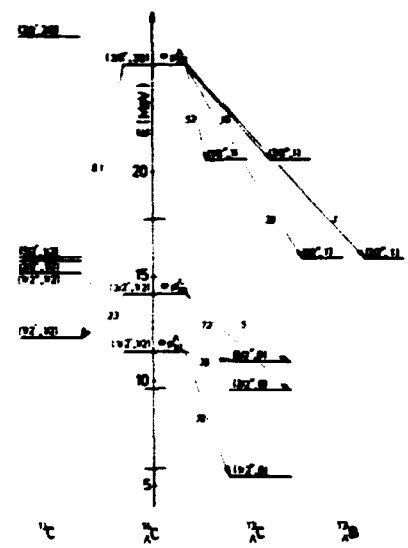

Fig. 1
Calculated level schema and partial decay widths (in per cent) of the $^{14}_{\Lambda}C$ hypernucleus.

/1/ R. Wünsch, L. Majling and J. Žofka, Proc. III. Int. Conf. on Mesons and Light Nuclei, Bechyně, 1985; Czech. J. Phys. B27 (1986)

/2/ R. Wünsch, L. Majling and J. Žofka, Proc. Int. Conf. on Hypernuclear and Kaon Physics, Brookhaven, 1985

ELECTROMAGNETIC RADIATION OF ROTATING NUCLEI

F. Dönau

Zentralinstitut für Kernforschung, Rossendorf, Bereich KF

Basing on the well-known concept of the rotor plus particle coupling an intrinsic representation of the radiative multipole operators is derived /1/ which enables one to calculate directly electromagnetic transition amplitudes with Cranking states. In this way both the orientation of the intrinsic system in space and the structure of the quasiparticles can be properly taken into account. This method is then applied to M1 and E2 properties of a high-j one-quasiparticle orbital treated in Cranking approximation and it is compared to the results of an equivalent rotor plus particle model. In considering the case of multi-quasiparticle configurations one can establish the semi-classical vector coupling scheme which has been successful in describing M1 enhancement effects as observed in several experiments (cf. ref. /2/).

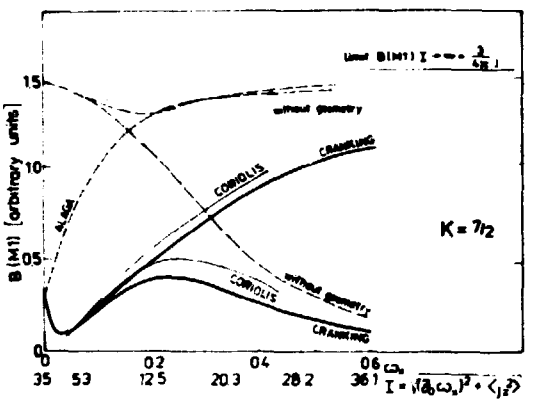

Fig. 1

B(M1) values for a j = 13/2 quasiparticle as a function of the transitional frequency ω_x placing the Fermi level at K = 7/2. For comparison the respective spin value I is given at the abscissa. For simplicity the gyromagnetic factor is chosen to be g = 1. The rotor calculation ("Coriolis") is performed using the rotational parameter A = 8.33 keV. The Alaga value is obtained by taking $K(\omega_x)$ = constant (7/2) and neglecting all K-mixing. The dashed curve "without geometry" is calculated with Cranking states but taking not care of the actual orientation of the intrinsic system in lab space. The branching corresponds to the different transitions I → I-1 and I → I+1, respectively.

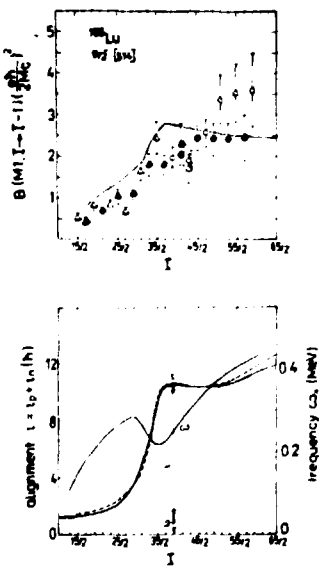

Fig. 2

Frequency ω_x, alignment $i = i_p + i_n$ and B(M1) values as a function of the spin I for the band 9/2 [514] in ^{165}Lu ref. /2/. The theory (full line) is compared to the experimental B(M1) values (triangles) as obtained by assumming a constant intrinsic quadrupole moment /2/ for this band.

References

/1/ Dönau, F., NBI-85-36 (1985)

/2/ Johnson, S. et al., Nucl. Phys. A442 (1984) 397

Critical Behaviour Of Collective Fluctuations

A. Pfitzner

Zentralinstitut für Kernforschung Rossendorf, Bereich KF

During the contact phase of a low-energy heavy-ion collision the mutual influence of collective and intrinsic motion shows specific features. A consistent treatment requines to consider not only the mean field, but also the impact of collective fluctuations on the intrinsic evolution [1]. Especially the feed-back of the coupling between collective and intrinsec motion on the collective potential, showing up in a renormalization of the stiffness, is decisive for the asymptotic behaviour of the collective variances [2], in contrast to a statement made in [3].

The master equation for the single-particle occupation numbers ϱ_α [1] is approximated by a relaxation equ. [2], specified by an equilibration time τ_{eq} and a (fermi-like) equilibrium distribution with diffuseness β^{-1} It forms together with the equation for the variance $\chi(t) = \langle \delta R^2 \rangle_t$,

$$\dddot{\chi} + 3\gamma\ddot{\chi} + (\gamma^2 + 2\eta^2)\dot{\chi} + 4\gamma\eta^2\chi = \frac{4\gamma}{\mu}(D/\mu\gamma + d), \qquad (1)$$

a coupled system which is highly non-linear because τ_{eq} and β^{-1} depend on the variances, and the transport coefficients γ, D, d as well as the renormalized stiffness $\eta^2 = \Omega^2 - \varkappa^2$ depend on ϱ_α (Ω^2 is the original stiffness). For $\eta^2 > 0$ we obtain damped, for $\eta^2 < 0$ exponentially increasing solutions of (1). In the critical point $\eta^2 = 0$ the asymptotic solution increases linearly with time. To estimate the influence of this different behaviour on the intrinsic evolution, we calculate the transport coefficients microscopically in a schematic model [2], using smoothed step functions for the occupation numbers characterized by a small parameter β_0^{-1}, and consider the dependence of τ_{eq} and β^{-1} on $\gamma_0 \equiv \gamma\tau^* = g^2|F|^2\pi/\mu$. Here, g is the level-density parameter, $|F|^2$ the coupling strength, μ the reduced mass and $z = \Omega^2\tau^{*2}$ (τ^* is the memory time). For $\eta^2 > 0$ we find asymptotically ($t \gg 1/\gamma$) values independent of time and of the initial variances $\chi(0)$ and $\varphi(0) = \langle \delta P^2 \rangle_{t=0}$, and a dependence on the coupling strength like $\tau_{eq} \propto 1/\gamma_0$. At variance to this we obtain for $\eta^2 = 0$ asymptotically

$$\beta^{-1}(t) = \frac{\mu}{\tau^{*2}} z_{cr}\chi(0) + \frac{{}_1F_1(-\frac{1}{2},\frac{1}{2},z_{cr})^2}{\pi z_{cr}}\left(\frac{\varphi(0)}{\mu} - \beta_0^{-1}\left[1 + \frac{1}{12}\frac{z_{cr}}{(\tau^*\beta_0^{-1})^2}\right]\right) + \frac{2}{\sqrt{\pi}} e^{z_{cr}} \beta_0^{-1} \frac{t}{\tau^*}, \qquad (2)$$

and $\tau_{eq} = g\,{}_1F_1(-\frac{1}{2},\frac{1}{2},z_{cr}) / \sqrt{\pi}\,\tau^*\beta^{-1}(t)$. Here, ${}_1F_1$ is a degenerated hypergeometrical function, and the critical stiffness z_{cr} results from the condition $\eta^2 = 0$, which reads

$$\sqrt{\pi}\, z_{cr}\, e^{z_{cr}} = \gamma_0\tau^*\, {}_1F_1(-\tfrac{1}{2},\tfrac{1}{2},z_{cr}). \qquad (3)$$

Equ. (3) establishes a unique relation between z_{cr} and γ_0, i. e. for a given system the ratio of a typical intrinsic time τ^* to a typical collective time $\tau_{coll} = 1/\Omega$ determines the coupling strength $|F|^2$. This changes the dependence of β^{-1} and τ_{eq} on γ_0 essentially: fig. 1 showes a remarkable increase of β^{-1} and a faster decrease of τ_{eq} with increasing coupling strength. We conclude that collective fluctuations may act like an equilibration mechanism which is most operative at the critical point.

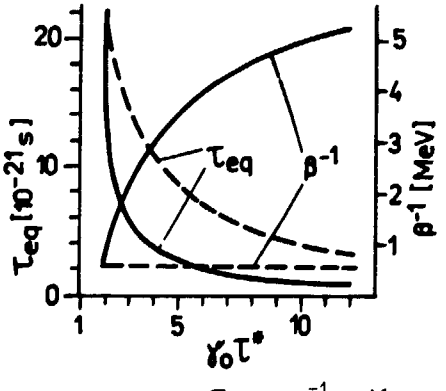

Fig. 1: Dependence of τ_{eq} and β^{-1} on γ_0
dashed curves : $\eta^2 > 0$, solid curves: $\eta^2 = 0$
$g = \frac{A}{10}\,\mathrm{MeV}^{-1}$, $A = 100$, $\tau^* = 10^{-22}$ s
$t = 10\tau^*$, $\beta_0^{-1} = 0.1$ MeV
$\chi(0) = 0.09\ \mathrm{fm}^2$, $\varphi(0) = (\frac{\hbar}{2})^2/\chi(0)$.

References

[1] L. Münchow, A. Pfitzner, Z. Phys. A 314(1983) 97
[2] A. Pfitzner, L. Münchow, to be published
[3] R. W. Hasse, Nucl. Phys. A 318 (1979) 480

TARGET-MASS DEPENDENCE OF PREEQUILIBRIUM NEUTRON YIELDS IN HEAVY ION COLLISIONS

P. Mädler
Vereinigtes Institut für Kernforschung Dubna, Laboratorium für Theoretische Physik

Recently, at the JINR, Dubna, inclusive double-differential cross sections for neutron emission have been measured for the $^{12}C + {}^{12}C$, ^{27}Al, ^{56}Fe, $^{114,124}Sn$, ^{181}Ta, ^{238}U reactions at 105 MeV incident energy [1] . As in a similar series of experiments for light charged particle emission [2] the target-mass dependence of fast neutron yields appears to be weak.

To analyze the data we have applied the two-stage model (TSM) for fast particle emission [3] taking into account the realistic neutron binding energies Bn of the colliding ions [1] (instead of Bn = 8 MeV as in [3]) that decrease monotonically in the given series of target nuclei from 18.7 to 6.1 MeV. Without changing the standard parameters [3] , a good description of the absolute double-differential cross sections could be obtained despite the comparably low incident energy.

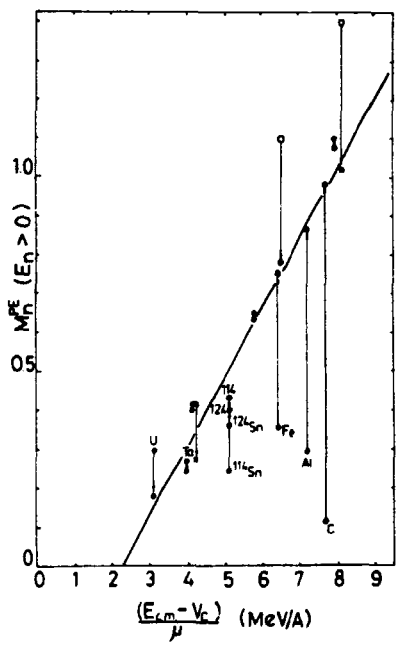

Fig. 1.
Total preequilibrium neutron yields for the present series of reactions. For details, see text. The open symbols belong to other reactions discussed in [1] .

In Fig. 1 the calculated total neutron preequilibrium yields are shown as a function of the energy/nucleon above the Coulomb barrier (μ -reduced mass number) both for realistic Bn (full circles) and for Bn = 8 MeV (asterisks connected by a thin line with the corresponding full circles). Note that while Bn strongly increases from left to right, the energy/nucleon above the barrier strongly increases too. Hence, the weak target-mass dependence (full circles) turns out to be a result of the compensation of two tendencies, and the conclusion of [2] that the target acts as a spectator and the process is a peripheral one seems to be oversimplified.

The Bn = 8 MeV calculations (asterisks) reproduce the known [4] linear energy dependence for a given system for which we have shown [1] that the influence of the actual binding energyies (compared to 8 MeV) decreases exponentially with increasing energy. Thus, in the intermediate energy domain the TSM can be applied in its original form [3] while at lower energies the individuality of the ions should additionally be characterized by their realistic binding energy.

The present interpretation provides a qualitative understanding of the strong correlation of fast α -particle yields with the α -particle binding energy in the target nucleus that have been observed for the reactions $^{22}Ne + {}^{159}Tb$, ^{197}Au, ^{181}Ta, ^{232}Th at 178 MeV incident energy [5] .

R e f e r e n c e s

[1] Kozulin, E.M., et al.; submitted to Z. Phys. A
[2] Pulmer, C.B., et al.; Phys.Lett. 100B (1981) 305
[3] Biedermann, M., and Mädler, P.; Preprint JINR E7-85-575 (1985), to appear in Z.Phys. A323 (1986)
[4] Holub, E., et al.; Phys. Rev. C28 (1983) 252
[5] Borcea, C., et al.; Nucl.Phys. A351 (1981) 312

INCIDENT-ENERGY AND PROJECTILE-MASS DEPENDENCE OF PREEQUILIBRIUM NEUTRON YIELDS IN HEAVY ION REACTIONS

M. Biedermann
TU Dresden, Sektion Physik, Wissenschaftsbereich Theoretische Physik
P. Mädler
Vereinigtes Institut für Kernforschung, Dubna, Laboratorium für Theoretische Physik

In the two-stage model for fast particle emission (TSM) [1] two physically distinct approaches have been combined: In the early stage we calculate particle emission in the spirit of the model of "prompt emitted particles" (PEP) [2]. In the later stage, after vanishing of the single-particle potential wall between the ions, particles are assumed to be emitted from a rapidly expanding hot zone (HZ) of appreciably large dimensions, which is strongly anisotropic in momentum space. The initial radius of the HZ we fix in accordance with recent results on the extraction of source radii from two-perticle correlation measurements. The radial velocity of the effective temperature front of the HZ is assumed to be o.2 c (sound velocity).

We have compared TSM calculations [1] with experimental results [3] on neutron emission in coincidence with evaporation residue for the $^{20}Ne+^{165}Ho$ reaction (Fig. 1). Obviously, at both incident energies, the model which does not contain any free parameter well accounts for shapes and absolute values of the high-energy tails of the neutron spectra.

In Fig. 2 the projectile-mass dependence of the TSM model predictions of the total cross section for fast neutron emission ($E_n > 12$ MeV) is compared to a few existing experimental values (taken from [4]). Here the target nucleus as well as the incident energy /nucleon above the Coulomb barrier are fixed. It is seen that the TSM quantitatively reproduces the strong increase of fast neutron yields with the projectile mass number - opposite to pure PEP calculations [1] which are also shown in Fig. 2. A slight underestimation of the experimental points for ^{12}C and ^{20}Ne projectiles is due to a certain contamination by evaporation of neutrons at $E_n > 12$ MeV which is not present in the calculations. The investigation of neutron emission for heavy projectiles at similar energies would be a further proof of the TSM.

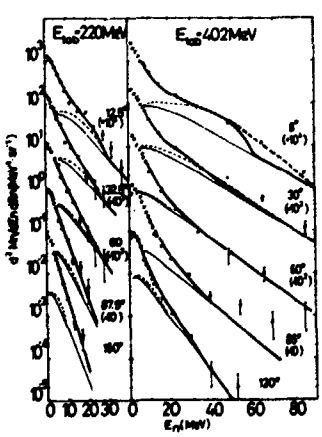

Fig. 1

Double-differential neutron multiplicities for the $^{20}Ne + ^{165}Ho$ reaction. Thin full lines: HZ contribution. Thin dashed lines: HZ + PEP contributions. Heavy full lines: TSM + evaporation. Heavy dashed line: TSM + evaporation, if a finite temperature is u used in the PEP calculations [1].

References

[1] Biedermann, M. and Mädler, P.; report JINR E7-85-575, to appear in Z. Phys. A323 (1986)

[2] Bondorf, J.P.,et al.; Nucl.Phys. A333 (1980) 285

[3] Holub, E., et al.; Phys. Rev. C28 (1983) 252

[4] Kozulin, E.M., et al.; report JINR P7-85-31 (1985)

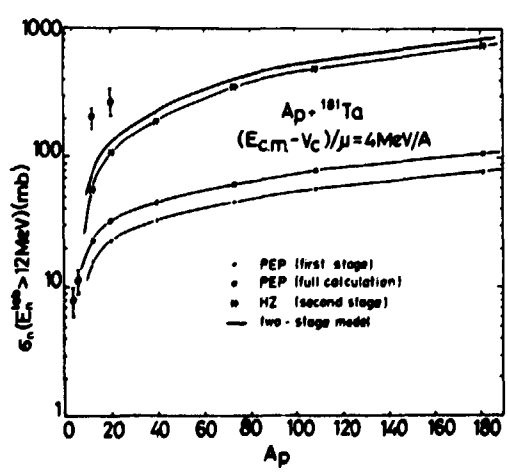

Fig. 2

COUPLING BETWEEN ENERGY- AND MASS-EQUILIBRATION IN HIC

R. Schmidt
TU Dresden, Sektion Physik, Wissenschaftsbereich Theoretische Physik

We continued and completed the analysis of the mass drift in heavy-ion collisions (HIC) within a modified diffusion model (MDM) [1].

Within the MDM the initial excitation and transfer of nucleons are calculated microscopically within the mean free path limit based on TDHF-physics. During the equilibration of the intrinsic energy nucleons are preferrentially transferred from the light to the heavy fragment until a common temperature has been established. The nucleon exchange during the joining transport stage is treated within a diffusion model with modified initial conditions for the mean value of the mass-asymmetry taking into account the net mass exchange during the previous stages of the collision. The application of this concept to HIC within a broad range of initial mass-asymmetries ($A_P/A_T \approx 1/10 \ldots 1/2$), total masses ($A_P+A_T \approx 80 \ldots 250$) and incident energies ($E/A \approx 4$ MeV/N ... 20 MeV/N) allows a consistent interpretation of rather different phenomena of the mass transport observed experimentally (see fig.). Partial lack of mass drift (Kr + Er), total lack of mass drift (Ar + Mo), drift against the static driving force (Ne + Cu) and vanishing production cross section for elements heavier than the projectile (Ne + Au) are explained on a common basis in terms of a continuous evolution mainly generated by the $(A_P-A_T \,/\, A_P+A_T)$-dependence of the number of exchanged particles prior to the transport stage.

The analysis of experimental data within the MDM strongly suggests that energy- and mass-equilibration in HIC are coupled. Thus, in any microscopic theory of the equilibration process of intrinsic energy in HIC the mass asymmetry degree of freedom should be taken into account. It is expected that the inclusion of this degree of freedom may also influence considerably the equilibration times.

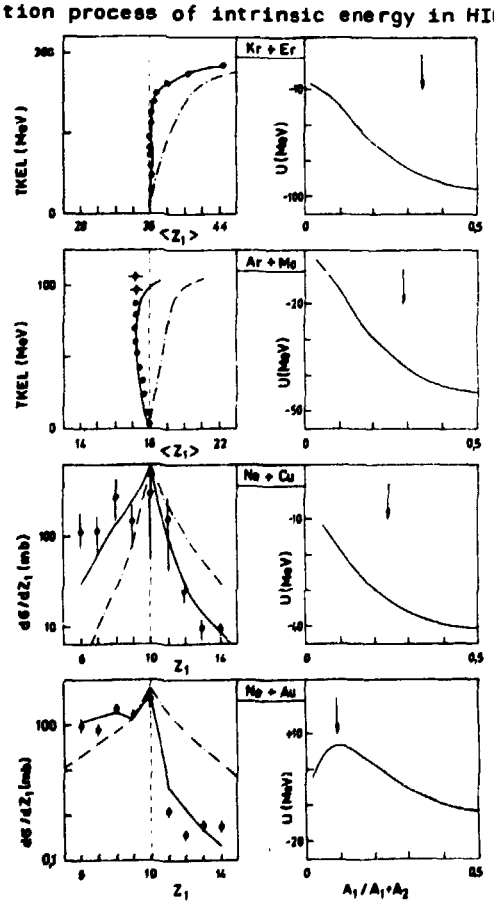

References
[1] Schmidt,R.; Nucl.Phys. A445 (1985) 534
[2] Schmidt,R.,et al.; Nucl.Phys.A311 (1978) 247
[3] Rudolf,G.,et al.; Nucl.Phys. A330 (1979) 243
[4] Bohne,W., et al.; Z. Phys. A313 (1983) 19
[5] Mathews,G.J.,et al.;Phys.Rev.C25 (1982) 300

Left: Exp. correlation TKEL($\langle Z_1 \rangle$) and charge distributions $d\sigma/dZ_1$ (dark points) for different HIC [3 - 5]. Dash-dotted lines: theoretical predictions of a standard diffusion model [2]. Solid lines: theoretical calculations within the MDM.

Right: Calculated driving potentials for representative partial waves, arrows indicate the target-projectile combinations.

A SIMPLE MODEL TO APPROXIMATE TDHF RESULTS ON FAST PARTICLE EMISSION

M. Biedermann
TU Dresden, Sektion Physik, Wissenschaftsbereich Theoretische Physik
P. Mädler
Vereinigtes Institut für Kernforschung, Dubna, Laboratorium für Theoretische Physik

In [1,2] it has been demonstrated that TDHF calculations in slab geometry well compare with numerically stable realistic TDHF evolutions for central collisions if integral characteristics of fast nucleon emission are concerned. This is because fast particle emission in TDHF occurs preferentially along the collision axis, while on the corresponding short time scale ($1...2\cdot10^{-22}$s) the transverse dynamics is of minor importance. Despite this, even in slab geometry large numbers of numerically stable calculations for particle emission require very large computer times [1,2].

We have investigated a seemingly extremely oversimplified model and compared to corresponding TDHF calculations for fast particle emission: The self-consistent mean-field of nuclear slabs we approximate by rectangular potential wells of depth V_o=-50.4 MeV. This value corresponds to the saturation density for the simplified Skyrme force used in [1,2]. The initial conditions are fixed as in the TDHF initial value problem. The trajectory of the "slabs" is replaced by a sudden release of the potential wall between the "slabs" at contact. The continuum of the composite system we have discretisized in a sufficiently large numerical box. Repeating systematically the TDHF calculations of [2] we have obtained surprisingly good results [3]:

i) The density evolution of the orbital initially representing the projectile slab in a A_1=0.2 fm^{-2} + A_2=2.0 fm^{-2}, $(E/A)_{Lab}$=5 MeV collision (Fig.1) is very close to the corresponding TDHF evolution (Fig.1 of [2]) outside the potential well (emitted particles). Differences for the corresponding densities inside the composite slab are due to a different reflection behaviour at the sharp/ diffuse edges.

ii) The percentage of emitted nucleons A/A (Figs.2 and 4 in [2]) are somewhat larger than in TDHF but come closer to them with increasing energy. For example, for a A_1= A_2=2.0 fm^{-2}, $(E/A)_{Lab}$=5 MeV collision our values exceed the TDHF value by a factor of 2.1.

iii) Except extremely small ($A \lesssim 0.4$ fm^{-2}) slabs the "slab mass table" is very similar to the HF mass table (Fig.3 in [2]).

In the present case no numerical iteration of the one-particle Schrödinger equation is needed: The density $\rho(z,t)$ is analytically expressed in terms of the energies of bound and discrete continuum states of the composite system.

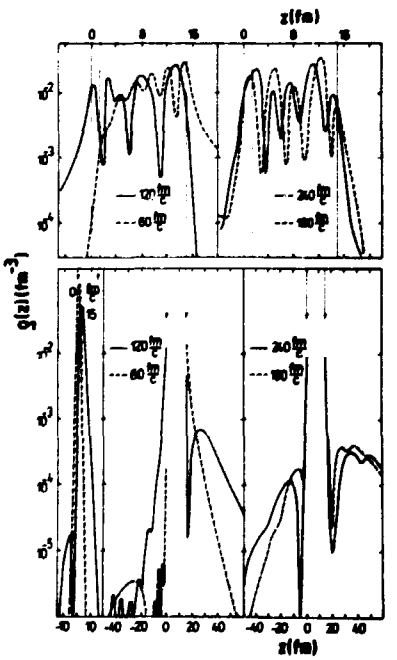

Fig. 1
Density evolution of the projectile wave packet outside (lower part) and inside (upper part) of the potential well of the composite system (indicated by arrows or vertical thin lines).

R e f e r e n c e s :
[1] Mädler, P.; Z.Phys.A318 (1984) 87
[2] Mädler, P.; JINR Communication E7-84-690 (1984)
[3] Biedermann, M., and Mädler, P.; in preparation

AZIMUTHAL CORRELATIONS BETWEEN TWO FAST PARTICLES WITHIN THE TWO-STAGE MODEL

M. Biedermann
TU Dresden, Sektion Physik, Wissenschaftsbereich Theoretische Physik
P. Mädler
Vereinigtes Institut für Kernforschung Dubna, Laboratorium für Theoretische Physik

The parameter-free two-stage model (TSM) for fast particle emission [1] is very succesful in describing single particle inclusive cross sections. The comparison of TSM predictions with more exclusive measurements should be a further fact for the validity of the model. Therefore, for the $^{20}Ne + ^{165}Ho$, E_{lab} = 402 MeV, reaction, we have calculated azimuthal correlations between two fast neutrons ($E_n \geq 30$ MeV) at fixed angles relative to the beam axis ($\Theta_x = 50^o$, $\Theta_y = 70^o$). Fig. 1 illustrates the calculated ratio of the coincidence cross section divided by the singles cross sections $\sigma_{xy} / \sigma_x \sigma_y$ as a function of the azimuthal angle ϕ. Here $\phi = 0^o$ / 180° corresponds to the emission of two neutrons to equal (opposite sides of the beam axis. The calculation clearly demonstrates that emission in one plane with the beam is favoured. This is in agreement with experimental results for the ^{197}Au (^{16}O, pp), E_{lab} = 400 MeV reaction with a low energy threshold $E_p \geq 36$ MeV at similar proton angles relative to the beam axis ($\Theta_x = 40^o$, $\Theta_y = 70^o$) [2]. Although different systems and ejectiles are concerned, for qualitative comparison, the experimental points from [2] are also shown in Fig. 1. Since ratios of cross sections are considered and low-energy ejectiles (neutrons) are excluded in the calculations, we claim that such a comparison makes some sense. A semiquantitative comparison of our results with the experimental points shows a slight overestimation of emission of two fast particles to the same side of the beam axis ($\phi = 0^o$). Possibly this is a consequence of the neglect of recoil effects, which (although of minor influence for heavy targets) strongly favour emission to opposite sides of the beam in the case of light systems [2]. Calculations for proton-proton correlations and direct quantitative comparisons with corresponding experiments are in progress [3].

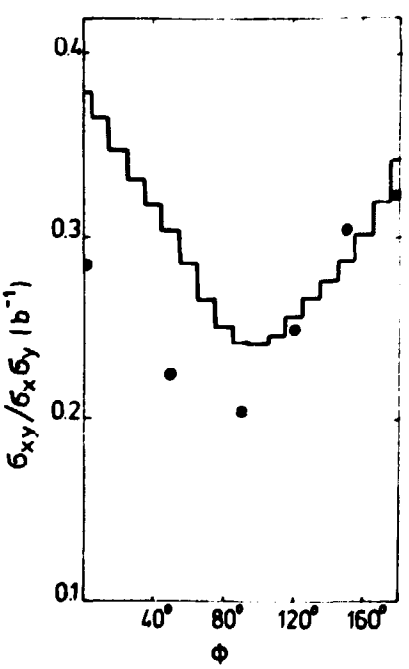

Fig. 1

References

[1] Biedermann, M., and Mädler, P.; report JINR E7-85-575 (1985), to appear in Z. Physik A 323 (1986)
[2] Tsang, M.B., et al.; Phys. Letters 148 B (1984) 265
[3] Biedermann, M., and Mädler, P.; in preparation

COMPARISON OF THE TWO-STAGE MODEL FOR FAST PARTICLE EMISSION WITH HOT-SOURCE PARAMETRIZATIONS

M. Biedermann
TU Dresden, Sektion Physik, Wissenschaftsbereich, Theoretische Physik

P. Mädler
Vereinigtes Institut für Kernforschung, Dubna, Laboratorium für Theoretische Physik

Inclusive data on fast particle emission are well reproduced if assuming isotropic emission from a moving hot source (MHS)[1] . The fit parameters of this model (temperature and velocity of the source, and an overall normalization factor) are smoothly varying functions of the incident energy.

The parameter-free two-stage model (TSM) for fast particle emission[2] provides a dynamical understanding of the MHS model and allows one to calculate time and impact-parameter avaraged effective source parameters:

i) The mean-velocity field introduced in the TSM to characterize the anisotropy of the nucleonic momentum distribution in the expanding hot zone (HZ) includes velocity components from the velocity of the target up to the projectile velocity. As a consequence, calculated effective source velocities are close to half the beam velocity above the Coulomb barrier (as in the MHS model).

ii) The calculated effective source temperatures are close to the MHS fit values.

iii) The calculated effective nucleon number in the source are close to the MHS fit values (slightly larger than twice the projectile mass number for asymmetric systems).

Furthermore, the (angle dependent) effective temperatures which result from the "rotating hot spot" parametrization (RHS)[1] are grouped around the calculated TSM values.

For example, for the $^{12}C + ^{181}Ta$, E = 105 MeV reaction the TSM yields an effective temperature of 3.8 MeV compared to 4.3 MeV (MHS,[3]) and valves ranging from 3.7 to 4.7 MeV (RHS,[3]). For the effective nucleon number, the TSM yields 27 compared to 24 (MHS,[3]). Since in the TSM translational as well as rotational motion of the HZ are incorporated in a natural way, the good agreement with the MHS and RHS fits is not surprising. Slightly larger temperatures from the MHS fit and from the RHS fit at forward angles are due to the fact that the TSM besides HZ emission includes also a certain amount of non statistical (PEP) emission which does not enter the calculated effective source values but implicitly influences the MHS/RHS fits of the total fast particle cross sections.

An extrapolation of the TSM to higher bombarding energies naturally leads to the expectation of a mid-rapidity high-temperature, a projectile-rapidity intermediate-temperature, and a target-rapidity low-temperature effective source[2] . The temperature hierarchy of these three sources is expected to increase with incident energy. This is exactly what has been observed for the $^{12}C+^{58}Ni \rightarrow p + X$ reaction[4] , where the fitted temperatures are 4.2/5.5/7.7 MeV at 25 MeV/A and 6.7/10.2/19.2 MeV at 84 MeV/A.

R e f e r e n c e s :

[1] Awes, T.C., et al.; Phys.Rev. C24 (1981) 89

[2] Biedermann, M., and Mädler, P.; Preprint JINR E7-85-575 (1985), to appear in Z.Phys. A323 (1986)

[3] Kozulin, E.M., et al.; Preprint JINR P7-85-31 (1985)

[4] Glasow, R., et al.; Proc. Workshop on Coincident Particle Emission from Continuum States, Bad Honnef, 1984, eds. Machner, H., and Jahn, P. (World Scientific, Singapore, 1984) p. 299

POLAR PARTICLE EMISSION IN SPONTANEOUS FISSION

B. Milek and R. Reif
TU Dresden, Sektion Physik, Wissenschaftsbereich Theoretische Physik
J. Revai
Central Research Institute for Physics, Budapest, Hungary

Emission and transfer of nucleons in heavy-ion collisions may be investigated by modelling the reaction dynamics as a particle in the field of two single-term separable potentials moving uniformly along straight-line trajectories. For this case in a Fadeev-like formulation the probabilities for the elastic, transfer, and breakup channel have been calculated in dependence on the basic reaction parameters [1, 2].

This three-body model for the dynamics of heavy-ion collisions has been extended to simulate spontaneous fission. As an initial state two spherical mean fields, approximated as one-term separable potentials, have been located at a certain separation distance, with a neutron as a third particle being bound by 8 MeV with a two-center wave function, which goes asymptotically to two 1s-states in the separated wells. For a given trajectory for the relative motion of the fragments during the fission process, the single particle wave function is followed in time by solving the corresponding time-dependent Schrödinger equation. From the asymptotic wave function the escape probability can be calculated in dependence of the non-adiabatic features of the fission dynamics implied in the chosen trajectory. First calculations for ^{252}Cf, s.f. indicate the following results, rather independent from the details of the trajectory in the overlap region:

(1) The total emission probability is a few percent, increasing only very slightly with the mass asymmetry.
(2) The average energy of the emitted particles is in the range of a few MeV, with high-energetic particles of about 2o MeV being decreased by a factor of $1o^5$ - $1o^6$. The emission spectrum is hardened with increasing mass asymmetry.
(3) The particle is emitted preferentially in polar direction (fission axis), with the emission probability in perpendicular direction diminished by about two orders of magnitude for the case of symmetric fission.
(4) Concerning the correlation with the mass asymmetry, the particle emission along the direction of the light fragment is favoured by about one order of magnitude compared to the flight direction of the heavy fragment, if high-energetic particles are emitted.

The general trends expressed in these results are reflected in the experimental data on polar particle emission in fission [3, 4].

References

[1] Revai, J.; Nucl. Phys. A 438 (1985) 512
[2] Milek, B., Reif, R., Revai, J.; Phys. Letters 15oB (1985) 65
[3] Kordyasz, A.J., et al.; Nucl. Phys. A 439 (1985) 28
[4] Theobald, J.; XV. International Symposium on Nuclear Physics, Gaussig, November 1985

ANGULAR DISTRIBUTIONS FROM GAMOW STATES IN $^{17}O + ^{16}O$

J. Fandrich, B. Milek and R. Reif
TU Dresden, Sektion Physik, Wissenschaftsbereich Theoretische Physik

While in nucleon induced reactions the relaxation of the compound system starts from an initial state with already one particle in the continuum which favours nonstatistical emission during various stages of the reaction, in heavy-ion reactions nucleons, at the beginning of the reaction occupying bound states of the mean potentials, have to be lifted at first to decaying states by the nucleus-nucleus interaction. Therefore, it is meaningful, to seperate the Gamow states, represented by wave functions with purely outgoing waves in the asymptotic region, from the remaining single-particle continuum. Supposing the two ions to move along given classical trajectories, quasistationary states are occupied by dynamical coupling in the adiabatic basis consisting of bound and Gamow states in a two-center potential. From the population of the basic states single-particle emission spectra, inelastic excitation, and transfer probabilities can be derived [1, 2]. The final occupation numbers after the interaction stage for different m-substates allow for the calculation of in- and out-of plane correlations during the sequential decay of quasistationary states.

Angle integrated spectra for neutron emission from Gamow states have been calculated [1] in a two center potential with finite depth potentials corresponding to the $^{17}O+^{16}O$ system. Initially, the $1d_{5/2}$ level is occupied by a valence nucleon in ^{17}O above e ^{16}O core. The quasistationary part of the basis $|\phi_{i\Omega\Lambda}\rangle$ for a given position of the center $\vec{R}_1$ and $\vec{R}_2$ has been labeled by the projection Ω of the angular momentum (rotational symmetry), parity Λ (identical cores), and a count number i. The required asymptotical behaviour is guaranted by the Green operator [1]

$$\hat{G}_0^{(+)}(E_{i\Omega\Lambda} - i\Gamma_{i\Omega\Lambda}) = \left(\lim_{\varepsilon\to 0} \frac{1}{E - H_0 + i\varepsilon}\right)_{E \to E_{i\Omega\Lambda} - i\Gamma_{i\Omega\Lambda}} \tag{1}$$

Expressing each potential in a finite rank oscillator basis $|I\rangle$ the Schrödinger equation $|\phi^+\rangle = \hat{G}_0^{(+)}\hat{V}|\phi^+\rangle$ can be solved in momentum representation by algebraization. Using the procedure (1) for fixed position of the two center, in space representation a angle dependent amplitude of the outgoing waves for $|\vec{r}| \to \infty$ can be derived

$$\begin{aligned} \langle \vec{r} | \phi^+_{i\Omega\Lambda} \rangle &\underset{|\vec{r}|\to\infty}{=} f(\hat{r}) \cdot \frac{e^{ik_{i\Omega\Lambda} r}}{r} \\ f(\hat{r}) &= \int d^3\vec{r}\,' \, e^{ik_{i\Omega\Lambda}\frac{\vec{r}}{|\vec{r}|}\vec{r}\,'} \sum_I \langle \vec{r}\,' | \hat{c}_I^{\,i\Omega\Lambda}(\vec{R}_1, \vec{R}_2) | I \rangle \end{aligned} \tag{2}$$

The operator $\hat{c}$ contains known coefficients as well as the translational operators for the localization of the centers. The wave number k is determined approximately by the real part of the complex energy ($\Gamma \ll E$) of the state under consideration. A double-differential spectrum arises by time integration over three time-dependent factors: the rate of emission between time t and t + dt, the probability to find the particle at an emission energy ε between ε and $\varepsilon + d\varepsilon$ (Lorentz-distribution) and finally the probability $|f|^2$ to find the particle in a space direction outside of the system. Various types of calculations for peripheral collisions are under investigation like neutron-projectile angular correlations for selected trajectories and averaged spectra.

References

[1] Milek, B. and Reif, R.; TU-Information 05-9-85, 05-10-85, 05-11-85 (1985) and submitted to Nucl. Phys. A

[2] Milek, B. and Reif, R.; Phys. Letters 157B (1985) 134

MODEL INVESTIGATIONS ON NITROGEN IMPLANTATION IN SILICON

E. Sobeslavsky and K. Wollschläger
Zentralinstitut für Kernforschung, Rossendorf, Bereich KF

The implantatation of high doses of energetic N^+-ions into silicon ($N_\square \cong 1.5 \cdot 10^{18}$ N^+ cm^{-2}, $E \cong 200$ keV per ion) leads to the formation of buried Si_3N_4-layers. SOI structures using such layers have been shown to be suitable for a complete dielectric insulation of microelectronic components, they also acts as a diffusion barrier against dopants and other unwanted impurities.

The present investigation deals with the modelling of as-implanted nitrogen concentration curves. In this case, if nitrogen concentration exceeds the characteristic stoichiometric value of Si_3N_4, the experimental curves show an approximately Gaussian nitrogen distribution in the vicinity of the projected range of the stopped ion R_p. The model was originally developed to describe high dose O^+-implantation in silicon /1/. It takes into account sputtering, volume swelling and the change in range profiles due to the formation of Si_3N_4. If the Si_3N_4 stoichiometry threshold is exceeded, the excess nitrogen is allowed to diffuse both to the surface and to the bulk in order to form Si_3N_4. A Deal-Grove rule for such a nitridation is assumed. The excess nitrogen which reaches the surface diffuses out.
Comparing the experimental data with the model calculations one obtains the following results:

- Above the Si_3N_4 stoichiometry threshold nitrogen is not found to diffuse. Hitherto a radiation enhanced diffusion (as known in the case of high dose oxygen implantation in silicon) could not fully be excluded /2,3/.
- For an energy of E = 20 keV per nitrogen atom ion mixing does not play a remarkable role.
- The nitrogen concentration of Si_3N_4 is reached, first at the profile maximum, at a dose N_{crit} of approximately $N_{crit} \cong \frac{3}{4} \cdot \sqrt{2\pi} \cdot d \cdot \Delta R_p$, where d is the molecular density.
- Compared with the model distributions the experimental ones show longer tails at the bulk side of the curves. This can be explained by an additional volume swelling effect caused by the excess nitrogen, which is assumed to be in a solid or liquid phase.
- The model describes well the formation of Si-N compounds at concentrations of nitrogen in silicon below the stoichiometric value of Si_3N_4. In this region the nitrogen distribution can be approximated by

$$n''(z,t) \cong \frac{n}{\Delta\Omega} \cdot \frac{\mathrm{erf}\left(\frac{R_p - z'}{\sqrt{2}\cdot\Delta R_p}\right) - \mathrm{erf}\left(\frac{R_p - z'}{\sqrt{2}\cdot\Delta R_p} - \frac{j_{impl}\cdot\Delta\Omega}{2\cdot\sqrt{2}\cdot\Delta R_p}\cdot\left[\mathrm{erf}\left(\frac{R_p}{\sqrt{2}\cdot\Delta R_p}\right) - \mathrm{erf}\left(\frac{R_p - z'}{\sqrt{2}\cdot\Delta R_p}\right)\right]\cdot t\right)}{\mathrm{erf}\left(\frac{R_p - z'}{\sqrt{2}\cdot\Delta R_p}\right) - \mathrm{erf}\left(\frac{R_p}{\sqrt{2}\,\Delta R_p}\right)}$$

where $z' = z - Y^N_{n_{Si}}$, Y is the sputtering yield, n_{Si} denotes the atomic number target density, j_{impl} and t are implantation current and time, respectively; $N_\square = j_{impl} \cdot t$.

$= \frac{1}{4} \cdot (\Omega_{Si_3N_4} - 3 \cdot \Omega_{Si})$, where $\Omega_{Si_3N_4}$ and Ω_{Si} stands for the volume of nitride molecule and silicon atom, respectively.

References

/1/ Jäger, H.-U. et al., Thin Solid Films 123 (1985) 159

/2/ Lezheiko, L.V. et al., J. Tech. Phys. 51 (1981) 818

/3/ Bayerl, P. et al., Radiat. Eff. 47 (1980) 217

MODELLING OF THE OXYGEN REDISTRIBUTION DURING FORMATION OF BURIED SiO_2 LAYERS BY HIGH DOSE OXYGEN IMPLANTATION

H. U. Jäger
Zentralinstitut für Kernforschung, Rossendorf, Bereich KP

Using a model [1] which takes into account changes in the ion range, target widening, surface sputtering and internal oxidation due to unbonded oxygen, the depth profiles obtained after high dose oxygen implantation into silicon have been calculated for a broad range of ion energies and implanted doses (fig. 1 and ref. [2]).

In a recent paper [3] the formation of buried SiO_2 layers has been monitored by the implantation of ^{18}O tracer atoms and subsequent analysis by negative ion SIMS. The oxygen isotope depth profiles measured in this experiment can be well reproduced by our phenomenological model [4] provided that a perfect exchange of migrating oxygen with matrix oxygen in the buried layer is postulated. In fig. 2 we present model predictions for the somewhat fictitious situation that the two oxygen doses (^{16}O and ^{18}O) implanted are equal to each other and amount to $D = 0.8 \times 10^{18}$ cm^{-2} (upper part) or $D = 1.2 \times 10^{18}$ cm^{-2} (lower part). The oxygen depth profiles shown refer to

(i) single implantation to dose D (thin line),
(ii) final distribution of the initially implanted isotope (dashed line),
(iii) distribution of the secondly implanted isotope (dotted line), and
(iiii) total oxygen distribution after the two successive implantations (thick line).

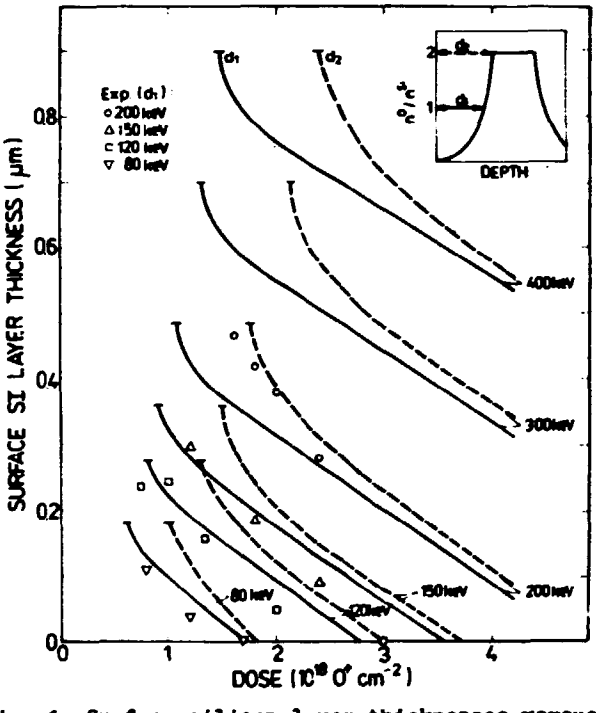

Fig. 1. Surface silicon layer thicknesses versus implanted oxygen doses for various implant energies.

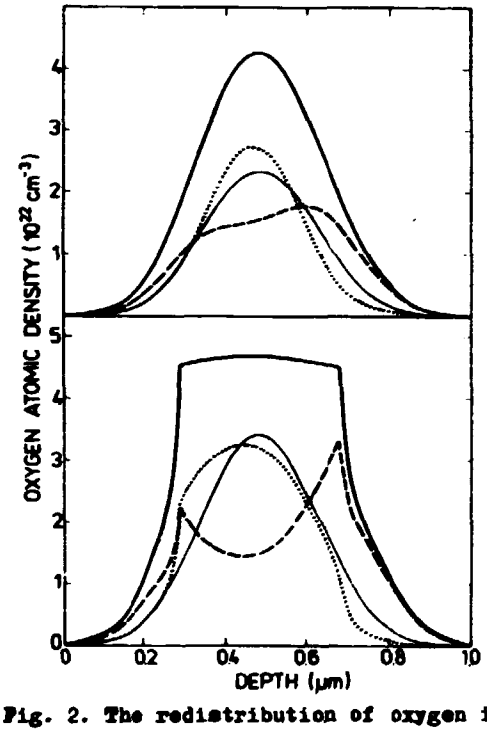

Fig. 2. The redistribution of oxygen in silicon during two successive implantations of 200 keV O^+ ions.

References

[1] Jäger, H. U., et al.; Thin Solid Films 127 (1985) 159
[2] Jäger, H. U.; Nucl. Instr. and Meth. B, in print
[3] Kilner, J. A., et al.; Nucl. Instr. and Meth. B 7/8 (1985) 293
[4] Jäger, H. U., et al.; to be published

ON THE CHOICE OF THE ELECTRONIC STOPPING FORMULA FOR RANGE PROFILE CALCULATIONS IN THE MEV REGION

M. Posselt, W. Skorupa, Zentralinstitut für Kernforschung, Bereich KF
A. Beyer, W. Markgraf, Technische Hochschule Karl-Marx-Stadt, Sektion Physik/Elektronische Bauelemente

It is well known that theoretical range profiles calculated by Monte-Carlo simulations or analytical transport theories are strongly influenced by the following inputs: (i) the interatomic potential or the nuclear stopping and (ii) the electronic stopping. We have studied the influence of the second input in the case of 990 keV phosphorous implantation into silicon where the slowing down of the incident ions is dominated by electronic losses. The ion range profiles have been determined by Monte Carlo simulations using (i) the Varelas-Biersack equipartition (cf. /1/) of the Lindhard-Scharff and the Bethe-Bloch electronic stopping formulas and (ii) the scaling of the electronic stopping cross-sections of protons. The first approximation interpolates between two limits: (i) At low velocities $v_1 \ll v_F \sim v_0$ and relatively high atomic numbers $0.75 v_F \ll v_0 \; Z_1^{2/3}$ the stripping of the projectile is small and independent of v_1. If $v_1 < v_F \sim v_0$ only the valence electrons of the target may be excited(Lindhard-Scharff). v_1, Z_1, v_0, v_F are the velocity and the atomic number of the projectile the Fermi velocity of the target and the Bohr velocity, respectively. (ii) At high velocities $v_1 \gg v_0 \; Z_1^{2/3}$ the projectile is fully stripped and all target electrons can be excited $v_1 \gg v_0 \; Z_2^{1/2}$ (Bethe-Bloch). Z_2 is the atomic number of the target. In the second model (cf. /2/) the well-known proton stopping cross-sections are multiplied by the effective charge Z_1^* of the projectile. Z_1^* is calculated by the Brandt-Kitagawa approach taking into account a certain stripping criterion. The upper limit of the Brandt-Kitagawa theory may be given by $v_1 \sim v_0 \; Z_2^{1/2}$ where all target electrons are excited.

In fig.1 the computed range profiles are compared with experimental values determined by pulsed CV measurements after 990 keV phosphorous implantation. The theoretical profile obtained from the second model (heavy lines) agrees well with the experimental data. The first model (thin lines) yields a deeper range profile. This difference may be interpreted as follows. In our example the initial velocity of the projectile is about $1.1 v_0$. In that region the stripping already depends on the projectile velocity. This is well described in the second approach. On the other hand, this effect is not considered in the first model which leads to a lower electronic stopping. Both profiles in fig.1 are calculated using the Biersack interatomic potential. Nearly the same results are obtained by applying the Moliere potential. Furthermore, in fig. 1 the ranges corresponding to the maximum of the profiles which would be obtained from the Gibbons (a) and the Burenkov (b) tables are shown.

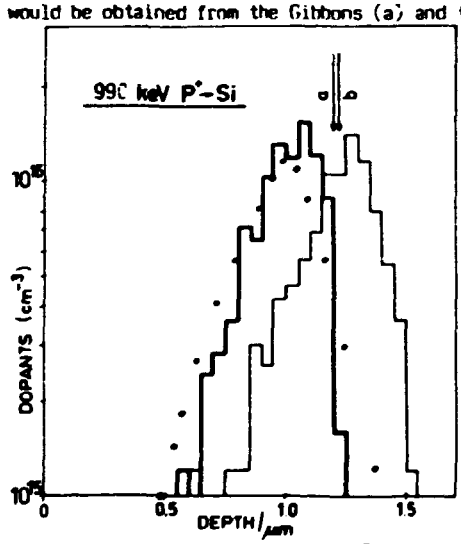

Fig. 1 Theoretical and experimental range profiles for 990 keV $^{31}P^+$ implantation into silicon (dose: $5 \cdot 10^{11}$ cm^{-2}, annealing: 1100 ^{0}C, halogen lamp, further experimental details see /3/)

/1/ Biersack, J. P. and Haggmark, L. G. , Nucl. Instr. and Meth. 174 (1980), 257
/2/ Biersack, J. P. and Ziegler, J. F., "Ion Implantation Techniques" (Ed. by H. Ryssel and H. Glawischnig, Springer 1982), 121
/3/ Skorupa, W. et. al. , this report, p. 45

INFLUENCE OF THE ENERGY TRANSPORT BY RECOILS ON ENERGY-LOSS PROFILES

H. Posselt, Zentralinstitut für Kernforschung Rossendorf, Bereich KF

Two Monte Carlo simulation schemes are applied: The first which was originally made up for range distributions [1] describes the slowing down of the incident ions until their energy drops below E_{min}.
The subcascades initiated by the primary knock-on atoms (PKA) are not followed and the deposition of the PKA energy is assumed to take place at the position of the PKA generation (local energy deposition). This approximation leads to a relatively fast computer code. In the second scheme [2][3] which is also used for sputtering and ion mixing purposes recoils of all orders are followed until E_{min}. Below E_{min} local energy deposition is assumed. E_{min} is chosen so that the corresponding particle range is smaller than the interval size in the calculated histograms. The disadvantage of the second scheme is its higher computer time consumption. In comparison with the first scheme (fig.1-thin lines) this method (heavy lines) yields depth profiles which are shifted into the depth and broader lateral profiles, due to the spatial energy transport by the recoils. In general for heavy ions incident on light targets this effect is considerable, both for electronic and nuclear loss profiles.
The following rough estimation may be useful to decide if the computer time consuming second method must be applied to calculate the energy-loss profiles or not. The nuclear stopping power of the incident ions determines the average energy transfer to the PKA per path length. Therefore, the portion of the energy dissipation into the subcascades and the energy transport by the recoils increase with increasing nuclear stopping. At sufficiently high ion energies ($\varepsilon > 0.3$ [4]) the maximum nuclear stopping of all ion-target combinations can be characterized by [2][3]

$$f = \frac{(M_1/M_2)^2}{(1+M_1/M_2)(1+(M_1/M_2)^{1/2})^{2/3}} \; \rho \; M_2^{2/3}$$

M_1, M_2, ρ are the ion mass, the target mass and the target density, respectively. In fig. 2 the quantities r and r_1 which globally characterize the longitudinal and the lateral energy transport by the recoils are drawn vs.f (data from [2][3]). r and r_1 increase with increasing f.

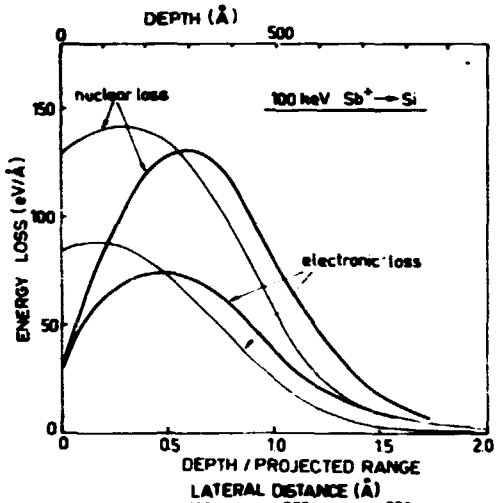

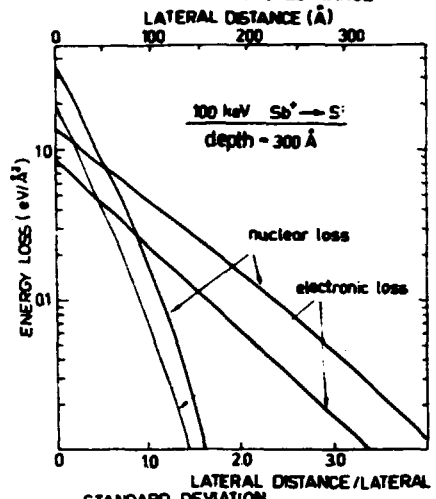

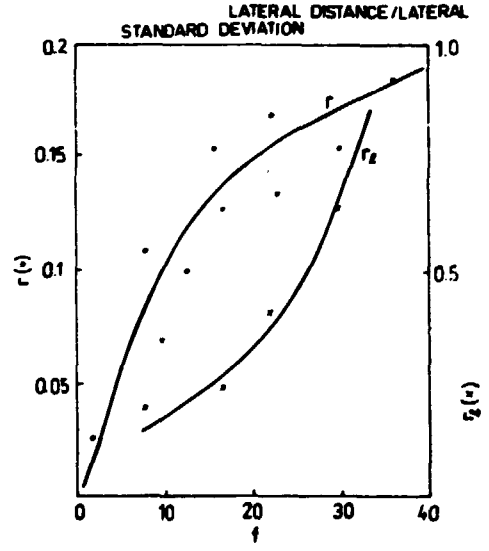

[1] Biersack, J. P. and Haggmark, L. G., Nucl. Instr. and Meth. 174 (1980), 257
[2] Posselt, M. and Biersack, J. P., to be published in Nucl. Instr. and Meth. B (1986)
[3] Posselt, M. , to be published in phys.stat.sol.(a) 94 (1986)
[4] Biersack, J. P. and Ziegler, J. F. , "Ion Implantation Techniques" (Ed. by H. Ryssel and H. Glawischnig, Springer 1982),149

COMPUTER SIMULATION OF THE EVOLUTION OF LOW-ANGLE GRAIN BOUNDARY NETWORKS DURING ZONE-MELTING OF SOI-LAYERS

K.-H. Heinig, H.-J. Müller and G. Otto
Zentralinstitut für Kernforschung, Rossendorf, Bereich KF

Silicon-on-Insulator (SOI) is attractive for high-density MOS-integrated circuits. One novel approach to forming device-quality single-crystalline layers on insulating substrates is lateral zone-melting (by halogen lamps, graphit stripe heaters or lasers). By means of this recrystallization technique monocrystalline layers with low-angle grain boundaries or subboundaries are obtained /1,2/. These randomly distributed subboundaries can deteriorate device quality. Therefore, experimental and theoretical investigations have been started in order to understand the pattern formation of subboundary networks with the aim to find means for its preventation or control.

At present there is experimental evidence /1,2/ that (i) the single-crystalline SOI-films grows preferably in ⟨010⟩ direction and tends to have (100) texture, (ii) the melt-solid interface consists of alternating (111) and (11$\bar{1}$) facets, and (iii) that subboundaries are formed at the interior corners of the faceted solidification front.

Starting from these rules and assuming that the normal growth velocity of the facets is determined only by the nucleation of new (111) lattice planes, a quantitative model for the evolution of subboundaries have been proposed recently /3/. Within this bidimensional model, after one growth step the change of the length L_{2i} of a (111) facet,i.e. a facet with an even index, is given by

$$dL_{2i}/dt = (v_{2i-1} - v_{2i+1}) / \sin (\theta_1 + \theta_2) , \qquad (1)$$

where θ_1 and θ_2 are the angles between the growth direction and the (111) and (11$\bar{1}$) facets, respectively, and v_{2i} is the normal growth velocity of the $(2i)^{th}$ facet, i.e.

$$v_{2i} = k_2 \int_{x_{2i}}^{x_{2i-1}} (x_m - x) \, dx / \cos \theta_2 \quad . \qquad (2)$$

Solidification proceeds in x-direction, where x_{2i} and x_{2i+1} are the positions of the corners of the $(2i)^{th}$ facet and $x_m = vt$ is the actual position of the melting isotherm. The kinetic factors k_1 and k_2 of the odd and even facets, respectively, are mainly determined by the nucleation rate, the temperature gradient at the solidification front and the texture. Using periodical boundary conditions, the system (1),(2) of coupled, non-linear differential equations for the 2*N facets has been solved numerically by means of a Runge-Kutta procedure (N is typically 10...100). For the "birth" and "death" of facets special numerical routines have been developed.

The results of the computer simulation can be summarized as follows /4/: (i) Independent of the initial conditions, the evolution of the loci of the interior corners (=subboundaries) results in a random, stationary pattern (see e.g. ref. /5/). (ii) Adjusting the parameters v, θ and k, all experimentally observed types of subboundary pattern can be explained. (iii) It has been proven numerically that $N \sim v^{-0.5}$. (iv) Misalignment between the growth direction and the ⟨010⟩ crystal direction leads to a certain self-confinement of subboundaries.

References

/1/ Scharff, W., J.-W. Erben, C. Höppner, A. Wolf, R. Klabes, J. Matthäi, M. Voelskow, and E. Wieser, Proc. Int. Conf. Energy Pulse Modification of Semiconductors and Related Materials, Ed. K. Hennig, ZfK-555 (1985) 397
Weissmantel, C., ibid. p. 383
/2/ Geis, M.W., H.I. Smith, D.J. Silversmith, R.W. Mountain, and C.V. Thompson, J. Electrochem. Soc. 130 (1983) 1178
/3/ Pfeiffer, L., S. Paine, G.H. Gilmer, W. van Saarloos, and K.W. West, Phys. Rev. Lett. 54 (1985) 1944
/4/ Heinig, K.-H. and G. Otto, Working Meeting Ion Implantation in Semiconductors ..., Balatonaliga (Hungary) 1985 and to be published
/5/ Fromm, U., Fromm, W.-D., K.-H. Heinig and G. Otto, this report p. 137

COMPUTERSIMULATION VERSUS ANALYTICAL FORMULAE: A CRITICAL DISCUSSION OF THEORIES OF TRANSFORMATION

H.-J. Müller and K.-H. Heinig
Zentralinstitut für Kernforschung, Rossendorf, Bereich KF

Mathematical studies of crystallization kinetics for the interpretation of experimental findings have been carried out for about four decades. The first attempts were made independently by Johnson and Mehl /1/ and Avrami /2/ in the early fourties. Their formula have been proved to be in accordance with many experimental data but there are also serious differences. These differences are to be expected because drastic approximations have been used for the derivation of the formula.

Ruckenstein and Ihm /3/ suggested a formula wich deals the problem of the so-called extended volume in Avrami's derivation somewhat better. However, as they did also fail to include the grain impingement in an appropriate manner, their formula can be used only for the early stage of transformation. Up to now the grain impingement could be taken into consideration by Speich and Fisher /4/ in an empirical way only. The broad discussion about the various models of phase transformation kinetics stimulated recently Price /5/ to compare them critical with experiment. As no practical theory of grain impingement is available he maintains that at present the empirical Speich-Fisher relation is the best alternative to describe experiments. Another problem not solved so far is the inclusion of the time lag into analytical transformation formulae.

Our computer simulation /6/ allow to take into full account the grain impingement as well as the time lag. Thus we are in a position to test analytical formula and to modify them. The main results of an extensive investigation of the solid-phase transformation a-Si into poly-Si in the framework of the computer simulation can be summarized into the following items:

(i) The Avrami formula is well adopted to transformation kinetics of processes if the time-lag does not play a role, ie where it is small compared to the transformation time scale. That results from the fact that Avrami's approximation with respect to the extended volume gives by accident a pre-factor which describes the growth stagnation by grain impingement rather good.

(ii) In contrast to discussions about transformation kinetics (see e.g./5/) we prove that if there are difficulties to fit experimental data by Avrami's law, then they are wether an evidence against it nor does they support other formulae. In reality, the time lag is the crucial quantity which determines the first stage or even the whole process of transformation.

(iii) Due to the complex interplay of time lag, grain impingement and other influences on the transformation kinetics, investigations of time dependent transformation processes on the base of Avrami's or other analytical formulae give no reliable information.

/1/ Johnson, W.A. and Mehl, R.F.; Trans. AIME 135 (1939) 416
/2/ Avrami, M.; J. Chem. Phys. 7 (1939) 103; 8 (1940) 212; 9 (1941) 212
/3/ Ruckenstein, E. and Ihm, S.K.; J. Chem. Soc. Faraday I 72 (1976) 764
/4/ Speich, G.R. and Fisher, R.M.; in Recrystallization, Grain Growth and Textures, New York 1981
/5/ Price, C.W.; Scripta Met. 19 (1985) 669
/6/ Müller, H.-J. and Heinig, K.-H.; this report p.44

COMPUTER SIMULATION OF THE PRIMARY CRYSTALLIZATION a-SI TO poly-SI

H.-J. Müller and K.-H. Heinig
Zentralinstitut für Kernforschung, Rossendorf, Bereich KF

The kinetics of crystallization has an increasing impact on the development of materials for microelectronic devices. It is a result of the collective interaction of extrinsic parameters (temperature-time-regime; starting and boundary conditions) and intrinsic laws of the transformation. There have been many efforts to formulate universal analytical laws for the transformation kinetics, but due to the complex interaction of kinetical and geometrical aspects no generally accepted formula exists. Therefore in the last few years a renewed interest in this subject inspired by the increasing possibilities of computer simulations (CS) can be observed. It has been shown that they give a deeper understanding of crystallization processes, because they allow a thorough insight into the fundamental microscopic motions. On the other hand CS are able to prove existing empirical or semiempirical laws by a systematical study of the influence of extrinsic and intrinsic parameters and laws on the kinetics of crystallization. Thus a variety nf CS has been established /1,2,3/ for the description of the second step of crystallization, the so-called grain growth, occuring upon annealing a polycrystalline aggregate after primary crystallization is complete. Up to now analogous extensive CS of the primary crystallization process are missing, although such models are very useful for the investigation of rapid thermal processing (e.g. a-Si to poly-Si) where this plays the dominant role.

Primary crystallization is caused by nucleation and growth of the crystalline phase within the amorphized Si. The kinetics of transformation is a result of the competitive process of nucleation and growth and the growth stagnation induced by grain impingement during crystallization. The latter depends on the actual grain ensemble of the crystalline phase. It is impossible to give an exact analytical description of the growth stagnation.

All these effects were included into a two-dimensional computer simulation of the primary solid-phase crystallization of thin layers of amorphous-to-polycrystalline Si. Classical nucleation theory and the growth rate of solid phase epitaxy serve as basic ingredients. The statistical aspects of nucleation are incorporated by a grand-canonical Monte-Carlo-Procedure. Thus the model is based on well-established, phenomenological laws, whereas most of the other CS work on a more microscopic scale using additional assumptions. An almost real geometrical situation of the grain ensamble is realized by a division of space and time into finit elements using bit-mapping techniques for the transformation area /4/.

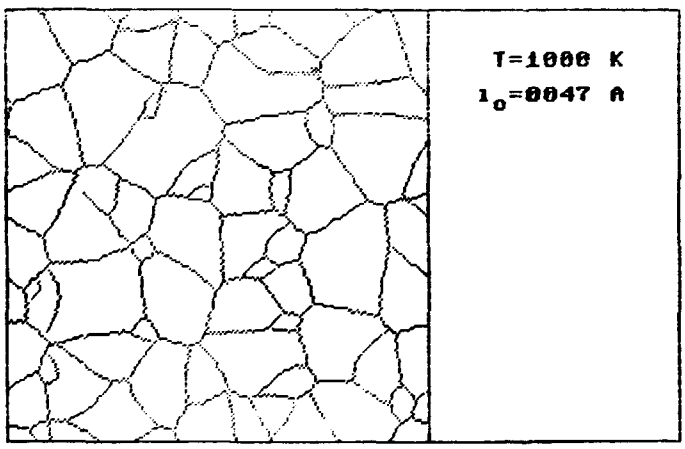

Plot of a calculated polycrystalline structure of a Si layer

Results on the grain size distribution, the grain-boundary topology and the transformation kinetics in two-dimensional Si layers are obtained in dependence on the transformation temperature. Furthermore the developed computercode permits an extensive investigation of the growth stagnation by grain impingement, which has been a fundamental problem in the derivation of analytical formulae for the kinetics of crystallization in the last years.

/1/ Anderson, M.P., Srolovitz, D.J., Grest, G.S. and Sahni, P.S.; Acta Met. 32 (1984) 783
/2/ Ceppi, E.A. and Nasello, O.B.; Scripta Met. 18 (1984) 1221
/3/ Yabushita, S., Hatta, N., Kikuchi, S. and Kokado, O.; Scripta Met. 19 (1984) 853
/4/ Müller, H.-J. and Heinig, K.-H.; to be published

APPLIED METHODS OF NUCLEAR PHYSICS

HIGH ENERGY (0.99 MeV) PHOSPHORUS IMPLANTATION INTO SILICON

W. Skorupa, E. Wieser, R. Grötzschel and M. Posselt
Zentralinstitut für Kernforschung, Rossendorf, Bereich KF
A. Armigliato und A. Garulli
CNR Istituto LAMEL, Bologna

Recently, ion implantation with energies in the MeV range has become of increasing importance for semiconductor technology /1,2/.

In our first experiments, P^{3+} ions have been accelerated with a voltage of 330 keV to reach an end energy of 0.99 MeV. The beam power density was ≤ 0.8 W cm^{-2} maintaining the target temperature at about 300 K. The substrates were monocrystalline silicon wafers with <100> orientation coated by 100 nm thermally grown SiO_2. The implanted doses ranged from $5 \cdot 10^{11}$ cm^{-2} to $7.5 \cdot 10^{14}$ cm^{-2}. After implantation, annealing was carried out by furnace (900 °C, 30 min, N_2), flash lamp (~1350 °C, 17 ms, air) and halogen lamp (~1100 °C, 10 s, air). This contribution will be concerned with radiation damage after implantation of $7.5 \cdot 10^{14}$ cm^{-2}.

In fig. 1 RBS spectra are shown. After implantation a peak due to direct backscattering is visible in the aligned spectrum at a depth of 0.83 µm. This value added with the SiO_2 thickness of 0.1 µm corresponds well with the position of the maximum of the energy deposited into nuclear processes as calculated by the BRICE theory (0.98 µm) and MONTE CARLO simulations (0.97 µm). No amorphisation took place there although the deposited energy in this depth is higher than 10^{21} keV cm^{-3}, the amorphisation threshold level at 300 K /3/. No defects were found by cross section TEM.

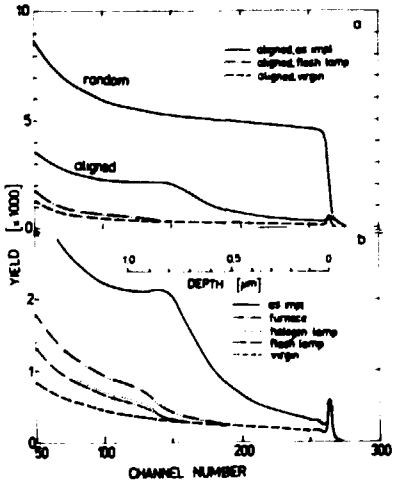

Fig. 1
RBS spectra (1.7 MeV, $^4He^+$) after 0.99 MeV phosphorus implantation a) random and aligned, b) aligned with higher magnification (for experimental details see text)

After annealing, the yield of the aligned spectra (fig. 1b) is in all cases for depths $\geq$ 0,65 - 0.85 µm slightly higher than that one of a virgin crystal. These higher yields are induced by dechanneling. Annealing with the short time methods was more effective. Only a narrow defect band was evaluated by cross section TEM between 0.88 µm and 1.13 µm for these cases. After furnace annealing dechanneling begins already at 0.65 µm. The TEM results confirmed that the defect band is broader and ranges from this depth to about 1.1 µm. Generally, the residual defects are dislocation loops and stacking faults. The surface region is free of defects.

References

/1/ Proc. 5th Int. Conf. Ion Impl. Equipment, Jeffersonville 1984, Nucl. Instrum. Methods B6 (1985)

/2/ Skorupa, W., Literatur-Report: Hochenergieimplantation in Silicium, ZfK/KFH 3.85 (1985)

/3/ Vook, F.L., Radiation Damage in Semiconductors, Inst. Phys. Conf. Ser. 16 (1973) 60

FORMATION OF BURIED SILICON NITRIDE LAYERS IN SILICON BY ION IMPLANTATION-NEW RESULTS

W. Skorupa, K. Wollschläger, H. Oertel and R. Grötzschel
Zentralinstitut für Kernforschung, Rossendorf, Bereich KF
H. Bartsch
Institut für Festkörperphysik und Elektronenmikroskopie, Halle

The ideal SOI (silicon on insulator)-structure may be characterised by a monocrystalline silicon layer free of defects above an ideal electrical insulator with a steep interface between them. A first step into this direction has been reported recently /1,2/. High dose nitrogen implantation (330 keV, 1.2 x 10^{18} cm^{-2}) followed by furnace annealing at 1200 °C, 5 h, N_2 leads to the formation of buried silicon nitride layers with steep interfaces and rectangular nitrogen profiles /1/. This method was investigated in more detail. Formerly, the aligned yield within the whole silicon top layer as determined by channeling was about 20 %. By optimisation of the annealing scheme (see below) it was found that it is possible to reach aligned yields comparable to such of unimplanted silicon (see Fig. 1, spectrum a). By cross section TEM only dislocations were found in the silicon top layers. Up to now only SOI structures with more complicated defects as grain boundaries, precipitates, twins etc. were possible to produce.

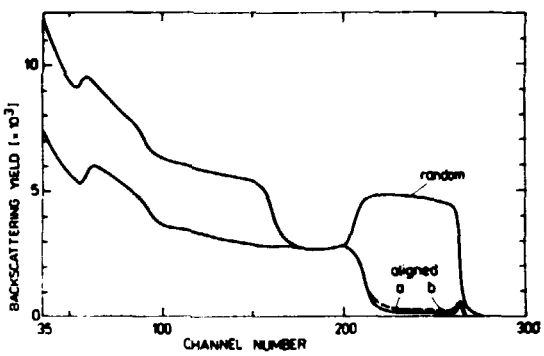

Fig. 1

RBS spectra after nitrogen implantation (330 keV, 1.2 x 10^{18} cm^{-2}) into silicon and furnace annealing (1200 °C, 5 h, N_2)

Annealing of the bare silicon wafers with buried Si_3N_4 layers at 1200 °C in nitrogen atmosphere led to a strong erosion of the polished surfaces. For this manner it was proved to use a thermal oxide as a protective layer. It was found to be sufficient to drive in the wafers into the furnace in oxygen atmosphere and changing the ambient gas to nitrogen after five minutes. In this case, the surfaces of the wafers were free of defects after annealing. From RBS aligned spectra (Fig. 1), it is visible the surface damage peak to be comparable to that of virgin silicon.

The mechanism of minority carrier lifetime increase above buried silicon nitride layers /3/ was investigated in more detail at the original structure i.e. epitaxial layers on the buried layer system. Clearly, it could be shown that Si_3N_4 precipitates lead to a gettering effect /4/.

References

/1/ Skorupa, W. et al., Gemeinsamer Jahresbericht 1984, ZfK-559 (1985) 96
/2/ Hemment, P.L.F. et al., Appl. Phys. Lett. 46 (1985) 952
/3/ Skorupa, W. et al., Electron. Lett. 20 (1984) 426
/4/ Skorupa, W. et al., Working Meeting on Ion Impl. in Semicond., Balatonaliga, 1985

ANODIC OXIDATION AS SECTIONING TECHNIQUE FOR THE DETERMINATION OF HIGH DOSE B^+ AND As^+ IMPLANTATION PROFILES IN Si

G. Mende

Zentralinstitut für Kernforschung, Rossendorf, Bereich KF

The profile determination in Si by electrical measurements or neutron activation analysis is often performed by successive layer removal with the help of anodic oxidation in combination with dissolving of the oxide in dilute hydrofluoric acid.

In the present work the influence of various doses of B^+ ($2 \cdot 10^{14}$ and $2 \cdot 10^{16}$ cm^{-2}, energy = 50 keV) implanted into n-type Si (5,0 Ohm cm) and As^+ ($2 \cdot 10^{14}$, $6 \cdot 10^{15}$ and $2 \cdot 10^{16}$ cm^{-2}, energy = 100 keV) implanted into p-type Si (10 Ohm cm) on the oxidation rate and the thickness of removed layers has been investigated after flash lamp annealing (17 ms at 1350 °C).

The samples were anodised with a constant current density (7 mA/cm^2) in 0.04 N solution of KNO_3 in ethylene glycol containing 1 Vol.-% H_2O. The thickness of removed layers from B^+ implantation profiles in Si was calibrated by means of neutron activation analysis after annealing (30 min at 750 °C in a N_2 stream) of the samples /1/. The thickness of removed layers from Si implanted with As^+ was measured by a Talystep.

After B^+ implantation with a dose of $2 \cdot 10^{14}$ cm^{-2} the thickness of removed layers does not change in comparison with unimplanted material (Fig. 1a) and the oxidation rate is constant (Table 1). However, after B^+ implantation with a dose of $2 \cdot 10^{16}$ cm^{-2} the thickness of removed silicon layers is reduced (Fig. 1b) and the oxidation rate is enhanced (Table 1), provided that the concentration of implanted boron is higher than $5 \cdot 10^{20}$ cm^{-3}.

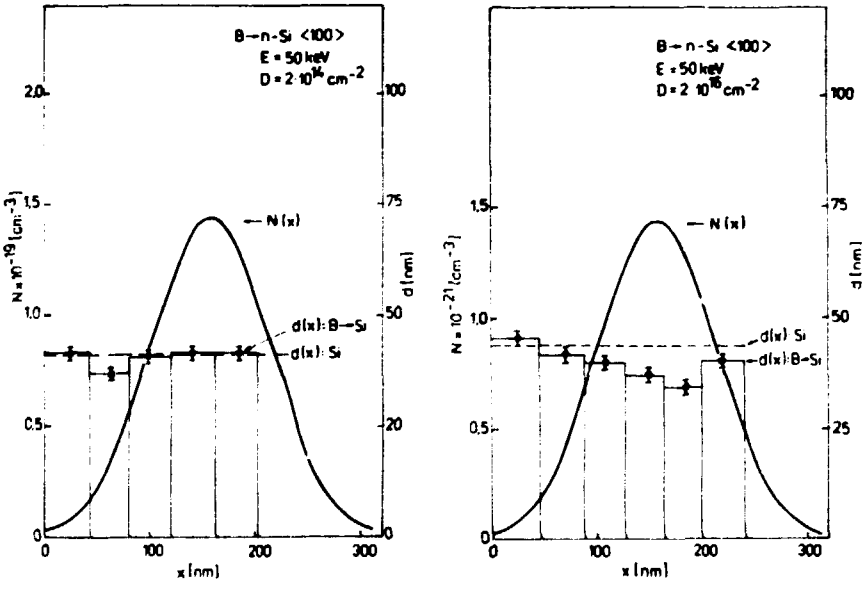

Fig. 1a, 1b

Removed layer thickness of silicon implanted with boron in comparison with unimplanted Si vs. depth x and the B^+ implantation profile $N_{(x)}$ according to the LSS theory

A similar effect can be stated after As^+ implantation with a dose of $2 \cdot 10^{16}$ cm^{-2}, provided that the concentration of implanted arsenic is larger than $2 \cdot 10^{21}$ cm^{-3}. But in this case not only the oxidation rate but also the thickness of removed layers is increased.

Therefore the oxidation rate is a good monitor for thickness change during anodisation of silicon implanted with sufficiently high doses ($2 \cdot 10^{16}$ cm^{-2}) of boron (energy = 50 keV) or arsenic (energy = 100 keV). In this case the thickness/voltage increments during anodisation of unimplanted materials are not valid and the thickness of removed layers must be determined step by step.

Table 1

Anodisation time t of Si implanted with boron during successive anodisation steps (V = 210 V)

dose /cm^{-2}/	t_1/min/	t_2/min/	t_3/min/	t_4/min/	t_5/min/	t_6/min/
$2 \cdot 10^{14}$	18.9	18.56	18.68	18.60	18.46	-
$2 \cdot 10^{16}$	19.55	18.81	17.20	11.31	10.76	11.83

Reference

/1/ Mende, G., J. Electrochem. Soc. 127 (1980) 2085

DIFFUSION ENHANCEMENT AND ELECTRICAL ACTIVATION DURING RAPID ISOTHERMAL ANNEALING (RIA) OF B AND As IMPLANTED Si

W. Kögler and E. Wieser

Zentralinstitut für Kernforschung Rossendorf, Bereich KF

Diffusion enhancement and electrical activation of B and As implanted in Si during RIA were investigated by comparison of experimental carrier or dopant profiles with computer simulations of diffusional broadening.

Experiment: Boron and Arsenic were implanted in ⟨100⟩-Silicon through 30 nm SiO_2. The dose was between $5 \cdot 10^{15}$ cm^{-2} and $2 \cdot 10^{16}$ cm^{-2} and the implantation energy was 30 keV and 100 keV respectively. RIA was carried out at a maximum temperature T_{max} between 800 °C - 1300 °C with a holding time t_h between 5 and 20 seconds.

Carrier profiles of B were measured by anodic oxid stripping and incremental sheet resistance and Hall effect measurements. Dopant profiles of As were determined by RBS measurements.

Computer simulations: For the computer simulations of diffusional broadening the following diffusion coefficients were used:

$$D_B = f \cdot D_o\left(1+\beta \frac{p}{n_i(T)}\right)(1+\beta)^{-1} \quad \exp(-3.43/kT)$$

$$D_o = 3.33 \cdot 10^9 \, \mu m^2/min, \quad \beta = 3$$

$$D_{As} = f \cdot D_o\left(1+\beta \frac{n}{n_i(T)}\right)(1+\beta)^{-1} \quad \exp(-4.1/kT)$$

$$D_o = 1.37 \cdot 10^{11} \, \mu m^2/min, \quad \beta = 100$$

The diffusion enhancement factor f was fitted in such a way, that calculated and measured profiles were in agreement.

In the case of arsenic the computer simulation included the cluster model by Tsai /1/. Clustered Arsenic does not diffuse and is electrically inactive.

Results:

B /3/
- The diffusion enhancement factor f is in all cases greater than 1. It decreases with increasing T_{max} and t_h, respectively. The observed values lie between f = 25 and f = 4.
- In the temperature range T_{max} 1000 °C - 1100 °C our time averaged enhancement factor f is comparable with an expression given by Fair /2/.
- For temperatures above 1100 °C the data (Fig. 6 /3/)disagree with the Fair formula.
- Full electrical activation is reached for annealing temperatures $T_{max} \geq$ 1100 °C.
- The maximum carrier concentration lies above the equlibrium solubility in the investigated temperature range.

As
- Also in the case of As enhanced diffusion has been stated. The f values are lower than in the case of B (typical values between 6 and 2).
- Full electrical activation was not reached in the investigated temperature regime because the formation of inactive As proceeds faster at higher concentrations and at higher temperatures T_{max}.
- At temperatures $T_{max} \leq$ 1000 °C the data indicates non-equilibrium states with maximums carrier concentrations above the equilibrium value.

Reference

/1/ M.Y. Tsai, F.P. Morehead, J.E.E. Baglin, A. E. Michel
J. Appl. Phys. 51 (1980)3230

/2/ R. B. Fair, J.J. Wortman, J. Liu
J. Electrochem. Soc. 131 (1984)2387

/3/ S. Guimarães, R. Kögler, E. Landi, S. Solmi, E. Wieser
phys. stat. sol. (a) 93 (1986) 577

ELECTRICAL ACTIVATION OF IMPLANTED GaAs BY SHORT-TIME ANNEALING

D. Pankin, C. Döring, J. Hüller, C. Weise, E. Wieser
Zentralinstitut für Kernforschung, Rossendorf, Bereich KP

Short time annealing of Si-implanted GaAs in the solid-phase regime has been investigated by light-pulse heating using halogen-lamps. Semi-insulating Cr-doped (100) GaAs was implanted with Si (200 keV) in the dose range of 10^{13} to 10^{15} Si/cm^2 at different temperatures (20-200 °C).

The dose dependence of the sheet carrier concentration (N_s), the mobility (μ) and the sheet resistivity ρ_s is shown in Fig. 1 for an annealing treatment at 900 °C for 5s without cap layer. For implantation at room temperature N_s increases up to the dose $1 \cdot 10^{14}$ Si/cm^2 and approaches a saturation value of $N_s \approx (3\text{-}4)\ 10^{13}$ cm^{-2}, valid also for higher doses. For high temperature implantation a similar dependence on the dose is obtained, but the saturation level of N_s is lower. The saturation behaviour of N_s can be explained by the amphoteric character of Si in GaAs, which is especially dominating at high doses. The weak dose dependence of μ points on a dominating influence of the chromium content. Therefore the dose dependence of ρ_s is mainly determined by the dose dependence of N_s.

The normally observed prevention of amorphization by T_{impl} =200 °C plays no role under our conditions. The RBS spectrum proves that also "room temperatur" implantation does not results in an amorphous layer. Obviously the temperature is >20 °C and the amorphization threshold depends very strongly on the real T_{impl}. This explains the lower saturation value of N_s at T_{impl} = 200 °C.

The dependence of N_s on the annealing temperatur and the annealing time is shown in Fig. 2. The dependence of N_s on the temperatur as well as on the time shows a maximum. This maximum shifts with higher temperatur to a shorter time and with longer time to a lower temperature, respectively. This means, there is a set of temperature-time pairs for a optimium temperature treatment. These pairs are mainly determined by the dissociation of the GaAs surface.

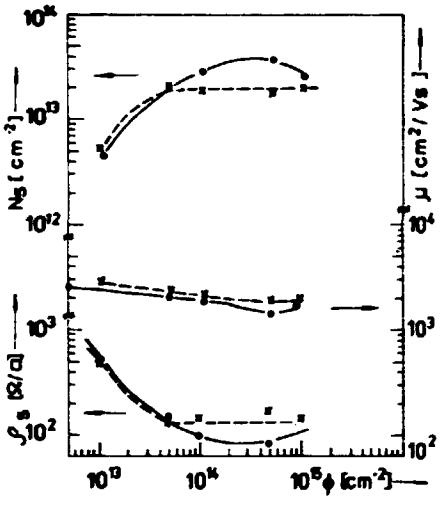

Fig. 1: Dose dependence of the sheet carrier concentration, mobility and sheet resistivity.
T_{impl} = room temperature
T_{impl} = 200 °C
annealing : 900 °C, capless, 5s

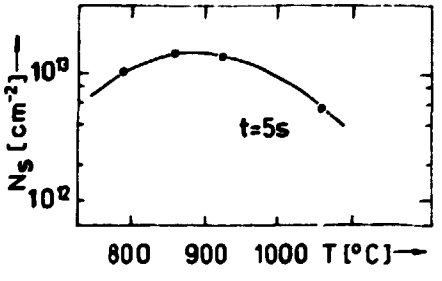

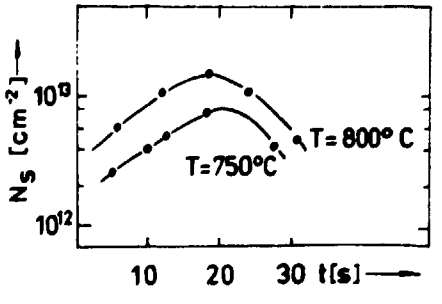

Fig. 2: Dependence of the sheet carrier concentration on the annealing temperature and the holding time.
($5 \cdot 10^{13}$ Si/cm^2)

FORMATION OF SCHOTTKY BARRIERS AND DEEP LEVELS

H. Morgenstern

Zentralinstitut für Kernforschung Rossendorf, Bereich KP

Metal-semiconductor systems show rectifying behaviour at suitable material pairing. The reason for this consists in the difference between the metal work function W_M and electron affinity W_χ of the semiconductor, which builds up a resulting electric field and therefore charge displacements in the contact region. The conductivity of the semiconductor is usually much lower than those of the metal, so that the charge displacement and the resulting bandbending will occur in the semiconductor. The width of the space charge layer can be varied by an additional external voltage and can be studied so. It is observed that the deposition of a metal on a silicon surface at enhanced temperatur will lead to a reaction between both materials resulting in the formation of silicides. The composition will possibly vary from a metal-rich silicide at the metal side to a silicon-rich one at the semiconductor side /1/, /2/. During this reaction deep levels are formed in the metal region of the semiconductor. A suitable material combination is the system molybdenum silicon. The process for the preparation of the structure (Fig. 1) is the following: P implantation 50 keV, 10^{15} cm^{-2}, activation 600 °C, 30 min, N_2; anodic oxidation for 100 nm oxide, annealing at 500 °C, 30 min, N_2; after oxide removal back contact by evaporation of aluminium, annealing at 450 °C, 20 min, N_2; front side oxide structurization by photolithography, evaporation of Mo (30 nm) at different substrate temperatures (400...200 °C).

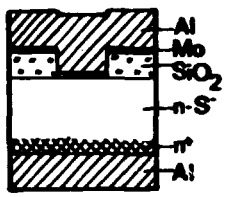

Fig.1: Cross section of Mo -n-Si structure

Results: Current-voltage measurements show the diode behaviour of the structure. It is visible (Fig. 2) that the substrate temperature during the Mo evaporation influences the shape of the curve. Higher temperatures (400...250 °C) give lower forward and reverse currents than the lowest (200 °C). Barrier height measurements give information about a possible variation of the internal structure of the barrier. Fig. 3 shows the results: A weak decreasing of the barrier height for decreasing temperature is noticable. DLTS measurements presents Fig. 4. With decreasing temperature the number of levels also decreases. Some levels seem to be typically for the

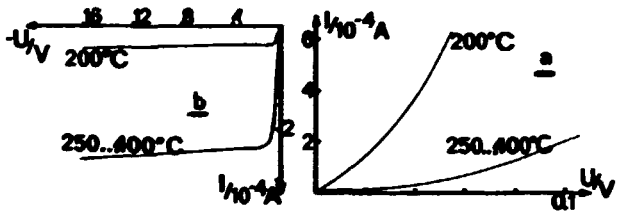

Fig.2: Current-voltage characteristics in forward (a) and reverse (b) direction

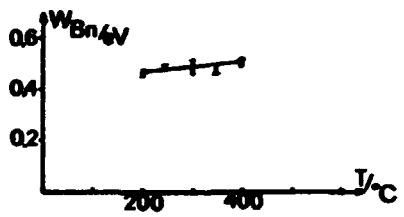

Fig.3: Variation of barrier height versus substrate temperature

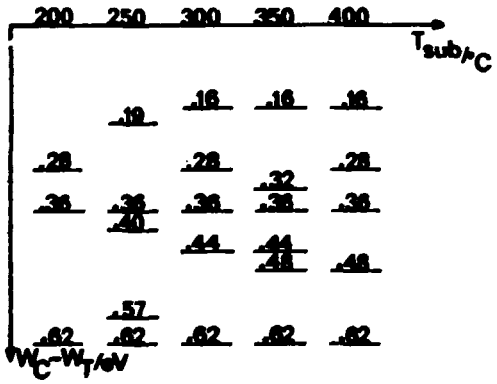

Fig.4: Deep levels in the Mo-n-Si structure at different substrate temperatures

barrier (0.28 eV; 0.36 eV; 0.62 eV), the other one are only traceable at certain temperatures. The level at 0.57 eV appears only after forward current stress of the structure. The capture cross sections lie between 10^{-15} and 10^{-18} cm^2; except the level at 0.19 eV, which has one of 10^{-13} cm^2. Densities of the levels are high, from 10^{14} to 10^{16} cm^{-3}. All levels are of donor type.

R e f e r e n c e

/1/ Asilova, S.P., Budberg, P.B.; Diagrammy sostojanija metalličeskich sistem 17(1971), Vsesojuznij institut naučnoj i techničeskoj informacii, Moskva

/2/ Thin films- Interdiffusion and reactions, ed. J.M. Poate, K.N. Tu, J.W. Mayer, John Wiley and Sons, New York

MINORITY CARRIER LIFETIME IMPROVEMENT OF HIGH RESISTIVITY NTD-SILICON AND ITS APPLICATION FOR COUNTING DETECTORS

L. Bischoff
Zentralinstitut für Kernforschung, Rossendorf, Bereich KF

High resistivity FZ-p-Si (ϱ_p = 2...5 kΩcm, τ = 0.5...1 ms) was used to produce n-Si with $\varrho_n \leq 100$ kΩcm by the Neutron Transmutation Doping technique. Lattice defects, caused by the fast neutrons from the nuclear reactor as well as impurities (heavy metals) inside the crystal and/or impurities diffusing into the crystal and its electrical activation during the annealing lead to a strong decrease of the minority carrier lifetime (MCL). Propper is to use gettering techniques to increase the MCL again. The results of these investigations are shown in Table 1.

Table 1
Results of the gettering investigations
∂-sample thickness; τ_{NTD}/τ_p-MCL-ratio of NTD-Si to p-Si

process	∂/mm/	τ_{NTD}/τ_p /%/	remarks
standard annealing	all	15...35	
ion implantation of Ar^+ and annealing at 600 °C	≤ 1 ≤ 2	~ 100 70...80	technology is very expensive
Ar^+-Impl. and HCl-oxidation at 1100 °C	~ 2	~ 80	technology is very expensive
HCl-oxidation at 1100 °C	~ 2	~ 65	out diffusion effects of phosphorous
600 °C-annealing and HCl-oxidation oxidation at 1000 °C	1...2	50...70	good compatibility with the technology
2-step annealing a) 750 °C, 2 h, N_2 b) 650 °C 8 h, N_2	≤ 1	40...80	long time process

From this NTD-Si (ϱ_n = 2...50 kΩcm) detectors with sensitive areas of 0.5...3 cm^2 were manufactured. The energy resolution amounts to FWHM = 15...40 keV for α-particles and ≳6 keV for 60 keV-γ-rays, respectively. These detectors were tested in transmission- and backscattering arrangements for high energy electrons for industrial applications. The maximum possible irradiation dose for spectrometric detectors depends on the demands of the measuring task and amounts to 5...50 · 10^{12} cm^{-2} for electrons and 2...5 · 10 cm^{-2} for α-particles, respectively. For counting detectors these values increase of one to two orders of magnitude. A partial or even a complete annealing of the radiation damage could be observed at 400 °C, N_2, 30 min. Therefore a re-use of the detectors is possible.

Another application field of NTD-silicon with $\varrho \geq 10$ kΩcm, τ > 200 µs is its use as detectors for backscattered electrons with E ~ 30 keV in control and analyzing systems for microelectronic structures (scanning electron microscope, type ZRM 20, from Carl Zeiss Jena).

TWO-STEP-ANNEALING OF HIGH RESISTIVITY NTD-SILICON

L. Bischoff

Zentralinstitut für Kernforschung, Rossendorf, Bereich KF

The standard annealing process of high resistivity NTD-Si at 750 °C (2 h, N_2) leads to a decrease of the minority carrier lifetime (MCL) up to 65 %. A second long time annealing at T = 400...650 °C allows to increase the MCL for thin slices (d ≤ 1 mm) again /1/. The dependence of the ratio τ/τ_0 (τ after-, τ_0 before the 2nd annealing) on the temperature is shown in Fig. 1. A gettering effect was only measured on n-type-Si, which is caused by phosphorous centres working as drains for heavy metal atoms. At temperatures about 700 °C these phosphorous-heavy metal pairs dissociate again. The assumption of a phosphorous gettering is supported by two facts:

a) The decrease of the electrical active phosphorous concentration ΔN_p at temperatures of about 650 °C (Fig. 1).

b) No effect in p-type-Si, and so oxygen-related gettering effects can be excluded.

Because of the relative low diffusion constant of heavy metals at these temperatures very long annealing times are necessary, see Fig. 2. After 12...18 h a saturation of gettering efficiency is observed. The clearer effect at Iwamatsu /1/ can be explained by the higher P-concentration of his samples (/1/: CZ-Si, $N_p \sim 5 \cdot 10^{14}$ cm^{-3}; this work: $N_p \sim 1 \cdot 10^{12}$ cm^{-3}). The increased MCL and the related higher resistivity (correspondending to $\Delta N_p = 1...2 \cdot 10^{12}$ cm^{-3}) are stable at room temperature. During a following 400 °C-annealing (30 min, N_2) these parameters don't change. A 500 °C-annealing leads to a MCL-decrease to 80 %.

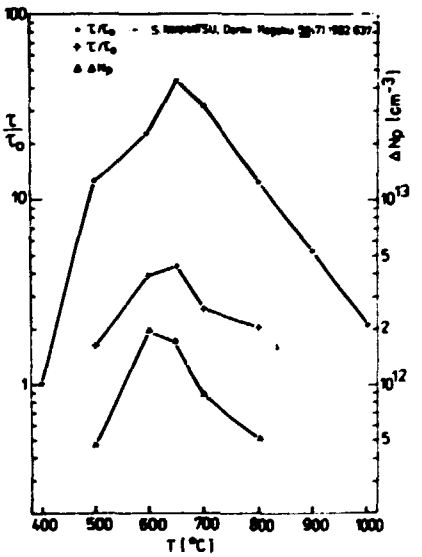

Fig. 1

Dependence of the MCL-ratio and the phosphorous concentration on the temperature
(t = 48 h /1/; t = 12 h this work)

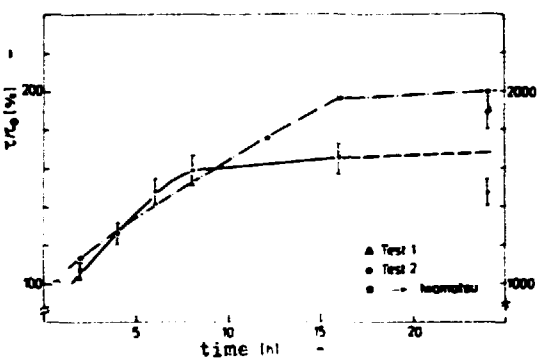

Fig. 2

Dependence of the MCL-ratio on the annealing time; T = 650 °C

Reference

/1/ Iwamatsu, S., Denki Kagaku 50(7) (1982) 637

FUNDAMENTAL STUDIES TO SENSORS MADE BY SILICON-ON-INSULATOR TECHNOLOGY

D. Schubert and U. Lorenz
Zentralinstitut für Kernforschung, Rossendorf, Bereich KF
W. Janschke and T. Uhlig
Zentrum für Forschung und Technologie Mikroelektronik Dresden

Sensitive elements of polycrystalline and zone melt recrystallized silicon enable an expansion of their operating temperature range and a reduction of their temperature dependence. Resistor structures were used to study the effect of thermic and mechanic signals. The spectral photoresponse was measured at the diodes /1/.
The temperature coefficients of resistance α_R of mono-, polycrystalline and recrystallized silicon is shown in Fig. 1. The sign and the value of α_R of polycrystalline silicon can be adjusted by the dopant concentration. Resistor films of silicon-on-insulator can be used up to much higher temperatures (500 °C). The longitudinal strain gauge factor K_L (resistors in direction of strain) of polycrystalline silicon is by a factor 2 to 3 less than that of monocrystalline material (Fig. 2). The transverse gauge factor K_T is even much less. The K_L- and K_T-factors of recrystallized silicon films with /100/-oriented surface and resistors in /110/-direction correspond to that of monocrystalline silicon (Fig. 3). Fig. 4 shows the spectral photoresponse of a diode with a small sensitive area (0.05 mm^2) on a 0.5 µm thick polycrystalline silicon film (distance of contact strips: 20 µm). By the increasing of the operating voltage U the dark leakage current is raised much more than the photoresponse.
The experimental studies enable to design temperature, rate of flow, pressure and radiation sensors /2/.

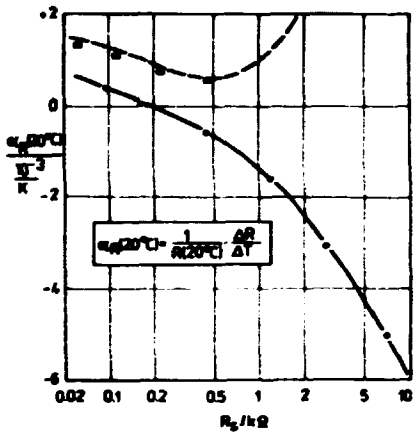

Fig. 1
Temperature coefficients α_R as functions of sheet resistance R_S
----- mono, -·-·- poly., ▭ recryst. Si

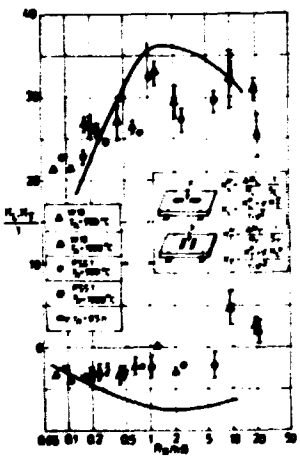

Fig. 2
Gauge factors K as functions of polycrystalline Si

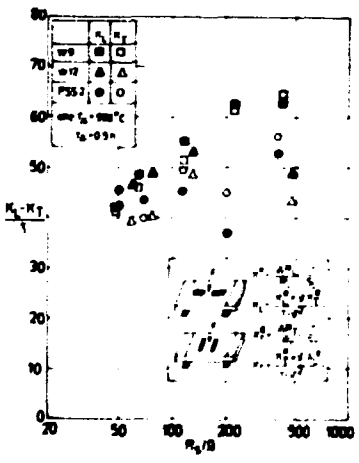

Fig. 3
of sheet resistance R_S of recrystallized Si

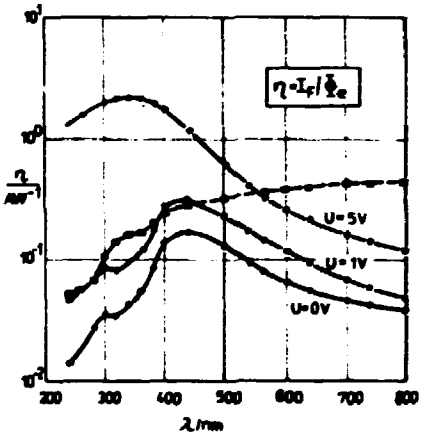

Fig. 4
Photoresponse η as a function of the wavelength λ of a polycrystalline Si diode

References

/1/ Schubert, D., U. Lorenz, Proc. 10. IMEKO World Congress, Prague, April 1985
/2/ Schubert D. et al., Proc. 19. Fachkolloquium Informationstechnik, Dresden, Januar 1986

CONSTRUCTION AND PERFORMANCE OF A LARGE AREA ΔE-E SILICON DETECTOR TELESCOPE

M. Deutscher, R. Förster, G. Mende, H.-G. Ortlepp and W. Seidel
Zentralinstitut für Kernforschung, Rossendorf, Bereich KF

For future experiments with the spectrometer DEMAS /1/ a ΔE-E silicon detector arrangement is necessary in order to measure high-energetic charged particles in addition to the heavy fragments. A first variant of such a telescope has been realized. It consists of a 0.2 mm thick ΔE detector and a 2 mm thick Si(Li) total absorption detector. The diameter of the Si-slices and of the sensitive areas amount to 51 and 45 mm, respectively.

The thin detector was prepared using 1000 Ωcm n-type silicon*). Both surfaces were polished as usually in the microelectronic technique**). It results in a microinhomogeneity within 20 nm for both plane surfaces. A parallelity deviation of 5 % was measured by electron transmission spectroscopy. The ion implantation has been used for doping the junction and the accumulation layers. A 100 nm thick thermal oxide layer serves for the edge protection.

The base material*) of the Si(Li) detector consists of dislocation free p-type silicon with a resistivity of 200 Ωcm and a minority carrier live time of 0.2 ms. The cross section of a typical detector is shown in fig. 1a. The drift proceeded under following conditions: Temperature: 110 °C, reverse voltage: 120 V, drift time: 170 hours. Fig. 1b shows the obtained current voltage characteristic. A minimum carrier life time of 1 ms has been estimated from it neglecting the diffusion- and surface contributions to the junction current.

With 5.5 MeV α-particles an energy resolution of 120 keV was obtained. A first test experiment has been performed at the external beam of the heavy ion cyclotron U-300 of the JINR, Laboratory of Nuclear Reactions, in Dubna. The self-supporting ^{197}Au target was bombarded in the reaction chamber of the spectrometer DEMAS by ^{12}C ions of 83 MeV energy. The ΔE-E telescope was located 21 cm apart from the target under 15° forward angle, covering a solid angle of 36 msr. A 150 μm thick Al absorber was placed in front of the telescope in order to stop elastically scattered particles. The standard electronics setup of the DEMAS spectrometer /2/ was used. Data were recorded event by event on magnetic disk for off-line analysis /3/. Fig. 2 shows the contour plot of the measured energy loss ΔE versus energy E for α, t, d and p. The setup is able to distinguish unambiguously between α-particles and hydrogen ions.

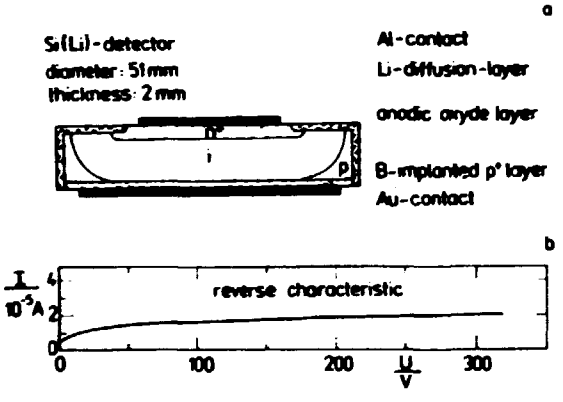

Fig. 1

a) Cross section of the large area Si(Li)-detector
b) U-I reverse characteristic of the detector

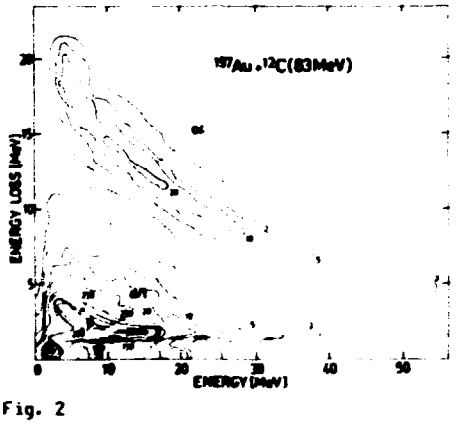

Fig. 2

Contour plot of energy loss versus energy for the system $^{197}Au + ^{12}C$ at 83 MeV incident energy

References

/1/ Gippner, P. et al., annual report 1983, ZfK-530 (1984) 115
/2/ Will, E. et al., Report JINR 13-85-754, Dubna (1985)
/3/ Fromm, W.D., W. Enghardt, annual report 1981, ZfK-488 (1982) 189

*) The material was produced by VEB Spurenmetalle Freiberg
**) D. Franco, Institut für Halbleiterphysik Frankfurt/Oder

CAPACITY MODEL OF A SILICON STRIP DETECTOR

M. Teichfuß and L. Bischoff
Zentralinstitut für Kernforschung Rossendorf, Bereich KP

Today silicon strip detectors are one of the most advanced electronic spatial resolution detectors, especially for photon and particle radiation. The minimum evidential energy of the position sensitive detector is determined by the energy resolution of the discrete detector elements. This talk discuss the capacity-voltage-characteristic of single diodes, which are influenced by their neighbours. Therefore a new capacity model (SDC-model)+ was developed and tested with ten strip detectors. The structure of three neighbouring diodes of such a detector is shown in Fig. 1. Nevertheless, the capacities are contained, which affect to the capacity-voltage-measurement at the kth diode. Corresponding to equation (1), the capacity C_k of this diode is greater than the capacity C_k^p expected by application of the plate-capacitor-model.

$$C_k = \frac{C_{kl} \cdot C_l^p}{C_{kl} + C_l^p} + \frac{C_{ki} \cdot C_i^p}{C_{ki} + C_i^p} + C_k^p > C_k^p \qquad (1)$$

The maximum parasitical capacity C_r^{max} of all remaining diodes was estimated with equation (2) on the understanding $C_{ki} \approx C_{kl} \approx C_{dd}$.

$$C_r^{max} \approx n \cdot C_{dd} \qquad (2)$$

with n - number of nearest neighbours

The capacity of one strip diode is then found to be

$$C_k = C_k^p + n\, C_{dd} \qquad (3)$$

with $C_k^p = \varepsilon \cdot A_k / d_k \qquad (4)$

(A_k strip plane, d_k depletion layer depth)

C_{dd} depends on the diode geometry. The model of two parallele half-cylinders (corresponding to the form of the depletion layers) has been used to describe the capacity between strip diodes. By using CAUCHY-RIEMANN's differential equations (6) the solution of the two dimensional potential equation $\Delta U(x,y) = 0 \qquad (5)$ can be found as a result of a function-theoretical problem, with conjugate complex potential V.

$$\frac{\partial V}{\partial y} = \frac{\partial U}{\partial x} \quad ; \quad -\frac{\partial V}{\partial x} = \frac{\partial U}{\partial y} \qquad (6)$$

Substituting C_k^p by equation (4) the diode capacity amounts to /1/:

$$C_k = \varepsilon\left[A_k / d_k + WLn / \ln(K_k / K_i)\right] \qquad (7)$$

with $K_k / K_i = r_i / r_k \; |(1-b+2a)/(1+b+2a)|$

$l = (r_i^2 - r_k^2)/b$

$2a = (l^2 + b^2 - 2(r_k^2 + r_i^2))^{1/2}$

r_i cylinder radius of the neighbour diode
r_k cylinder radius of the kth diode
b distance between two cylinder axis
L strip length

In the case of a single diode detector structure equation (7) is equivalent to the plate-capacitor-model. The SDC-model enables the description of the experimental obtained strip diode capacity (see Fig. 2). Further on, the model gives informations relative to the degree of the capacitive connection between the strip diodes, which are standing in need of application of special readout principles (capacitive charge division).

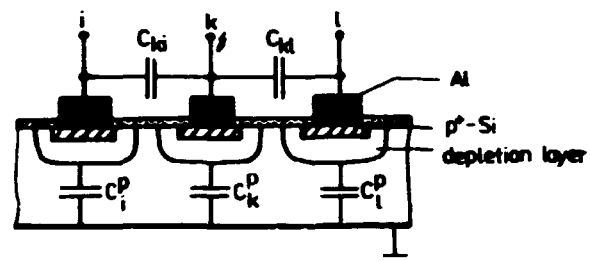

Fig. 1 Strip diodes structure with capacitive equivalent circuit

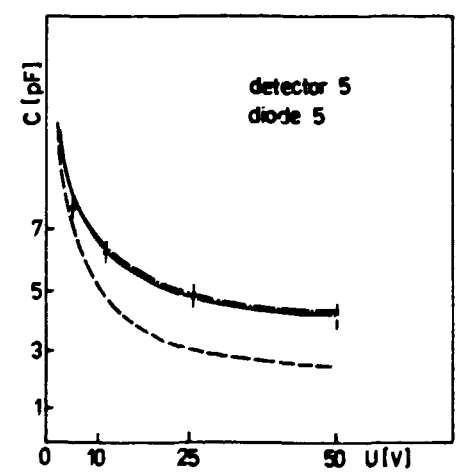

Fig. 2 Capacity-voltage-characteristics of a representative strip diode
—•—experimental capacity
---plate-capacitor-model
-·-SDC - model

Reference

/1/ Teichfuß, M.; Diploma project, Technical University Dresden (1985)

+ SDC = Strip Detector Capacity

PERFORMANCE OF SILICON NUCLEAR RADIATION DETECTORS

J. von Borany, L. Bischoff and B. Schmidt

Zentralinstitut für Kernforschung Rossendorf, Bereich KF

ZfK's semiconductor nuclear radiation detectors are ion implanted oxide passivated silicon p^+n - type diodes, produced by a special planar process.

PARAMETERS:

Active Area	:	10...1300 mm^2
Sensitive Depth	:	up to 300 µm; ≤ 1000 µm
Reverse Current	:	100 nA/cm^2/100 µm
Operating Voltages	:	+50...+200 V
Window Thickness	:	≤ 0.2 µm
Pulse Rise Time	:	≤ 5 ns
Time Resolution	:	≤ 200 ps for A ≤ 25 mm^2
Working Conditions	:	Room Temperature, Vacuum or Air
Mounting Configurations	:	BNC Rear Connector (P,T series)
		Microdot Side Connector (T series)

FEATURES AND APPLICATIONS:

- High resolution spectroscopy of charged particles, i.e. electrons, protons, deuterons, α - particles or heavy ions with a penetration depth ≤ 300 µm; ≤ 1000 µm*
- Counting measurements of charged particles with high counting efficiency
- Particle identification or any type of ΔE measurements
- Spectroscopy of soft γ- and X-rays at room temperature ($15 < E_\gamma < 100$ keV)
- Possibility of baking in vacuum systems or annealing after high radiation exposition

PROPERTIES OF DETECTOR SERIES

Active Area A / mm^2	Guaranteed Max. Resolution / keV α**	β***	Partially Depleted Detectors, w ≧ 100 µm Model -No.	Totally Depleted Detectors, w=300 µm Model - No.
10	13	6	P-0010-100-13	T-0010-300-13
20	15	8	P-0020-100-15	T-0020-300-15
50	17	10	P-0050-100-17	T-0050-300-17
100	20	13	P-0100-100-20	T-0100-300-20
180	25	18	P-0180-100-25	T-0180-300-25
350	30	25	P-0350-100-30	-
1300	unspecified<100keV		P-1300-100	-

Table 1: Standard detector series (w - depth of depletion layer)

Active Area A / mm^2	Material	Guaranteed Max. α-Resolution / keV**	· Remarks
50	NTD - Si	25	w = 0.5...1.0 mm
100	NTD - Si	30	w = 0.5...1.0 mm
280	NTD - Si	50	ring structure
40...590	FZ - Si	18...40	position-sensitive six - ring structure
21...56	FZ - Si	15	rectangular active area, special mount

Table 2: Special detector series*

*Restricted availability **Total system resolution FWHM for ^{210}Po, 5.304MeV alphas using standard ORTEC-electronics ***Beta resolution approximated by pulser width FWHM

TWO-DIMENSIONAL POSITION-SENSITIVE PHOTODETECTORS

B. Schmidt, H. Schott

Zentralinstitut für Kernforschung Rossendorf, Bereich KF

The two-dimensional position-sensitive photodetector (xy-PSPD) is a dual axis full area optoelectronic sensor that provides continuous analog position information (x,y) about a centroid of a light spot as the spot moves on the sensor surface. The sensor is fabricated by a proprietary ion implantation process [1] which gives very good linearity and uniformity. The dual axis position-sensitive detector consists of two layers: a high resistivity implanted p-layer with p^+-implanted contact areas and an i-layer in high resistivity silicon with implanted n^+-contact areas also on the front side. This used structure is based on the device structure proposed by NOORLAG and MIDDELHOEK [2].
As shown in Fig.1 in the equivalent circuit each position signal (photocurrents I_{x1},I_{x2} and I_{y1},I_{y2}) is only divided into two parts by the two resistive layers, and therefore, this type has a higher position detecting ability in comparison with tetra-lateral position-sensitive detectors, where four electrodes are placed on the top p-layer and one electrode on the underneath n-layer [3]. The photocurrent collected by the electrodes is inversely proportional to the distance between the incident light beam position (x,y) and the electrodes. The conversion formula is given in Fig.1, ,where I_{x1}, I_{x2} and I_{y1}, I_{y2} are the photocurrents collected by the electrodes. 2L and I_{ph} respectivily stand for the interdistances between the contacts and the total photocurrent.
The mean features and applications of the x,y-PSPD are the same as noted in [4]. The sensor is manufactured and available in chip form. The mean device parameters are given in Table 1.

Parameter	x,y-PSPD
Recommended Mode of operation	Photoconductive
Spectral range (10 % of peak)	400...1050 nm
Radiant responsivity at peak	$\geq 0.45\ A \cdot W^{-1}$
Nonuniformity of radiant responsivity	< 2 %
Position sensitivity	$50...60\ \mu A \cdot mW^{-1} \cdot mm^{-1}$
Position nonlinearity (from center to 75 % of center-contact distance)	≤ 1 %
Dark current (30 V bias)	≤ 200 nA
Rise time (10 % - 90 %, 50 Ω load, 30 V bias)	1...2 µs
Active area	10,0 x 10.0 mm^2
Chip dimensions	14.0 x 14.0 mm^2

Table 1:

Device parameters of the two-dimensional position-sensitive photodetector

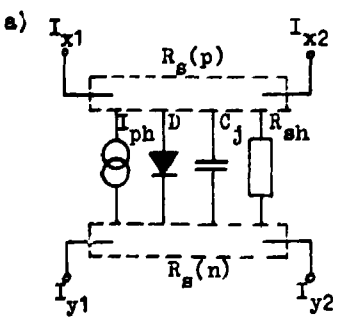

I_{ph}: photocurrent generator
D : ideal diode
C_j : pn-junction capacity
R_{sh}: shunt resistor
$R_s(p)$: p-layer resistivity
$R_s(n)$: n-layer resistivity

$$I_{ph} = I_{x1} + I_{x2} = I_{y1} + I_{y2}$$

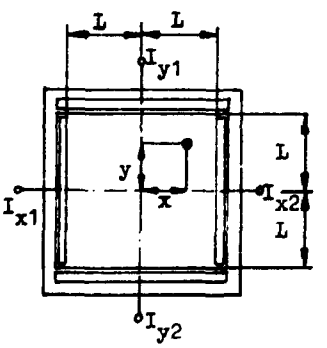

$$\frac{I_{x2} - I_{x1}}{I_{x1} + I_{x2}} = \frac{x}{L}$$

$$\frac{I_{y2} - I_{y1}}{I_{y1} + I_{y1}} = \frac{y}{L}$$

Fig.1: Equivalent circuit (a) and conversion formula (b) of the x,y-PSPD

Literature

[1] Schmidt, B.,and R. Ross, Sensors and Actuators 4 (1983) 439
[2] Noorlag, D.J.W. and S.M. Middelhoek, Solid State & Electr. Dev. 3 (1979) 3, 75
[3] Dünnebier, G. et al., Feingerätetechnik 30 (1981) 4, 170
[4] Schmidt, B. and H. Schott, this report p.58

ONE-DIMENSIONAL POSITION-SENSITIVE PHOTODETECTORS

B. Schmidt, H. Schott

Zentralinstitut für Kernforschung Rossendorf, Bereich KF

The one-dimensional position-sensitive photodetector (also called strip-photodiode - SPD) is an optoelectronic sensor that provides continuous position data of a light spot, which travels over its surface along one axis (x). The SPD consists of three layers: implanted p - layer, implanted n^+- layer underneath and i - layer in a high resistivity silicon substrat [1]. Incident light beam falling on the SPD is photoelectrical transduced in a photocurrent and detected by two electrodes on the p- typ resistive layer (Fig.1). Since the resistivity of the p - layer is uniform, the photocurrent collected by one electrode is inversely proportional to the distance between the incident light beam position (x) and the electrode. The conversion formula is given in Fig.1, where I_{x1} and I_{x2} are the photocurrents collected by the electrodes and 2L and I_{ph} stand for the electrode interdistance and the total photocurrent (proportional to the light beam intensity) respectively.

Predominant features and applications of this optoelectronic sensor are:

Features	Applications
• Continuous position signal	• Remote optical alignment
• Position accuracy independent on light spot size	• Machine tool alignment
• Electrically variable null point	• Vibration analysis
• Simultaneous power and position signal	• Process control
	• Guidance systems

The mean device parameters are given in Table 1. The SPD is manufactured and available in chip form.

Parameter	SPD
Recommended Mode of operation	Photoconductive
Spectral range (10 % of peak)	400...1050 nm
Radiant responsivity at peak	$\geq 0.45\ A \cdot W^{-1}$
Nonuniformity of radiant responsivity	< 2 %
Position sensitivity	$27.5\ \mu A \cdot mW^{-1} \cdot mm^{-1}$
Position nonlinearity (from center to 75 % of center-contact distance)	≤ 1 %
Dark current (30 V bias)	100 nA
Rise time (1o % - 90 %, 50 Ω load, 30 V bias)	0.5 µs
Active area	3.0 x 36.5 mm^2
Chip dimensions	5.0 x 40.0 mm^2

Table 1:

Device parameters of the one-dimensional position-sensitive photodetector

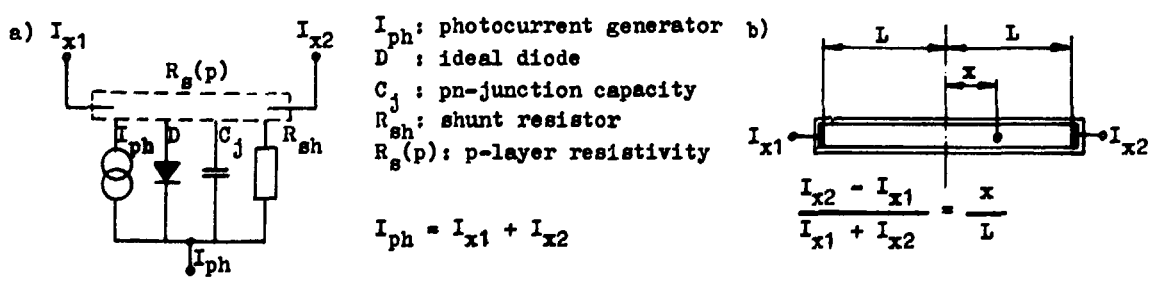

Fig.1: Equivalent circuit (a) and conversion formula (b) of the one-dimensional position-sensitive photodiode

Literature

[1] Schmidt, B. and R. Ross, Sensors and Actuators 4 (1983) 439

METHODS OF PRODUCING GRAIN BOUNDARY FREE SILICON STRIPES ON INSULATING SUBSTRATES

J. Matthäi and M. Voelskow
Zentralinstitut für Kernforschung Rossendorf, Bereich KF
K. Höppner and W. Scharff
Technische Hochschule Karl-Marx-Stadt, Sektion Physik/Elektronische Bauelemente
D. Gerisch and K.-H. Stegemann
VEB Zentrum für Forschung und Technologie Mikroelektronik Dresden

During the last few years fabrication of crystalline silicon on insulating substrates has gained much interest, since it promises many advantages for device applications in comparison to bulk silicon. The zone -melting recrystallization of large area thin silicon layers on insulating substrates is a favourable technique for producing SOI -structures.

In the present work, the zone-melting process was realized by preheating the sample up to 1100 K-1200 K using a set of 12 halogen lamps and moving the light stripe of an additional lamp in an elliptical mirror across the wafer with velocities of 0.5 mm/s to 2.0 mm/s. This process results in an ⟨100⟩-oriented crystalline layer with the typical subgrain boundary pattern ("feather structure"). For circuits with high packing density, i.e. with small active areas of elemental devices, it is necessary and sufficient to obtain grainboundary free areas at desired positions. In the paper, three methods of producing such areas will be presented.

One method to approach this goal, proposed by Geis /1/, is the transversale modulation of the temperature by an array of absorbing or reflecting stripes on the top of the encapsulated silicon layer. We used fotolithografically patterned stripes of $MoSi_2$. The distance between stripes and the width of them were varied from 10 µm to 150 µm. Since the reflection coefficient of molten silicon is greater than the reflection coefficient of the silicide hence the coolest areas are between the silicide stripes, and the grain boundaries are located under the stripes.

A transversale modulation of the temperature can also be obtained with patterned polycrystalline silicon stripes embedded in the encapsulating SiO_2 layer. In this case the different temperatures were obtained by additional heat production of the molten polycrystalline silicon stripes during solidification. As shown in Fig. 1 subgrain boundaries are located under the stripes.

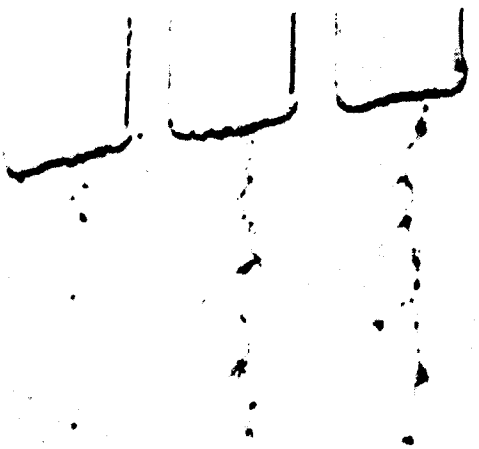

Fig. 1: Optical micrograph of a recrystallized silicon layer after Schimmel- etch

A third method of producing defect- free silicon areas on insulating substrates is the recrystallisation of long silicon stripes embedded in the system of the SiO_2/Si_3N_4 layers. Stripes with a width below 40 µm recrystallize to grain boundary- free monocrystalline silicon islands. If the width exceeds the typical distance between subgrain boundaries in large area recrystallized films, one obtain monocrystalline stripes containing subgrain boundaries.

Reference

/1/ H.W. Geis et al., Appl. Phys. Lett. 40, 158 (1982)

ELECTRICAL PROPERTIES OF MOS-STRUCTURES FABRICATED IN LAMP RECRYSTALLIZED Si FILM ON OXID

M. Sieber, K. Voelskow, H. Oertel

Zentralinstitut für Kernforschung Rossendorf, Bereich KP

The effects of process variables, such as preoxidation, HCl-oxidation and front surface damage gettering on electrical properties of MOS-structures in silicon-on-insulator, have been investigated.

The effect of preoxidation has been studied by growing a thermal oxid approximately 60nm and 120 nm thick in dry O_2 which was subsequently etched away. Some other samples were prepared only by chemical cleaning of recrystallized silicon films.

In order to investigate the influence of front surface damage gettering argon was implanted at a dose of 10^{15} ions/cm^2 through the 50 nm thick SiO_2 into the recrystallized films. After annealing at 1000 °C for 60 min in N_2-atmosphere the implanted layer was removed.

Planar MOS-capacitors were fabricated by growing a 80 nm thick gate oxide in dry O_2 at 1000 °C with and without HCl on the approximately 0.44 µm thick recrystallized Si films. Al-gates and Al-contacts to the recrystallized Si were prepared by electron-beam deposition, photolithography and annealing in forming gas at 450 °C for 30 min.

The electrical characteristics of MOS-structures have been investigated using high-frequency and quasistatic capacitance-voltage (c-v)- measurement as well as by triangular voltage-sweep (TVS) at 250 °C and by Hall effect measurements.

Generation lifetime in recrystallized Si films have also been determined by the high frequency c-v characteristics derived in response to a triangular-voltage sweep /1/.

All these measurements indicate that the recrystallized Si exhibits an n-type conductivity. The doping concentration N_D in the film is $1.4 \cdot 10^{16}$ cm^{-3}, as evaluated from the ratio of high frequency depletion layer capacitance in inversion to oxid capacitance,

This high doping level is likely due to diffusion of contaminations from the oxide cap layer during the recrystallization.

The other electrical properties, such as the interface state density at midgap N_{ss}, the effective charge density at flat band N_{eff}, mobile ions density in oxid N_m, effective minority carrier lifetime $\tau_{g\,eff}$ and carrier mobilities μ_H, are summarized in Tab. 1.

Tabelle 1

Process	N_{eff} /cm^{-2}/	N_{ss} /ev^{-1}cm^{-2}/	N_m /cm^{-2}/	$\tau_{g\,eff}$ /µs/	μ_H /cm$^2 \cdot$ v^{-1}s^{-1}/
Chemical cleaning and O_2-oxidation	$5.6 \cdot 10^{10}$	$4.1 \cdot 10^{10}$	10^{10} ./. $8 \cdot 10^{10}$	0.1	750
Preoxidation and O_2-oxidation	$5.3 \cdot 10^{10}$	$4.0 \cdot 10^{10}$	10^{10} ./. $8 \cdot 10^{10}$	0.1	760
Surface damage gettering and O_2-oxidation	$5.3 \cdot 10^{10}$	$4.3 \cdot 10^{10}$	10^{10} ./. 10^{11}	<0.1	700
Chemical cleaning and 3 % HCl-oxidation	$4.6 \cdot 10^{10}$	$3.8 \cdot 10^{10}$	$\leq 10^{10}$	2.4	860 ./. 900
Preoxidation and 3 % HCl-oxidation	$4.6 \cdot 10^{10}$	$3.0 \cdot 10^{10}$	$\leq 10^{10}$	2.4 ./. 2.6	~900

These results show that the HCl oxidation is a very effective process for improving of electrical characteristics of MOS-structures, especially for achiving a high lifetime of minority carriers in recrystallized Si.

Reference

/1/ K. Taniguchi, Solid-State Electronics, vol. 21, pp 1057-1061

CHARACTERIZATION OF PECVD NITRIDE LAYERS

C. Bauer, D. Grambole, C. Heiser, F. Herrmann and W. Rudolph
Zentralinstitut für Kernforschung, Rossendorf, Bereich KF

Thin nitride layers (400 nm) were deposited on silicon wafers using the plasma enhanced CVD- technology (SiH_4 + NH_3 gas inlet). Hydrogen concentration, stoichiometry, density and refractive index of the layer material were studied by a suitable combination of nuclear methods as well as optical and mechanical measurements:

- the $^1H(^{15}N,\alpha\gamma)^{12}C$ resonance reaction at E_R= 6.84 MeV for H- concentration analysis and H- depth profiling / 1 /
- Rutherford backscattering / 2 / to obtain both stoichiometry N_{Si}/N_N and area density (N-at/cm^2) of the nitride layer,
- thickness measurements by means of Taylor-Hobson taly step, together with
- ellipsometry to get information about the refractive index.

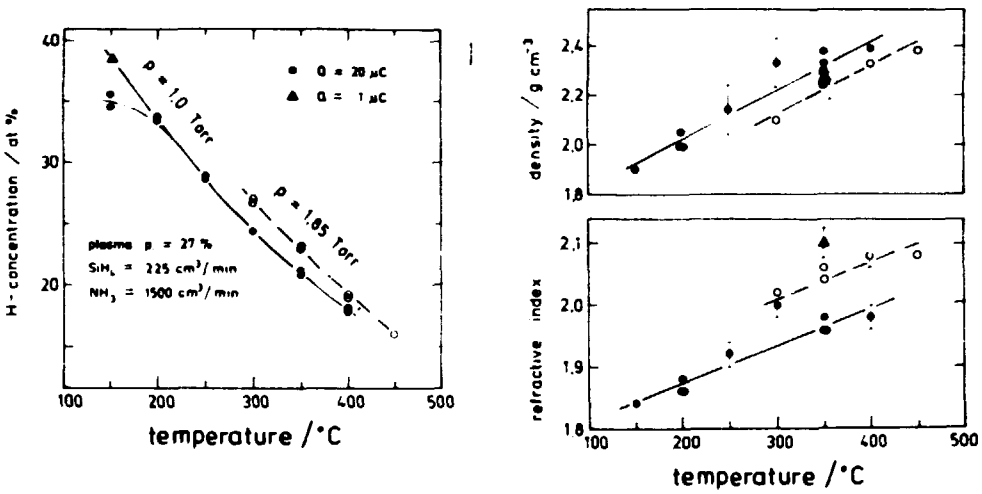

Fig. 1: Hydrogen concentration, density and refractive index of PECVD nitride layers as a function of the substrate temperature

As can be seen from Fig. 1 , substrate heating leads to a significant reduction of the average hydrogen concentration, whereas the stoichiometry was found to remain stable (N_N/N_{Si}= 1.15 and 1.32 for p= 1.85 and 1.0 Torr, respectively). With increasing temperature the hydrogen loss increases the density of the layer material, consequently the refractive index grows up. No other parameter variation as SiH_4 flow and plasma power , respectively, led to a comparable drastic change of the hydrogen concentration. A rise of the SiH_4 flow (100...300 cm^3/min) changes the stoichiometry (N_N/N_{Si}= 1.2...1.0) and increases the refractive index (n= 2.0...2.1).

References

/ 1 / Rudolph, W. et al., J. Radioanal. and Nucl. Chem. 83 (1984) 99
/ 2 / Chu, W.-K., Academie Press (New York,SanFrancisco,London) 1978

BORON DEPTH PROFILING BY THE $^{11}B(d,\alpha_0)^9Be$ REACTION

W. Rudolph, C. Bauer, C. Heiser and P. Urwank
Zentralinstitut für Kernforschung, Rossendorf, Bereich KF

At deuteron energy E_d= 1.55 MeV and detection angle ϑ = 160° we measured the particle spectrum due to deuteron bombardment of a 180 nm thick natural boron target and estimated the cross sections for the strong particle groups. For these strong transitions the yield functions were measured in the energy region E_d= 0.8...1.7 MeV. According to our results the $^{11}B(d,\alpha_0)^9Be$ reaction is best suited for boron depth profiling using deuteron induced reactions. A small plateau of the yield function is obtained for $E_d \approx$ 1.4...1.5 MeV and this reaction gives the greatest yield except the very broad $^{10}B(d,\alpha_1)2\alpha$ peak.
The $^{11}B(d,\alpha_0)^9Be$ reaction at E_d= 1.50 MeV was employed to measure boron depth distributions in 500 nm thick boron doped silicon oxide layers produced by plasma enhanced chemical vapour deposition.

CHARACTERIZATION OF BORON DOPED SILICON OXIDE LAYERS BY HELIUM BACKSCATTERING AND PROMPT NUCLEAR REACTIONS

W. Rudolph, C. Bauer, C. Döring, D. Grambole, R. Groetzschel, C. Heiser, F. Herrmann and P. Urwank
Zentralinstitut für Kernforschung, Rossendorf, Bereich KF

The oxide layers were produced by low-temperature and low-pressure CVD at 420 °C (deposition rate $\approx$ 100 nm/min). Different (B_2H_6 + Ar) admixtures to the (O_2 + SiH_4) flowing through led to different boron concentrations within the 500 nm thick layers deposited on thick silicon substrates.
The silicon and oxygen areal densities (in at/cm^2) and the O/Si ratios were determined by 1.7 MeV He backscattering, whereas the boron and hydrogen contents were measured using the $^{11}B(p,\alpha)2\alpha$ and $^1H(^{15}N,\alpha\gamma)^{12}C$ reactions, respectively. A 180 nm thick boron target and plastic foils with well known hydrogen content served as standards. In this way the layer compositions were determined in dependence upon the (B_2H_6 + Ar) flowing through and a full characterization of the main layer components was realized. Using special backings and optimum experimental conditions the concentrations can be determined with an accuracy of 1...2 % .

PLASTIC FOILS AS PRIMARY HYDROGEN STANDARDS FOR NUCLEAR REACTION ANALYSIS

W. Rudolph, C. Bauer, K. Brankoff, D. Grambole, R. Groetzschel,
C. Heiser and F. Herrmann
Zentralinstitut für Kernforschung, Rossendorf, Bereich KP

Plastic materials contain large amounts of hydrogen and their compositions are well known. However, these materials are not stable during ion bombardment and the hydrogen signal depends on the ion fluence applied in the measurement / 1 /. By means of a rotating sample holder we realized large irradiated foil areas (up to 10 cm^2) and measured the differential γ- ray yields y(Q) of the $^1H(^{15}N,\alpha\gamma)^{12}C$ resonance reaction (E_N= 6.5C MeV) at low current densities (1...2 nA/cm^2) in dependence upon the collected charge / 2 /.

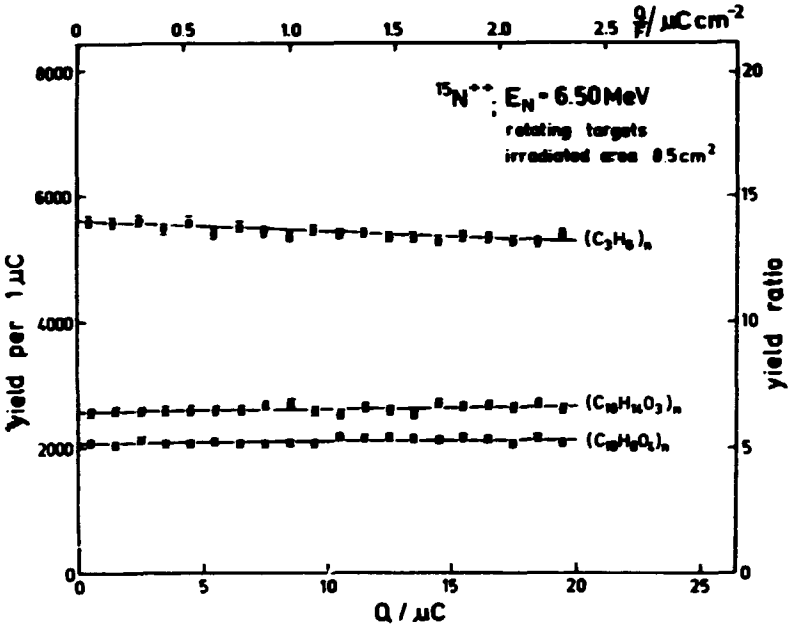

Fig. 1

Differential γ- ray yield curves measured at low $^{15}N^{++}$ fluences, Q/P $\leq$ 2.5 μOcm^{-2}, current density 1...2 nA/cm^2. Yield ratios relative to an a-Si:H sample containing 13.6 at% hydrogen.

In Fig. 1 the results are shown for the polypropylene $(C_3H_6)_n$, polyester $(C_{10}H_8O_4)_n$ and polycarbonate $(C_{16}H_{14}O_3)_n$ foils, respectively. As can be seen the γ- ray yields change only slightly at these measuring conditions and the initial yields y_o= y(Q=0), which correspond to the known foil compositions, can be determined with good accuracy. In this way the experimental errors can be kept well below the uncertainties inherent to the stopping cross section data / 3 / and the plastic foils are suitable as primary hydrogen standards for nuclear reaction analysis.

R e f e r e n c e s

/ 1 / Westerberg, L. et al.,Nucl. Instrum. Methods B9 (1985) 49
/ 2 / Rudolph, W. et al.,Proc. of the 7. Int. Conf. Ion Beam Analysis, July 1985
/ 3 / Ziegler, J.F. , Handbook of Stopping Cross Sections for Energetic Ions in all Elements, Vol. 5, Pergamon Press. 1980

50 kV FINE FOCUSED ION BEAM APPARATUS

A. Hoffmann, A. Kahn, U. Kreißig and F.K. Naehring
Zentralinstitut für Kernforschung, Rossendorf, Bereich KF

To study the angular distribution of ion emission from a Gallium liquid metal ion source an automatically driven device including a stepping motor was developed. Fig. 1 shows how the emitted angular intensity varies with the emission angle α. For ion currents greater than 10 µA we observed a small peak at the edge and another close to the axis of the distribution. The plateau becomes structurated because of growing protrusion at the apex of the liquid metal cone. These results agree well with other experiments /1/ and theoretical calculations /2,3/.

The ion micro beam laboratory equipment /4/ has been implemented. An ion source power supply (instability $< 10^{-4}$) allows to set both the extraction voltage, determining the ion current and the energy width of the beam, and the energy of the ions entering the focusing lens independently. For beam trimming and size measurements the edge method is used. The ion current profile is monitored by moving the beam across the meshes of an aluminium grid. The collected current behind the grid is displayed on the oscilloscope, see Fig. 2.

A solid state detector for target imaging by secondary electrons is prepared. An octupule ion beam deflector has been optimized for high uniformity of the electrical field within the deflector by a simple model calculation /5/. Fig. 3 shows the geometry of the device that gives ten times better uniformity compared to previous ones.

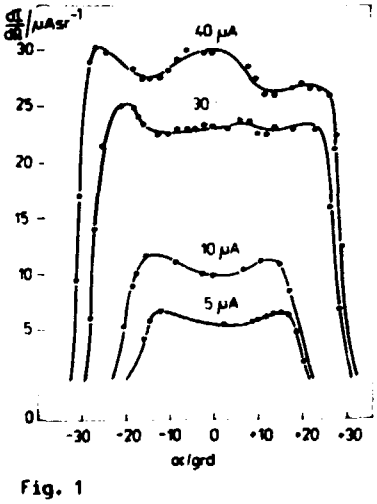

Fig. 1

Angular intensity distributions from Gallium liquid metal ion source at different ion emission currents

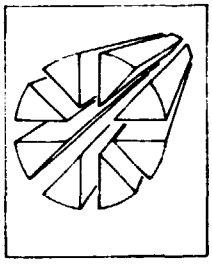

Fig. 3

Octupole ion deflector geometry

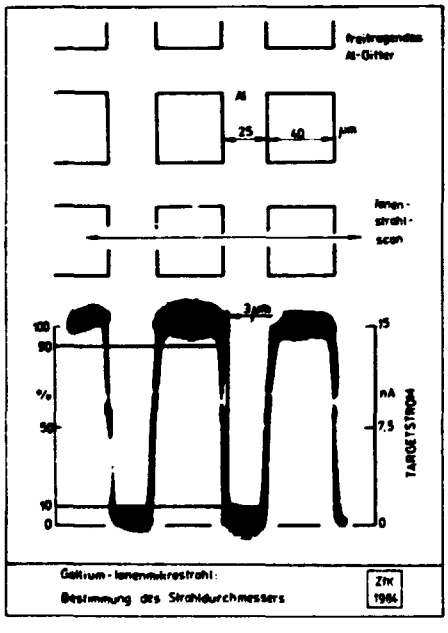

Fig. 2

Determination of the beam diameter at the edges of an aluminium grid structure

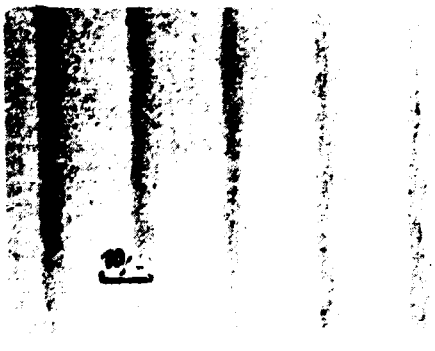

Fig. 4

Scanning electron micrograph of a lattice written by an ion beam into a Au layer on Si

The ion beam was used to write lines into a layer of 30 nm Au on a Si substrate. Fig. 4 is a SEM image of a typical detail caused by an ion beam of 10 nA Ga^+ with an energy of 30 keV. The smallest width is about 2 µm.

References

/1/ Wilkens, B., T. Venkatesan, J. Vac. Sci. and Technol. B1, 4 (1983) 1132

/2/ Kang, N.K., L.W. Swanson, Appl. Phys. A30 (1983) 95

/3/ Kingham, D.R., L.W. Swanson, Appl. Phys. A34 (1984) 123

/4/ Naehring, F.K., A. Kahn, ZfK-559 (1985) 93; Proc. Int. Conf. on Electron Beam Technologies (Varna 26.5. - 2.6.1985) Sofia 1985, pp. 523

/5/ Naehring, F.K., G. Otto, Phys. Status Solidi A94, 2 (1986)

ON GEOMETRICAL ABERRATIONS OF THIRD AND HIGHER ORDER IN TUBE LENSES OF FINITE LENGTH

R.R.Bartl
Zentralinstitut für Kernforschung, Rossendorf, Bereich KF

Aberrations of higher than 3rd order in rotational-symmetrical electrostatic systems usually are neglected, if the beam diameter inside the lens is one half or less of the diameter of the electrode boring. 3rd order aberrations are known for tube lenses, whose length L is large in comparision with the diameter D. For practical application tube lenses with finite L/D ratios and aberrations of higher order were investigated /1/.

For each lens geometry were calculated: the potential U(x,z) (using the method of Hoch et.al. /2/, a linear superposition of analytical elementary fields), the paraxial particle trajectory, the cardinal elements, the 3rd order aberrations (trajectory and value in the image plane) and the exact trajectory. The calculation of paraxial trajectory and 3rd order aberrations bases on the axial potential $\phi(z)$ and a power series in x, for the exact trajectory we had to compute the potential and its derivatives for every point of the trajectory.

It was shown, that the cardinal elements and aberration coefficients for ratios L/D ≥ 2 obtain the asymptotic values. For smaller L/D the focal length, the image distance and the magnification decrease, while the aberration coefficients increase. In the investigated range of starting distances from the axis x_o and starting slopes x_o' the spherical aberration term is dominating. Its coefficients at the image z_i are defined by the equation

$$x(z_i)=B_3(x_o')^3+B_5(x_o')^5+B_7(x_o')^7+\ldots$$

The values of B_5 and B_7 were extracted from the difference between exact calculated and 3rd order trajectories.

The figure1illustrates the ratio A of the aberrations of 5th and higher order to the aberrations of 3rd order at the image for various values of x_o' and L/D (curve parameter), $x_o = 0$. All points represent trajectories, whose maximal distance from the axis is smaller then one half of the lens radius.

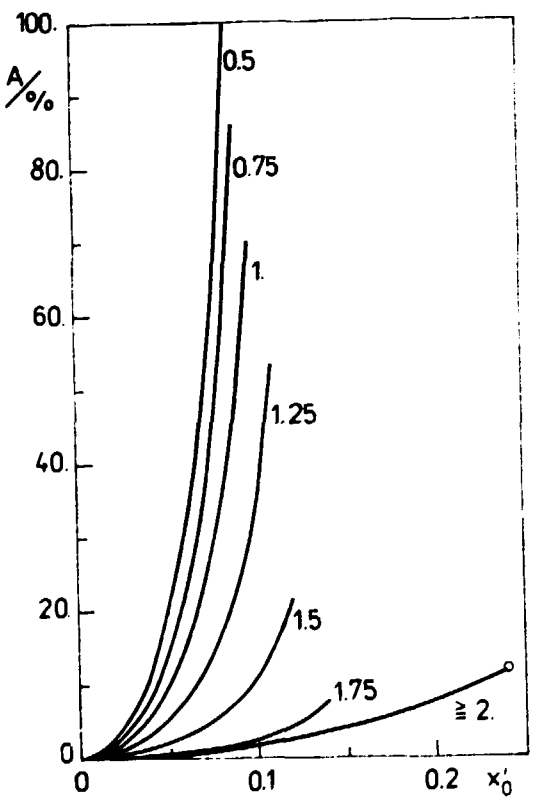

fig.1
Ratio A of the aberrations dependent on the starting slope x_o', curve parameter L/D

REFERENCES

/1/ R.R.Bartl, to be published in Exper. Technik Physik
/2/ H.Hoch et.al., Optik 50(1978)413

THE MAGNETIC FORM FACTOR OF IRON IN AMORPHOUS $Fe_{75}B_{25}$

W. Matz
Zentralinstitut für Kernforschung, Rossendorf, Bereich KF

The neutron diffraction intensity of an amorphous alloy in the ferromagnetic state contains nuclear and magnetic contributions. For amorphous $Fe_{75}B_{25}$ the latter contribution is given by:

$$\frac{d\sigma}{d\Omega}_{magn.} = \frac{2}{3}\left(\frac{e^2\mu}{2mc^2}\right)^2 \mu_{Fe}^2 \, f_{Fe}^2(Q) S_{Fe-Fe}(Q) \qquad (1)$$

Here μ_{Fe} is the magnetic moment, $f_{Fe}(Q)$ the magnetic form factor and $S_{Fe-Fe}(Q)$ the partial structure factor for the iron-iron atomic pairs, respectively.
The magnetic neutron scattering contribution for amorphous $Fe_{75}B_{25}$ was determined as the intensity difference from measurements without and with a saturating magnetic field parallel to the scattering vector $\vec{Q}$. The partial structure factor $S_{Fe-Fe}(Q)$ was estimated from the results of neutron and X-ray diffraction experiments on this material [1]. The magnetic moment of iron at room temperature can be deduced from Mössbauer spectroscopy and was taken to be $\mu_{Fe} = 1.79\ \mu_B$ [2].
According to [3] the magnetic form factor of iron can be given in a parametrized form. Introducing a width parameter W [4], which accounts for the broadening of f(Q) in the amorphous material, one gets:

$$f_{Fe}(Q) = 0.3854 \cdot \exp(-0.08517\ WQ^2) + 0.6326 \cdot \exp(-0.3209\ WQ^2) - 0.0173 \qquad (2)$$

The magnetic cross section of equ. (1) was fitted to the experimental magnetic intensity (points in fig. 1) in order to estimate the parameter W in the magnetic form factor (2). The best fit (full line) was achieved for $W = 0.9 \pm 0.03$. In fig. 2 the corresponding magnetic form factor of iron in amorphous $Fe_{75}B_{25}$ is compared with the magnetic form factor of pure iron. The width parameter $W < 1$ indicates a tendency of 3d-electron localisation for iron in amorphous $Fe_{75}B_{25}$. This result is consistent with observations for other amorphous alloys [4,5].

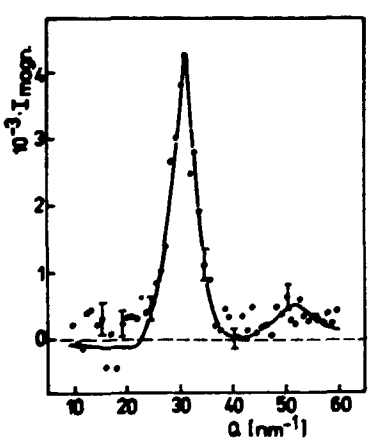

Fig. 1
Experimental magnetic neutron diffraction intensity (points) and calculated intensity using equations (1) and (2) (full line)

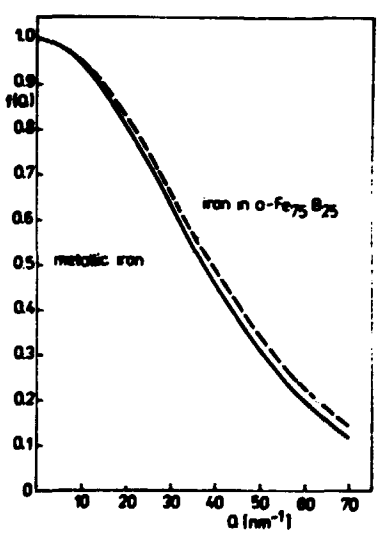

Fig. 2
Comparison of the magnetic form factor of iron in metallic iron (full line) and iron in amorphous $Fe_{75}B_{25}$ (dashed line)

References

[1] Matz, W. et al., Gemeinsamer Jahresbericht 1983, ZfK-530 (1984) p. 64
[2] Matz, W., H. Hermann, subbmitted to Phys. Status Solidi
[3] Lisher, E.J., J.B. Forsyth, Acta Crystallogr. A27 (1971) 545
[4] Bletry, J., J.F. Sadoc, J. Phys.F5 (1975) L110
[5] Wu Guan, N. Cowlam et al., J. Phys. 43, C7 (1982) 71

METHODICAL INVESTIGATIONS VIA TEXTURE OF ROCK SALT

M. Betzl and W. Voitus
Zentralinstitut für Kernforschung, Rossendorf, Bereich KF
A. Ertel
Karl-Marx-Universität Leipzig, Sektion Chemie, WB Kristallographie

In a former paper /1/ the importance of neutronographic texture analysis of rock salt was already underlined. It was referred to the coarse-graining of these rocks whereby in the case of usual sample dimensions the grain statistics is not sufficient.
As it could be demonstrated by methodical investigations the majority of samples cut show a grain size distribution with a maximum near 2 - 4 mm in diameter independent of the mineral deposit. About 22 % of grains are bigger than 5 mm and about 1 % is bigger than 10 mm. Taking as a basis for neutronographic texture investigations a minimum number of 1000 grains the minimum sample dimensions for the sphere-technique (approximated by a cube) should not fall below 30 x 30 x 30 mm^3. Due to the integral measurement of neutrons scattered in $2\theta_{hkl}$, the needed increasing of cross-section of the incident beam and the changes of cross-section of the scattered beam during the sample rotations for the pole figure scanning a larger detector aperture must be required. Fig. 1a shows the (200)-Halit-pole figure of the sample B4 measured with a BF_3-detector of 38 mm in diameter. In Fig. 1b the same pole figure measured by means of a ^3He-detector of 90 mm in diameter is given. The averaging of intensities due to the broadening of the detector slit can be clearly seen.
Additional improvements are possible by measuring of neighbouring sample ranges and the superposition of their results in composite pole figures. In general their is no significant improvement of superposition of more than two single measurements. Fig. 2a-c show two single (200)-pole figures and the composite pole figure obtained from the former ones.

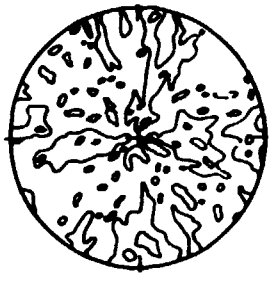

Höhenlinien: 1.0, 1.5
Meß-Nr.: 583391152
Halit (200) Probe B4

Fig. 1a

Höhenlinien: 1.0, 1.5, 2.0
Meß-Nr.: 584191152
Halit (200) Probe B4

Fig. 1b

Höhenlinien: 1.0, 1.5, 2.0
Meß-Nr.: 585071152
Einzelmessung zur Compositpolfigur
Halit (200) Probe 1.2.A(1)

Fig. 2a

Höhenlinien: 1.0, 1.5, 2.0
Meß-Nr.: 585091152
Einzelmessung zur Compositpolfigur
Halit (200) Probe 1.2.A(3)

Fig. 2b

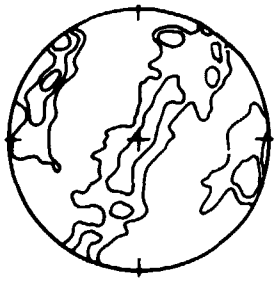

Höhenlinien: 1.0, 1.5, 2.0
Meß-Nr.: 585821152
Compositpolfigur Probe 1.2.A
Halit (200)

Fig. 2c

An additional increasing of the influence of coarse-graining can be expected by an oscillatory movement of sample performed during the measurement.

Reference

/1/ Betzl, M., Gemeinsamer Jahresbericht 1981, ZfK-488 (1982) 108

NEUTRONOGRAPHIC TEXTURE INVESTIGATIONS OF HALIT

M. Betzl and W. Voitus
Zentralinstitut für Kernforschung, Rossendorf, Bereich KF
A. Ertel
Karl-Marx-Universität Leipzig, Sektion Chemie, WB Kristallographie
P. Bankwitz and H. Kämpf
Zentralinstitut für Physik der Erde Potsdam, Bereich Geologie

The GDR has available large Halit-Sylvin-mineral deposits representing an important base of resources for chemical industry and agriculture. Behind the USSR and Canada the GDR holds the third place of the world hauling. Simultaneously during the last 10 years plans of secondary storage containments for various materials have become more and more important. In both cases the interest in texture analysis for investigating of salt tectonics and salt properties has increased. The Werra-Kali-Area, the Region of Northern and Southern Harz and the Clod of Calvörde are the main mineral deposits of the GDR.

First neutronographic texture investigations were performed at samples of the called regions with special consideration of the faulting pertubation zone of the mineral deposit of the Clod of Calvörde.
Fig. 1 and 3 show the (200)-Halit pole figure of the sample B2 of the Region of Southern Harz and of the sample 3.1 of the Clod of Calvörde, resp. In Fig. 2 the (220)-pole figure of the sample B6 of the Werra-Kali-Area is given. For all samples investigated a (100)-fibre texture can be observed (Fig. 1,3). Only the tectonically strongly deformed sample B6 of the Werra-Kali-Area additionally shows a (110)-fibre texture (Fig. 2). Especially considering the examples of Fig. 1 and 3 it must be concluded that a transformation of the corrected pole figures from the coordinate system of measuring into those of the place where the sample was cut (topographical system) must be carried out before analysing the data by calculation of the three-dimensional orientation distribution function. Only when this step is done the results obtained for the different regions can be compared among one another. The hitherto existing investigations of the mineral texture of Halit give rise to the following conclusions:

1. For all of the three regions a (100)-fibre texture can be universally observed. Therefore a planar deformation texture should exist.
2. The texture do not turn with the layered material (salt fault of the Clod of Calvörde) but it is comparable with a cleavage texture superimposed with the faulting structure and in general possessing about the same orientation.
3. Likely the obtained Halit-mineral textures are caused by recrystallization because the investigations of salt-dome samples /1/ show a (100)-fibre texture too. Therefore the recrystallization behaviour of rock-salt should have a comprehensive importance being not supposed until now and existing independent of the primary structure.

Höhenlinien: 1,0, 1,5, 2,0
Meß-Nr.: 584181152
Halit (200) Probe B2

Fig. 1

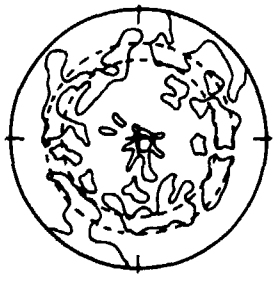

Höhenlinien: 1,0, 1,5
Meß-Nr.: 584161153
Halit (220) Probe B6

Fig. 2

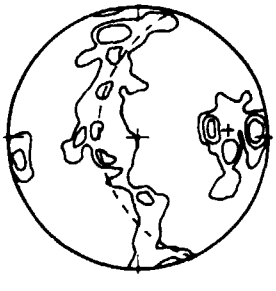

Höhenlinien 1,0, 1,5, 2,0
Meß-Nr 785101152
Halit (200) Probe 3.1

Fig. 3

References

/1/ Brokmeier, H.G., Thesis Clausthal-Zellerfeld (1983)

TEXTURE DEVELOPMENT IN PASS-ROLLING OF FCC METALS

P. Klimanek and K. Cyrener
Bergakademie Freiberg, Sektion Metallurgie und Werkstofftechnik
A. Mücklich and U. Scholz
Zentralinstitut für Kernforschung, Rossendorf, Bereich KF

In addition to recent texture investigations of hot-rolled steel rods produced by pass-rolling in a groove sequence of the type ROUND - OVAL /1,2/ the orientation changes occuring during pass-rolling of technical pure Cu and Al in groove sequences ROUND - OVAL and SQUARE - OVAL were measured by neutron diffraction. The plastic deformation was performed in one step (total strain $\varphi \approx 0.9...1.0$) with strain rates $\dot{\varphi} \approx 1\ s^{-1}$ at 293 K (cold-rolling; $T/T_s < 0.5$) or at T(Al) = 673 K and T(Cu) = 923 K, resp. (hot-rolling; $T/T_s \approx 0.7$). For quantitative analysis of the rod textures pole figures {111}, {200}, {220} and {311} of the sample material were used. The experimental technique is explained in /3/. Fig. 1 illustrates the choice of the sample related coordinate system. The results of the inv· igation give rise to the following conclusions:

- As expected from the deformation geomet. ıe texture of the pass-rolled rods is very inhomogeneous (see also /1,2/). In the regions near the surface . .rregular orientation distribution is observed, but in the midsection of the rods well-defined texture components can be found. As it follows from measurements of complete (i.e. four quadrants) pole figures as well as from orientation distribution functions, which were calculated without restricting suppositions concerning the sample-related coordinate system, these midsection textures can clearly be interpreted in terms of orthorhombic sample symmetry.

- In both groove sequences the midsection textures formed by cold-rolling at room temperature can be described by the main components
  {110}<001>, {110}<111> ... {110}<112>, {112}<111> and {112}<110>.
  Just these orientations were also observed after hot-rolling of austenitic stainless steel X8CrNiTi18.10 in the groove-sequence ROUND - OVAL /1,2/. The independence of the midsection textures of the groove geometry may be surprisingly at first, but can be understood because of the very similar deformation geometry near the rod axis (Fig. 1).

- After hot-rolling at $T/T_s = 0.7$ the textures of both sample materials and groove sequences include the cube component {001}<100>. Because of the fact, that the total strain was chosen sufficiently large and the material was quenched immediately after the deformation, the formation of this texture component should be a consequence of dynamical and postdynamical recrystallization.

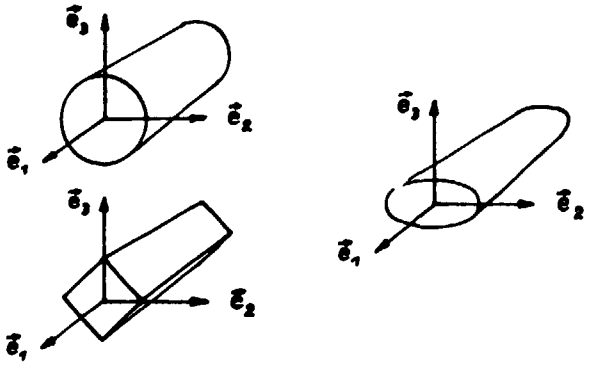

Fig. 1
Rod rolling geometry and sample coordinate system for groove sequences ROUND - OVAL

Although the texture of pass-rolling can be described by components {hkl}<uvw> partly occuring in connection with flat rolling too, they have to be considered as a special type of deformation textures (compare /2/). Together with /1,2/ the present paper gives a first contribution to a more systematic analysis of these textures, the practical importance of which becomes clearly increasing in connection with the development of modern rolling techniques.

References

/1/ Schubert, A. et al., Gemeinsamer Jahresbericht 1983, ZfW-530 (1984) 65
/2/ Schubert, A. et al., Proc. 7th ICOTOM, Nordwijkerhout/Holland 1984, S. 133
/3/ Kleinstück, K. et al., Kristall und Technik 11 (1976) 409
/4/ Bunge, H.J.: Texture Analysis in Materials Science. London: Butterworth 1982

TEXTURE DEVELOPMENT DURING COLD ROLLING OF (α + β)-BRASS

P. Klimanek and A. Kühl
Bergakademie Freiberg, Sektion Metallurgie und Werkstofftechnik
A. Mücklich and U. Scholz
Zentralinstitut für Kernforschung, Rossendorf, Bereich KF

The orientation changes occuring in cold rolling of (α + β)-brass CuZn39Pb with different microstructures (Table 1) were measured by means of the neutron diffraction technique described in /1/ and quantitatively analysed by use of orientation distribution functions, which were calculated from complete pole figures {200}, {220} and {311} of the f.c.c. α-phase and {200}, {211} and {321} of the b.c.c. β-phase by series expansion /2/. In all microstructures taken under investigation the spatial arrangement of the phases corresponded to that of a so-called dual phase structure. The plastic deformation of the material was carried out at room temperature with thickness reductions $\Delta\varepsilon$ = 5 % up to a maximum deformation ε = 50 %.
The results of the texture analysis can be summarized as follows:

- According to the prehistory of the alloy (Table 1) in all unstressed samples relatively sharp initial textures were found which can essentially be explained by recrystallization (α-phase) and texture inheritance (β-phase) occuring in the α-β transition during the annealing procedures. The connection between the textures of the phases is based on the KURDJUMOV - SACHS relationship $\{111\}_\alpha \parallel \{110\}_\beta$; $\langle 110\rangle \parallel \langle 111\rangle_\beta$ and the sharpness of the β-texture indicates significant variant selection. The main texture components of the phases are summarized in Table 2.

Table 1
Structure characteristics of the sample material

annealing structure 2 ←	initial state obtained by cyclic TMT	→ annealing structure 1	→ TMT structure
893 K/1.5 h quenching	rolling: RT/50 % annealing: 893 K/8 h slow-cooling	733 K/1 h quenching	rolling: RT/40 % annealing: 573 K/72 h quenching
v_β = 42.5 %	v_β = 8.1 %	v_β = 13 %	v_β = 30.7 %

TMT - thermomechanical treatment; v_β - volume fraction of the β-phase

Table 2
Texture components of the (+ β)-brass

α-phase			β-phase	
annealing structure	TMT structure	annealing structure		TMT structure
	A* = {011}⟨733⟩		A, A'	= {443}⟨338⟩
	Z_1A* = 011 344			
	B* = {338}⟨443⟩		B, B'	= {225}⟨110⟩
	Z_1B* = {011}⟨211⟩			
C* = {011}⟨100⟩	S* = {123}⟨643⟩	(C)		C = {001}⟨110⟩
Z_1C* = {112}⟨211⟩	d* = {011}⟨100⟩	(W)		W = {001}⟨100⟩

Z_1 - first twinning generation

- As in the case of the -phase the texture components of the β-crystallites also correspond to the rolling texture of singe-phase b.c.c. materials. But contrary to the α-phase, the orientation changes during the deformation are closely related to the microstructure of the sample material.

- As it can be expected for solid solutions with low SFE, in the plastically deformed α-phase a typical brass-type texture is formed. In addition orientations of the copper-tube can be found, whose orientation densities are higher than in single-phase brass and more significant in the annealing structures 1,2 than in the fine-grained TMT structure. The maximum sharpness of the α-texture is already observed after thickness reductions of about 20 %.

In comparison with the texture development in two-phase steels with micro-duplex structures /3,4/ the interrelations between the deformation textures of the phases in (α + β)-brass seem to be very weak. Such a behaviour is in agreement with the ideas concerning the plasticity of dual-phase structures.

References

/1/ Kleinstück, K. et al., Krist. Tech. 11 (1976) 409
/2/ Bunge, H.J.: Texture Analysis in Materials Science. London: Butterworth 1982
/3/ Klimanek, P. et al., Proc. 6th ICOTOM, Tokyo 1981, Vol. 2, S. 901
/4/ Klimanek, P. et al., Proc. 4th RISØ Int. Symp. Metallurgy and Materials Science, Roskilde (Dänemark) 1983, S. 339

SMALL-ANGLE NEUTRON SCATTERING ON HYDRATING CEMENT PASTE

F. Eichhorn
Zentralinstitut für Kernforschung, Rossendorf, Bereich KF
F. Häußler und U. Miehe
Technische Hochschule Leipzig, Sektion Naturwissenschaften

Hardened cement paste is the hydration product of cement powder. It consists of hydrated phases of clinker minerals, pores of different size, water and remaining unhydrated clinker phase particles.

By small-angle neutron scattering (SANS) compact samples can be investigated without special preparation because of the small absorption coefficient of the cement paste constituents. Using a double-crystal diffractometer with perfect crystals (neutron wavelength = 0.101 nm) for SANS measurements variation of the microstructure in the particle size region 30 nm ... 10 µm can be observed. For preparing the sample Portland cement powder of the type PZ 1/40 A was mixed with 38 % water by weight and then filled in a container of 6.8 mm thickness. The SANS intensity is given by

$$I_{SANS} \sim (\varrho_P - \varrho_M)^2 \left|F_P(\beta)\right|^2 \qquad (1)$$

$\varrho_{P,M}$ - scattering length density of particles and matrix, respectively, F_P - particle form factor.

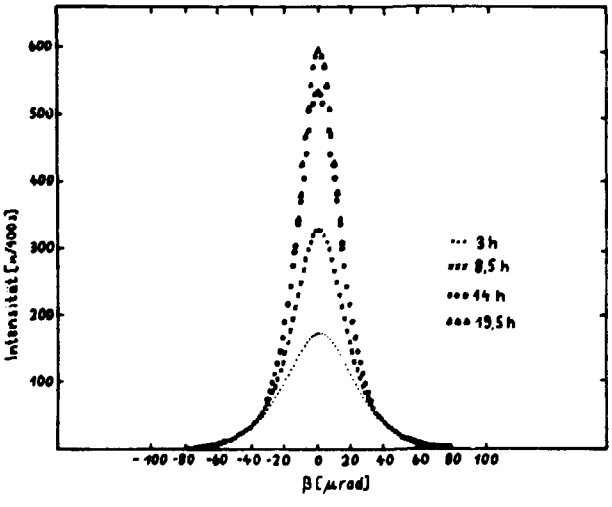

Fig. 1
Intensity of SANS from hydrating cement paste for different time after the beginning of hydration versus the scattering angle

Scattering curves of the cement paste for different time after the beginning of hydration are shown in Fig. 1. Their half-widths decrease during the first hydration day. Assuming spherical particles this corresponds to an increase of the particle diameter from 2.4 µm (3 h) to 3.6 µm (25 h). At the used water-to-cement ratio no capillary pores may grow up /1/. Therefore the observed effect in the early hydration state is caused by particles of clinker minerals. The generation of hydration products on the surface of the original clinker mineral grains is equivalent to an effective increase of the particle size. Moreover the integral SANS intensity decreases (Fig. 2), because the value of factor $(\varrho_P - \varrho_M)^2$ determining the intensity is reduced during the hydration. Immediately at beginning of the hydration this factor amounts to $20.6 \cdot 10^{28}$ m^{-2} taking into account water and the mean value of all cement phases. It reaches $6.1 \cdot 10^{28}$ m^{-2} in the completely hydrated state.

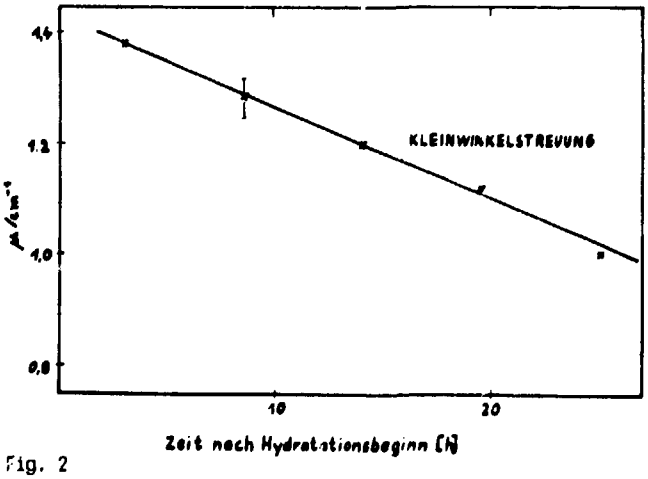

Fig. 2
Coefficient of SANS from hydrating cement paste versus the hydration time

Literature

/1/ Wesche, K.: Baustoffe für tragende Bauteile. Band 2. Wiesbaden

DEPTH DISTRIBUTION OF F, Na, AND P IN TOOTH ENAMEL MEASURED BY MEANS OF NUCLEAR REACTIONS

H.-E. Zschau, J. Vogt, and G. Otto
Karl-Marx-Universität Leipzig, Sektion Physik, WB Angewandte Kernphysik

Nowadays the application of nuclear methods for the determination of elemental concentrations is a growing field of research [1]. High resolution spectrometry of x-rays, γ-rays, and backscattered particles produced by ion beam bombardment of very different materials is used to measure lateral and depth concentration profiles of main and trace elements in the near surface region.

We continued our measurements [2] of the fluorine distribution in tooth enamel after application of fluorine containing drugs to prevent the teeth against caries. Also the knowlegde of P and Na depth distributions in a surface layer up to some hundred nanometers is helpful for a better understanding of demineralization processes during formation of caries cavities and the caries preventing activity of the drugs. In the interesting region up to 0,5 μm the fluorine depth profile was obtained by means of the narrow resonance (Γ = 2,5 keV) of the reaction $^{19}F(p,\alpha\gamma)^{16}O$ at a proton energy of E_p = 340 keV. The emitted γ-rays with energies of E_γ = 6.129 MeV, 6.916 MeV, and 7.115 MeV were used for the evaluation of the concentration values. The depth resolution of the profile was about 25 nm.

The phosphorus depth profile was measured using the resonance at E_p = 1148 keV (Γ = 4 keV) of the reaction $^{31}P\ (p,\gamma)\ ^{32}S$ (E_γ = 2237 keV) with a depth resolution of 65 nm and simultaneous the resonance reaction $^{23}Na\ (p,\alpha\gamma)\ ^{20}Ne$ (E_p = 1163 keV, $\Gamma \approx 5$ keV, E_γ = 1634 keV) was used for the determination of the sodium depth profile with a resolution of about 80 nm.

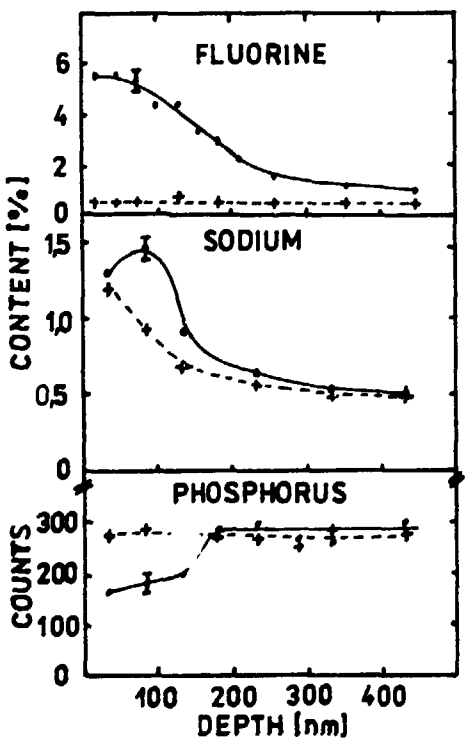

The obtained depth distributions of fluorine, phosphorus, and sodium (Fig. 1) in the outer surface of tooth enamel are helpful for dentists for the development and the optimization of the application of prophylactic treatments against caries.

[1] 3rd PIXE Conference, Heidelberg 1983 Nucl. Instr. and Meth. in Phys. Res. B 3 (1984).

[2] Wolf, U. et. al.: Jahresbericht 1984, ZfK - 559 (1985) 84

Fig. 1 F, Na, and P depth distributions of prepared tooth (full line) and an unprepared tooth (dashed line)

INVESTIGATION OF EPITAXIAL $(Ca,Sr)F_2$/GaAs HETEROSTRUCTURES BY RBS/CHANNELING TECHNIQUE

R. Flagmeyer, and B. Schumann,+
Karl-Marx-Universität Leipzig, Sektion Physik und Sektion Chemie+

Group II fluorides have received considerable attention as epitaxial insolators on semiconductors because of their properties like cubic structure, the good lattice match and the ease of evaporating stoichiometric films. The interest originates from a potential use for a three dimensional device stapeling. MBE growth of CaF_2, SrF_2 and BaF_2 and their mixed crystals on Si or GaAs substrates [e.g. 1,2] has already been reported. We presented first RBS/Channeling investigations of $Ca_{0.43}Sr_{0.57}F_2$ films on GaAs (100) which were deposited by a simple flash evaporation technique [3] [4]. Films with thicknesses from 10 to 250 nm were deposited in a high vacuum equipment ($p \approx 2 \cdot 10^{-3}$Pa) on chemo-mechanically polished GaAs substrates. Epitaxial growth was found in the substrat temperature range from 725 to 850 K.

Typical aligned and random backscattering spectra are shown in Fig. 1 a. The standard scattering angle of $\theta = 120^0$ gives good depth resolution and the Sr part of spectra appears as a "background-free signal" to characterize the film thickness and quality. For grazing exit geometry (Fig. 1 b) the surface depth resolution becomes better than 5 nm. In this way, surface minimum yields X_{min} were determined exactly behind the surface peak. Best values of 4,5 % and 10 % are found. Generally, the crystalline perfection increases with decreasing film thickness. SEM and TEM investigations yielded that cracking takes place at layer thicknesses exceeding about 100 nm. Cracks arise from strains caused by large differences in thermal expansion coefficients.

Grazing exit channeling is very sensitive to surface films on an epitaxial layer. We found area densities of $2 \cdot 5 - 3 \cdot 5 \cdot 10^{15}$ at.cm^{-2}(Sr) which point out disordered surface regions of 2 - 3·5 monolayers, resulting from oxidation and/or reconstruction. Furthermore, accordant with AES profiles RBS spectra (cp. Fig. 1 a) show a sharp transition from GaAs substrate to fluoride film within an interface region of 15 - 20 nm. Investigating depth and energy dependence of normalized minimum yield X(d), a strong increase of X(d) with increasing ion energy as well as a distinct decrease behind the interface has been observed. Dechanneling by edge dislocations or loops (R > 20 nm) and direct scattering from curved atomic rows [5] has been found to be proportional to $E^{1/2}$ and E^1, respectively. Thus we assume that relative high dislocation densities in present films lead to strong dechanneling as well as direct backscattering of ions. From increase of $X(d) - X_{perf}(d)$ with depth we conclude dislocation densities up to 10^{11}.cm^{-2}.

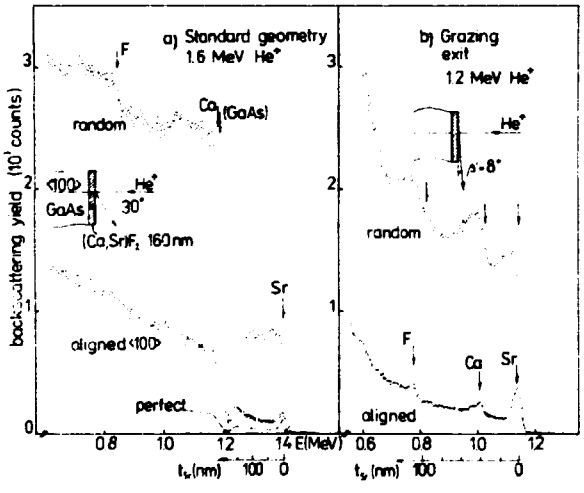

Fig. 1 RBS/Channeling spectra of an 160 nm thick $(Ca,Sr)F_2$ film on GaAs (100)

References

[1] Schowalter, L.J., et al.; J. Appl. Phys. 58 (1985) 302
[2] Siskos, S., Fontaine, C., and Munoz-Yague, A.; J. Appl. Phys. 56 (1984) 1642
[3] Flagmeyer, R., and Schumann, B.; phys. stat. sol (a) 93 (1986), in press
[4] Schumann, B., et al.; J. Cryst. Growth, to be published
[5] Wielunski, L.S., et al.; 11th Int. Conf. Atomic Collisions in Solids, Washington 1985, to be published in Nucl. Instrum. Meth. Phys. Res. B

MICROHARDNESS OF PROTON BOMBARDED GAP SINGLE CRYSTALS

C. Ascheron, H. Neumann, G. Dlubek+, R. Krause+

Sektion Physik, Karl-Marx-Universität Leipzig
+Sektion Physik, Martin-Luther-Universität Halle

Proton bombardment of III-V compound semiconductors has been shown to provide effective electrical and optical isolation in device fabrication /1/.
The irradiation induced changes in the mechanical properties of proton bombarded semiconductors may influence the operational performance and lifetime of the devices /2/.
We report first results regarding the influence of proton bombardment on the microhardness of GaP single crystals.
On (111) and (100) GaP, irradiated with $(0.1-8)\cdot 10^{17}cm^{-2}$ 1 MeV H^+ ($R_p \approx 13\,\mu m$) at 300 K and annealed at 720 K, a load of 20 g was applied for a period of 15 s. Since the indentation depths were far below the penetration depths of the protons, the measured microhardness is characteristic of the surface region. On unimplanted GaP we found a microhardness of 7.6 GPa for the (111) face and of 8.0 Pa for the (100) face. This trend in hardness anisotropy of GaP agrees with that reported for InP /3/. In implanted crystals within the error of our measurements no anisotropy could be revealed. With rising fluence the microhardness increases as shown in fig. 1. For both faces at the fluences studied maximum microhardness changes of about 50 % are observed.
Since GaP is elastically strained by the proton bombardment induced defects and since strain is nearly proportional to damage density /4/ the relation of changes in microhardness to strain is of interest. By comparing fig. 1 a with fig. 1 b it can be seen, that both functions increase sublinearly with fluence and exhibit a tendency to saturation behaviour at higher fluences. The correlation between hardness changes ΔH and lattice strain $\Delta d/d$ can roughly be described by $\Delta H \sim \sqrt{\Delta d/d}$. On He^+ bombarded steel /5/ an according dependence of ΔH on the dislocation loop density has been observed. Within the error of our measurements the given relation holds also for the annealing behaviour.

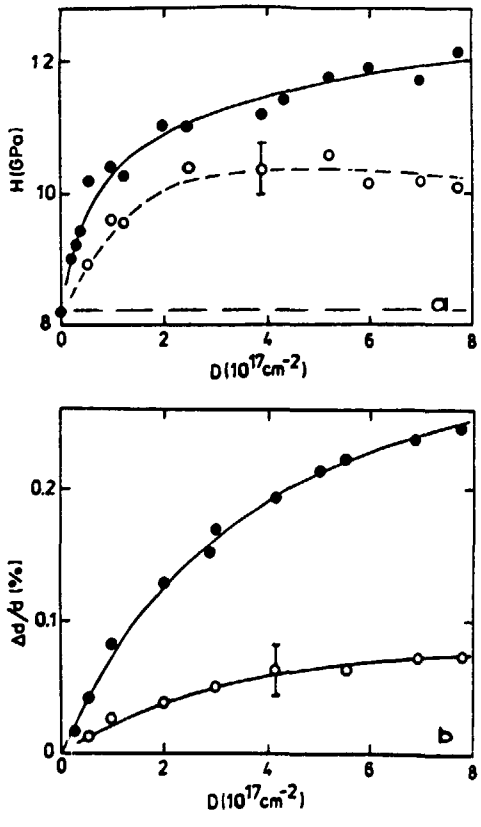

Fig. 1: Fluence dependence of the microhardness H (a) and of the strain $\Delta d_{111}/d_{111}$ of (111) GaP immediately after bombardment at 300 K (•) and after annealing at 720 K for 30 min (o)

References

/1/ R.C. Newman, J. Woodhead, Rad. Eff. 53, 41 (1980)
/2/ D.Y. Watts, A.F.W. Willoughby, J. Appl. Phys. 56, 1869 (1984)
/3/ D. Brasen, J. Mater. Sci. 11, 791 (1976)
/4/ C. Ascheron et al., Phys. Stat. Sol. A 92, 169 (1985)
/5/ K. Shiraishi, K. Fukai, J. Nuc. Mat. 117, 134 (1983)

HYDROGEN DEPTH PROFILING IN IMPLANTED GaP USING ELASTIC RECOIL DETECTION

D. Lehmann and C. Ascheron
Karl-Marx-Universität Leipzig, Sektion Physik, WB Angewandte Kernphysik

Hydrogen isotopes, especially ^1H, are very difficult to detect in nondestructive elemental analysis. With the usual RBS method it is rather complicated to measure H distributions because of the low mass. Nuclear reactions, commonly used to profile H isotopes, require heavy-ion beams of several MeV kinetic energy in the case of ^1H. In the last decade a new method has been developed, experimentally based on the ordinary RBS equipment. The so-called elastic recoil detection (ERD) [1] uses the recoil of low-mass atoms from the sample after an impact with heavier energetic projectiles.
We measured the depth distribution of hydrogen in proton implanted GaP by means of ERD using 1.5 MeV He^+ ions. The experimental arrangement is shown in fig. 1a. Since only depths up to 250 nm can be profiled under these conditions, the implanted sample was bevelled by sputtering with 1 keV Ar ions. In this way the measurable depth interval was increased (from 250 nm to 3 µm) at the expense of the depth resolution (reduced from about 25 nm to 160 nm). Fig. 1b shows ERD spectra obtained at different positions on the bevelled sample. Behind the sharp surface peak, which is mainly attributed to hydrocarbon and water contaminations, the spectra of recoiled protons increase with rising H content.

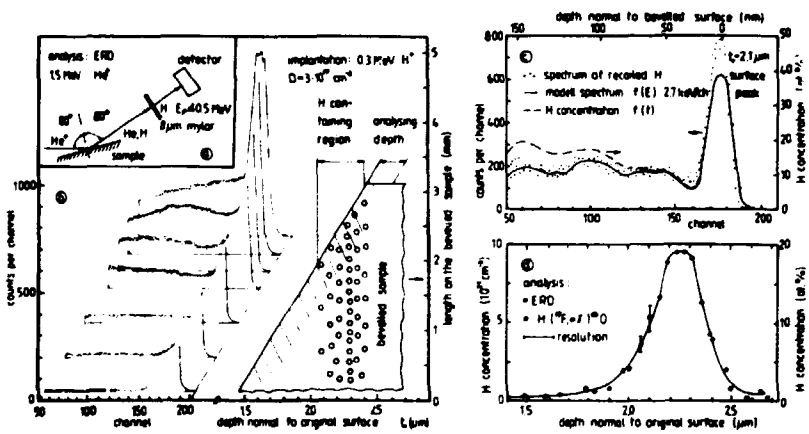

Fig. 1
Depth profiling of H implanted GaP using the ERD method

The hydrogen concentration profile was extracted from the measured spectra with an iterative modelling procedure, which consists of the following routines:
- computation of the concentration dependent energy-depth conversion in the H spectra;
- modelling of a theoretical spectrum with an initial H distribution and a recoil cross-section, deviating from the pure Coulomb case [2] ;
- convolution of the theoretical spectrum and its fit to the smoothed experimental one;
- extraction of a corrected depth distribution of hydrogen and
- start of the next iteration from the beginning.

3 to 4 iteration loops are enough to obtain reasonable agreement between experimental and fitted spectra (fig. 1c). Under the chosen conditions the sensitivity of the method is about 10^{15} H atoms/ cm^2 within a depth interval of 20 nm.
The combination of all spectra from the bevelled sample gives the implantation profile, which is shown in fig. 1d. The hydrogen distribution measured with the nuclear reaction technique on the same sample [3] is also included in fig. 1d. The good agreement between the two methods enables ERD to be used as a standard-free method for hydrogen profiling.

References

[1] L' Ecuyer, J. et al.; J. Appl. Phys. 47 (1976) 881
[2] Ingram, D. C. et al.; Nucl. Instr. Meth. B 6 (1985) 430
[3] Ascheron, C. et al.; Phys. Stat. Sol. A 89 (1985) 549

DEPTH RESOLUTION IN DIFFERENTIAL HALL-EFFECT MEASUREMENTS FOR SHALLOW IMPLANTATION PROFILES

B. Lukasch
Humboldt-Universität zu Berlin, Sektion Physik - Bereich Atomstoßprozesse der Festkörperphysik

For the differential Hall measurement of low energy ion implantation profiles in silicon below for example 10 keV implantation energy a stepwise removement of about 2 nm is necessary. In this paper possible depth resolution, even after a lot of stripping procedures by anodic oxidation is examined.
It is well known /1/ that layers, fully amorphized by implantation, recrystallize epitaxially with an atomically sharp interface. For the profile shown in Fig. 1 the interface of recrystallization has stoped at a critical concentration of foreign atoms of about 10^{21} As/cm^3 /2/. To prove the resolution of the method the so generated edge in the doping profile has been analysed.
Calibration of the stripping procedure has been made by epitaxially recrystallized As-implanted profiles, where fully activation appears and chemical profile is well known from RBS-measurement. The thickness of removed silicon after anodic oxidation and HF-stripping is given within an error of about 20 % by

$$t\ [\mathrm{nm}] = 1 + 0{,}25\ U_P\ [\mathrm{V}]\ ,$$

where U_P is the voltage drop between the bulk silicon and the electrolyte in the moment of oxidation stop. As electrolyte a solution of KNO_3 in ethylene glycol with 10 % water has been used. Within the given error the thickness of the layer seems to be undependent on structure of the silicon target and on current density witch has been varied strongly to realise oxidation times grater then 20 seconds.
Obviously a surface near layer of about 1 nm is deactivated by atmospheric oxidation within a few minutes. For all points in Fig. 1 shown in one row, no change in the integral Hall-Effect was visible. After the 20th step a deviation is visible but no differential evaluation was possible. But allready the next point reaches nearly the chemical As-concentration. Ooviously even after the 20th step of 1.5 nm removing the resolution is better then 3 nm.

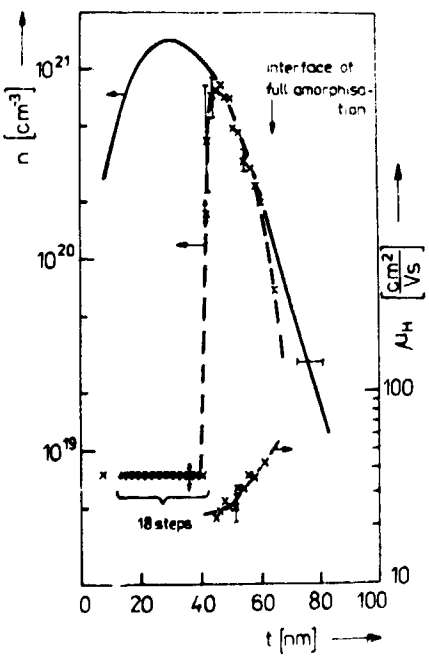

Fig. 1: Carrier concentration and Hall mobility profile of a 5×10^{15}cm^{-2} As-implantation, 50 keV, annealed at 520 °C, 15 min. Full line represents RBS-measurement.

/1/ J. Narayan; J. Appl. Phys. 53 (1982) 8607
/2/ H. Kerkow, G. Kreysch, B. Lukasch; phys. stat. sol. (a) 82 (1984) 125

THE USE OF SECONDARY ION MASS SPECTROMETRY FOR STEEL ANALYSIS

S. Mechahougui, G. Lehmann, and U. Müller-Jahreis
Sektion Physik der Humboldt-Universität zu Berlin, Bereich "Atomstoßprozesse der Festkörperphysik"

The secondary ion mass spectrometry (SIMS) is one of the most effective methods in microanalysis. The sensitivity for trace elements is normally in the range of ppm and in the order of ppb in the most favorable cases. Secondary ion signals depend not only on primary ion density, sputter rate of the target and concentration of the investigated elements in the sample but also on chemical effects in the matrix material caused by its composition and modified by primary ion implantation. Generally, the so called matrix effect is not favorable in quantitative analysis but it can be used in microanalysis for the investigation of both concentration and chemical state.

Vanadium secondary ion signals were used to charcterize different crystallographic phases of a low-alloyd steel (C: 0.12 %, Mn: 1.3 %, V: 0.05 %, Nb: 0.08 %, Al: 0.005 %).

The steel probes were submitted to successive thermal treatments for producing alternating two different states: solid solution of vanadium (states X_n, with n = 0 to 4) and precipitation (states Y_n). The states of solid solution were obtained by austenitic transformation by heating (1200°C, 10 min, air) followed by quenching in water. The Y_n-states were produced by a low-rate cooling ($dT/dt \leq 0.5\ Ks^{-1}$).

As it can be seen in Fig. 1, the vanadium concentration (measured by emission spectroscopy) has not been changed by the thermal treatment, whereas the carbon concentration decreases. The SIMS-signals of vanadium are found to be constant, too, but different in the two states (the Fe^{57}-signal has been used as reference). The vanadium secondary ion emission from the X-states (solid solution) was about 30 % smaller than that from the Y-states (precipitation). This result was expected because of the ionic bonds of vanadium carbide and/or nitride in the precipitation state.

But this information is not sufficient for a quantitative microanalysis because of the superposition of concentration and matrix effect. Our proposition is now to use and additional information from the ratio of vanadium molecule and atomic emission $I(V_2)/I(V)$. This ratio has been found to be more dependent on the matrix effect than the vanadium emission. Here the Y-values exceeded the X-values by a factor of about 5 (Fig. 2). The great straggling of the experimental values in the Y-states is not caused by a limited accuracy in the measuring process but it is an expression of local inhomogeneities.

The use of both informations (V/Fe and V_2/V) seems to be a promising way in the determination of the concentration and the state in microscopic areas of the steel samples. Such a method could also be applied in other problems of SIMS-microanalysis because of the non-existence of standards for inhomogeneous samples.

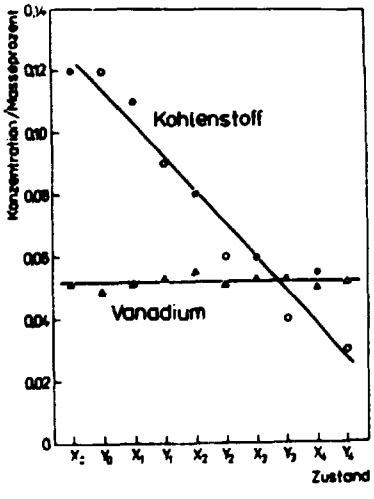

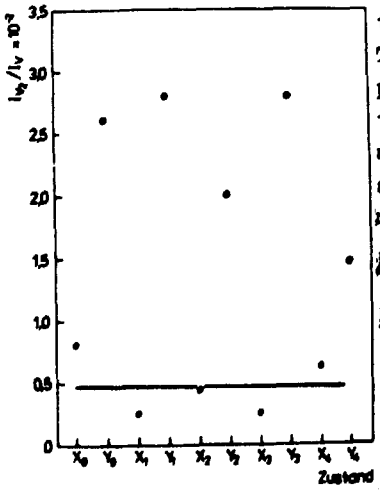

Fig. 1: Vanadium and carbon concentration in dependence on the thermal treatment

Fig. 2: V_2/V-ratio in dependence on the thermal treatment

[1] R. Namdar, D. Loison, and R. Texier, J. de Physique, Colloque C2, Suppl. 45, 673 (1984).

[2] S. Mechahougui, Int. Sem. on Mater. Sci., Anaba (Algeria), Oct. 1985.

[3] D. Stulik, Rad. Eff. Letters 87, 117 (1985).

A METHOD OF QUANTIFICATION OF MASS SPECTRA IN SECONDARY ION MASS SPECTROMETRY (SIMS)

H. Düsterhöft and A. Lüders
Sektion Physik der Humboldt-Universität zu Berlin, Bereich Atomstoßprozesse der Festkörperphysik

One of the most serious problems of SIMS is its quantification without standards. To confine the large number of influence parameter on secondary ion yield investigations were carried out on special glasses /1/. In case of such ionic crystals the emission follows laws of 'bond breaking' without strong influence of oxygen /2/.
The instrumental data were published elsewhere /3/.
The composition of the glasses was:
type SVI Ca8: 50 SiO_2 + 16,7 Al_2O_3 + 33,3 CaO (mol %)
type CaSP-92: 50 SiO_2 + 6 Al_2O_3 + 38 CaO + 6 Fe_2O_3 (mol %).
The samples were polished (untreated samples) ore deposited after 2160 h at room temperature in a special solution on 0,9 g CaO/l + 42 g KOH/l + 8 g NaOH/l (treated samples).
The preparation was carried out in ZIAC of AdW.
The energy window of the energy analyser corresponded with the maximum energy (E_{max}/eV) of the Si^+-ion. In comparision with treated and untreated samples the mass spectra showed a linear connection between the ratio of the relative secondary ion yield of the elements and the ratio of the mol % in the samples (table 1). This table shows a mean deviation $\bar{s}$ of the ratio on the counts (a/b) to the ratio on the mol % (A/B).

Table 1 ($\bar{s}$ = 2,22):

	rel. SI yield (counts/s) a: S VI Ca8	b: CaSP-92	a/b	A/B	$s = \frac{A/B}{a/b}$
Si	1127	2731	0,42	1	2,38
Al	3038	2434	1,25	2,78	2,23
Ca	13743	31294	0,44	0,88	2,00

By means of normalisation of the mass spectra of the sample CaSP-92 with $\bar{s}$ we got a comparable mass spectra to the sample SVI Ca8. Same results we obtained from some other samples of glasses of this type. The composition of the treated samples was unknown. For the standardisation we took this mass line which had the smallest deviation. Fig. 1 shows that all other lines were decreased. Using the ratio between (a/b) and (A/B) on the mass spectra of treated samples we obtained a quantitative survey about surface conditions. The obtained formula 50 SiO_2 + 6,8 Al_2O_3 + 36,6 CaO + 6,9 Fe_2O_3 (mol %) nearly described the surface conditions of treated sample CaSP-92. The results were reproducible. If the surface was covered by oxygen the ratio $\bar{s}$ changed its magnitude but the arised mass spectra were very similar to these without oxygen coverage.

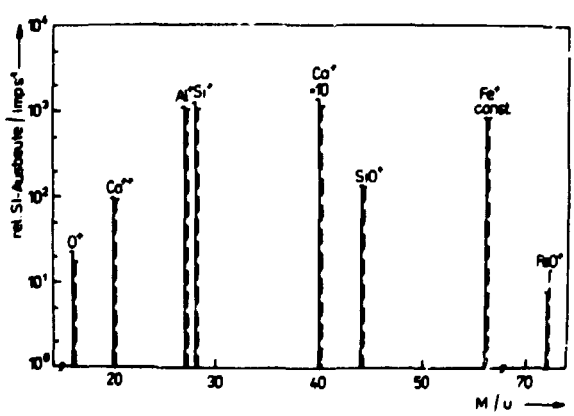

Fig. 1: Relative Secondary Ion Yields
-------- CaSP-92, untreated, $\bar{s}$=2,22 normalised on S VI Ca8
- - - - CaSP-92, treated, normalised on Fe of untreated sample (primary ions 10 keV Ar^+)

[1] Engelhardt, G., Phys.Chem.Glasses, 26, 157 (1985)
[2] Blaise, G., Slodzian, G., Surface Sci., 40, 708 (1973)
[3] Düsterhöft, H. et.al., Exp.Tech. Phys. 32, 131 (1984)
[4] Düsterhöft, H., Lüders, A., to be published

DEEP LEVELS IN n-Si CAUSED BY LOW ENERGY ION IMPLANTATION

J. Bollmann, H. A. Klose, and A. Mertens
HU Berlin, Sektion Physik, Bereich "Atomstoßprozesse der Festkörperphysik"

The low-energy ion implantation can be used to produce surface-near shallow profiles with projected ranges R_p between 10 nm and some 100 nm for the shrinkage of feature sizes in VLSI, but implantation defects are simultaneously created in depths of some R_p. Because it is possible to perform Schottky junctions by a low-energy high-dose implantation of heavy metal ions [1] the process-induced defects can be studied in the as-implanted state as well as after annealing procedures. How expected the implantations generate typical vacancy-coupled defects (E1, E3, E4) and two levels (E2, E5) independent of implanted ion species. Annealing procedures reduce drastically the concentration of these defects contrary to the increasing amount of implanted ion-correlated defects (see table in the case of Ag^+ implanted n-Si samples). By using DDLTS measurements in connection with a precise interpretation of the raw data [2] depth profiling of different deep levels was carried out (see Fig. 1). Because the metal-correlated defect profiles show a similar shape compared to the other defects it must be assumed that a small amount of implanted metal ions is channeled. It should be pointed out that these long tails of defect distributions achieve values of many R_p and depend on crystal orientation.

$e_n = A\,T^n \exp(-\Delta E/kT)$			
level	ΔE/eV	$A\,T^2/s^{-1}$	features of levels
E 1	0.42	2.7×10^{11}	PV^-, V_2^- acceptor
E 2	0.32	4.3×10^{10}	?
E 3	0.25	5.8×10^{11}	V_2^{--} acceptor
E 4	0.15	5.7×10^{10}	VO^-(A-centre)
E 5	0.14	4.9×10^{11}	?
1 E	0.44	2.7×10^{12}	assumed Ag corr.
2 E	0.37	1.0×10^{12}	
3 E	0.35	2.3×10^{12}	after 775K/30min
4 E	0.32	1.2×10^{12}	heat treatment
5 E	0.17	1.7×10^{11}	
E I	0.56	3.8×10^{12}	Ag- acceptor
E II	0.09	1.4×10^{10}	O- donor (after 575K/
	0.06	7.0×10^{8}	30 min annealing)

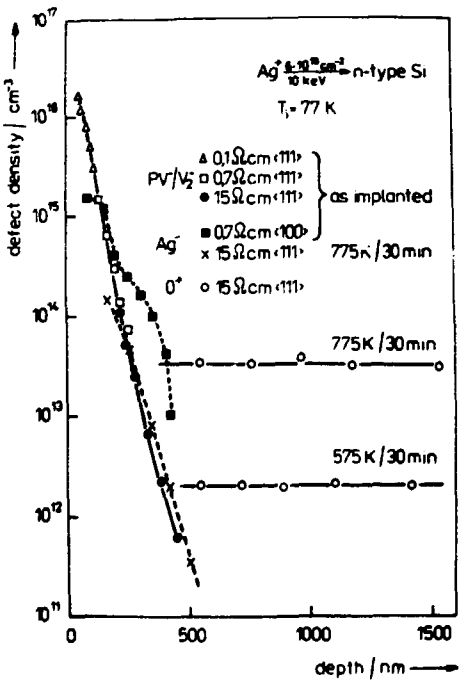

Fig.1: Depth profiling of some typical implantation defects determined by DDLTS

References:

[1] Bollmann, J., Klose, H. A., and Mertens, A.; Proc. Phys. Halbleiteroberfläche 16 (1985) 267
[2] Maass, K., Irmscher, K., and Klose, H. A.; phys.stat.sol. (a) 91 (1985) 667

STRUCTURE DEPENDENCE OF QUADRUPOLE COUPLING CONSTANTS IN $A^{II}B^{IV}C_2^V$ CHALCOPYRITE COMPOUNDS

S. Unterricker, Bergakademie Freiberg, Sektion Physik

Some of the so called probe methode (NQR, ME, TDPAC, ...) determine the quadrupole coupling constant $\nu_Q = eQV_{zz}/h$ and with it the electric field gradient (efg) V_{zz} at the nuclear probe. V_{zz} reflects the charge distribution in the probe environment. To obtain all the informations which contains V_{zz} one needs a good theory of efg. In priciple such a theory must start from the electronic charge distribution $\varrho(\vec{r})$. Normally, $\varrho(\vec{r})$ is not exactly known and a calculation of the efg with a fine structured $\varrho(\vec{r})$ is very time consuming. Therefore, by far the most cases, only approximative solutions of the problem are possible. Very hopeful is a theoretical investigation of the lattice structure dependence of efg. Here simplifying models proved entirely successful [1,2] .

In a first step geometric efg are calculated with the definition $a^3q = a^3V_{zz}(1-\gamma_\infty)^{-1}\, 4\pi\, \varepsilon_0 e^{-1}$, which are numbers independent on the cell volume. $(1-\gamma_\infty)$ is the STERNHEIMER correction. The a^3q show a simple dependence from the axis ratio for instance in the cases of substances with wurtzite lattice [2] , with $CdCl_2$ lattice or for ternary $A^{II}B^{IV}C_2^V$ semiconductors with chalcopyrite structure. In Table 1 the TDPAC measured ν_Q for $A^{II}B^{IV}C_2^V$ compounds are listed.

Table 1
Quadrupole coupling constants for $A^{II}B^{IV}C_2^V$ semiconductors. Probe nuclei ^{111}Cd; $\tau = 2-c/a$.

substance	ν_Q/MHz	$a^3q(A)$	τ
$CdSiP_2$	110.1(9)	23.9(2)	0.164
$CdGeP_2$	88.1(17)	19.8(4)	0.123
$CdGeAs_2$	75.7(20)	18.8(5)	0.113
$ZnSiP_2$	53(2)	9.9(4)	0.067
$CdSnP_2$	37.3(7)	9.1(2)	0.048
$CdSnAs_2$	31.6(6)	8.4(2)	0.044

Though the substances cover a wide range of tetragonal compressions the $a^3q(A)$ show a striking linear τ dependence. This is surprising because the chalcopyrite structure is characterized not only by $\tau = 2-c/a$ but also by the different cations A and B and by the anion displacement $\delta = x-1/4$.

We have calculated the geometrix efg $a^3q(A)$ by a lattice summation of a point ion lattice using the $\delta(\tau)$ relation of ABRAHAMS-BERNSTEIN for ideal sp^3-configurated B^{IV} atoms. The result $a^3q(A) = 3.152(Z_A - Z_B) + (25.8\, Z_A + 30.6\, Z_B)\tau$, with charge numbers Z_A, Z_B and Z_C at the lattice points, depends linearly on τ .

The following statements are possible if we compare theory and experiment:

- If the Z_A, Z_B and Z_C are explained as effective charge numbers it follows $Z_A > Z_B$.
- The spread of the Z_A, Z_B and Z_C for the different substances should be relatively small.
- The case $\tau = 0$ is comparatively simple (exact tetrahedral arrangement of the nearest neighbour charges). With the free ion STERNHEIMER correction of $(1-\gamma_\infty) = 30$ we got $Z_A - Z_B = 0.69$.
- The effective charge state of the Cd probes is < 2. This can be considered by a valence electron correction factor $F^{val} > 1$ beside $(1-\gamma_\infty)$.
- The value of F^{val} is unknown. With $F^{val} \sim 3$ the effective charges of HÜBNER [3] agree with our experiments.
- Between the spherical ion cores there are extended bond charge distributions, which in a point charge approximation yield efg proportional to τ and of the same order and sign as $a^3q(A)$.

R e f e r e n c e s

[1] Bodenstedt, E., and B. Perscheid; Hyp. Int. 5 (1978) 291
[2] Unterricker, S.; Proceedings of the XX Winter School on Physics, 13 - 26 April 1985, Zakopane-Poland, p. 437
[3] Hübner, K.; phys. stat. sol. (b) 52 (1972) K 33

MÖSSBAUER STUDY OF FE $^{2+}$ - FE^{3+} ORDERING IN NATURAL CHROMITES

C. Pietzsch, Bergakademie Freiberg, Sektion Physik

Natural chromite spinels are chemically complex and therefore offer the possibility of a variety of hypothetical cation ordering schemes. In the literature there are different opinions on this problem. Osborne et al. [1] assumed an "ordered" spinel structure with divalent cations on the tetrahedral (T) sites and trivalent cations on the octehedral (O) sites. Da Silva et al. [2] have interpreted the Mössbauer spectra of chromite as a disordered distribution of Fe^{2+} and Fe^{3+} on both T and O sites. In some cases electron hopping occurs if Fe^{2+} and Fe^{3+} both are situated on octahedral sites.
This paper reports a Mössbauer investigation of three chromites from different locations, the Mössbauer parameters of which are given in Table 1.

Table 1
Mössbauer parameters of chromites

	T = 295 K				T = 77 K			
chromite	I rel.	δ/mm·s^{-1}	Δ/mm·s^{-1}	Γ/mm·s^{-1}	I rel.	δ/mm·s^{-1}	Δ/mm·s^{-1}	Γ/mm·s^{-1}
I	140(6)	0.497(5)	0.585(5)	0.25(1)	210(11)	0.61(1)	0.470(9)	0.47(4)
	335(23)	1.023(5)	1.086(9)	0.47(2)	170(22)	1.12(2)	2.02(3)	0.51(9)
	293(22)	1.023(6)	1.95(1)	0.50(3)	457(12)	1.173(4)	2.935(6)	0.41(5)
II	162(8)	0.481(9)	0.578(7)	0.33(2)	205(10)	0.54(2)	0.61(2)	0.54(4)
	285(33)	1.046(7)	1.13(2)	0.48(4)	109(13)	1.1[illegible](3)	2.06(3)	0.53(8)
	258(13)	1.018(8)	1.89(1)	0.47(3)	476(9)	1.169(4)	2.923(6)	0.43(2)
III	432(13)	0.370(5)	0.931(6)	0.51(2)	509(21)	0.52(2)	0.84(1)	0.57(5)
	-	-	-	-	59(15)	0.91(3)	2.17(3)	0.34(9)
	394(17)	1.05(1)	1.478(9)	0.74(3)	339(17)	1.178(7)	2.920(7)	0.42(2)

I - intensity, δ - isomer shift (rel. α-Fe), Δ - quadrupole splitting, Γ - line width.

The best fit of the room temperature spectra allows the following interpretation. Chromite I and chromite II show nearly the same parameters. One doublet is characteristic of Fe^{3+} occupying T sites with a relatively large quadrupole splitting owing to a random cation distribution on the O sites (perturbed spinel) and the other one corresponds to Fe^{2+} O sites. For the third doublets two distinct possibilities of coordination exist. Either Fe^{2+} occupies T sites or due to electron hopping between Fe^{2+} and Fe^{3+} on the same crystallographic sites a doublet with the average valency of $Fe^{2.5+}$ appears. The spectra of chromite III were fitted with two doublets, one to Fe^{3+} and the other one to Fe^{2+} both on octahedral sites. The line width of the Fe^{3+} doublet is very broad in this case.
To clarify the problem of electron hopping Mössbauer spectra at 77 K were recorded. The 77 K run of the three chromites shows three distinct doublets in any case. Remarkably is the decrease of the intensity of the $Fe^{2.5+}$ doublet in favour of the other two doublets compared with the room temperature spectra. This result leads to the conclusion that electron hopping exists in inverse natural chromites.

R e f e r e n c e s

[1] Osborne, M. D., et al.; Contrib. Mineral. Petrol. 77 (1981) 251
[2] Da Silva, E. G., et al.; Appl. Phys. 22 (1980) 389

RARE EARTH ELEMENT AND YTTRIUM CONTENTS IN FLUORITE SAMPLES

D. Degering, S. Unterricker and W. Stolz
Bergakademie Freiberg, Sektion Physik
O. Leeder and G. Wendebaum
Bergakademie Freiberg, Sektion Geowissenschaften

The small concentrations of the rare earth elements (REE) in geological samples play an important role for investigations of the geochemical source aspects. Because of the small differences in their electronic configurations they behave like a coherent group with little variations. Yttrium which is not a lanthanide may show rare-earth-like characteristics originating in its similar electronic configuration. On the other hand, the absence of one electronic shell in comparison to the REE must have some effect on its behaviour. Therefore, yttrium is possibly a more sensitive indicator for the history of formation of the sample as the variations between the REE. Unfortunately, contrary to the most REE Y is not detectable by the instrumental neutron activation analysis (INAA). So, Y is often not considered in geochemical works.

Here we report investigations on a fluorite deposit in Ilmenau-Gehren. The contents of La, Ce, Sm, Eu, Tb, Dy and Yb were determined by the INAA method. The Y-determination was performed as presented in [1] by means of the ^{89}Y (d,2n) ^{89}Zr reaction. Pulverized specimens from the Ilmenau deposit, a fluorite standard (XXK) and a limestone standard (KH) were activated with deuterons (E_d=13.5 MeV, 1 µA for 1h). The peak area of the ^{89}Zr γ-line was determined by a special fitting procedure with Gaussian curves on an energy-dependent background. The chondrite-normalized contents of the REE vs. the ionic radii for the fluorite standard XXK and a sample from Ilmenau are shown in Fig.1. The abundances of the standard except the Y-value were taken from [2] , the ionic radii from [3] and the chondrite contents are the same as in paper [4] . All samples showed a REE distribution pattern with a continous growth for increasing radii. Eu has an anomalous behaviour based on its two possible oxidation states. For the standards XXK and KH the measured Y-concentrations were (61 ± 4) ppm and (14 ± 2) ppm, respectively. These results are in agreement with the values (59 ± 6) ppm and (13 ± 0.6) ppm from [2] obtained by an interpolation between the neighbouring elements. Nevertheless, along the vein of Ilmenau the Y-abundances were in the range from 20 to 50 ppm and thus apparently larger as expected by an interpolation (2 to 20 ppm). This fact is illustrated in Fig.1 where the REE- and Y-concentrations are presented for a characteristic sample. These results demonstrate that the interpolation provides not always right yttrium contents. Thus the introduction of yttrium in the fluorite lattice for geological samples depends obviously on the growing conditions and is only under certain circumstances similar to that of the REE.

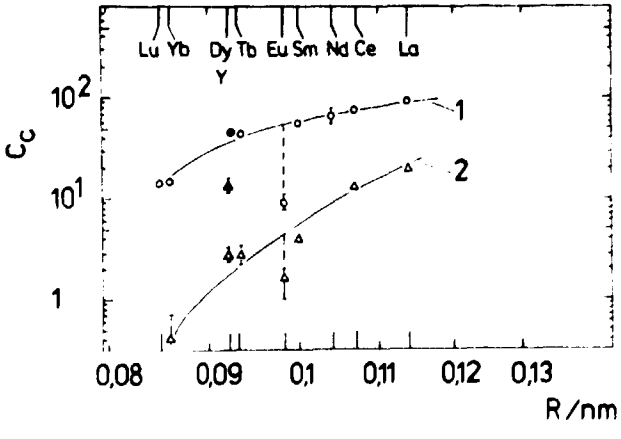

Fig. 1
Plot of the REE abundances related to chondrite contents (C_c) vs. ionic radii (R). Curve 1 connects the relative contents of the fluorite standard XXK (open circles) and curve 2 that of a typical sample from Ilmenau (open triangles). Also shown are the Y-values of these specimens (filled signs).

References

[1] Degering, D., and S. Unterricker; Gemeinsamer Jahresbericht 1984, ZfK - 559 (1985) 83
[2] Saupe, M., and G. Loos; 3. Tagung Nukl. Analysenverfahren, Dresden 1983, Preprints 155
[3] Ahrens, L. H.; Geochim. Cosmochim. Acta 2 (1952) 155
[4] Loos, G., and M. Saupe; 3. Tagung Nukl. Analysenverfahren, Dresden 1983, Preprints 109

DEFECTS IN LASER ANNEALED ION IMPLANTED GaAs LAYERS

W. Wesch, P. Ressel, E. Wendler
Friedrich-Schiller-Universität Jena, Sektion Physik

Ion implanted GaAs layers capless annealed with nanosecond laser pulses exhibit a pronounced tail of the absorption coefficient near the fundamental absorption edge with an exponential dependence on the photon energy characterized by an energy $E_1 \approx 0.1$ ... 0.5 eV depending on the laser energy density and almost no refractive index change. Laser irradiation of virgin GaAs created the same near edge optical behaviour [1], and an identical behaviour is also observed in weakly ion implanted GaAs layers [2]. It was shown recently [1-3], that the measured optical properties can be understood assuming high concentrations of vacancies, anti-site defects and/or complexes of them. It was furthermore deduced that also for the extremely short anneal times the surface decomposition of the material must be prevented. Because the experiments with the commonly used cap layers yielded poor reproductibility of the electrical parameters laser annealing in a highpressure ambient atmosphere was proposed [4]. First investigations of samples irradiated at 125 bar in an Ar atmosphere carried out in our laboratory show a reduction of the near edge absorption exponent Kd (Fig. 1a). The characteristic energy has a constant value E_1 = 0.22 eV independent of the laser energy density (Fig. 1b) indicating a reduced average defect concentration in the resolidified layers (under normal pressure E_1 increases with the laser energy density). The high pressure annealing significantly increases the degree of electrical activation, but the electron mobility is yet too low [5]. Thus, the prevention of material degradation is not sufficient to produce optimum electrical parameters. Obviously defects created as a consequence of the high regrowth velocity play an important role in the binary III - V compounds. This problem may be overcome by reducing the resolidification front velocity, e.g. by elevating the sample temperature during irradiation.

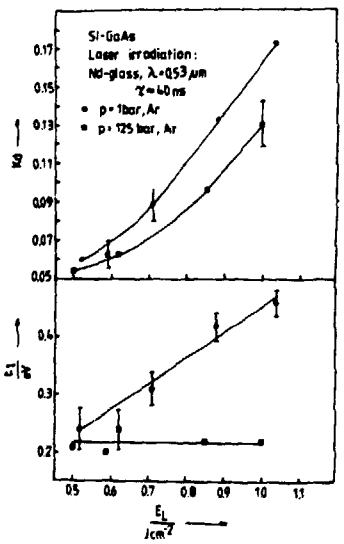

Fig. 1: Absorption exponent Kd and characteristic energy E_1 versus the laser energy density E_L for virgin SI- GaAs irradiated with 40 ns pulses of a Nd-glass laser (λ = 0.53 µm) at normal pressure (O) and at a pressure of 125 bar (□) in an argon atmosphere.

[1] W. Wesch, E. Wendler, G. Götz, K. Unger, H. Röppischer, Chr. Resagk, phys. stat.sol. (b) 130, 539 (1985)
[2] E. Wendler, W. Wesch, G. Götz, phys. stat. sol. (a) 93, 543 (1986)
[3] E. Wendler, W. Wesch, K. Unger; Proc. Int. Conf. Energy Pulse Modification of Semiconductors and related Materials, ed. K. Hennig, Dresden 1984, p. 535
[4] F. Sato, T. Sunada, J. Chikawa, Mater. Lett. 1. 111 (1983)
[5] W. Wesch, G. Götz; phys. stat. sol. (a) 1986, in the press

RBS INVESTIGATIONS OF DEFECTS IN WEAKLY DAMAGED GaAs

W. Wesch, K. Gärtner, E. Wendler
Friedrich-Schiller-Universität Jena, Sektion Physik

Weakly damaged ion implanted GaAs layers show characteristic near edge optical properties: a highly increased absorption coefficient depending exponentially on the photon energy and almost no refractive index change. As discussed in [1, 2, 3], these results of the optical measurements can be understood by the assumption of a high relative concentration ($\approx$ 50%) of matrix specific point defects (anti-site defects, vacancies) characteristic for compound semiconductors.

Recently in [4] it was shown that the temperature dependence of the RBS minimum yield for a crystal with point defects is characteristic for the position r_a of displaced atoms from the string of atoms. Therefore it is possible to determine the defect concentration $n_{pd}(z)$ as well as the position r_a from the depth dependence of the minimum yield measured for different temperatures. In Fig. 1a the difference of the minimum yield of implanted and virgin GaAs $\Delta\chi_{min}(z)$ is depicted for two temperatures. From the smoothed experimental curve $\Delta\chi_{min}(z)$ at 293 K we have calculated the relative concentration of point defects, $n_{pd}(z)$, assuming different fixed values of the distance r_a from the string and for randomly distributed r_a (no preferred position) (see Fig. 1b). For these defect distributions with the corresponding r_a values the differences in the minimum yield $\Delta\chi_{min}(z)$ at 60 K were calculated (dashed curves in Fig. 1a). In spite of the large experimental errors of the RBS data the temperature dependence of $\Delta\chi_{min}(z)$ is negative and can be confirmed only for r_a = 0.025nm and r_a = 0.03nm. Taking further into account that for r_a = 0.05nm and randomly distributed r_a negative defect concentrations are obtained for depth $z > 0.8\mu m$ (omitted in Fig. 1b), we concluede from our RBS investigations that high concentrations of displaced atoms (maximum values of 50 ... 90%) with prefered positions in the lattice cell at a mean distance of about 0.025 ... 0.03nm from the atomic string exist in weakly damaged GaAs layers. The results distinctly exclude interstitials and confirm the suggestions indicated by the results of the optical measurements.

[1] E. Wendler, W. Wesch and G. Götz; phys. stat. sol. (a) 93, 543 (1986)
[2] W. Wesch, K. Gärtner, E. Wendler and G. Götz; Int. Conf. Radiation Effects in Insulators, Guildford 1985, to be published in Rad. Effects.
[3] E. Wendler, W. Wesch and K. Unger; Proc. Int. Conf. Energy Pulse Modification of Semiconductors and Related Materials, ed. K. Hennig, Dresden 1984, p. 535.
[4] K. Gärtner, K. Hehl and G. Schlotzhauer; Nucl. Instr. and Meth B4 (1984) 55

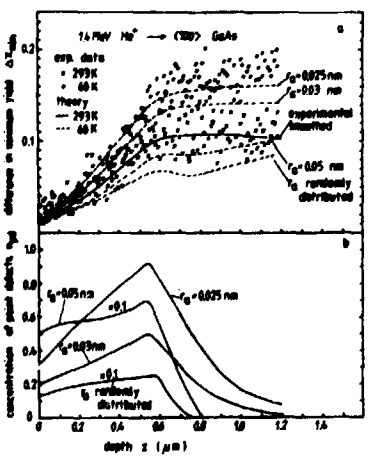

Fig. 1 Depth dependence of the difference of minimum yield $\Delta\chi_{min}(z)$ for 1.4MeV He^+ ions incident on perfect ⟨100⟩ GaAs and ion implanted GaAs ($5\times10^{15} N^+cm^{-2}$ at 293 K), measured at 293 K and 60 K (part a). The relative concentrations of point defects $n_{pd}(z)$ were calculated for different distances r_a from the string using $\Delta\chi_{min}(z)$ at 293 K (part b, negative part of $n_{pd}(z)$ omitted). The theoretical curves in part a (dashed lines) were received with the corresponding distributions $n_{pd}(z)$ given in part b.

ACCELERATORS

OPERATION OF THE CYCLOTRON U-120

B. Anders and H. Guratzsch

Zentralinstitut für Kernforschung Rossendorf, Bereich G

In the past year the total operation time of the cyclotron has been 4794 hours. The beam has been used mainly for basic nuclear research (1366 hours) and isotope production (1466 hours). Table 1 shows the complete time distribution. Table 2 gives the survey of accelerated particles with their percentages of beam time.

In the course of cyclotron improvement new ion sources have been tested and the acceleration at higher harmonics has been studied. Ions of $^{20}Ne^{3+}$ (12 MeV) and $^{20}Ne^{4+}$ (21 MeV) have been accelerated at the third harmonic and extracted into the beam line. To improve the beam handling system, the quadrupol doublet has been extended to a triplet.

Table 1

Beam time distribution for 1985

Cyclotron operational	5817 h
Turning on and off; Maintenance	591 h
Scheduled revision	432 h
Total beam time:	4794 h
Nuclear physics	1366 h
Isotope production	1466 h
Neutron therapy	197 h
Thin-layer activation	196 h
Cyclotron improvement	1038 h
Other users	531 h

Table 2

Accelerated ions and their percentages of beam time

D^+	52 %
H_2^+	5 %
$^4He^{2+}$	40 %
$^{6;7}Li^{3+}$	3 %

OPERATION OF THE ELECTROSTATIC ACCELERATORS IN 1985

W. Bürger and S. Turuc

Zentralinstitut für Kernforschung Rossendorf, Bereich G

Tandem-Accelerator

The accelerator was operated in a 3-shift mode. It was used for experiments of nuclearphysics, solid-state-physics, thin-layer-activation with respect to abrasion investigation, irradiation of polymer-foils for filter production and for accelerator-experiments and development.

Characterizing parameters are given in table 1 und 2.

Table 1

	hours
Available time	5970
Accelerator under voltage	4048
Experiments with beam	3243
Development	861
Maintenance and planned stand	848

Table 2

species of ions	rel. op. time
p	5,5 %
d	22,7 %
d (pulsed)	16,7 %
^{15}N	17 %
^{19}F	4,5 %
^{35}Cl	27,7 %
O, Cu, Br, Ge, Si, Se	5,9 %

The life-time of the charging belt (Greengate) is now 8200 hours. The acceleerator-tubes (stainless steel electrodes, ceramic insulators, inclined field) have been used up to now about 48000 hours.

The injector-platform supporting the two ionsources (duoplasmatron, sputter-ionsource) was elevated 1000 mm. This was necessary to get place at the entrance of the accelerator for beam-diagnostic elements.

The equipment for foil irradiation was tested under different conditions. In a pilot production a quantity of 2000 m^2 of polymer-foil was irradiated in a appropriate quality.
In connection with our development of simple and reliable sputter-ionsources we came to a sale contract for one ionsource MISS 483 with the University of Helsinki.

Van-de-Graaff-Accelerator

The 2-MV-vdG-Accelerator was used 2675 hours mainly for nuclear analysis protons, deuterons and heliumions.
The activities for improving the beam quality, started in the last year have been continued.

NUCLEAR ELECTRONICS AND METHODS

FIRST INVESTIGATIONS WITH A STATIONARY POSITRON CAMERA

P. Manfraß, W.D. Fromm, M. Sobiella and D. Wohlfarth
Zentralinstitut für Kernforschung, Rossendorf, Bereich KF

Investigations of the properties of a stationary positron camera with gas-filled detectors /1/ were started in 1985. As detectors two 20*20 cm² MWPC are combined with four 5 mm thick multihole converters in order to absorb the γ-radiation from the annihilation. The converters are operated in the normal drift regime with a field strength of ~1 kV/cm. The effectivity for E_γ=511 keV was 8 %. The time window of 120 ns was selected from the FWTM-width of the coincidence spectrum.

The algorithm for the filtering of the backprojected tomograms assumes, that for all source points the same aperture can be provided. For an acceptance of ± 15 degrees and a distance of 32 cm between the MWPC's this condition is only in a volume of 8*8*12 cm³ fulfilled. The dimensions of the 7 longitudinal tomograms recorded are chosen identical to the detectors which results in a pixel size of 3.125*3.125 mm² (64*64 channels).

The measured resolution for a ^{22}Na line-source (diameter 2 mm, length 50 mm) was 5 mm FWHM. This relatively poor resolution is mainly caused by parallax error which amounts to 4 mm in the given geometry with a distance of 25 mm between the converters. The reconstruction of the measured tomograms was performed applying the method of Townsend et al./2/.

Tests of the filtering programs with simulated data-sets revealed a good reproduction of the shape and intensity of the object distributions. The defocused intensities were damped by a factor of 1/8 compared to the backprojected distributions. For measured data-sets using the ^{22}Na line-source in different picture planes the achieved damping factor of 1/3 is worse. This may be caused by the finite spatial resolution of the positron camera which was neglected in the filtering program and manifests itself as a widening of the source perpendicular to the picture plane.

Another test with a spatial activity distribution was performed using a white rat with ^{18}F enriched in the sceleton after injection of Na_3AlF_6 (Fig.1). The mean coincidence rate was 150 c.p.s. Only 30 % of the total coincidences (N_{tot}=642000) were used for the picture generation according to the aperture condition. Therefore, every picture plane contains about 26000 events with 18000 true coincidences.

References

/1/ P. Manfraß et al.; Gemeinsamer Jahresbericht 1984, ZfK-559(1985)148
/2/ D. Townsend et al.; Phys.Med.Biol. 23(1978)325

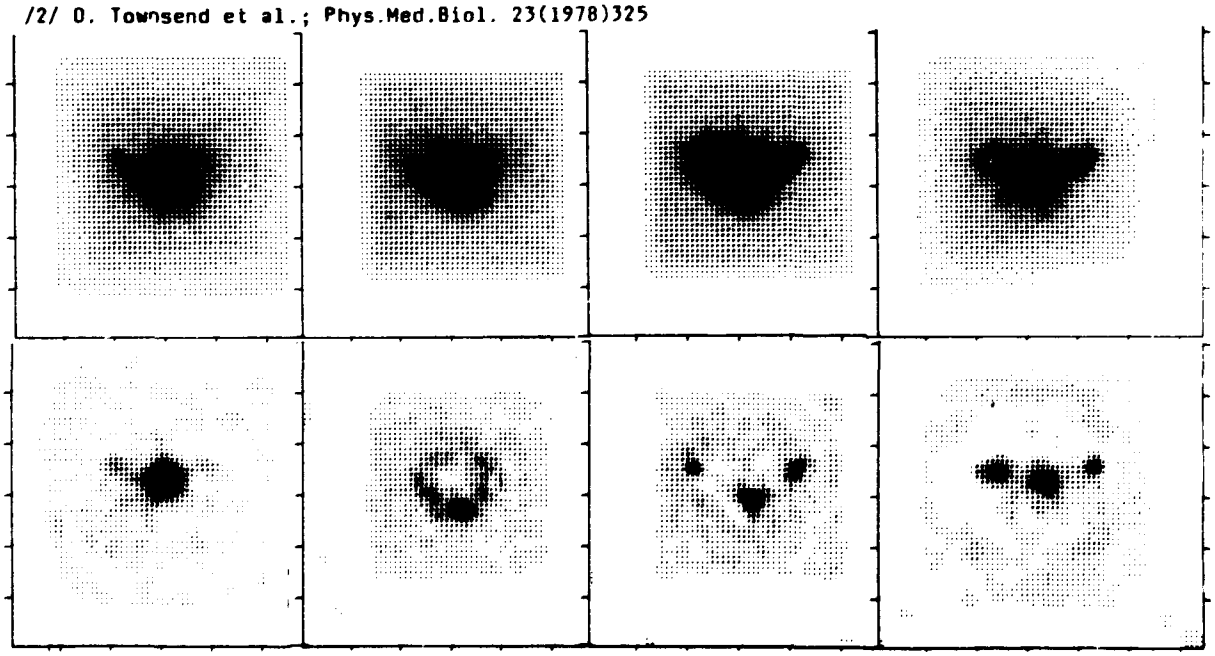

Fig.1 Positron emission tomograms of the sceleton of a rat: raw data and reconstruction (below)

THE CONVERTER-MWPC IN THE MULTI-STEP AVALANCHE MODE

P. Manfraß, W.D. Fromm, M. Sobiella and D. Wohlfarth
Zentralinstitut für Kernforschung, Rossendorf, Bereich KF

The investigations for the improvement of the properties of the detectors used for the positron camera were continued. With the application of the multi-step avalanche amplification principles /1/ for MWPC's with hole-converters critical parameters like time-resolution and discrimination against background radiation can be substantially improved /2/. The field strength within the converter is so large that electron multiplication takes place. The following amplification of the electron avalanche in the MWPC field yields signal amplitudes about 100 times larger as in the normal drift regime of the converter.
The main topic of the investigations was the measurement of the time-resolution for selected detector gas admixtures with Ne as main component. The converter with a total thickness of 4 mm was fabricated from ten 0.2 mm thick PbSb3Sn2.5 foils with electrically isolating layers of 0.2 mm Prebeg. The diameter of the holes and the distance between hole centers were 0.8 and 1.0 mm respectively. The best time-resolution of 15 ns FWHM was achieved with Ne + 5 % Hexan and a homogenous field strength of 8.0 kV/cm at the converter and 1.1 kV anode voltage. The use of CO_2 as faster quenching gas did not improve the time-resolution.
The measurement of the detection effectivity for γ-radiation of 511 keV with respect to converter and anode voltages has shown, that the practically reachable effectivity is limited by the large dynamic range of the signal amplitudes. This follows from the exponential dependence of the multiplication factor $M = e^{\alpha x}$ from the pathlength x in the homogenous electric field. The dynamic range of the signal amplitudes is reduced if the field strength applied to the first 5 Pb-foils is diminished in such a way that only in the second half of the converter electron multiplication can occur. In accordance to /3/ for the homogenous field a maximal effectivity of 2.4 % (1.2 % per mm Pb) was measured. In the second case the effectivity growed to 3.3 % (1.65 % per mm Pb). Our investigations confirm that by an optimal choice of the electric field in the converter the effectivity of the detector can be further improved.

References

/1/ A. Breskin et al.; Nucl.Instr.Meth. 161(1979)19
/2/ A. Jeavons et al.; Nucl.Instr.Meth. 176(1980)89
/3/ A. Jeavons et al.; CERN-EP/82-201, Dec. 1982

A MICROPROCESSOR CONTROLLED MÖSSBAUER SPECTROMETER

P. Reichel, W. Matz and W. Boede
Zentralinstitut für Kernforschung, Rossendorf, Bereich KF

The Mössbauer spectrometer 4S 1D was reconstructed using the microprocessor system MPS 4944. For this purpose the coil of the velocity transducer was rewound to allow for a low resistant feeding (± 10 V). The microprocessor has 1024 analyser channels and two Mössbauer spectra were independently recorded in the experiment. Quartz-stabilized 1 ms time pulses were given to an up-down-counter (-511...0...511...0...-511) and are used as the binary input signal of a DAC. The output signal is a triangle function. It is integrated to give a double parabole and drives the transducer via a power amplifier. Linearity control is performed by comparison of the triangle function with the signal of a reference coil in the transducer. The 1 ms pulses initiate interrupts in the microprocessor. The address of the multiscaler is computed from the binary information of the up-down-counter. The detector counting rate within the 1 ms time interval is than added to the appropriate channel.

The software of the microprocessor allows for the output of the spectra on a printer and a paper tape puncher. The width of the multisceler is 24 bits, but for output only 16 bits can be used. The measuring time can be presented between 1 and 255 hours. In the output regime it is possible to sum up 2, 4 or 8 succesive channels.

Test experiments were performed with a standard absorber of α-iron (25 µm thickness) and a ^{57}Co-Mössbauer source in rhodium host. For different maximum Doppler velocities, ranging from v_{max} = ± 6.9 mm/s to v_{max} = ± 11.6 mm/s, the Mössbauer spectra were analysed. Each of the two spectra and the sum spectrum were created separatly. The sum spectrum was determined by calculating at first the velocity zero of the two parts and than the shift between them. In order to estimate the linearity of the velocity scale, the velocity-channel-relation was computed by a lesst square fit. The calculated error of the slope of the linear relation don't exceed ± 0.2 % in the mentioned velocity range. The single absorption line positions differ from the calculated positions in the most cases by less than 0.1 channel. The shift between the two spectra depends on the maximum velocity. It is between 0.25 and 1 channel, if each spectrum is measured with 512 channels. The line width (FWHM) of the absorption lines was measured for v_{max} = 6.9 mm/s with two different discriminator windows for the 14.4 keV γ-line of iron. With high discrimination (window width equal to half-width of γ-line) the inner two absorption lines of the Mössbauer spectrum have a line width of Γ = (0.263 ± 0.003) mm/s. This is essentially the same as the value of 0.26 mm/s given by the producer for the source used. For relaxed discrimination (window covers the whole γ-line) the comparable line width is Γ = (0.286 ± 0.005) mm/s. For higher maximum velocities the mean width of the absorption lines is about 0.3 mm/s. The summation of the two spectra with proper shift between them do not broaden the line width of the absorption lines.

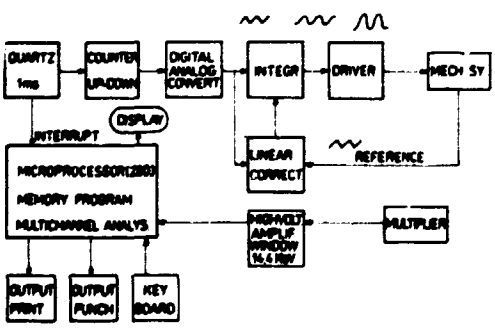

Fig.1 Scheme of the Mössbauer-spectrometer

A NUCLEAR MICRO-BEAM PROBE FOR THE INVESTIGATION OF SURFACES

W.D. Fromm, D. Grambole, F. Herrmann and F. Schwarzenberg
Zentralinstitut für Kernforschung, Rossendorf, Bereich KF

The nuclear microprobe is an analytical instrument to get information about the lateral sample composition in the surface region in the micrometer range. For this prompt radiations (X-rays, backscattered particles, secondary electrons or γ-rays) are measured which are emitted when the target is irradiated with charged particles of high energies ($\geq$2 MeV) focussed by an electromagnetic quadrupole triplet to a diameter of about 5 µm /1/. A two-dimensional elemental map will be got if the beam is scanned over an area of about 500*500 µm² by means of a computer-controlled electromagnetic deflection system placed before the lens /2/.
The microprobe is connected to an intelligent CAMAC-System (Fig.1).The apparatus is controlled by the autonomous crate controller AMCA-80 constructed on the base of the 8 bit microprocessor U880. All the used CAMAC-units are manufactured in the Central Institute for Nuclear Research. The scan of the beam spot over the surface of the sample is realized by means of a twofold 10 bit Digital-to-Analog converter. Only 7 bits (128 steps) are used for the deflection in the X- and Y-direction. The program MIKROS allows 8 different settings of the stepwidth and the selection of the starting values for X and Y. Therefore, it is possible after an overview measurement of the sample to look for certain regions in more detail. The beam current at the given position is monitored by a presetable counter which counts the current-integrator pulses delivered from the Faraday cup. Therefore, by normalization to the charge a correction for beam intensity variations is applied. The radiation emitted in the interaction of the sample and the beam is recorded by a γ-ray or X-ray detector. Pulses are fed to the Analog-to-Digital converter. The recorded pulse height is placed in an 8 Kbyte buffer memory together with the corresponding positional information. If the charge limit chosen for the measurement at one position is reached, the beam spot is deflected to the next position. If the buffer is filled, the registered events are written to a magnetic tape cassette drive. During this operation the beam is switched off to prevent damage of the sample. The total capacity of one tape cassette of 512 Kbyte is sufficient for measurements of a few hours. For the immediate evaluation of the measurement an on-line sorting procedure was implemented. The energy-spectrum of the used detector can be registered and displayed on the graphic display unit which also serves as operator console. Up to four peaks corresponding to certain reaction types can be chosen as windows for the sorting. For every event fulfilling one of the conditions the corresponding two-dimensional spectrum (128*128) is incremented. The four two-dimensional spectra are stored and displayed by means of an attached color display unit /3/. Using this on-line technique the sample can be seen in the light of the selected reaction channel during the data-taking. The programs are written in assembly language.

R e f e r e n c e s

/1/ Grambole, D. et al.; Gemeinsamer Jahresbericht 1982, ZfK-503(1983)p.140
/2/ Grambole, D., Herrmann, F.; Gemeinsamer Jahresbericht 1984, ZfK-559(1985)p. 92
/3/ Fromm, W.D., Kahlenbach, M.; Gemeinsamer Jahresbericht 1983, ZfK-530(1984)p.131

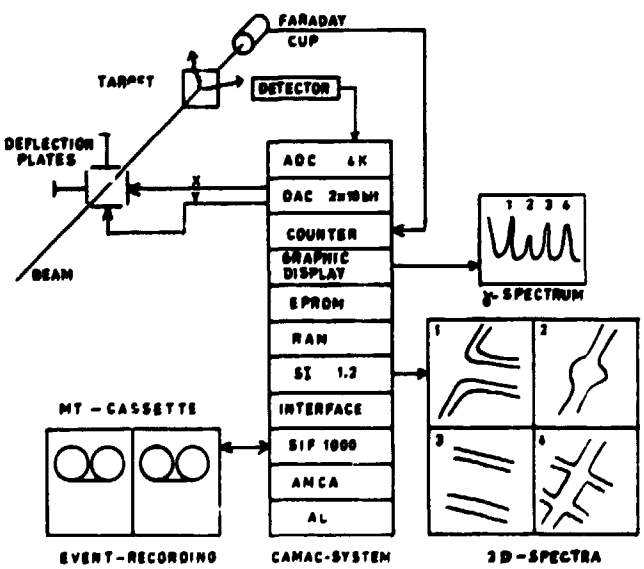

Fig.1 Schematic representation of the CAMAC-system used for the control of the Rossendorf nuclear microbeam probe

INVESTIGATION OF SCINTILLATION MATERIALS

J.Rüdiger
Zentralinstitut für Kernforschung Rossendorf, Bereich KF

In the beginning of the 70-s the most convenient γ-ray scintillation detector - NaI(Tl) - did not satisfy users anymore, in particular because of its hygroscopy and its relatively poor timing properties, compared to organic scintillators. Therefore, a great effort was done to find out new scintillation detectors. At present, the most promising "new" materials for efficient scintillation detectors seem to be $Bi_4Ge_3O_{12}$(so called "BGO")[1] and BaF_2 [2]. Some success was also acchieved with CdS(Te), $CdWO_4$ [1] and the "old" CsI(Tl) [3].

With regard to future experiments at the cyclotron tandem U 400 - U 400 M at the JINR Laboratory of Nuclear Reactions in Dubna, USSR, we checked our possibilities for the preparation of scintillation detectors for γ-rays and for light charged particles of high energy. The following materials were investigated [1)]: CsI(Tl), CaF_2, CaF_2(Eu), CaF_2(Ce), BaF_2, BaF_2(Ce), $Bi_4Ge_3O_{12}$("BGO"), $Y_3Al_5O_{12}$(Ce), TlBrI ("KRS-5"), and a plastic scintillator from TESLA (CSSR): SPB 31. We considered their most important parameters, like relative pulse height, energy resolution, α/β-ratio, and the pulse shape obtained from the anode of the photomultiplier tube (PMT) and observed on an oscilloscope. Several types of PMT were used: M 12 FS 100, M 12 FVC 51, K 14 FQS 51, XP 1020. To increase the light output the scintillators were surrounded with various reflectors (aluminium, aluminized mylar or teflon foils, MgO or Al_2O_3 powders), and were coupled to the front-end of the PMT with silicon grease NP12 or with silicon oil NM 1 - 100 000.

Here, only preliminary results can be given.

1. For the detection of light charged particles of high energy the most promising scintillators seem to be CaF_2(Ce) and CsI(Tl). Fluorite (CaF_2) has a low γ-ray sensitivity, and its activation with Ce leads probably to the highest scintillation efficiency for α-particles (see also ref.[4]). Also, the α/β-ratio for CaF_2(Ce) has the largest value after CsI(Tl). The second scintillator has the highest α/β-ratio of all materials investigated (see table), but there are large fluctuations between different pieces. The reason for this is not yet clear.
2. For the detection of γ-rays we investigated various samples of BaF_2 in order to test the possibility for its use as anticompton shielding. In part, we found that the best of all tested reflectors for the UV-scintillating BaF_2 is MgO, in contradiction to ref.[5]. Teflon tape seems to be an overall good reflector for all scintillators.

Table 1: Preliminary results for some materials

Scintillator	Energy resolution, % γ-rays (662keV)	α-particles (6.0MeV)	α/β-ratio for 6 MeV α-particles
BGO	22	7.5	0.21
BaF_2	15	8.5	0.28
CaF_2	—	9.0	0.32
CaF_2(Eu)	—	8.5	0.42
CaF_2(Ce)	—	7.0	0.52
CsI(Tl)-1	10	4.0	0.58
CsI(Tl)-2	16	5.6	0.74
SPB 31	—	~11	~0.08

3. In table 1 some values of approximate α/β-ratios are listed. These values correspond to the ratio between the γ-ray energy and the α-particle energy at the same pulse height.

References: [1] Farukhi M.R.; IEEE Trans.Nucl.Sci. NS-29 (1982) 1237.
[2] Wisshek K. et al.; Nucl.Instr.Meth.Phys.Res. 227 (1984) 91.
[3] Grassmann H. et al.; Nucl.Instr.Meth.Phys.Res. 228 (1985) 323.
[4] Czirr J.B. et al.; Nucl.Instr.Meth. 143 (1977) 487.
[5] Wong W.-H. et al.; IEEE Trans.Nucl.Sci. NS-31 (1984) 381.

1) The constant support of the VEB Carl Zeiß Jena, WOBI, where most of these samples have been prepared, is gratefully acknowledged. We thank also Dr.Schulze (ZOS Berlin) for providing us with the BGO sample.

DEVELOPMENT AND TEST OF A ΔE - E ANNULAR DETECTOR TELESCOPE

P. Kleinwächter, J. Rüdiger, J. Döring, L. Funke, H. Freitag, H. Rotter, Th. Scholz, W. Schulze, R. Schwengner, E. Will and G. Winter

Zentralinstitut für Kernforschung Rossendorf, Bereich KF

A special ΔE - E annular detector telescope was developed to identify light charged particles emitted in heavy ion induced reactions under forward and backward angles. The ΔE detector was made from a 200 μm thick n-Si slice (50 mm Ø) and consists of six concentric annular diodes ranging from 0.4 ... 5.9 cm^2 sensitive areas. The width of each ring amounts to 2.3 mm. The ion beam passes through a hole of 9 mm diameter. Thus, it is possible to get information on the angular distribution of the emitted reaction products in an efficient way. More detailed informations on the annular Si-detector and the electronic signal processing is published elsewhere [1]. If all rings are connected together an energy resolution of 3‰ for 6 MeV α-particles is obtained.
As E detector serves a plastic scintillator (SPW 31, TESLA) coupled by a light pipe (placryl) to the photomultiplier tube of the type XP 1020. The plastic scintillator has a hole of 10 mm diameter for the beam passage and a thickness of 8 mm that allows a stop of 27 MeV protons completely. The energy resolution for 6 MeV α-particles is found to be 12 ‰.
Some properties of the detector system such as the noise and the timing behaviour as well as the energy resolution were tested at the Rossendorf cyclotron by bombarding ^{27}Al with beams of protons, deuterons and α-particles of different energies. The time resolution of the telescope was determined by using a ^{227}Ac source (providing α- and γ-radiation in coincidence) to be 5 ns. In a first experiment the telescope was installed in a reaction chamber at the U-200 cyclotron of the JINR in Dubna utilizing the reaction $^{16}O + ^{27}Al$ at an incident energy of 140 MeV. The data were recorded online on magnetic tape by a SM-3 computer. The result of this test experiment is plotted in fig. 1 where no ring selection of the ΔE detector was made. It shows a rather good separation of the p, d, t and α-particles. The relatively high yield of accidental coincidences is due to the large coincidence time (1 μs) used in this preliminary experiment.

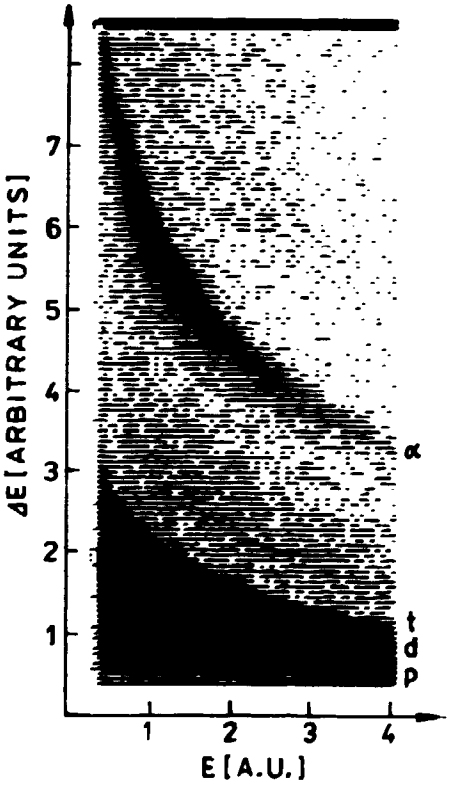

Fig. 1

ΔE - E plot showing the p, d, t and α-particles emitted in the reaction $^{16}O + ^{27}Al$

References:

[1] Schmidt, B. et al. Annual Report ZfK-559 (1984), p. 152

CONSTRUCTION OF A PLUNGER FOR COINCIDENCE EXPERIMENTS

G. Winter, M. Freitag and W. Schulze
Zentralinstitut für Kernforschung Rossendorf Bereich KF

The reliability of plunger measurements can be considerably improved when the γ-ray transitions are measured in coincidence with other signals which are either characteristic for the desired reaction channel or for a certain cascade in the final nucleus. Such signals can be derived from additional detectors that must be arranged near the beam spot on the target. The total efficiency of such coincidence measurements depends quite strongly on the geometry of the plunger chamber and on the absorption properties for all radiations to be detected. Thus, a plunger of small volume and high transparency for the radiations is necessary. However, these properties must be considered in connection with the demand for high mechanical stability and precise adjustments. For the first test experiments a small and simple arrangement was constructed (see figure 1) that allows us to reach a minimum distance between target and plunger of 20 μm. The target of thickness 0.20 mg cm^{-2} was evaporated on 0.5 mg cm^{-2} aluminized polyesther foil. The same polyesther material was also used for the plunger. Examples of lineshape analyses for measurements carried out in the $\gamma\gamma$-coincidence mode /1/ are shown in figure 2.

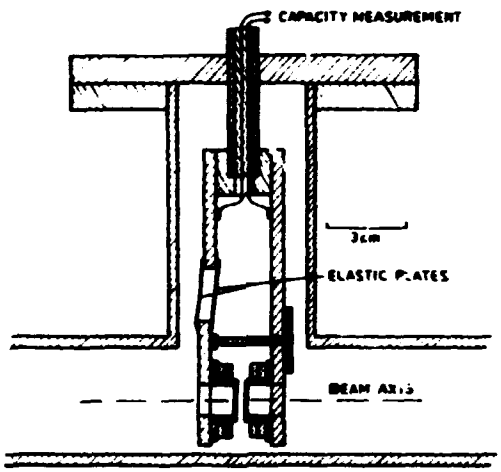

Figure 1. Schematic view on the new plunger arrangement in a plastic vacuum chamber for $\gamma\gamma$-coincidence experiments.

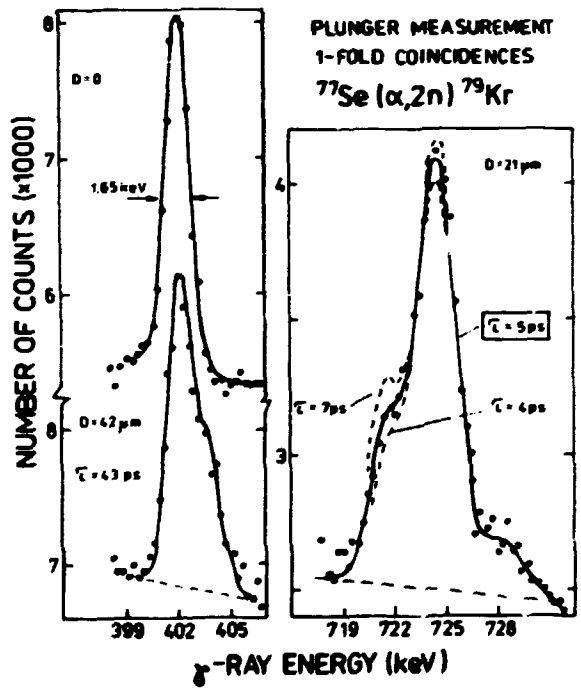

Figure 2. Lineshape analyses for the 402 keV transition and for the doublet at 722 - 726 keV in ^{79}Kr /2/. The observation angle was 24 $\pm$ 8 degrees.

References:
/1/ Winter, G., Schulze, W., and Will, E.; this report p. 102
/2/ Winter, G., Schwengner, R., Funke, L., and Döring, J.; this report p. 21

DOUBLE GRID AVALANCHE COUNTER WITH LARGE DYNAMIC RANGE

W. Seidel, H.-G. Ortlepp and J. Fiedler
Zentralinstitut für Kernforschung, Rossendorf, Bereich KF

Parallel plate avalanche counters (PPAC) have been shown to be well suited as large area timing detectors for heavily ionizing particles. We present here the prototype of a double grid avalanche counter (DGAC) /1,2/ with an active area of 13 x 13 cm^2 designed for the inner detector layer of the 4π spectrometer PHOBOS /3/. The detector consists of a 50 $\mu g/cm^2$ thick Formvar foil with 40 $\mu g/cm^2$ gold layers on both sides as a common cathode and two orthogonal anode wire grids. The wire planes are located at 3 mm distance on either side of the cathode and consist of 50 µm Cu-Be wires, equally spaced by 1 mm soldered on printed circuit boards. Each wire is connected to ground through a 500 kΩ resistor. For detecting the X and Y positions of the avalanches, delay line read out is used /4/. All electrode frames were made of epoxy resin plates. The electronics employed has been described elsewhere /4/. The detector was operated in a vacuum chamber filled with n-pentane gas in the pressure range of 1 - 10 Torr. The DGAC counting efficiency was measured relative to an ion implanted silicon detector (SD). For different gas pressures the ratio between the DGAC-SD coincidence and the SD singles count rates was measured as function of the DGAC applied reduced voltage. With 5.5 MeV ^{241}Am α-particles the detection efficiency of 100 % can be obtained only at a pressure of $p \geq 3$ Torr. For fission fragments of a ^{252}Cf source a wide plateau of 100 % detection efficiency is obtained down to p = 1 Torr. At lower pressure values it is difficult to apply voltages high enough for 100 % efficiency without parasitic discharges between the electrodes. Test measurements for the time resolution were performed with a conventional PPAC (5 cm^2 area, 2 mm gap width) and a DGAC in coincidence. For α-particles of an ^{241}Am source the intrinsic time resolution of the DGAC was 290 ps at U = -615 V and p = 4 Torr. Fig. 1 shows time-of-flight (TOF) spectra for different flight paths, measured with a ^{252}Cf source. The TOF spectrum for fission fragments and α-particles at a cathode voltage of U = -570 V and p = 4 Torr, is shown in part a. For the α-particles the intrinsic time resolution amounted only to Δt = 570 ps. The detection efficiency was determined to be 100 % for the fission fragments and the α-particles. The PPAC timing signal was derived from a preamplifier with logarithmic amplitude response /5/. Fig. 1b shows the TOF spectrum of the light and heavy fission fragments with an α-particle pulse height below the trigger threshold. The light fragments show FWHM = 320 ps which corresponds to an intrinsic time resolution of the DGAC of $\Delta t <$ 200 ps, taking into account the energy-loss straggling in the start counter and the intrinsic velocity distribution of the fission fragments. A ΔE-resolution of 20 % and a position resolution of $\Delta X = \Delta Y \leq 1.5$ mm was obtained for a 100 % α-particle as well as fission fragment efficiency. A further optimization of the position resolution is under work.

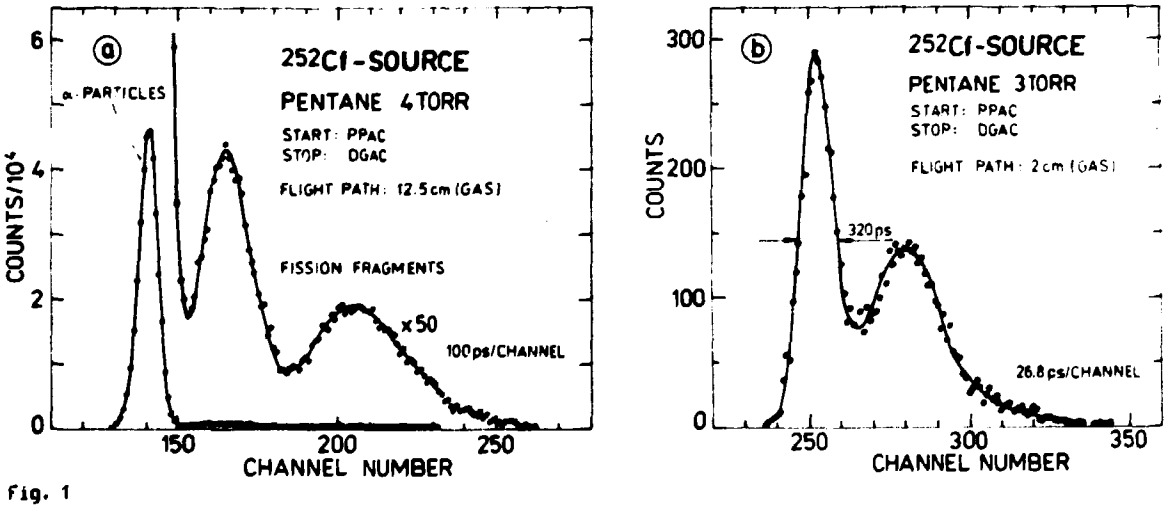

Fig. 1
Time-of-flight spectra for 12.5 cm (a) and 2 cm (b) flight paths

References

/1/ Shenhav, N., H. Stelzer, GSI scientific report; GSI 84-1 (1984) 253
/2/ Hazui, C., H. Ribrag, Nucl. Instrum. Methods 212 (1983) 201
/3/ Soderq, H. et al., annual report 1984, ZfK-559 (1985) 144
/4/ Ortlepp,H.-G., W. Seidel, annual report 1984, ZfK-559 (1985) 149
/5/ Ortlepp, H.-G., this report, p. 95

TIMING WITH FAST PARTICLE DETECTORS

H.-G. Ortlepp

Zentralinstitut für Kernforschung, Rossendorf, Bereich KF

If usual constant fraction triggers (CFT) are operated with the short timing signals of fast particle detectors as micro channel plate detectors (MCP) or parallel plate avalanche counters (PPAC) several difficulties may occur. With shaping delays in the order of 1 ns a proper operation of the zero-crossing detection circuit becomes problematic. Furthermore, intolerable output pulse shifts may occur near threshold /1/ due to a wrong logical combination of the informations from the threshold discriminator and the zero crossing detector in the following circuit, e.g. a D-type flip-flop. During the last two years some new solutions for CFT circuits were tested by us.

If the conventional "fraction" attenuator is replaced by the RLC filter shown in fig. 1 the free time,before the time-defining low-high transition (full circle) at the output of the comparator becomes long enough to guarantee a proper operation of the following logics.

In order to avoid the time shifts for near-threshold pulses /1/ caused by too short signals of the lower level discriminator output leading to an insufficient covering of the "clock" transition by the "D" input signal of the above mentioned flip-flop (FF1 in fig. 2) a second one (FF2) was introduced. The output signal of the "zero crossing" comparator is delayed by del. 2 (~5 ns) until the Q-response of FF1 has reached an unambiguous state.

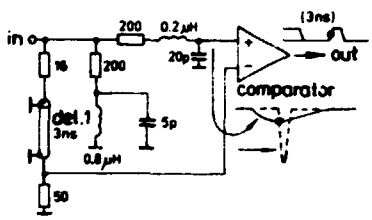

Fig. 1

RLC filter
+ delay - crossover formation

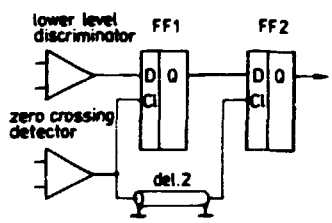

Fig. 2

Modification of the CFT logics

Several investigations were performed concerning the timing electronics for parallel plate (PPAC) or parallel grid (PGAC) avalanche counters. The typical current pulse shape of a PPAC shown in fig. 3 suggests that the best timing information should be derived from the fast trailing edge. A current amplifier with ~ 0.5 ns transition time and an amplification factor selectable between 100 and 800 was applied. In the CFT the "fraction" attenuator was removed (f=1.0), and the delay time between the two inputs of the "zero-crossing" comparator was chosen as Δt = 2 ns (see fig. 3).

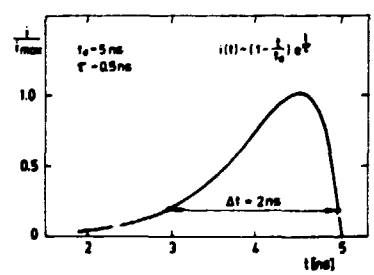

Fig. 3

Current pulse of a PPAC
t_0: drift time through the whole gap
τ: time constant of the electron avalanche
Δt: shaping delay of the CFT with f=1

Thus the comparator fires in that instant when the second of two equal values of the curve i(t) separated by Δt is reached. An advantage of this method is not only the timing at the fastest part of the signal, but also the possibilitiy to extend the dynamic range replacing the fast linear current amplifier /2/ between the PPAC and the CFT by a logarithmic one. The logarithmic response was achieved with the help of a forward biased Schottky type diode KD 514 (USSR) as feedback resistance of the first stage. If comparator chips of the type KR 597SA1 (USSR) were used a walk less than ± 100 ps was achieved for CFT input pulses between 150 mV and 3 V. The corresponding dynamic range of the signals at the input of the logarithmic amplifier amounted, however, to 300 : 1.

With a PGAC the logarithmic principle yielded very bad timing results, probably caused by pulse shape variations at different impact points. In this case a "classical" CFT scheme with f = 0.3 and Δt = 1.5 ns built around a SP 9687 chip (PLESSEY) yielded better results /3/.

References

/1/ Kotte, R. et al., Gemeinsamer Jahresbericht 1983, ZfK-530 (1984) 125

/2/ Ortlepp, H.-G., W. Seidel, Gemeinsamer Jahresbericht 1984, ZfK-559 (1985) 149

/3/ Seidel, W., et al., this annual report, p. 94

A BRAGG CURVE IONIZATION CHAMBER

R. Kotte

Zentralinstitut für Kernforschung, Rossendorf, Bereich KF

Bragg curve spectroscopy (BCS), first proposed by Gruhn et al. /1-5/, is a new method for particle identification in heavy ion reactions. It is based on the generation of an ionization current signal with a time dependence that contains information on the specific ionization along the particle track. If the particle is stopped inside the active volume of the detector, the specific ionization distribution has a characteristic shape known as the Bragg curve, which contains the information required for a Z-identification of the particle and the determination of it's energy.

In this paper we report on an ionization chamber with the electrical field lines parallel to the particle trajectory (Bragg ionization chamber BIC). The chamber is mounted on a piacryle flange (fig. 1). The particle enter the active volume through an entrance window of 2.5 cm diameter. The entrance window was made of stretched polypropylene foil of thickness δ = 100 µg•cm^{-2} supported by an etched brass grid (180 µm broad strips, 2 mm mesh width, 83 % transmission) which serves as cathode together with the brass entrance window holder and an aluminium flange supporting the whole detector construction. The design of the entrance window and the grid holder allows a rapid and simple window exchange. A set of such holders is permanently prepared by glueing with windows of different thickness. The distance between the cathode and the Frisch grid (FG) is chosen as L = 5,3 cm. It is possible to extend this distance to L = 10 cm or even more. Equidistant guard rings with an inner diameter of 4 cm maintain a homogeneous electrical field between the cathode and the FG. A divider chain of 8 x 20 MΩ/0.1 W supplies the voltages for these electrodes. The cathode is held on negative potential with the feedthrough across the high vacuum in front of the chamber. The FG-to-anode distance amounts to G = 0.65 cm. The grid consists of 70 µm copper/beryllium wires with 0.5 mm spacing (sceening inefficiency 1.0 %). The anode is a brass disk maintained at positive potential through the input of the charge sensitive preamplifier. N-pentane was used as stopping gas purified from water and oxygene by a threefold destillation /6/. The pressure was chosen such that the particles with the longest range provide a 5 cm track length. The cathode-to-FG potential was fixed to a reduced field strength E_-/p = 3.8 V/cm•torr corresponding to a drift velocity $v_d \sim$ 3 cm/µs delivering a maximum pulse length of 1.8 µs. In order to guarantee an effective collection of all the electrons drifting to the anode a ratio of the anode-to-FG field to the cathode-to-FG field $|E_+/E_-|$ = 3.5...4.0 was chosen. The signal from the preamplifier was fed into two different shaping amplifiers. The first one was a standard spectroscopic amplifier with 2 µs shaping time for the energy determination. The second one was a special new developed BCS-amplifier+peak stretcher unit /7/ with a short shaping time (adjustable in three steps: 47, 100, 220 ns) which is comparable to the electron transit time through the anode-to-FG gap. This signal when viewed on an oscilloscope should be representative of the Bragg curve. Both signals were digitized and fed into a two-dimensional analyzer with colour display.

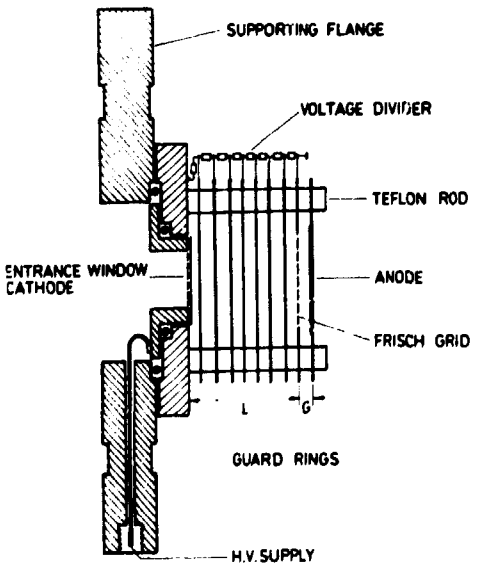

Fig. 1
Bragg chamber cross section

References

/1/ Gruhn, C.R. et al., NIM 196 (1982) 33
/2/ Schiessl, Ch. et al., NIM 192 (1982) 291
/3/ Asselineau, J.M. et al. NIM 204 (1982) 10'
/4/ McDonald, R.J. et al., NIM 219 (1984) 508
/5/ Shenhav, N.J. et al., NIM 228 (1985) 359
/6/ Walzog, D. et al., ZfK-559 (1984) 155
/7/ Ortlepp, H.-G., this annual report p. 98

TEST MEASUREMENT WITH A BRAGG IONIZATION CHAMBER AT THE ROSSENDORF TANDEM ACCELERATOR

R. Kotte, H.-G. Ortlepp, H.-J. Keller and F. Stary
Zentralinstitut für Kernforschung, Rossendorf, Bereich KF

First experimental results are reported on the Bragg ionization chamber (BIC) presented in a former paper /1/. The alpha particle resolutions of the BIC obtained with a pressure of 150 torr n-pentane are given in table 1. After subtracting the contributions of the electronics ΔE_e = 18 keV and the straggling in the entrance window ΔE_w = 19 keV, determined with a high resolution surface barrier detector, the intrinsic BIC energy resolution for alpha particles amounts to ΔE_{BIC} = 22 keV (FWHM). The BIC properties for heavy ions were proved at the Rossendorf 5 MV tandem accelerator. The following ions were used for the measurement of the energy and Bragg peak resolutions as well as for the determination of the response functions of these parameters: 22.75 MeV $^{12}C^{4+}$, 26.0 MeV $^{16}O^{5+}$, 36.0 MeV $^{35}Cl^{7+}$, 32.2 MeV $^{28}Si^{6+}$, 36.8 MeV $^{28}Si^{7+}$, 41.4 MeV $^{28}Si^{8+}$, 31.5 MeV $^{32}S^{6+}$, 36.0 MeV $^{79}Br^{7+}$. These particles were elastically scattered from a 10 µg·cm^{-2} ^{197}Au target evaporated on a 10 µg·cm^{-2} carbon backing fixed on an aluminium target holder. The scatter products were observed at an lab. angle ϑ = 30° and a distance l = 70 cm between the target and the entrance window with a solid angle $\Delta\Omega$ = 1 msr. In order to produce a continuous energy distribution of the scattered particles in some cases a cellulose absorber was set behind the target. In table 1 resolution parameters (FWHM) for different heavy ions are presented. The given energy value E is the energy of the particles deposited in the active gas volume of 60...150 torr n-pentane as measured with the BIC. For the estimation of the BIC energy response the elastic scatter peaks of the projectiles and a few recoil peaks of target, backing and target holder components are used. For the heaviest particles (^{79}Br, ^{197}Au) the energy response function is no more linear due to an increasing contribution of recombination effects in the gas. In first approximation the response of the Bragg peak which is a measure of the element number Z is also a linear function. A typical two-dimensional plot of BP over E is given in fig. 1. The charge resolving power of the detector is obvious from the corresponding BP single spectrum (fig. 2). The BP resolution may be improved by increasing the BCS amplifier shaping time constant τ (table 1), but, the energy point at which the BP becomes independent of the energy will rise, too. We found a compromise of τ = 100 ns corresponding to half the transit time of the electron through the Frisch grid-anode-gap.

Table 1

BIC resolution parameters (FWHM)

$^{A}_{Z}X$	ΔE keV	E MeV	$\frac{Z}{\Delta Z}$	τ ns
$^{4}_{2}He$	34	5.3	31 45	100 220
$^{12}_{6}C$	250	21.7	37	100
$^{16}_{8}O$	400	23.9	42	100
$^{28}_{14}Si$	400	35.4	27 35 47	47 100 220
$^{32}_{16}S$	480	28.6	28 35 47	47 100 220

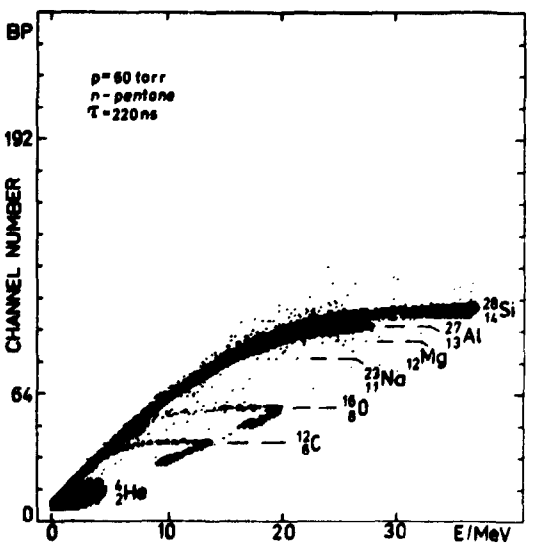

Fig. 1

Bragg peak vs. energy distribution of elastical scattered 41.4 MeV ^{28}Si ions and recoils from target (^{197}Au), backing (^{12}C) and target holder (^{27}Al,Mg, ^{23}Na, ^{16}O)

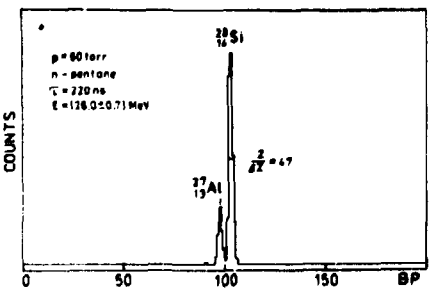

Fig. 2

Bragg peak spectrum for a given energy window deduced from fig. 1

References

/1/ Kotte, R., this annual report p. 96

SHAPING AMPLIFIER FOR BRAGG CURVE SPECTROSCOPY

H.-G. Ortlepp
Zentralinstitut für Kernforschung, Rossendorf, Bereich KF

The introduction of the Bragg curve spectroscopy technique /1/ for heavy ion Z identification requires a shaping amplifier with a time constant comparable with the electron drift time between the grid and the anode of the Bragg ionization chamber. Usually this drift time is in the order of 0.1 to 1 microseconds. Most of the available spectroscopy amplifiers, have, however, shortest shaping times of 0.25 or 0.5 microseconds. Therefore, a new shaping amplifier was developed meeting the requirements of Bragg curve spectroscopy. The amplifier together with a peak stretcher is housed in a 40 mm wide EGS module. The simplified circuit diagram of the amplifier part is shown in fig. 1. The three operational amplifiers are built up from discrete components. The shaping is performed by one pole-zero compensated differentiation just at the input and four decoupled RC-integration networks between the second and the third amplification stage. Time constants of 22; 47 and 105 ns are selectable by a switch, resulting in shaping times (with the commonly used normalization) of 47; 100 and 220 ns, respectively.

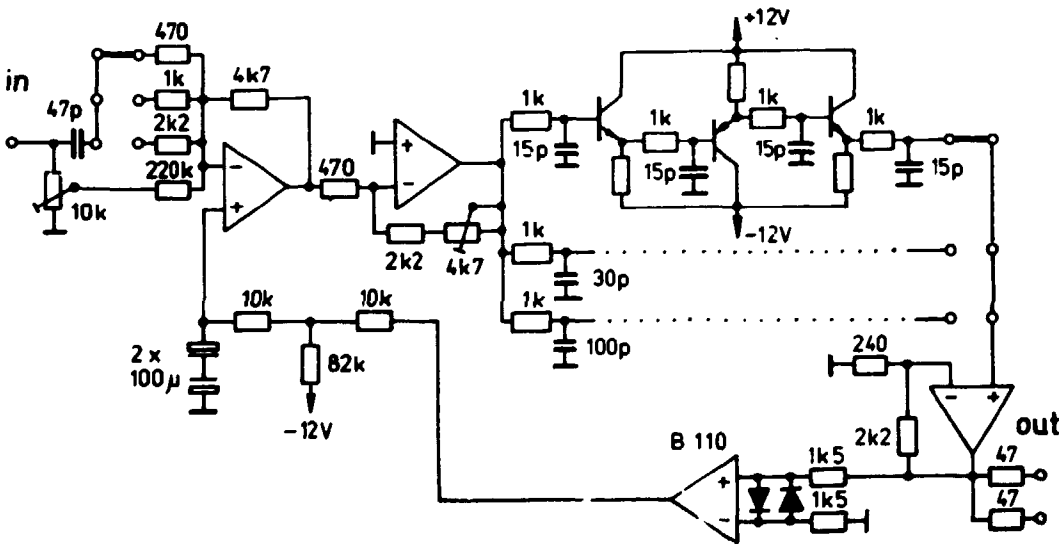

Fig. 1
Simplified circuit diagram of the Bragg curve spectroscopy amplifier

The amplification factor defined as the step response amplitude divided by step height, may be adjusted in the second stage by the 4.7 kΩ potentiometer from 50 to 150 (at 100 ns shaping time). Both the input and output polarities are positive. Baseline stabilization is performed by a feedback loop including a B 110 voltage comparator (µA 710) and an RC low pass. Different from usual amplifiers the change of the differentiation time constant is performed by changing the resistance before the virtual ground of the first stage. In this way the step response amplitude becomes proportional to the inverse of the shaping time. The Bragg curve signal, however, remains nearly independent of the shaping time. Therefore, the amplification needs not be changed when the shaping time is changed. The Bragg peak amplitude decreases only slightly with increasing shaping time because the peak becomes broader and more flat. The shaping times were chosen shorter than usually utilized in order to extend the Bragg curve spectroscopy to lower heavy ion energies.

References

/1/ Kotte, R., this annual report, p. 96

AN AXIAL IONIZATION CHAMBER FOR FRAGMENT DETECTION

L.N. Andronenko, V.V. Janofsky, A.A. Kotov, L.A. Vaishnene
Leningrad Nuclear Physics Institute, Gatchina, U.S.S.R.
W. Neubert
Zentralinstitut für Kernforschung Rossendorf, Bereich KF

Fig. 1 shows a cross section of the ionization chamber provided for Bragg curve spectroscopy of fragments emitted in proton-nucleus collisions. The distance between the cathode mesh and the anode is 140 mm. The anode made from polished copper-plated epoxy resin is screened by the Frisch grid at 20 mm distance. In order to achieve an electrical field parallel to the incoming particles between the cathode and the anode, ten equidistant guard rings are mounted. The inner diameter of these field shaping rings increases like a cone to have regard to the different diameters of the meshes of the cathode (20 mm) and of the Frisch grid (80 mm). The guard rings are spaced and insulated by glass cylinders fixed on brass holders. A divider chain supplies the voltages for these electrodes. In order to keep the pollution of the gas as low as possible the case of the ionization chamber is made from steel covered by nickel. The particles to be detected enters the chamber through a thin foil of Formvar supported by a nickel mesh wire of 97 % transparency. An additional electrode is placed at 2 mm distance in face of the cathode mesh. Both electrodes are made from a nickel mesh of 6 strips per mm and form an avalanche counter provided for timing measurements.
The ionization chamber was operated with n-heptane and n-pentane purified using the following procedure. Both liquids were deep-frozen by means of liquid nitrogen, then the rest gases were pumped out from the reservoir and pentane (or heptane) were distilled into the ionization chamber volume. Usually, this procedure was repeated once more before the voltage to the electrodes was switched on.
First test experiments were carried out with a ^{252}Cf source. The gas pressure was adjusted such that the maximum range of fission fragments corresponds to the effective length of the chamber. The anode pulses were fed into a charge sensitive preamplifier and processed by a CAMAC data acquisition system.
The pulse height distribution measured with heptane had a shape typical an energy spectrum of fragments slowed down by an absorber. This effect, which is due to the increased recombination probability of heptane, was also observed for n-butane /1/. Finally, purified pentane was found to be a suitable gas. The energy spectrum (fig. 2) gives a peak-to-valley ratio p/v = 2.6 ± 0.4 which agrees with the result in ref. /1/ obtained with a constant gas flow of isobutane.

References

/1/ A. Ocd, P. Geltenbort, P. Gönnenwein, T. Manning and D. Gouque; Nucl. Instr. Meth. 205 (1983) 455

Fig. 1

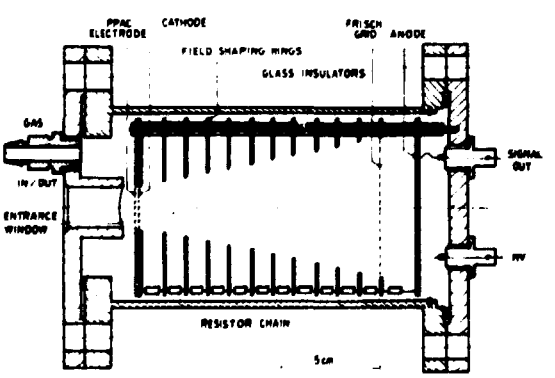

Fig. 2

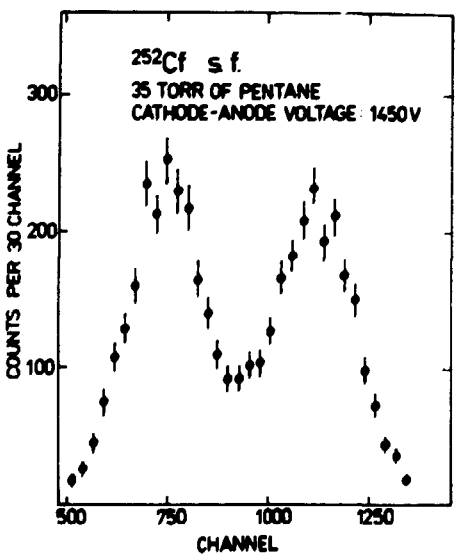

A FAST DISCRIMINATOR WITH LOW-LEVEL THRESHOLD

A.I. Iljin+) and W. Heubert
Zentralinstitut für Kernforschung Rossendorf, Bereich KF

Fast preamplifiers connected to parallel plate avalanche counters (PPAC) provide pulse heights which may vary from several tens up to some hundreds of millivolts. In timing measurements with such detectors it is advantageously to use a fast discriminator which allows to adjust a low threshold. Here we present a simple fast discriminator on the basis of electronic components available at present time. The circuit diagram is shown in fig. 1. Two discriminators are assembled on a double-sided printed circuit board in CAMAC standard. Starting with physical events this discriminator allows an adjusting the low-level threshold at about 30 mV. An univibrator for the stretching of the output signal and a delay adjustment are provided for further improvements. Special applications require the corresponding option of the entrance part of the discriminator.

Timing measurements (fig. 2) were made with generator and detector pulses both fed through a fast preamplifier with a rise time of about 3 ns. For generator pulses an attenuator was used to vary the signal level at the discriminator input. The transit time was measured with a TAC connected between the discriminator output and the pulse generator synchron output (left part of fig. 2). We achieved a walk of $\lesssim$ 550 ps in the dynamical range from 40 mV up to about 1 V. The discriminator was also tested with a TOF arrangement of two PPAC's. The voltage of the start detector was changed whereas the voltage of the stop detector was kept constant. The points of the right part of fig. 2 refer to the peak position of the light fragments of ^{252}Cf separated from the heavy ones by a flight path of 7 cm. If the start PPAC is operated at low voltage a full resolution of both groups is prevented and some uncertainties are introduced. We repeated the measurements with the fast discriminator SD 5034 manufactured in series at the ZfK. It is obviously, that this discriminator cannot be applied to precise timing measurements.

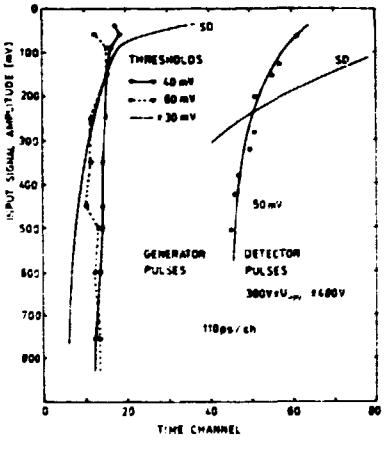

Fig. 2

+) On leave from Leningrad Nuclear Physics Institute, Gatchina, U.S.S.R.

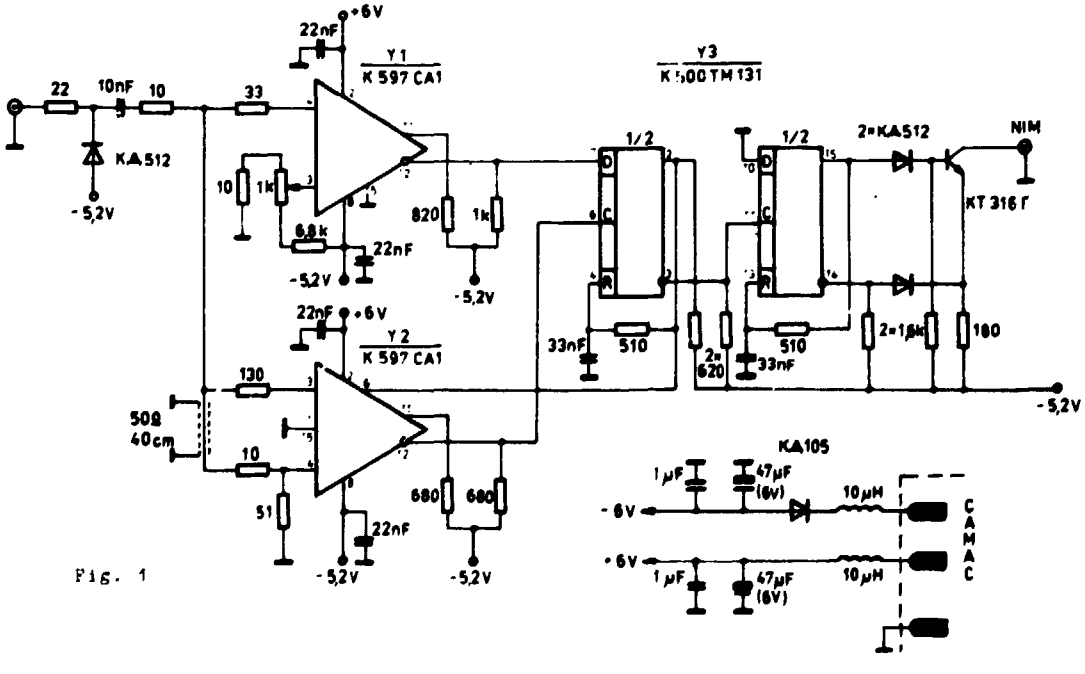

Fig. 1

PREAMPLIFIER FOR SILICON PARTICLE DETECTORS

H.-G. Ortlepp and E. Schuster
Zentralinstitut für Kernforschung, Rossendorf, Bereich KF

For several years an increasing number of silicon particle detectors has been produced at the CINR nuclear and solid state physics departement /1/. Devices with rather different geometrical and electrical parameters are used e.g. for alpha-spectroscopy and in-beam charged particle detection including fast timing.

Therefore, a preamplifier for broad range applications was developed (fig. 1). Since detector capacities of more than 1000 pF have to be expected a high transconductance FET was used. Selected devices of the power type KP 903 (U.S.S.R.) with g = 50...80 mS at I_d = 20 mA yielded values of the noise line width in the order of 4 keV + 10 eV/pF at 2 µs shaping time. In order

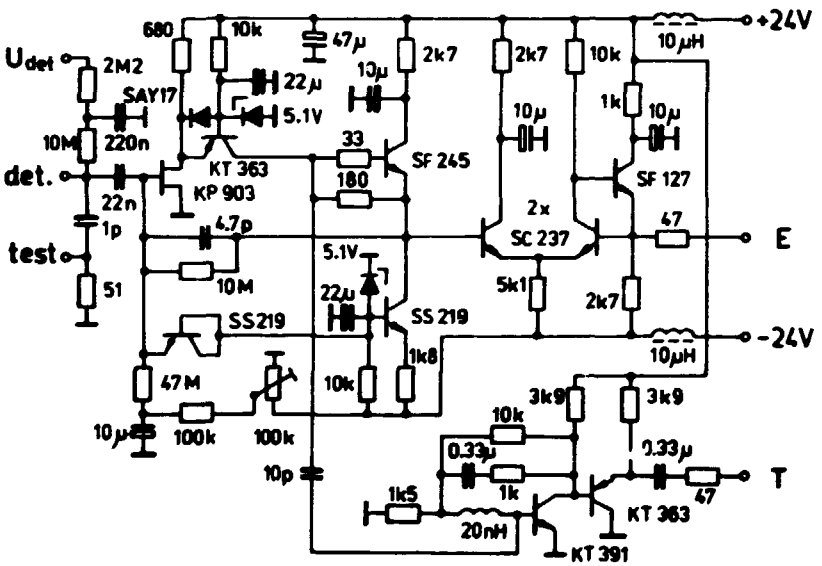

Fig. 1
Circuit diagram of the preamplifier

to get a linear response up to ~ 1000 MeV, necessary for heavy ion experiments, the sensitivity had to be kept low. On the other hand, at a too low sensitivity the input noise of the shaping amplifier influences the resolution. The chosen value of 8 mV/MeV seems to be a reasonable compromise. The 1000 MeV dynamic range is reached only if the detector bias is positive. With the help of the 100 kΩ Potentiometer the potential of the E-output is adjusted to zero. The timing signal is coupled from the high impedance point of the charge sensitive loop via a 10 pF capacitor to a current to voltage converter. The risetime of the timing output (T) signal amounts to 0.8 ns if a pulse of 0.2 ns risetime is fed into the test input.

The preamplifier was used in a time of flight-energy spectrometer for low mass charged particles. A small parallel plate avalanche counter (PPAC) with about 150 ps (FWHM) time resolution for alpha particles acted as start detector. The PPAC timing system is described in ref. /2/. For Si detectors of 13; 50; 800 and 1250 mm^2 active area time resolutions of the whole spectrometer of 200; 260; 450 and 700 ps (FWHM), respectively, were achieved.

References

/1/ Borany, J. von et al., this annual report, p. 56
/2/ Ortlepp, H.-G., this annual report, p. 95

SUPPRESSION OF LOW-MULTIPLICITY γ-RADIATION IN PLUNGER EXPERIMENTS BY MEANS OF COINCIDENCE TECHNIQUE

G. Winter, W. Schulze and E. Will
Zentralinstitut für Kernforschung Rossendorf Bereich KF

In-beam γ-ray spectra can be seriously contaminated by γ-rays arising from the β-decay of isotopes produced during the irradiation of the target, from inelastic neutron scattering on the surrounding material or from long-lived radioisotopes. In plunger experiments the beam of bombarding particles strikes not only the very thin target but also the plunger and the target backing. Nuclear reactions of the 27 MeV α-particle beam with these materials lead to an additional source of background radiation. Using a low-Z material for the plunger and the target backing (polyesther foil) all these background radiations are of low multiplicity compared to the multiplicity of the prompt radiation arising from (α,2n) reactions on nuclei of the A = 80 mass region where average multiplicities of about 5 are expected. Therefore, the background component in the γ-ray spectrum recorded by a Ge(Li) detector can be suppressed when multiple $\gamma\gamma$-coincidences with additional detectors are measured. In order to obtain the coincidence spectrum of the Ge(Li) detector with good statistical accuracy it is necessary to detect the γ-rays from the target with high efficiency. This condition was fullfilled by using a new plunger of small volume /1/ and high transparency for γ-radiation and by recording the emitted γ-rays in two NaI(Tl) detectors (7.5 cm diameter, 7.5 cm length) which both are arranged at a distance of 4 cm from the beam spot. The Ge(Li) detector was positioned at a distance of 12 cm from the target and recorded the emitted γ-rays at an angle of 24 $\pm$ 8 degrees with respect to the beam direction (see the insert of figure 1). In a computer simulation /2/ this arrangement has been found to give the desired properties.

Signals from the Ge(Li) detector are stored in different parts of the memory when they are found in coincidence with signals from either no, one ore two NaI(Tl) detectors resulting in spectra of 0-fold, 1-fold and 2-fold coincidences, respectively. The resolving time of the multiple coincidence circuit was 36 ns. The influence of the coincidence selection is illustrated in figure 1. The dominating peaks in the 0-fold spectrum are caused by reactions of the α-particles with the polyesther foils (each 0.49 mg cm^{-2}) and successive β^+ decays. In the 1-fold spectrum these peaks are suppressed by a factor of about 10 whereas the intensity of the desired peaks arising from the (α,2n) or (α,pn) reaction on ^{77}Se is not reduced. Moreover, due to the reduction of the general continuum the statistical uncertainties are about 3 times smaller in the 1-fold than in the 0-fold spectrum. Lifetimes of excited states in ^{79}Kr as deduced from these measurements are presented separately /3/.

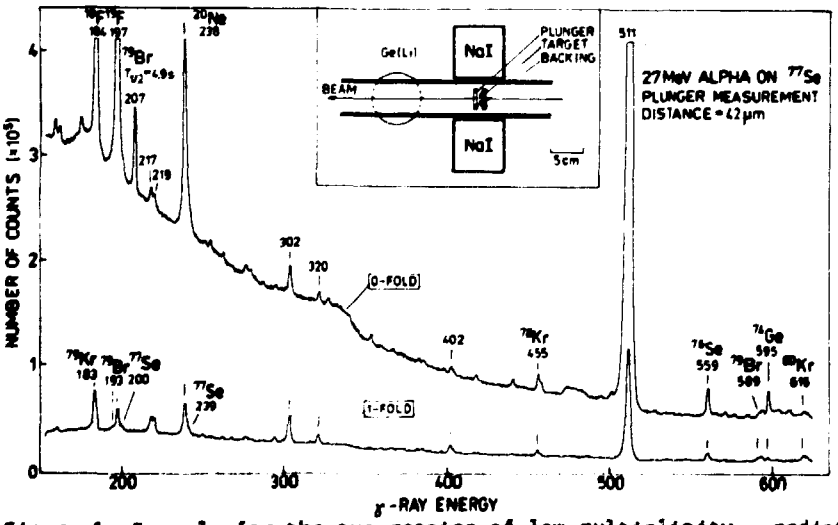

Figure 1. Example for the suppression of low-multiplicity γ-radiation. The insert shows the geometry of the coincidence arrangement.

References:

/1/ Winter, G., Freitag, M., and Schulze, W.; this report p. 93

/2/ Winter, G.; Nucl. Instr. Meth. A243 (1986) 192

/3/ Winter, G., Schwengner, R., Funke, L. and Döring, J.; this report p. 21

MAJORITY COINCIDENCE UNIT

E. Will
Zentralinstitut für Kernforschung Rossendorf, Bereich KF

Multidetector coincidence arrangements are frequently used in nuclear research. In such experiments coincidence events will only be recorded, if a desired number of detectors or a distinguished combination of detectors (pattern) have fired. For the interpretation of a coincidence event the number of detectors or the detector pattern have to be recorded. In order to process a high data rate special coincidence modules are used for this aim. Therefore, a majority coincidence with the following properties was constructed:

- The number of detectors (majority) and/or the detectors which have to see an event (master) can be specified.
- The coincidence time can be chosen between 30 ns and 20 µs.
- A separate strobe input is possible for realising a fast-slow coincidence. The strobe time can be adjusted between 0.5 and 5 µs.
- The coincidence allows 12 coincidence input signals.
- A separate coincidence input can be used that is not included in the majority logic.
- Each input signal may be either in the TTL or in the NIM standard.
- The number of input signals and the input pattern is aveiable in the SI 1.2 standard.

In figure 1 the scheme of an experiment [1] is shown with one Ge(Li) detector (master) and two NaI detectors. The leading edges of the shaped pulses start the time and selection logic. An ECL logic adds the input signals and gives the result to the output and the multiplexer, which compares the sum with the demanded number of detectors (fold). In case of agreement and if also the signals of both the master logic (in this case only from the Ge(Li) detector) and the ADC come within the strobe time (3 µs) an output signal is generated, that starts the conversion in the ADC and gives a LAM to the computer. The computer reads the data from the ADC and from the coincidence unit with the help of a multiplexer [2]. After the data transfer a general reset of the module is carried out.

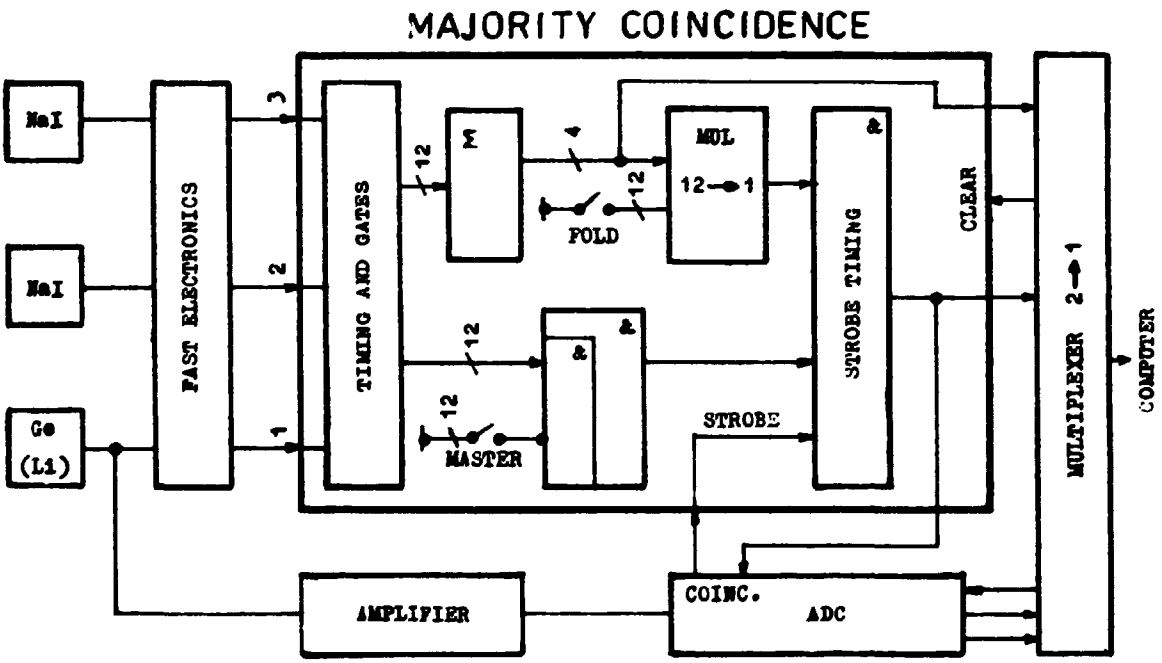

Figure 1: Scheme of an experiment with one Ge(Li) and two NaI detectors.

References

[1] Winter, G., Schulze, W. and Will, E.; this report p. 102
[2] Will, E.; Annual report ZfK 443 (1981) p. 205

ELECTRONIC DEVELOPMENTS OF THE KFM GROUP

H. Angermann, W.D. Fromm and F. Schwarzenberg
Zentralinstitut für Kernforschung, Rossendorf, Bereich KF

Magnetic Tape Cassette Controller 9958-20

On the base of the single board computer UPC 880 an intelligent interface unit for the Robotron K 5200 magnetic tape cassette drive was developed /1/. The controller provides the commonly used SIF 1000 Interface. The first batch was manufactured using wire-wrap technology to build the specific part of the interface-logic (IL). Later on this part was optimized and produced as a small printed circuit (PC) board adapted to the single board computer (SBC). With the version 9958-20 both parts (SBC + IL) are combined on a 170 * 205 mm² PC board in order to facilitate production. A description of the magnetic tape cassette interface is published in ref. /2/.

Small TV-Monitor

For the compact multichannel analyzer (MCA) a small display monitor had to be developed as a built-in unit. High resolution alphanumeric and graphic output is desirable. Display drivers supporting an addressable field of 256 * 512 pixels are available (VIS2A, GDD 5216) and generate signals according to the TV standard. Therefore, the TV-tube M17-111 (Tungsram, Hungary) with a screen diagonale of 155 mm has been used. The deflection electronic is realized on two PC boards with the dimensions of 95 * 150 mm² each. The power consumption is 10 W. The circuits were optimized for good linearity (< 1%) which is essential for graphic output. The unit is constructed as EGS-module of 160 mm width.

Small Functional Keyboard 9902

For the control of the compact MCA a keyboard with full alphanumeric capability is not the optimal choice. In addition to such drawbacks as large dimensions and weight the user may prefer a device-like communication with the instrument using dedicated buttons to invoke certain pre-programmed functions. A small keyboard constructed from conductive rubber with 32 keys arranged in 8 rows and 4 columns was developed. As interface a PIO was used. The scan of the keyboard is performed by software. The codes of the keys are taken from a table which can be easily changed. Four LED's of different color in the top row are used als visual feedback. The geometrical dimensions of the keyboard are 60 * 140 mm². A flat ribbon cable is used as connection to the interface module.

PROM-Programmer 9900

For the microcomputer development system MPS 4944 a PROM-programming module was developed for EPROM's of the types 2708, 2716 and 2732. The PC board 9900 (95 * 170 mm²)/3/ generates the programming voltage of 26 V. The data-, address- and control-signals are provided by two PIO and transistor switches. The programming regimes are implemented by software. The programmer was adapted to the MPS bus and mounted in a standard MPS board frame. A 24 pin ZIF socket is connected with a flat ribbon cable to the front panel. The monitor program of the MPS system was supplemented with commands for reading and programming the EPROM. A test for programmability before and correctness after the programming is performed automatically.

Hardware Multiplication Unit 4058

The 16 bit minicomputer KRS 4201 has no instructions for multiplication and division. In process automation as the main field of application these instructions are of minor importance. In scientific canculations however the emulation of these instructions represents a substantial part of the total running time. Therefore, a hardware multiplication unit for the KRS 4201 was developed /4/. The unit consists of 2 PC boards and attaches to the programmed channel of the computer. The multiplication of two 16 bit operands is carried out in 5 µs. A software package containing subroutines for floating-point multiplication and division (by successive multiplication) was implemented. The calculational speed improves by a factor of about ten.

References

/1/ F. Schwarzenberg and W.D. Fromm; Gemeinsamer Jahresbericht 1983, ZfK-530(84)p.129
/2/ F. Schwarzenberg and W.D. Fromm; radio, fernsehen, elektronik, 35(86)Nr.4
/3/ F. Gabriel et al.; Neuerervereinbarung NVe 19/83, ZfK Rossendorf, 1983
/4/ J. Zschau et al.; Neuerervereinbarung NVe 29/80, ZfK Rossendorf, 1980

HARD- AND SOFTWARE SUPPLEMENTS FOR THE COMPUTER Z 9001

P. Schwarzenberg
Zentralinstitut fuer Kernforschung, Rossendorf, Bereich KF

The standard version of the ROBOTRON homecomputer Z 9001 comes with 16K Dynamic RAM, 4K ROM for the operating system and 1K Static RAM for the video refresh memory. A 4-slot external U880-processor bus is implemented for memory expansions. ROBOTRON offers for memory expansions a 16K-DRAM and a 10K-ROM plug-in module. Standard software tools are a 10K-Basic-Interpreter and a 10K-Editor /Assembler.

Here some hard- and software tools for the Z 9001 are presented which has been developed to provide a wider range of applications in scientific institutes.

1. Software solutions

- Monitor/Debugger ZM-9001

  This program supports powerfully the implementation of machinecode programs. For this aim 25 commands can be used. Among them are commands for starting user programs with two breakpoints, for displaying and changing memory contents and processor registers, for moving, verifying or testing memory areas, for searching binary strings and for working with I/O-ports. Moreover, the program delivers a lot of I/O-routines to handle data transfer with peripheral devices. For this purpose the user-port (one PIO-port and one CTC-channel) has been taken to connect peripheral devices with the standard interface SIP-1000. Furthermore, an output-routine exists to apply a RS232-output-device like the thermal printer TD 40 for program listings or graphic applications.

  With the 'Assign'-command the user can assign the logical implemented devices CONSOLE, READ, PUNCH and LIST to different I/O-routines (physical I/O-devices).

  Another powerful feature of the ZM-9001 is its ability to switch the computer into a CP/M-compatible mode. A lot of well-known CP/M-programs (e.g.ZSID, MBASIC) can be used in this mode.

- Screen Editor BITEX-Z9001

  The CP/M-version of the screen editor BITEX-88/3 developed in the ZfK Rossendorf for the microprocessor system MPS 4944 has been adapted to the Z 9001. If no printer is available in the system configuration, the off-line output of the text files is carried out by data transfer to the magnetic cassette tape.

- Z 9001 Tape Protocol Interface

  On the MPS 4944-based CP/M-system a program was implemented that allows the Input/Output of Z 9001-magnetic tapes. Thus an off-line communication between the CP/M-system and the Z 9001-systems is possible.

2. Hardware solutions

- 10K-ROM-Module with bank switching

  To realize BASIC- and word processing applications without changing plug-in modules the standard ROM-Module was modified. This module occupies the address range C000H-E7FFH. The main feature of this module is the use of the bank switching principle. Thus, two or more of this modules may be plugged into the system at the same time. The actual module is selected by software. The above mentioned ZM-9001 also includes the switching technique for such modules. The system developed in the ZfK works with two of such modified modules and permits to operate 20K-ROM <u>and</u> 48K-RAM simultaneously.

- Communication module

  To provide the communication with other computers or peripheral devices, a module for serial communication has been developed. The module contains a SIO- and a CTC-device and includes one RS232- and one current-loop-channel. On the base of this module a system for word processing was installed using the following components:

  - one ROM-Module with ZM-9001 and BITEX
  - two RAM-Modules (==> 48K-RAM configuration)
  - typewriter S 6010 with RS-232-interface

  The text input and output proceeds directly from/to the S 6010 using BITEX-Z9001.

SOFT- AND HARDCOPY FOR HOMECOMPUTERS

H.-J. Müller, F. Schwarzenberg and W.D. Fromm
Zentralinstitut für Kernforschung, Rossendorf, Bereich KF

Homecomputers has been proved to be a useful tool for the effective solution of small and intermediate numerical problems in theoretical and experimental physics. To enlarge its field of application a COMMODORE 64 computer (C-64) was connected to other computers and peripheral devices. Thus it has become possible to receive and to send program- or textfiles and to make hardcopies of computer generated high-resolution graphics using dot matrix graphic printers (DMGP).

The C-64 provides an implemented software for using a RS 232-channel to communicate with other computers and peripheral devices. Thus it is possible to control such options as baud rate and parity as well as the number of start and stop bits with BASIC or machine language kernel routines, but no physical RS 232-channel exists in the standard configuration of the C-64. Therefore it is necessary to convert the TTL-level of the C-64 I/O-signals either to the standard level of RS 232 (+/- 3...25 V) or to a 20 mA-current loop. Because of the inexpensive hardware realization (two optocouplers; two transistors) and the complete galvanic seperation of the coupled devices the current loop was preferred. The C-64 was connected with a MPS 4944-based CP/M-development system. The communication software of the CP/M-system permits the received C-64 data to be transmitted to the console, to the print device (line- or type-wheel printer) or to a digital cassette drive /1/. At present time the C-64 hardcopy data will be sent to the DMGP (SD 1154) off-line by using the magnetic tape cassette drive /2/. It is planned to install a one board microcomputer /3/ inside the DMGP to realize an on-line contact with the C-64.

The hardcopy of high-resolution graphics (320 by 200 dots) takes some care because the bytes of the screen memory of the C-64 are arranged horizontally, while the bytes selecting the needles of the DMGP are organized vertically. A further complication arises from the demand of enlarging the x- and y- axis of the graphics twice to minimize the printing inaccuracies of the DMGP with respect to the graphic size. One short machine language program for the C-64 serves as a byte-generator of the bit-mapping memory acting horizontally, while an additional machine language program working in the receiving system transforms the bytes vertically and doubles the size of the graphics. This way has been shown to provide the most effective data transfer of the different versions proved. The transmission of one high-resolution graphics lasts about 40 sec. at a baud rate of 2400. The printing time is limited by the velocity of the DMGP only. On the other hand, the data transfer by magnetic cassette tape serves as an easy way to safe these graphics for later access.

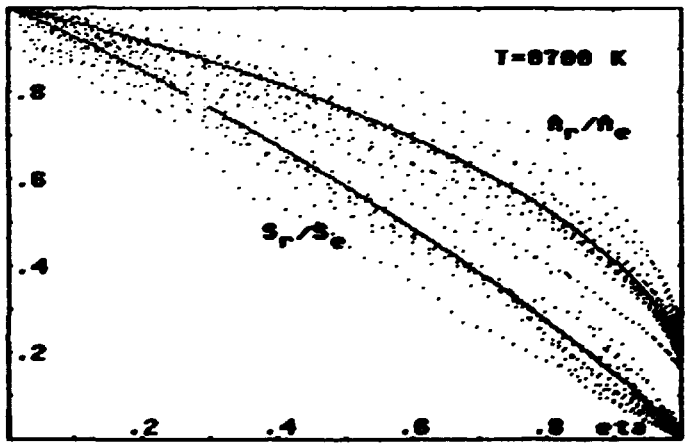

Hardcopy of a high-resolution graphics generated by the C-64

/1/ Schwarzenberg, F. and Fromm W.D.; radio, fernsehen, elektronik 35 (1986) Heft 4
/2/ Fromm, U., Fromm, W.D., Heinig, K.-H. and Otto, G.; this report p. 137
/3/ Schwarzenberg, F. and Fromm, W.D.; Proceedings of the XI. International Symposium on Nuclear Electronics, Bratislave 1983, D13-84-53, p.204, Dubna 1984

THE DATA-LINK- AND PHYSICAL-LAYER IN THE LAN GDP-NET

W.-J. Linnemann

Zentralinstitut für Kernforschung, Rossendorf, Bereich G

The software of a comput r network may be considered as a set of cooperating distributed processes organized as a hierarchical structure of layers. They are characterized by the services offered to the entities located in the next upper layer.

In the software package implemented in the distributed process-control system at tandem and cyclotron accelerator [1] the Application Layer is the highest one. It is offering the service for user tasks. The lowest level consits of the Data Link Layer and Physical Layer (Fig. 1). For each layer main data units are the Interface-Data-Units IDU and the Protocol-Data-Units PDU.

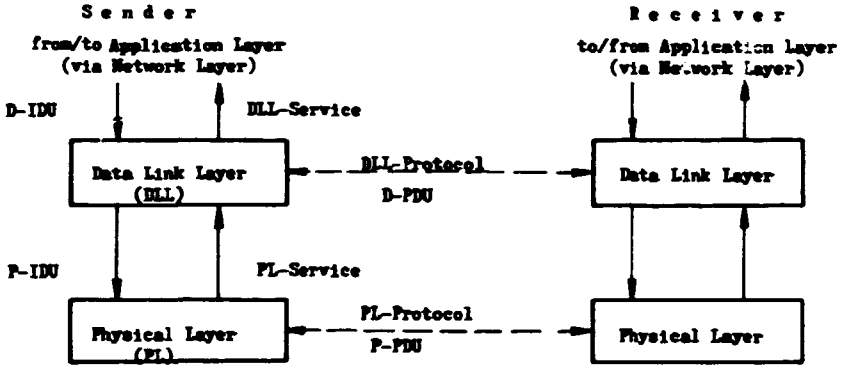

Fig. 1 Correspondence between layers, services and protocols

In our net we use a CAMAC system for Data transfer. Therefore, the logical parameters of the CAMAC medium access unit (Link-Modul 1471) determines the Protocol Data Units of the Physical Layer P-PDU.
The P-PDU (Fig. 2) is a set of LAN (look at me) signals and a transparent information.

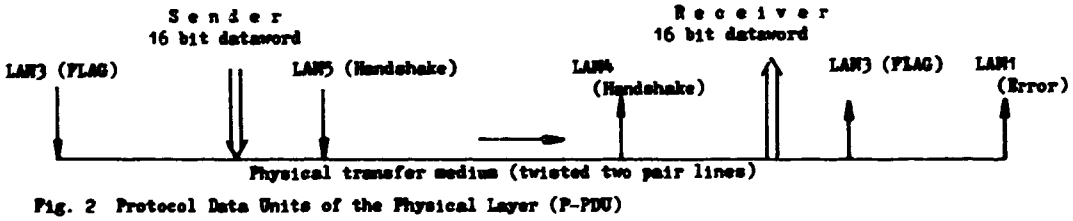

Fig. 2 Protocol Data Units of the Physical Layer (P-PDU)

The tasks of Data Link Layer realises the logical control, frame assembling and medium management. The Interface-Data-Units of the Data Link Layer (D-IDU) are: RECNER (receiver number), CTRL (for response handling) and BUFFER (user dates). The result of frame assembling is the Data Link Layer-PDU (D-PDU).
There are two types of the D-PDU.

- Control frame:	FLAG	RECNR	CTRL	CNTRL0-CNTRL 7	FCS	FLAG
- Inform. frame:	FLAG	RECNR	CTRL	DATABYTES (2-4092)	FCS	FLAG

FCS: Frame checking sequenz, CNTRL0-CNTRL 7: Protocol Control Unit (PCU).

[1] Hiekmann, S. and Fülle, R.; mer 25 (1982)621

A Variant for On-Line Rapid Extraction in Nuclear-Chemical Experiments with Crown Ethers

E. J. Langrock
Technische Hochschule Leipzig, SNW 2

K. Eichhorn
Zentralinstitut für Kernforschung Rossendorf, Bereich G

K. Gloe und P. Mühl
Zentralinstitut für Festkörperphysik und Werkstofforschung Dresden

For a number of nuclear-chemical investigations, an on-line rapid extraction system ought to be applied. In literature, systems have been described, in particular, where the recoil nuclei from a solid thin target are transported away by means of a He-jet and conveyed into a solution /1-4/.

Skarnemark et al. have described a system where HCl/N_2 carries out the transport in to the solution /5/.

The variant of irradiating a solution, where a (n,γ)-reaction taking place, applied by Aronsson et al. in 1973 was no longer presented in the literature published later on.

In the present case, it was intended to test the chemical fundamentals of the extraction under dynamic conditions described in /7/. For this purpose, the reaction $^{nat.}Hg + \alpha$ was chosen and an aqueous target solution, irradiated with He-nuclei of an energy of 26 MeV in the Cyclotron U-120 in Rossendorf. For irradiating the aqueous target solution, a flow chamber was developed. The ion beam (vacuum) entered the irradiation chamber (normal pressure) through thin foil window (6 μm Ti). A schematic sketch of the experimental setup is shown in Fig. 1. In order to separate the phases, a centrifugal extractor was used. A $HgCl_2$-solution at a pH-value of 4.6, was used as aqueous phase and a solution of 18-crown-6 in benzene, as organic phase. The concentrations corresponded to the conditions described in /7/. Already few seconds after the beginning of the experiment, aliquots were taken out of both phases and evaluated by γ-spectroscopy. The Pb-isotopes found are shown in Tab. 1.

Tab. 1

nuclide	energy	$T_{1/2}$
Pb-197M	239.5 keV 608.5 keV	42 min
Pb-199	353.4 keV 366.9 keV	1.5 h
Pb-202M	422.1 keV 960.7 keV	3.62 h
Pb-204M	374.7 keV 898.9 keV 911.4 keV	1.15 h

Fig. 1

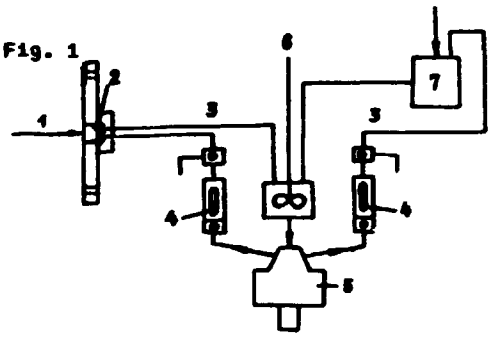

1-beam; 2-irr. chamber; 3-valve for samples; 4-rotameter; 5-centrifugal extractor; 6-mixer; 7-storage

The distribution coefficient of 24 found for Pb, for the extraction into the organic phase, did not change during the experiment, which four hours. Thus crown ethers may be considered suitable for the rapid extraction. The flow chamber for irradiating liquid targets has proved serviceable. Applying this method, first steps have been realized to extend the possibilities of nuclear-chemical methods for on-line investigations in the liquid phase.

Literature

/1/ Baker, J.D. et al., J. anorg. nucl. Chem. 42 (1980) 1547
/2/ Skarnemark, G. et al., Nucl. Instrum. a. Meth. 171 (1980) 323
/3/ Baker, J.D., et al., Radiochimica Acta 28 (1981) 51
/4/ Broden, K. et al., J. inorg. nucl. Chem. 43 (1981) 765
/5/ Skarnemark, G. et al., Radiochimica Acta 33 (1983) 97
/6/ Aronsson, P.O., et al., J. inorg. nucl. Chem. 36 (1974) 2307
/7/ Langrock, E.-J., et al., Radiochimica Acta 30 (1982) 229

OPTIMIZATION OF THE ASSOCIATED PARTICLE (AP) DETECTION SYSTEM USED FOR TCAPM FISSION CROSS-SECTION MEASUREMENTS IN THE 4.5 AND 8.5 MeV NEUTRON ENERGY RANGE

C.-M. Herbach, G. Musiol, G. Pausch
Technische Universität Dresden, Sektion Physik, WB Angewandte Kernphysik

E. A. Ganza
Khlopin Radium Institute Leningrad

The AP detection system, used in our TCAPM fission cross-section measurements at ~ 4.5 and ~ 8.5 MeV neutron energies [1,2], was optimized. Mean AP counting rates of 3600...3700/s ($\dot{N}_{AP,max}$ = 4800/s) at a solid angle $\Delta\Omega_{AP}$ ~ 1.4 sr for AP detection and corresponding background corrections of (1.5...2.5)% ± (0.3...0.4)% were reached [1]

- by changing the reaction kinematics at E_n ~ 4.5 MeV to get higher AP energies [1],
- by utilizing ΔE detectors with optimum thickness, diameter and homogeneity, and
- by applying a two-parameter unit with colour display [3] to optimize the eight electronic thresholds and the coefficients for particle identification [2].

Fig. 1 shows a ΔE-E_r representation in the AP channel at E_n = 4.8 MeV; in fig. 2 scattered deuterons are suppressed by an optimum ΔE timing threshold [2]. Fig. 3 shows the selected E_g window ($E_g = \Delta E + E_r$) which includes the ^{3}He-AP-peak. Because of the overlapping total energy, a complete separation of ^{3}He from the ^{4}He background is only possible by selecting an A_p window ($A_p = a\,\Delta E + b\,E_r$) (fig. 4).
At E_n = 8.65 MeV, four alpha groups have to be suppressed (fig. 5).

Figures:

1	5
2	3	4

REFERENCES

[1] C.M. Herbach et al., report 05-06-85, TU Dresden, 1985
[2] C.M. Herbach et al., report 05-07-85, TU Dresden, 1985
[3] W.D. Fromm, M. Kahlenbach, ZfK-530 (1984), p. 131

ANALYSIS OF ASSOCIATED PARTICLE SPECTRA IN TCAPM FISSION CROSS-SECTION MEASUREMENTS AT ~19 MeV NEUTRON ENERGY

C.-M. Herbach, K. Merla, G. Musiol, G. Pausch
Technische Universität Dresden, Sektion Physik, WB Angewandte Kernphysik

L.V. Drapchinsky
Khlopin Radium Institute Leningrad

In our TCAPM fission cross-section measurements at $E_n \sim 19$ MeV, selfsupporting Ti-T targets (2...3 mg/cm^2) covered by thin Al layers (~0.2 mg/cm^2) are used for neutron production. Unfortunately, (d,α) reactions occur at the Ti, the Al layer, and at the oxygen which is bound at the target surface and in the whole target volume /1,2/. The energy spectra of such alphas and "true" accociated particles (AP) overlap, and a background correction becomes necessary. In general, various Ti-T and Ti target foils are available during the cross-section measurement, but no pair of foils with identical Al layers and oxygen depth profiles. Therefore, the background correction must be based on a separate analysis of all background components, considering the true target composition (fig.):

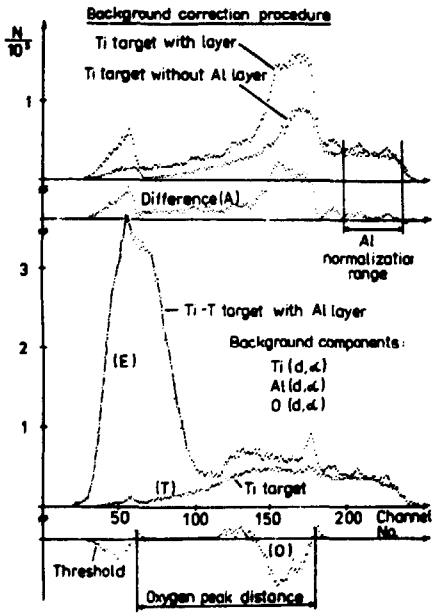

1) An "Al" spectrum (A) is obtained from a pair of Ti foils of comparable thicknesses with and without Al layer, considering a spectra normalization relative to the number of registered scattered deuterons.
2) A "Ti" spectrum (T) is obtained from a Ti foil without Al layer and of a thickness comparable to that of the used Ti-T target.
3) The "Al" and "Ti" spectra are normalized to the "effect" spectrum (E) of the Ti-T target. The normalization factors a, b are derived from the Al normalization range, where no oxygen component is present and the Al component consists of separated peaks. By calculating the difference (D) = (E) - a·(A) - b·(T), a spectrum is generated which consists only of the AP peak and a residual oxygen component caused by the difference of the oxygen profiles.
4) Considering the level scheme of ^{16}O and the reaction kinematics, the conclusion was derived that the $^{16}O(d,\alpha)$ component consists of two separated peaks. Because of the energy loss of alphas within the target, the peaks are broadened and the shapes correspond to the oxygen profiles. Using the peak distance and peak ratio determined from measured spectra (Ti foil; high oxygen component), the residual oxygen component within the AP peak is calculated from the oxygen component in (D) outside the AP peak. By calculating this "residual oxygen" spectrum (O), the energy threshold for alpha detection (caused by ΔE detector thickness) is taken into account.
5) The complete background spectrum (B) = a(A) + b(T) + (O) is used to calculate the background portion within the AP window.

This procedure was implemented at an SM-4 computer.

REFERENCES

/1/ C.M. Herbach et al., report 05-07-85, TU Dresden, 1985
/2/ C.M. Herbach et al., ZfK-559 (1985), p. 21

EXPERIMENTAL DETERMINATION OF THE $^3He(d,p)^4He$ BACKGROUND PORTION IN TCAPM-MEASUREMENTS OF ABOUT 19 MeV NEUTRON ENERGY

C.-M. Herbach, K. Merla, G. Musiol, G. Pausch
Technische Universität Dresden, Sektion Physik, WB Angewandte Kernphysik

L.V. Drapchinsky, E.A. Ganza
Khlopin Radium Institute Leningrad

The production of 18.8 MeV neutrons in absolute fission cross-section measurements by using the Time-Correlated Associated Particle Method (TCAPM) was performed based on the $T(d,n)^4He$-reaction by 6 MeV deuterons [1,2].
Because of the T-decay, the $^3He(d,p)^4He$-reaction can generate background α-events which are registered by the associated particle (AP) detector. For deuteron energies > 0.5 MeV the reaction cross-section is in the order of the $T(d,n)^4He$ cross-section [3], and background portions of ~1 % seem to be possible also for new Ti-T-targets (age ~ 30 days). The reaction kinematics are nearly the same, therefore the $^3He(d,p)^4He$ background events can not be discriminated from the AP's by means of pulse height analysis.
By performing the background correction only based on measured spectra at non-tritiated foils [2,4], certainly, this portion is not taken into account and would lead to a systematic error of the neutron flux measurement. In order to consider this additional background exactly, the correlated protons (P) were counted by a ΔE-E_R-semiconductor telescope which was placed inside the vakuum chamber (Fig. 1). An absorber foil was used to screen the detectors from the scattered deuterons. The application of the telescope-technique was favourable in order to discriminate the detector pulses caused by γ-ray.
In contrary to the figure, by employing a smaller AP detector diaphragm (Ø 3 mm) it was guaranteed, that the correlated P-cone was fully placed within the solid angle of the P-detector (diaphragm Ø 9 mm). The $^3He(d,p)^4He$ background portion was determined by counting the coincidences between AP- and P-events in relation to the number of the registered AP's. All electronic levels were set as in the cross-section measurement. To check up all conditions and to identify the P's, single and two-dimensional pulse height spectra of the P-detectors were registered.

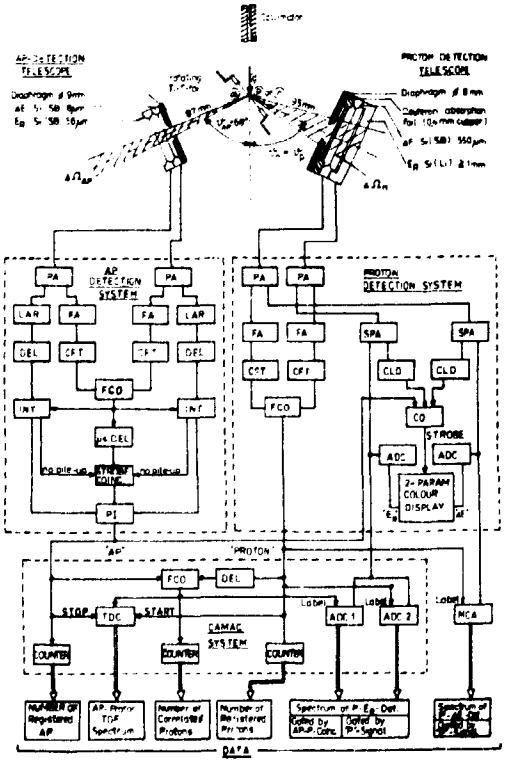

The measurements at three different Ti-T-targets ~30 days after their preparation resulted in values of (0.25±0.10)% for the P/AP-ratio. This confirmes the measurement which was performed after the cross-section measurements [5,6] by using a comparable system with the result of (0.35±0.30)% [2,7]. The difference to the theoretical estimation should be caused by the escape of ^3He-gas out of the foil.

REFERENCES

[1] C.M. Herbach et al.; ZfK-559(1985),p.21
[2] C.M. Herbach et al.; report 05-07-85, TU Dresden, 1985
[3] T.W. Bonner et al.; Phys.Rev. 88 (1952), p. 473
[4] C.M. Herbach et al.; this report p.110
[5] C.M. Herbach et al.; ZfK-559(1985),p.19
[6] C.M. Herbach et al.; ZfK-559(1985),p.20
[7] C.M. Herbach et al.; XV.Intern.Symp. on Nucl.Phys."Nuclear Fission", Gaussig, GDR, Nov. 1985; Proc.to be publ. as a ZfK-report
[8] C.M. Herbach et al.; this report p.112

Fig. 1: Block diagram of the P/AP-ratio measurement (geometry as in the proton cone measurement discribed in ref./8/)

CONE BROADENING IN TCAPM FISSION CROSS-SECTION MEASUREMENTS

C.-M. Herbach, G. Musiol, G. Pausch
Technische Universität Dresden, Sektion Physik, WB Angewandte Kernphysik

The only possible source of undetected systematic errors in fission cross-section measurements by means of the time-correlated associated particle method (TCAPM) which does not appear in other techniques of neutron flux determination, is a broadening of the correlated neutron cone due to scattering effects. The effect of neutron scattering is considered in the neutron scattering correction, whereas the scattering of incident deuterons or associated particles (AP) can produce errors if it leads to a considerable part of correlated neutrons which do not hit the fission foils. Therefore, much care was taken to an exact experimental determination of the neutron cone profile [1-3].

In various cone profile measurements carried out during TCAPM fission cross-section measurements [2-4] and using a scintillation detector placed outside the reaction chamber, a "tail" was observed at a level of about 10^{-3} of the cone maximum. Theoretical estimates and an additional cone profile measurement with a scatter which simulates a thicker vacuum chamber wall [3] suggested that this is an effect of neutron scattering at the fission chamber material and the vacuum chamber wall. This suggestion was proved by a direct measurement, making use of the nearly identical kinematics of the $T(d,n)^4He$ and the $^3He(d,p)^4He$ reactions: Because of the tritium decay, the Ti-T targets used for neutron production in our 18.8 MeV measurements contain noticeable amounts of ^3He, and ^4He particles from $^3He(d,p)$ contribute to the total AP counting rate [2]. By measuring the profile of the corresponding cone of correlated protons, the influence of deuteron and AP scattering within the target foil on the cone shape is taken into consideration, and the result of such a measurement can be used to estimate the systematic error due to this effect. In principle, also a measurement of the neutron cone profile inside the reaction chamber should allow to discriminate neutrons scattered at the chamber well because of the additional flight path and the enlarged time-of-flight; but in this case, the high gamma background limits the sensitivity of the cone profile monitor.

A proton cone measurement was performed using the proton telescope described in [5]. The measured profile (fig.) shows that the "tail" observed in a corresponding neutron cone measurement is caused only by neutron scattering, and the shape of the initial neutron cone outside the fission samples down to 10^{-6} of the maximum value can be described by an exponent. This fact was used to estimate upper limits of the error ε_{cb} caused by cone broadening in TCAPM fission cross-section measurements. A calculation for the geometry of the ^{235}U measurement at 4.45 MeV, based on cone profiles determined experimentally, resulted in $\varepsilon_{cb} < 0.1$ % [6].

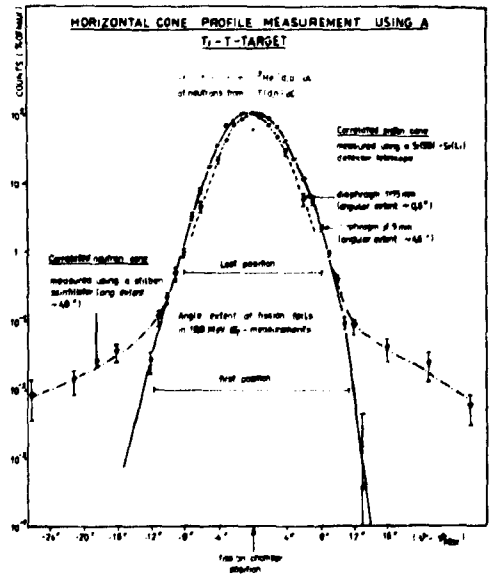

REFERENCES

[1] C.M. Herbach et al., ZfK-559 (1985) 24

[2] C.M. Herbach et al., report 05-07-85, TU Dresden, 1985

[3] R. Arlt et al., IAEA-TECDOC-335, p. 174 (1985)

[4] C.M. Herbach et al., report 05-06-85, TU Dresden, 1985

[5] C.M. Herbach et al., this report p. 111

[6] G. Pausch, Dissertation, TU Dresden 1986

CONSIDERATION OF THE $^{12}C(n,n')3\alpha$ -REACTION AS A BACKGROUND SOURCE WITHIN A METHAN FILLED FISSION CHAMBER FOR NEUTRONS OF ~19 MeV

C.-M. Herbach, K. Merla, G. Musiol, G. Pausch
Technische Universität Dresden, Sektion Physik, WB Angewandte Kernphysik

In order to detect the neutron induced fissions in cross-section measurements usually an ionization fission chamber (FC) is employed. Because of its high electron drift velocity (~10 ns/mm), the application of methan as the chamber filling gas is advantageously to get very short current pulses and therefore to minimize the pile-up probability of α-pulses from the natural acivity of the fission foils.
But in absolute cross-section measurements, the $^{12}C(n,n')3\alpha$ -reaction within the methan gas must be taken into account as a background source. For 18.8 MeV neutrons this reaction ($\sigma \approx 370$ mb [1], Q= -7.27 MeV) generates events with a rate in the order of the induced fission rate. For special trajectories of the three α-particles, energy losses up to ~11 MeV can be realized within the FC To identify the reaction, an experimental test was performed by using a methan chamber without fission foils. When the chamber was put into the neutron flux, pulses could be observed above the electronic noise (Fig. 1). The correlation of these pulses with neutrons was proved by a time-of-flight measurement.

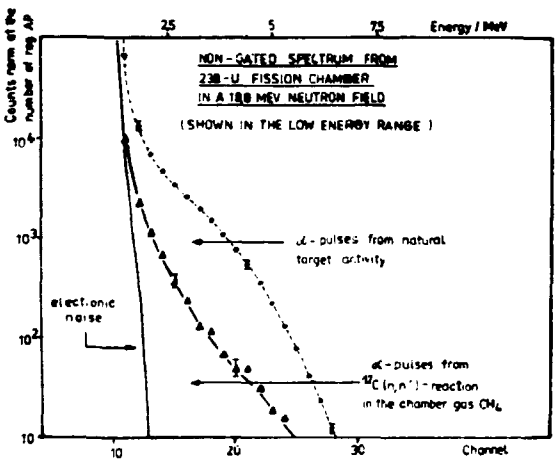

Fig. 1: Comparision of spectra with and without fission foils within the FC

In our TCAPM cross-section measurements at 18.8 MeV on U-235 [2], Pu-239 [3] and U-238 [4] it was not possible to discriminate the $^{12}C(n,n')3\alpha$-background events by means of the CFT-threshold, because it would lead to counting losses within the plateau region of the FC spectrum and therefore to a higher uncertainty of the threshold correction to zero. To consider the neutron correlated background in the FC channel, the following procedure was applicated (Fig. 2): A lower limit K_o was introduced which characterizes the lower end of the linear plateau region. The number of correlated events (N_u-N_α) below k_o was determined as the difference of the total number of events below k_o (N_u) and the number of random α-AP coincidences (N_α) which was calculated from the direct FC spectrum and the CFT efficiency curve (Fig. 2). The correlated events were subtracted from the number of coincident fissions N_f^c. Fission fragment pulses below k_o were determined by a linear extrapolation of the plateau region from k_o (N_{ex}). Though the ratio $(N_u-N_\alpha)/N_f^c$ can reach values up to ~6 % the additional uncertainty of the correction is very small and is only caused by the error of N_α calculation, if all coincident fissions were collected in the spectrum during the whole measuring time.

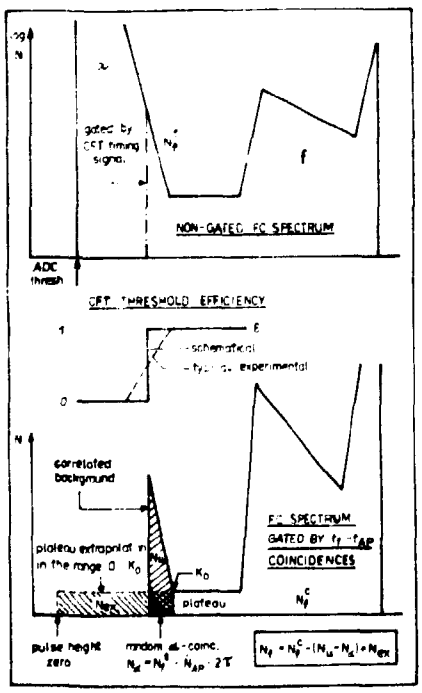

Fig. 2: Scheme of correction of the correlated background and the three

REFERENCES

[1] B. Anpolkovic et al.; Nucl.Phys. A394 (1983),p.95
[2] C.M. Herbach et al.; report 05-07-85, TU Dresden 1985
[3] C.M. Herbach et al.; this report p. 4
[4] C.M. Herbach et al.; this report p. 5

A CORRELATION BETWEEN FISSION FRAGMENT ABSORPTION LOSSES AND THE PLATEAU HEIGHT IN FISSION CHAMBER SPECTRA

C.M. Herbach and G. Pausch
Technische Universität Dresden, Sektion Physik, WB Angewandte Kernphysik

In most of the progressive fission cross-section measurements, the detection of fission events is based on the registration of fission fragments using parallel plate ionization fission chambers. In general, the absolute detection efficiency is determined by linear extrapolation of the "plateau" region in the fission chamber spectrum from the detection threshold to zero at the pulse height scale, and by calculating the counting losses due to absorption of both fragments within the target foil using a parameter R_o which describes the fission fragment range in the target material.

The relation

$$\varphi(E) = \frac{\partial K(t,x(E))}{\partial E} \quad ; \quad x(E) = R_o - R(E) \qquad (1)$$

between the energy spectrum $\varphi(E)$ of the fission fragments which leave the target layer and the absorption correction $K(t,R_o)$ (t: target thickness) allows to derive a correlation between absorption losses and the plateau height in the fission chamber spectrum [1], if the range-energy function R(E) for fission fragments in the target material is known. For thermal neutron energies the absorption correction becomes simple [2], and (1) results in

$$\varphi(E) = \frac{t}{2} \cdot \frac{1}{(R_o - R(E))^2} \cdot \frac{dR(E)}{dE} \quad \text{for} \quad x = R_o - R(E) \geq t \quad \text{(plateau region):}$$

$$\varphi(E) = \frac{1}{2t} \cdot \frac{dR(E)}{dE} \quad \text{for} \quad x = R_o - R(E) < t \qquad (2).$$

The ratio φ_p/K_o of the plateau height to the absorption losses then does not depend on the target thickness and on absolute R(E) values, but only on the shape of the range-energy function, if R_o is determined from R(E) and the known fission fragment kinetic energy.

A first estimate of the absorption losses for the fission foil configuration used in our ^{235}U fission cross-section measurements at 4.45 and 18.8 MeV [3] was performed [1], based on measured fission chamber spectra and a simple calculation of φ_p/K_o applying new stopping power data [4] (fig.). The calculated lower edge of the fission fragment peak for the experimental fission chamber geometry was employed to calibrate the energy scale in the plateau region [5]. This estimate results in an experimental range parameter $R_{exp} = 4.7$ mg/cm^2; an additional correction of 0.85 % was found due to the non-linear plateau shape at lower energies.

The described method allows to determine an individual range parameter for each fission foil which considers chemical composition and surface roughness. Further theoretical and experimental investigations are necessary to get detailed information on the sensitivity to stopping power data and on the uncertainty of the energy scale in measured fission chamber spectra.

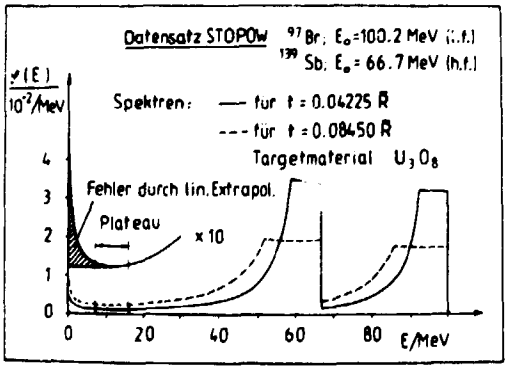

REFERENCES

[1] G. Pausch, Dissertation, TU Dresden 1986
[2] R. Arlt et al., report 05-5-79, TU Dresden 1979
[3] C.M. Herbach et al., report 05-07-85, TU Dresden 1985
[4] J. Henniger, W. Wagner, private communication
[5] C.M. Herbach, Dipl. work, TU Dresden 1982

DETERMINATION OF THE AREAL DENSITY OF THE PU-239 FISSION-FOILS

K. Merla, C.-M. Herbach, R. Perez
Technische Universität Dresden, Sektion Physik, WB Angewandte Kernphysik
O.I. Kostochkin, S.M. Solovjev
Khlopin Radium Institute Leningrad

In hitherto carried out Pu-239 fission cross-section measurements the parameters of the fissile layers were the main limitations for better accuracies of the result. [1,2,3] All used Pu-239 fission-foils were prepared at the KRI by thermo-sputtering using material of high isotopic purity (> 99.99 mass-% main nuclid). The determination of the areal densities were carried out at the KRI by low geometry α- counting. All published results are based on these values with total errors of about 1 %. At the TUD a low geometry counter [4,5] was built up to enable independent measurements. At first all Pu-foils used in the measurements at 4.6, 8.65 and 18.8 MeV were investigated. Each foil was measured by 2 different detectors to check independence of detector properties. But all results agreed within the statistical uncertainty of < 0.1 %.

The geometry factors of the used systems of apertures were calculated by the formula of Petrzhak [6] using results of geometrical measurements at a 3-dimensional set-up. Besides these calculations with 3 independent systems of nearly the same aperture-Ø at the target a comparison test with an target of excellent homogeneity was performed to check the calculations result. All the results of this test correspond within the error limits and the small divergences were used as corrections to the geometry factors (0.21 to 0.46 %) (fig.1). A typical α-spectrum is shown in fig. 2. At the spectra the following corrections had to be considered (in brackets typical values in the Pu-239 measurements):

- background correction determined by independent measurements before and after the runs (0.01 to 0.47 % - increasing because of insignificant contamination of detector and apertures during the runs)
- correction of α-pulses originating in the decay of Pu-238 within the layer (this amount was only determined out of the spectra to about 1.80 %)
- extrapolation of the spectrum from the discr. level to pulse height zero (0.1 to 0.2 %)
- pile-up correction (< 0.1 %)

Besides the error components by the corrections at the spectra and the geometry factor the following were considered:

- half-life period (employing $T_{1/2}$ = 2.411.10^{4}y) [7] 0.12 %
- backscattering out of the detector [8] 0.10 %
- large angle scattering [8] 0.25 %

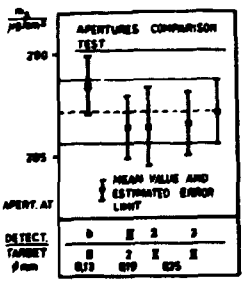

Fig.1

Tab.1

Foil-No.	m_s (ug/cm^2)
1	287.9 ± 1.7
2	163.9 ± 1.0
3	138.3 ± 0.8
5	160.6 ± 1.0
11	199.8 ± 1.2
13	198.1 ± 1.2
	1148.6 ± 6.9

In the table the results are given. The total error was estimated to about 0.61 %. The total areal density of all the foils differ from the KRI value (1145.2) 0.30 %. A revise of the ascertained cross-section values using these new areal density results of better precision is planned.

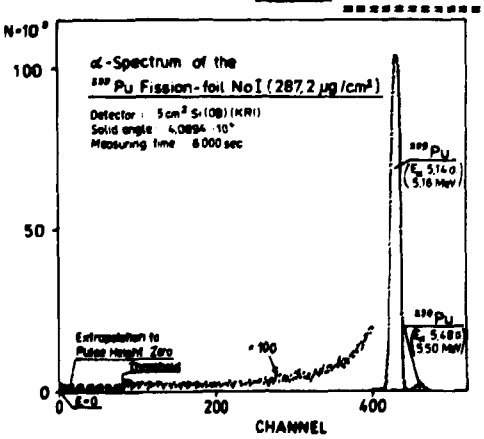

Fig. 2

REFERENCES

[1] C.-M. Herbach et.al., preprint TUD 05-06-95,1985
[2] C.-M. Herbach et.al., ZfK-559 (1985) 20
[3] C.-M. Herbach et.al., Proc.XV.Int.Symp.on Nucl. Phys., Gaussig 1985, to be published as an ZfK-report
[4] K. Merla, Dipl. work, TU Dresden, 1981
[5] R. Arlt et.al., ZfK-530 (1984) 119
[6] K.A. Petrzhak, M.A. Bak, Journ. techn. fizika XXV (1955) 636
[7] A. Lorenz (Ed.), INDC (NDS)-149/NC, Vienna 1983
[8] P.H. White, Nucl. Instr. and Meth. 79 (1970) 1

DETERMINATION OF THE INHOMOGENEITY OF U-238 FISSION-FOILS BY RBS-MEASUREMENTS

K. Merla
Technische Universität Dresden, Sektion Physik, WB Angewandte Kernphysik
R. Groetzschel
Zentralinstitut für Kernforschung, Rossendorf, Bereich KF

In the TCAPM fission cross-section measurements the inhomogeneity of the fissile layers is of interest because it makes a direct contribution to the total error of the σ_f-measurement. In case of materials of high enough own α-activity as Pu-239 and U-235 this parameter was determined by a scanning measurement as described in ref. /1,2/ but at U-238 with a lower α-activity measuring times of about 10 month would be necessary. Therefore at U-238 this parameter was determined by Rutherford-Backscattering measurements at the Van-de-Graaff-accelerator of the CINR Rossendorf with the following main exp. features:

- 1.7 MeV ^{4}He-ion beam of about 10 to 17 nA beam-current
- 15 mm^2 Si(SB)-detector, placed in an distance of 130 mm to the target (angle relative to the beam axis 190°)
- the normalization of the spectra was realised by an current-integator to an absolute value of 30 µC (statistical uncertainty $\lesssim$ 0.2 %)
- measuring points of 3 mm diameter were located in the centre of the foil (Ø 21 mm) and 8 on a circle (Ø 12 mm) in steps of 45°

The fig. shows the RBS-spectra of 2 fission-foils, which were prepared by different technologies (HF-sputtering, separation out of an metal-organic compound). The spectra show a main peak originating in the foil material Uranium. Its high energy edge arises from α-particles backscattered at the target surface, its low energy edge from α-particles backscattered at U-nuclei on the backing surface. Lighter elements from the backing give overlapping peaks at lower energies. The used ORTEC-7040 MCA disposes of software possibilities for a linear background subtraction using only the contents of the border channels for interpolation, so that the result shows a strong dependence on these both statistical varying numbers. Therefore the brutto area of the effect peak was used as a measure of the Uranium contents. It is possible because

- the backing of constant thickness gives a constant pile-up background
- the dependence of the Rutherford-scattering cross-section on the depth of the scattering position is negligible because of the nearly constant layer thickness.

Because the peak-width is a measure for the layers total thickness the ratio peak-area: peak-width should give additional informations about the layers real structure (perhaps ballast substances).

The stability of all the experimental components was controlled by the position of the high energy edge of the Uranium peak. All obtained results were reproduceable within the total error limits of 0.25 %. 8 fission-foils with the following parameters were investigated:

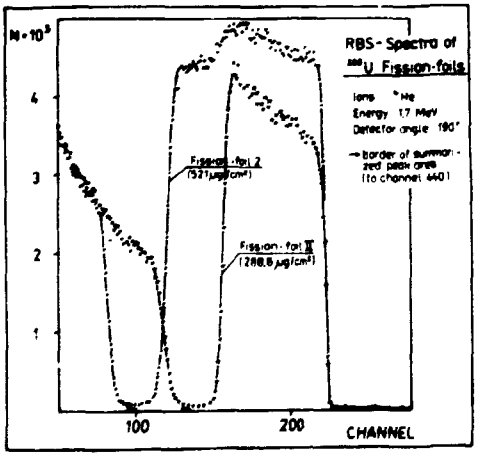

- areal density 289...521 µg/cm^2
- stand. deviation of the points outside the centre 0.51...2.94 %
- averaged difference to the central point 0.16...3.57 %
- total inhomog. 0.53...4.03 %.

By an optimization beetween the error contribution by the total inhomogeneity of the optimised fission-chamber (calc.mounting pos.of each foil so, that the stand.dev.of the round points will be a minimum)/2/ and the reachable statistical uncertainty in the fixed measuring time gave the best value for the use of the 5 best foils. This arrangement was used in the 18.8 MeV measurement /3/.

REFERENCES

/1/ K. Merla, Dipl.work,TU Dresden, 1981
/2/ C.M. Herbach et al.; preprint TUD 05-06-85 (1985)
/3/ C.M. Herbach et al.; this report p. 5

SEPARATION OF OUTER-SHELL SATELLITE X-RAY LINES AT SOURCES OF HIGHLY IONIZED ATOMS

W. Wagner
Joint Institute of Nuclear Research, Dubna
G. Zschornack
Technical University Dresden, Department of Physics

Calculations for the evolution of ionic charge states by multistep electron impact ionization in sources of highly ionized atoms have been published earlier in ref. [1]. It has been shown, that the width of the charge distribution keeps values of several charge units over the whole ionizing process up to high charge states.
We investigated the possibilities of a wavelength dispersive X-ray spectrometer to seperate satellite lines of neighbouring ionic charge states.

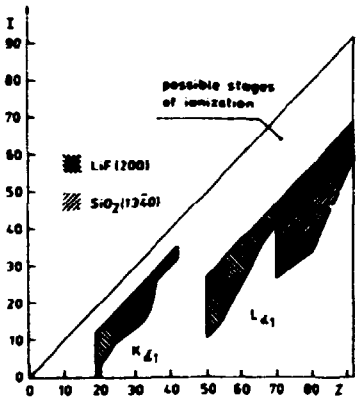

Fig. 1
Resolved outer-shell satellite lines for the $K_{\alpha 1}$ and $L_{\alpha 1}$ transitions (hatched areas) by the Dubna JOHANSSON spectrometer, using SiO_2(13$\bar{4}$0) and LiF(200) crystals.
I - stage of ionization.

The outer-shell satellite lines of the K- and L-series are shifted relative to the diagramme lines by 10^{-1} eV to 10^{2} eV [2]. Due to the natural line widths of radiation one can expect that high resolving crystal diffraction spectrometers are not able to seperate X-ray lines over the whole charge spectrum.
Estimations have been carried out for the Dubna JOHANSSON-spectrometer [3] assuming nearly real measurement geometry. We have examined the $K_{\alpha 1}$ and $L_{\alpha 1}$ lines which could be measured by use of a SiO_2 (13$\bar{4}$0) and a LiF (200) crystal.
The resolving power of a crystal diffraction spectrometer depends on the BRAGG-angle and the realized angular divergence $\Delta\vartheta$:

$$\left|\frac{\lambda}{\Delta\lambda}\right| = \left|\frac{E}{\Delta E}\right| = \left|\frac{\tan\vartheta}{\Delta\vartheta}\right|$$

where $\Delta\vartheta$ consists of the components $\Delta\vartheta_K$ - the width of the crystal mosaic distribution and $\Delta\vartheta_G$ - the geometrical width.
Because of the dominating influence of $\Delta\vartheta_G$ over a wide range of ϑ, assuming real measurement conditions, we took into consideration the natural line widths $\Delta\vartheta_\lambda$ and $\Delta\vartheta_G$, neglecting the qualitative parameter $\Delta\vartheta_K$. Therefore our estimations are to be understood as a lower limit of possible resolution. The geometrical aberrations have been simulated statistically by the computer code VERDI 1 [4].
Under the condition, that the resolution of the spectrometer has to be equal or better than the energy difference of neighbouring satellite lines (a very strong test!), we find the indicated areas of the (Z,I)-plot in fig. 1.

REFERENCES

[1] Lehmann, D. et. al., 9-10744, JINR, Dubna, 1977, Karrasch,C. et.al., Gemeinsamer Jahresbericht 1984, ZfK-559, p. 166
[2] Zschornack, G. et.al., "Dirac-Fock-Slater X-Ray Energy Shifts and Electron Binding Energy Changes for all Ion Ground States in Elements up to Uranium", to be published as ZfK- Report
[3] Wagner,W. et.al.,JINR,Rapid Communications, N6-85,1985,p.46
[4] Reichmann,A. et.al., Gemeinsamer Jahresbericht 1984, ZfK-559, p. 167

TEMPERATURE CONTROL OF ANALYZER CRYSTALS IN CRYSTAL DIFFRACTION SPECTROMETERS WITH DISCONTINUOUS OPTIMIZED CONTROLLERS

D. Kreiseler
Joint Institute for Nuclear Research Dubna, Division of New Acceleration Methods
G. Zschornack
Technical University of Dresden, Department of Physics, Division of Applied Nuclear Physics

To realize a working regime with high stabilized temperature on the analyzer crystal of crystal diffraction spectrometers, to use in precision measurements the high accuracy of the best known x-ray standards, a parameter optimized discontinuous controller was applied. The base for it was an available CAMAC-equipment for the temperature mesurement and control /1/ with a precission of 0.02 K and a deliver unit, generating adjusting values of 1024 heating steps for the current supply of a heating coil on the crystal holder.

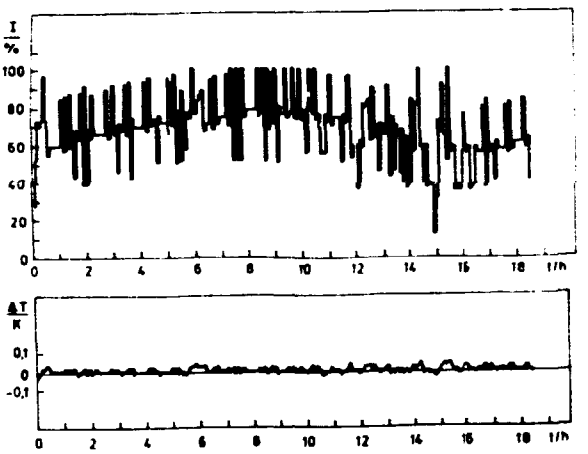

Fig. 1
Course of temperature ΔT and adjusting value I for with a parameter-optimized discontinuous PID-acting controller realized automatic loop.

After a choosen scanning time T_0 an interrupt of the running measurement programme by the computer MERA 60-30 takes place and a discontinuous control algorithm is started, which has the form of a difference equation

$$U(k) = U(k-1) + q_0 \; e(k) + q_1 \; e(k-1) + q_2 \; e(k-2)$$

with

U : value of adjusted parameter
e : control value deviation from reference input
q_i : control parameter
k : repetition step

The identification of the controlled system and design of discontinuous PID-acting controller are computer-aided and provided in dialogue with a system of connected computer MERA 60-30 and microcomputer INTEL 8080. Essential support for the design of the controller arises from graphical representation of results on a colour display. This possibility was used for a qualitative report of control and adjusting processes.
Basing on the developed program system for digital simulation the design of the controller was provided. For the disturbed process a maximum temperature deviation ΔT of 0.04 K was found. On Fig. 1 the course of the control and adjusting values for optimized control parameters is shown. The sampling time was 4 min.

REFERENCES

/1/ Dunin W.B. et al.; Preprint JINR, P 13-83-287, Dubna, 1983

A TWO-BEAM LASER ANGLE INTERFEROMETER FOR BRAGG CRYSTAL DIFFRACTION SPECTROMETERS

G. Zschornack
Technical University Dresden, Department of Physics

G. Müller
Technical University Dresden, Department of Information Processing

G. Karrasch, W. Schulze, W. Wagner
Joint Institute for Nuclear Research, Dubna

For a precise definition of the crystal angle position in diffraction spectrometers a laser angle interferometer was developed and applied at the JINR Dubna. The diffraction spectrometer works basing on a master drive with a transmission ratio $i_g = 37228$ and forms from the 1.5^o-angle increment of the stepping motor an angle step of 0.145 arcsec. This value has stochastic character and deviations from ideal values may be verry important (reasons: quality of keying, assembly conditions). Using the increments from the laser interferometer for the angle measurement, it is always possible to drive into the lock-in range of a slow-motion control device ($\Delta\vartheta \leq 2'$), realized with piezoelectric crystals. This device allows in connection with the laser interferometer a fine adjustment in the range $\Delta\vartheta \approx 0.2$ arcsec.

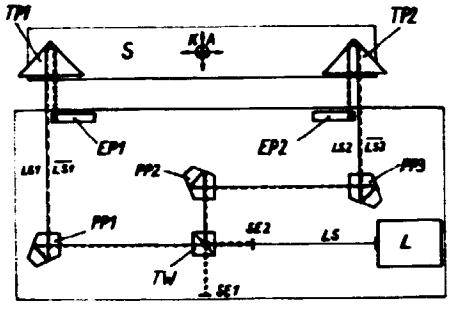

Fig.1 Opto-mechanical assembly of the interferometer.

Fig. 1 shows the opto-mechanical assembly of the interferometer. It is build up as a two-beam interferometer, that allows to analyze a maximum angular range of $\pm 26^o$. The laser beam LS, emitted with small divergence by the laser L, is splitted on the beam-splitting cube TW in two components LS1,2. The single beam components are reflected on pentagonal prismes PP1,2,3 in direction to the triple prismes TP1,2 which are mounted on the shoulder S, rotating around the crystal axis KA. Here they are reflected to the final prism EP1,2 and from EP1,2 vertically adjusted back to TW.

Owing to the rotation of S in both branches of the interferometer different Doppler shifts of the beam frequency f_L are generated. In TW both components superimpose to a beat frequency f_S, where $f_S \ll f_L$. After the receivers SE1,2 the signals are processed in the interferometer electronics [2]. In the signal processing device one signal is delayed and a frequency multiplication (8 times) for both channels take place. The angular increment $\lambda/32R$ has a maximum value of 0.012 arcsec for a given distance R of both triple prismes. All registrated values are counted in a bidirectional counter and topical determination of the angle in interferometer units occurs for an average of 300 counts.

Fig. 2 Uncertainities of angle determination due to influence outside of the optical branch.

In Fig. 2 the counter content without average is shown. This representation demonstrates the uncertainities of the angle determination due to influences outside of the optical branch. This uncertainities are in an average region of about 30 interferometer units, that corresponds to an angle interval of less than 0.4 arcsec. The two-armed construction provides the independence of the angle analyse from lateral position variations of the crystal, which can occur due to support conditions of crystal table and bottom drive in the order of some micrometers [3].

First measurements demonstrate the operating function of the interferometer in an angle range of 15°.

REFERENCES

[1] Karrasch,G. et.al.; JINR, P13-83-484, Dubna, 1983
[2] Müller,G. et.al.; JINR P13-83-55, Dubna, 1983
[3] Debler,E.; PTB-Me-8, Braunschweig, 1975

INVESTIGATIONS WITH THE AIM OF INSTALLATION A LOW-LEVEL γ-SPECTROMETER

J. H. Kim[+], S. Unterricker, W. Stolz, D. Degering and D. Hebert
Bergakademie Freiberg, Sektion Physik
D. Simon
ZIPE - Außenstelle im Kalibetrieb "Werra"
+ Aspirant, Kim Il Sung Universität Phjongjang, KVDR

Components contributing to the background of a γ-spectrometer are the natural activities of the U- and Th-chains and of 40-K decay in the environment of the detector, the shielding and the detector materials and events which are induced by cosmic rays. These background sources must be carefully investigated by establishing a low-level γ-spectrometer.

Beside shielding of the detectors by massive walls of low activity materials the background can be reduced very effectively by an additional geological shielding [1,2]. We determined with an overlay of 200 mwe an attenuation of the muon induced background to 10^{-2}, which is nearly energy independent in the energy range of 5 MeV to 200 MeV. In the energy range below 5 MeV this effect is not so obviously if natural γ-activities dominate.

We have measured γ-background spectra in the energy range up to 4 MeV by a NaI(Tl)- and a Ge(Li)-detector in the mining district of Freiberg (Reiche Zeche, overlay 140 m gneiss ~ 380 mwe) and a salt mine of the Werra district (overlay 500 m lower buntsandstein and salt ~1100 mwe). The cavity in the salt mine has an environment of more than 10 m of rock salt. Table 1 summarizes characteristic figures of the γ-background spectra measured by a 10 cm^3 Ge(Li)-detector and a 256 channel analyzer.

Table 1

Selected photopeak and integral rates (up to 4 MeV) in counts/10^4s

location	E_γ = 1.46	=1.76	=2.61 MeV	E_γ > 0.2	> 1.5	>2.7 MeV
surface lab.	539(9)	48(4)	76(4)	113000	2980	97(4)
R.Z. 1.Sohle ~380 mwe	1240(10)	65(5)	105(4)	133000	3540	0.9(4)
salt mine						
Merkers(Rhön)~1100mwe	180(20)	1(1)	1	10500	26	-

Up to the 208-Tl line at 2.61 MeV the values of the gneiss cavity are larger than corresponding surface values. This is a consequence of the high U, Th and K contents in this field. Coupled with this is a relatively high Rn concentration which strongly increases by the interruption of ventilation [2] . Of course the background above 2.7 MeV is strongly reduced.

In the salt mine the background results are much better. This environment has very low U and Th contents, which are below the detection limits of our natural activity and neutron activation analyses measurements (< 0.07 ppm of U and < 0.01 ppm of Th). Rn was also not detectable. The only problem is the K concentration, which results in a pronounced K-peak and the corresponding Compton background. We determined a K_2O equivalent of 0.21 % in the rock salt. This relatively high (0.1 ... 0.2 %) K content is characteristic for the rock salt of the Werra region. Much better results one can expect in the Staßfurt rock salt of the Bernburg district. In this case a minimum K_2O equivalent of 0.02 % in the environment of a location is possible, which must result in a very low natural γ-activity. In connection with a shielding by selected materials and also low activity construction materials for the detector complex a very low γ-background can be expected. Naturally such a location for a γ-spectrometer brings problems with the maintenance, the sample exchange and also the salt dust.

References

[1] Helbig, W.,et al.: Isotopenpraxis 20 (1984) 60
[2] Hebert, D.,et al.: Proceedings of the 3rd International Conference on Low Level Counting, Bratislava, CSSR, 21. - 25. 10. 1985. To be published in Nucl. Instr. Meth. Phys. Res.

FAST TRIGGER FOR NEUTRON TIME-OF-FLIGHT MEASUREMENT

P. Eckstein, A. Meister and U. Gohs
Technische Universität Dresden, Sektion Physik, WB Kernphysik

The experimental investigation of chemical induced shifts of neutron resonances /1/, Doppler-broadening of neutron resonances /2/ as well as other effects /3/ requires a registration of minute differences between the positions and shapes of neutron resonances observed with different samples. Neutron transmission measurements with the time-of-flight technique at the Dubna pulsed reactor IBR-30 operated in boaster mode with the linac LUE-40 guarantee for low-energy resonances the necessary energy resolution as well as a high counting-pulse rate needed for statistical accuracy. The neutron detector used for such measurements comprises a lithium-glass scintillator and a photomultiplier.
For a precise processing of detector pulses, the rate of which changes very strong and fast, a trigger was developed with ECL-technique /4/.

The trigger possesses the following parameters:
- input pulses: positive or negative polarity, pulse length $\geq$ 4 ns
- threshold: adjustable in digital manner (4 bit)
  from $\pm$ 10 mV to $\pm$ 150 mV with steps of 10 mV
- maximum pulse rate: 2 10^7 s^{-1}
- output pulses: $\pm$ 0.7 V at 50 Ω, adjustable pulse length > 25 ns
- dead time: adjustable $\gtrsim$ 45 ns
- current supply: + 6 V (150 mA), - 6 V (600 mA)
- case dimension: 55 x 100 x 140 mm^3

The detector pulses are fed by an emitter follower to a fast operational amplifier working as a comparator. The trigger has a logic devices guaranteeing a constant dead time after each registrated event, this is realized by charging and discharging a capacitor by constant current.

The presented trigger was used in transmission measurements and was working reliably up to a maximum pulse rate only determined by the scintillation time constant of lithium-glass scintillator (about 75 ns). Without dead time device the trigger was also successfully tested for input pulses having lengths of 1...2 ns.

References

/1/ Meister, A. et al., Nuclear Phys. A 362 (1981) 187
Mittag, S. et al., Nuclear Phys. A 435 (1985) 97
/2/ Seidel, K. et al., Conf. Neutron Physics, Kiev (USSR) 1983, Proc. Vol. 2, p. 379
/3/ Seidel, K. et al., Yad. Fiz. 42 (1985) 1041,
Ignatovich, V.K. et al., preprint P3-83-892 Dubna (1983)
/4/ Gohs, U., Diplomarbeit, TU Dresden, Sektion Physik (1984)

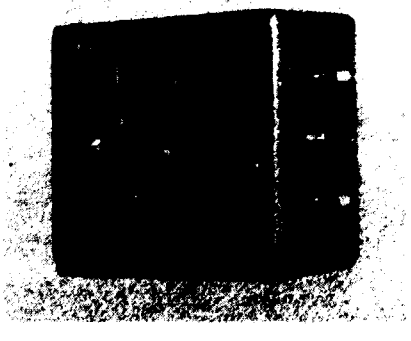

Fig. 1:
View on the trigger device described here.

GRADUALLY EVAPORATED FOILS FOR ABERRATION CORRECTION OF FISSION FRAGMENT TIME-OF-FLIGHT IN A DIRECTION-SENSITIVE ARRANGEMENT

H. Märten, D. Richter
Technische Universität Dresden, Sektion Physik, WB Kernphysik

W. Neubert, I. Probst
Zentralinstitut für Kernforschung Rossendorf, Bereich KF

Foils with a gradually changing thickness have been prepared by a stepwise evaporation of FORMVAR (~ 90 µg/cm^2) with aluminium (≳10 µg/cm^2 single-layer thickness) to correct for different fission fragment time of flights due to the geometrical aberration in a direction-sensitive detector arrangement. Fragment direction and time of flight are measured by the use of special set-up consisting of a single parallel-plate avalanche counter PPAC (transmission detector located beside the fission sample) and a position-sensitive one (PPAC(PS)) /1,2/. The PPAC(PS) is mounted in a straight frame. Hence, the fragment flight path and, consequently, the fragment time of flight for a given kinetic energy per nucleon depend on fragment direction. If this "aberration" is small, it can be corrected for by the use of a foil with gradually changing thickness to retard the fragments definitely. The preparation of such a foil requires an accurate evaluation considering the stopping power of the PPAC foils and the working gas (heptane at about 1300 Pa pressure) and varying the thickness of the stopping foil to obtain an unique fragment time of flight for all directions. The stopping foil position was chosen in the middle of the distance between both PPAC. This arrangement was assumed to be optimum. The evaluation procedure is carried out by the use of a FORTRAN code enabling the calculation of the total time of flight of a fragment characterized by mass number and initial kinetic energy.
All necessary stopping power data are introduced /3/. Obviously the fragment velocity is a local function. Hence, the whole fragment time of flight is obtained by integration. The deduced stopping foil thickness, which is a continuous local function, can be approximated by a stepwise function. This is the pattern for the evaporation procedure.

The described method of aberration correction is only reasonable if the maximum flight path distinction is lower than about 10 %.
It was testet with fragments from spontaneous fission of ^{252}Cf. In this case, the symmetric fragments had a unique time of flight to distinguish between the light and the heavy fragment group in a simple manner. An alternative method is a multi-parameter measurement including fragment time of flight and position and a corresponding off-line analysis (cf. /2/).

References

/1/ H. Märten et al., Gemeinsamer Jahresbericht 1984, ZfK-559 (1985) 10

/2/ W.D. Fromm et al., Proc. Int. Conf. on Nucl. Phys., Nov. 1985, Gaußig (GDR)

/3/ L.C. Northcliff, R.F. Schilling, Nucl. Data Tables A 7 (1970) 233

EXPERIMENTAL ARRANGEMENT FOR THE MEASUREMENT OF CORRELATIONS BETWEEN FISSION PRODUCTS AND NEUTRONS

H. Märten, D. Richter, D. Seeliger
Technische Universität Dresden, Sektion Physik, WB Kernphysik

W.D. Fromm, W. Neubert
Zentralinstitut für Kernforschung Rossendorf, Bereich kF

The application of a direction-sensitive method of fragment spectroscopy enables the measurement of the whole neutron emission distribution N(E,Θ), i.e. in dependence of lab. frame energy and emission angle with reference to light-fragment direction, simultaneously. Hence, several systematic errors are avoided /1,2,3/.
An extended spectrometer based on a fragment detector arrangement consisting of a single parallel-plate avalanche counter (PPAC) and a position sensitive one is used in connection with two fast neutron detectors. Fragment direction, fragment time of flight (FF-TOF) and neutron time of flight (n TOF) for both neutron detectors (D1, D2) are measured three-dimensionally (Fig. 1). The single PPAC located beside the fission sample (5 mm normal distance) provides the timing signal T-PPAC for the FF-TOF as well as the n TOF measurement. The time difference between T-PPAC and the anode signal T-A of the position-sensitive PPAC is a measure of FF TOF (about 100 mm flight path).

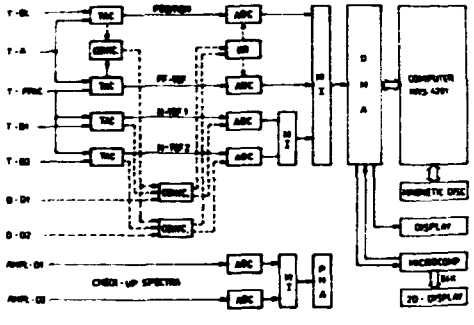

Fig. 1
Scheme of signal processing and data acquisition (see text). Dashed lines represent logical signals.
(TAC - time-to-amplitude converter, COINC - coincidence unit, ADC - analogue-to-digital converter, MI - multiplexer interface, DMA - direct memory access).

The cathode of the position detector (180 mm length) is subdivided into 36 segments, whose signals are coupled into a delay line inductively (220 ns maximum delay) yielding the time signal T-DL. Measuring the time difference between T-A and T-DL one obtains the position (FF direction) signal. Fig. 1 represents the scheme of data processing. T-D and D-D are the neutron detector timing signal and the discriminator signal (amplitude and particle discrimination) respectively. The corresponding amplitude spectra (AMPL-D) are stored for a continious check up of stability.
The computer KRS 4201 connected with a microcomputer-aided system for 2D-spectrum handling with coulor display is used for on-line data acquisition (including representation of single spectra and an eligible 2D-spectrum), complex off-line data sorting (assembler codes), and the final data analysis (FORTRAN programme system).
The deduced position spectra for selected neutron energy intervals and for a given fragment group are unfolded by the use of a rather simple Gaussian-fit algorithm (resolved peaks). The peak area for a given FF direction (angle Θ) and a chosen E interval divided by the geometrical PPAC(PS) segment efficiency (to be measured) is proportional to N(E,Θ).
The described experimental arrangement is employed to measure N(E,Θ) of neutrons from ^{252}Cf(sf) which is "standard" subject for the study of the mechanism of fission neutron emission. The measured angular distributions are characterized by a rather high point density (up to 120 in 180 deg) /2,3/.

References:
/1/ H. Märten et al., Gem. Jahresbericht 1984, ZfK-559 (1985) 10.
/2/ H. Märten et al., Proc.Int.Conf.on Nucl.Data for Basic and Appl. Sci. May 1985, Santa Fe (USA)
/3/ W.D. Fromm et al., Proc.Int.Conf.on Nucl.Phys., Nov. 1985, Gaußig (GDR)

IMPLEMENTATION OF SERIAL MULTI-MASTER BUS CONTROLLER USING SINGLE-CHIP MICROCOMPUTER

W. Meiling and R. Krause
Technische Universität Dresden, Sektion Physik, WB Kernphysik

In scientific instruments increasing amount of decentralized data processing executed by internal microcomputers reduces required data transfer rate between coupled devices of a complex measuring system to about 10 or 100 KByte/s. In these cases, serial data transfer mode can be recommended, expanded by multimaster capability if more than one device is able to control data transfer on the bus.
In last years some serial multimaster bus standards were defined. The local area computer network busses are characterized by high transfer rates and by expensive interface controllers which exclude application in scientific instruments. On the other hand, the inter-IC bus I^2C /1/ represents a serial multimaster component bus, which is designed to connect integrated circuits on a printed board or to couple printed boards in a frame with data rate up to 100 Kbit/s. Originally, the interface controllers are implemented on the chips of the 8400 microcontroller family and adapted peripheral circuits /2/. Parameters of I^2C and possible realization of interface controllers by use of a single-chip-microcomputer suggest application of I^2C to couple scientific instruments within distances which are typical in laboratory rooms.
In fig. 1 block diagram of the I^2C interface controller is shown. Serial data transfer protocol is program-controlled reducing the expense of the controller to one-chip-microcomputer U 882, 2 KByte EPROM circuit and 5 standard logical circuits which perform some logical and timing conditions. If one of the connected instruments wants to act as bus master, it gives the start condition which prevents all other instruments from bus control until master has finished its transfer mode. Wired-AND function by pull-up resistors at the bus lines SDA (serial data) and SCL (serial clock) secures clock synchronization of master and slave. More details of data transfer protocol, of arbitration procedure and of other parameters are given in /1/.
Using the interface controller of fig. 1, two K 1520 microcomputers and two I^2C peripheral circuits (PCD 8571 128 byte CMOS RAM, PCF 8573 clock/calendar) are coupled with a total bus length of about 5 m. The maximum transfer rate is about 25 Kbit/s. From the first investigations can be concluded that the I^2C bus controllers using U882 single-chip microcomputers are suitable to realize low-expensive serial bus coupling of "intelligent" scientific instruments /3/.

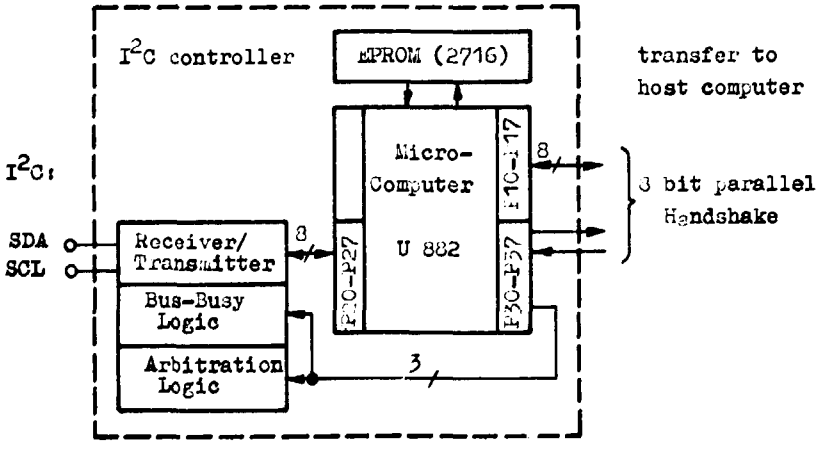

Fig. 1
I^2C interface controller

References
/1/ Philips/Valvo: I^2C Bus Specification, Philips Netherlands, 1983
/2/ Valvo: Integrierte Schaltungen für den I^2C-Bus. Schaltkreisinformationen, 1984
/3/ W. Meiling, R. Krause: Jahrestagung Mikrocomputertechnik der KDT, Dresden, 1985.

MASS SPECTROMETRY OF LIQUID METAL ION SOURCES

R. Mühle, F. Machalett
Friedrich-Schiller-Universität Jena, Sektion Physik

Recently there has been considerable interest in liquid metal ion sources for applications such as maskless ion doping of semicondors with submicron dimensions [1, 2]. Among these ion sources, alloy liquid metal ion sources offer a variety of ion species, so that for example n- and p-type dopants can be implanted using a single ion source. For many sources significant amounts of doubly charged ions are often observed. This is an advantage in obtaining high energy focused ion beams. In many cases liquid metal ion sources also emit a large percentage of their ions in the form of clusters. The composition of the emitted ions can be influenced for example by the source feed composition, the source ion emmision current and the operation temperature [3, 4]. In order to optimize the working conditions for the different applications it is necessary to investigate carefully the ion energy and mass distribution.

In the present work a magnetic mass spectrometer has been adapted for the registration of the mass distribution up to an energy-mass-product of about 5 MeV . u. The schematic diagramm is shown in Fig. 1. The emitted ions are accelerated to an energy of $q \cdot V_E$ (q is the charge of the ion and V_E the extractor voltage) and can be focused by a triple cylinder lens. The geometric parameters of the arrangement are the following: $l_1 = l_2 = 0.8$ m, $r = 0.1$m, $\phi = 41^\circ$. The slits s_1 and s_2 can be varied continously. The ions are collected behind the exit slit by a Faraday cage. The obtainable mass resolution at a slit width of 2 mm is about 50. The mass spectrometer was tested with an AuSi alloy liquid metal ion source of an atomic composition $Au_{94}Si_6$. The observed mass spectrum at 43 µA source current and 8.23 kV acceleration voltage is shown in Fig. 2. Primarily, Si^{++}, Si^+, Si_2^+, Au^{++}, Au^+, Au_2^+ and Au_3^+ ion species are emitted. Additionally, Au_nSi^{m+} clusters can be observed connected with the Au_n^{m+} ions. Since Au_2Si^{++} ions are present in the spectrum it can be supposed that the line designated as Au^+ is in reality a mixture of Au^+ and Au_2^{++} ions. The observed ion flux fractions are presented in Table I.

In order to have an impression of the mass resolution of the presented mass spectrometer the Si^+ line is shown in detail in Fig. 3. The isotopes $^{28}Si^+$, ^{29}Si and ^{30}Si can easily be separated even at a slit width of 2 mm.

Table I. The observed ion flux fraction of the $Au_{94}Si_6$ alloy liquid metal ion source

ion species	ion flux fraction (%)
Si^{++}	1.98
Si^+	0.99
Si_2^+	0.70
Au^{++}	5.19
Au^+	73.81
Au_3^{++}	0.17
Au_2^+	9.79
Au_3^+	4.43
$AuSi^{++}$	0.02
Au_2Si^+	0.81
$AuSi^+$	1.08
Au_3Si^{++}	0.06
Au_2Si^+	0.14
Au_3Si^+	0.83

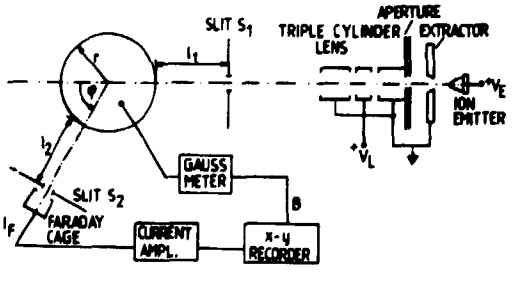

Fig. 1 Schematic diagramm of the mass spectrometer

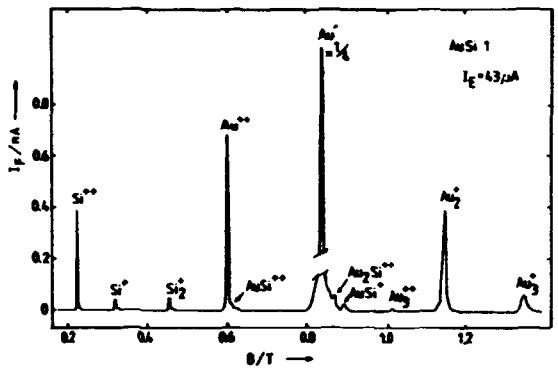

Fig. 2 Observed mass spectrum of the AuSi liquid metal ion source showing the ion current I_F vs. B field at 43 μA source current

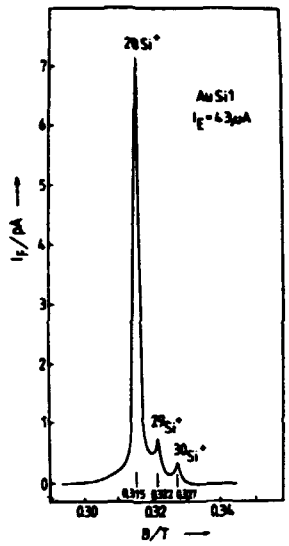

Fig. 3 Mass spectrum of the Si^+ ions showing the resolving power of the spectrometer at a slit width of 2 mm

References

[1] E. Miyauchi, H. Hashimoto: Nucl. Instr. and Meth. B 7/8 (1985) 851

[2] R.H. Reuss: Nucl. Instr and Meth. B 10/11 (1985) 515.

[3] K. Komuro, T. Kato: Proc. 6th Symp. ISIAT'82 (Tokyo, 1982) 63

[4] H. Arimoto, E. Miyauchi, H. Hashimoto: Jap. J. Appl. Phys. 24 (1985) L 288

BASIC CHARACTERISTICS OF AN AU-SI-LIQUID METAL ION SOURCE

R. Mühle, F. Machalett
Friedrich-Schiller-Universität Jena, Sektion Physik

Liquid metal field ion sources (LMIS) offer a high brightness ($\sim 10^6$A cm^{-2} sr^{-1} [1]) and also a variety of metal ion species [2] so that there has been increasing interest in recent years in their application for maskless ion implantation and microfabrication [3, 4]. But one drawback for such an ion source is that it is applicable only for elements having a relatively low melting point and a low vapour pressure at this point. For this reason the ionisation of elementary Si by LMIS is not possible and an eutectic alloy with Au is generally employed because of his good wetting properties. The melting of thie alloy starts at the eutectic temperature of T = 636 K.

The following measurements were carried out by means of the ion source described in [5] and an Au-Si-alloy with an atomic composition of $Au_{94}Si_6$. A typical current-voltage characteristic of the ion source is shown in Fig. 1. The emitter tip was mounted about 0.5 mm behind a concentric extractor electrode of 3 mm diameter. The ion source is turned on at a threshold voltage of 6.9 kV and the ion current I_E rises up to 100 µA corresponding to an angular intensity of 57 µAsr^{-1}. The heater current was set about 5% above the value necessary for complete melting. There is a hysteresis in the $I_E U_E$ charcteristic which is also observed by Komuro and Kawakatsu [6]. A typical angular distribution (dI/dΩ vs ϕ) with the source current as a parameter is shown in Fig. 2. For small emission angles ϕ the angular intensity is nearly constant. The observed mass spectrum is published in [7].

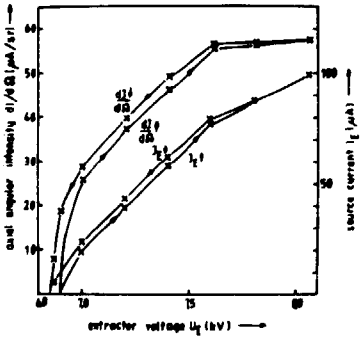

Fig. 1 Current-voltage characteristic of the Au-Si LMIS

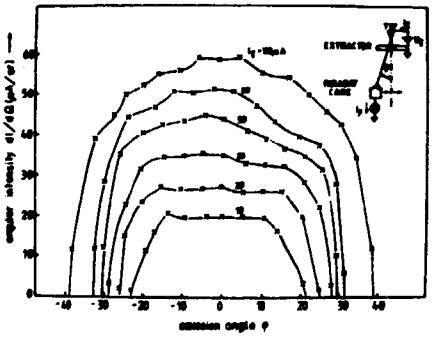

Fig. 2 Angular intensity dI/dΩ vs emission angle ϕ for different source currents I_E

References

[1] R. Clampitt, D.K. Jefferies: Inst. Phys. Conf. Ser. 38 (1978) 12
[2] D. Broughton, R. Clampitt: Vacuum 34 (1984) 275
[3] A. Wagner: Nucl. Instr. and Meth. 218 (1983) 355.
[4] R.H. Reuss: Nucl. Instr. and Meth. B 10/11 (1985) 515
[5] J. Mittenbacher: Gemeinsamer Jahresbericht 1984, ZfK-559 (1985) 94
[6] M. Komuro, H. Kawakatsu: J. Appl. Phys. 52 (1981) 2642
[7] R. Mühle, F. Machalett: this ZfK-report

COMPUTATIONAL METHODS AND CODES

FORTRAN PROGRAMMES FOR THE CALCULATION OF SINGLE-PARTICLE QUANTITIES IN HEAVY-ION COLLISIONS IN A TWO-CENTER BASIS

B. Milek
TU Dresden, Sektion Physik, Wissenschaftsbereich Theoretische Physik

With help of the programme EWBER the stationary Schrödinger equation can be solved in a three dimensional finite depth two-canter potential applying the separable-potential technique. For that purpose spherical potentials of a Woods-Saxon shape with spin-orbit forces, localized by translational operators at certain distance, are represented in a finite-rank oscillator basis. In this way the Schrödinger equation can be solved by algebraization in momentum representation [1]. The solvability condition for a corresponding system of equations is a vanishing complex determinant, which depends on the eigenvalue. The search for zeros of the determinant is performed with help of the Newton procedure. All solutions can be characterized in a complex k-plane:
solutions on the positive imaginary axis - bound states,
solutions on the negative imaginary axis - virtual states,
solutions in the lower half plane - Gamow or quasistationary states [2].
A further labeling follows by introducing symmetries of the problem (quantum numbers). The output of EWBER are single-particle energies and after solving the system of equations with vanishing determinant by a Gauß procedure the wave functions, too. For a given rank of the oscillator basis (in the present version 21) the accuracy of the eigenvalues (energies) can be choosen freely. The normalization of the wave functions is determined with an accuracy of about 5 %.

In the programme COUPLE radial couplings in the adiabatic basis are calculated of the typ $\langle \phi_\nu | \frac{\partial}{\partial R} | \phi_\mu \rangle$ for two levels ν, μ [2]. These couplings reflect nonadiabatic effects in the relative motion of the nuclei and influence the single-particle motion. Both bound and Gamow states can be coupled with each other.

Time dependent occupation numbers in the two-center single-particle basis calculated by EWBER are the output of the programme LANZEN. At first, a calculation of classical trajectories is performed governed by conservative nucleus-nucleus and Coulomb forces according to the method [3]. The change in time of the occupation numbers is determined by a first order system of differential equations which have been solved by the predictor-corrector method. The population of the levels is governed by the decay widths and by the coupling matrix elements calculated in COUPLE.

Physical applications of the programmes have been performed for the single-particle inelastic excitation and transfer in the system $^{17}O + ^{13}C$ (Landau-Zener effect) [4] and by the coupling of bound and quasistationary states in the system $^{17}O + ^{16}O$, which leads to an emission of the valence neutron in ^{17}O [2].

References

[1] Gareev, F.A., Gizzatkulow, M.Ch.,and Revai, J.; Nucl. Phys. A 286 (1978) 512
[2] Milek, B. and Reif, R.; TU-Information o5-9-85, o5-1o-85, o5-11-85 (1985) and submitted Nucl. Phys. A
[3] Schmidt, R., Teichert, J.; JINR-report E4-8o-527, E4-8o-735 (198o)
[4] Milek, B., Reif, R.; Phys. Letters 157B (1985) 134

PEP - A FORTRAN PROGRAM FOR CALCULATION OF FAST NUCLEON EMISSION IN HEAVY-ION REACTIONS

M. Biedermann
TU Dresden, Sektion Physik, Wissenschaftsbereich Theoretische Physik
P. Mädler
Vereinigtes Institut für Kernforschung Dubna, Laboratorium für Theoretische Physik

The model for "promptly emitted particles" (PEP) proposed in ref.[1] and its modifications are based on the assumption that at any time of the reaction the actual momentum distribution of the nucleons can be described by two Fermi spheres (T=C) shifted by the relative velocity. Adding the relative and the intrinsic velocity apart of the nucleons from the projectile (target) moving through the contact zone into the target (projectile) have sufficient energy to escape. The deflection at the nucleus surface is taken into account in a classical manner. The partial absorption of fast nucleons is taken into account according to the imaginary part of the optical potential for the nucleon- nucleus-scattering. A macroscopical, TDHF motivated model for the description of the trajectory as well as the evolution of the neck between the colliding nuclei [2] is used in the program PEP. In this way the friction force and the intensity of the flux of emitted particles could be treated in a consistent manner [3].
The present version of the PEP- model shows nearly identical shapes of the angular distributions and spectra in comparison with [1]. However, the absolute cross sections are smaller by a factor up to 1.5 due to the consistent description of the trajectory and particle emission and the neglecting of two body PEP [3]. Generally, the PEP- model shows too strongly forward peaked angular distributions and too small cross sections for the emission of very fast particles in comparison with the experiment. Due to the possibility to introduce a finite temperature for the nucleonic momentum distribution the emission probabilities of very fast nucleons may be enhanced formally.
The calculation of PEPs is stopped when either the momentary flux of emitted particles is zero or the turning point is reached in the trajectory. Moreover, the calculation can be stopped at the time t_0 when a compact neck occurs. The results obtained in this regime correspond to the emission in the first stage of the two- stage model proposed in [3].

The program calculates double- differential as well as energy- or angle- integrated cross sections (integrated over impact parameter) and prints separately the corresponding contributions of nucleons from the projectile/ target. Differential multiplicities for certain impact parameters can be calculated and the time evolution of the flux of emitted particles can be analysed. The results are printed in the labor or c.m.-system.

References:

[1] Bondorf, J.P., et al.; Nucl. Phys. A333 (1980) 285
[2] Biedermann, M., Mädler,P., and Reif, R.; Report JINR E7-84-415 (1984)
[3] Biedermann, M., and Mädler, P.; Report JINR E7-85-575 (1985)

HOT - A FORTRAN PROGRAM FOR CALCULATION OF FAST NUCLEON EMISSION FROM A HOT ZONE

M. Biedermann
TU Dresden, Sektion Physik, Wissenschaftsbereich Theoretische Physik
P. Mädler
Vereinigtes Institut für Kernforschung Dubna, Laboratorium für Theoretische Physik

The two- stage- model for the description of the prequilibrium emission of nucleons in heavy- ion reactions proposed in ref. [1] is based on the assumption that in the early stage of the reaction a slightly compressed hot zone forms in the contact zone of the ions with an effective temperature front expanding radially with velocity of sound (0.2c). In particular at the beginning of the collision the momentum distribution of the nucleons in this zone is very anisotropic. This can be described by introducing a mean velocity field, directed along the collision axis.
The nucleons can be emitted until the effective front of the hot zone reaches the outside surfaces of the nuclei. The angular distributions (for asymmetric systems) are forward peaked in the laboratory system (as a result of the anisotropy of the hot zone in momentum space).
In program HOT a trajectory model described in ref. [2] is used. The evolution of the hot zone starts, when in the trajectory model a compact neck occurs. The hot zone cools down as a consequence of the fast expansion inspite of simultaneous exitation (because of friction). Impact parameters where no compact neck occurs (quasi elastic collisions) are excluded.
The double- differential cross sections calculated with HOT represent the contribution of the second stage in the "two- stage- model" [1]. In addition to double- differential cross sections (or mean multiplizities) and angle- or energy- integrated values the program prints the time development of the temperature and the excitation energy in the hot zone as well as the actual flux of emitted particles.
The calculation can be carried out in the labor- or c.m.- system. The initial radius of the hot zone is fixed (motivated in [1]) with 3.6 fm, although other values can be used, too. The calculation for a given impact parameter is stopped at the time $t = \min(\max(t_u, t_w), t_{ww})$ (t_{ww}- interaction time; t_w- time for which the temperature front reaches the outside surface of the havier reaction partner; t_u- turning point).
The input data include quantities characterizing the specific reaction as well as the step sizes for integrations over time, impact parameter, angle, and energy, which determine the necessary calculation time. A sufficiently precise calculation for one reaction needs nearly 15-25 minutes calculation time at the CDC-6500 of the Joint Institute (JINR) Dubna.

R e f e r e n c e s :

[1] Biedermann, M., and Mädler, P.; Report JINR E7-85 575 (1985)
[2] Biedermann, M., Mädler, P., and Reif, R.; Report JINR E7-84-415 (1984)

FORTRAN CODE FOR THE CALCULATION OF "REALISTIC" DISTRIBUTIONS OF NEUTRONS PRODUCED IN HYDROGENE-ISOTOPE REACTIONS

H. Märten, A. Ruben
Technische Universität Dresden, Sektion Physik, WB Kernphysik

Predictions on neutron production distributions for any given field point are required for several applications (specifically for the measurement of microscopic nuclear data). The differences between realistic energy and intensity distributions and those calculated for a point source are expected to be large for rather extensive target arrangements and for short distances between the neutron-producing target and the given field point. The computer code to be described is suitable to calculate the distribution of neutrons produced by the use of a gas target /1/ via the reactions $D(d,n)^3He$, $T(p,n)^3He$, and $T(d,n)^4He$. Compared to Ref. 2, this work is extended concerning the numerical treatment of the beam stopping in the gas volume and the corresponding neutron production rates with reference to the considered field point.

The primary beam exhibits an energy width and divergence to be taken into account. Considering the energy and angle straggling in the entrance foil(s) as well as the foil inhomogenity the beam parameters are deduced for the target entrance point by a non-correlated superposition. The gas target length is subdivided into an eligible number i of single intervals numerically. In this way, it is possible to account for the energy width, the angle straggling, and the production cross-section as functions of the target length coordinate x. Specifically the average neutron energy, the neutron energy spread, and the differential cross-section are calculated for the actual lab. frame angle depending on x. We assume a rectangularly shaped energy loss in the gas for the step i. It has to be folded with the total projectile energy distribution of the preceding step. In a similar way, the angle straggling is taken into account.
The neutron distribution of each step i is deduced according to the kinematics /3/ of the reaction. Furtheron, an eligible angular spread of the field point is introduced in the calculation to account for the size of the neutron detector or the sample.
The total distribution in energy and intensity (per time unit and per beam current unit) is obtained by integration over x.
The formulae for the calculation of the energy loss, energy and angular straggling as well as the cross-section data were taken from the Refs. 4 and 5, respectively.
The following conclusions have been drawn from the calculations:

i) The calculated distribution is mostly influenced by the target geometry and projectile energy loss and straggling for field points close to the target at oblique angles. In this case, a large step number i_{max} is necessary.

ii) The width of the energy distribution composed of two main contributions, i.e. projectile energy spread and angular straggling, exhibits a remarkable behaviour as a function of angle due to the influence of the angular straggling of the beam. For realistic entrance foil thicknesses, one obtaines a maximum at oblique angles (cf. Ref. 2).

References

/1/ S. Mittag, W. Pilz, D. Schmidt, D. Seeliger, T. Streil, Kernenergie 22 (1979) 237
/2/ H. Klein, H.J. Brede, B.R.L. Siebert, Nucl. Instr. Meth. 193 (1982) 635
/3/ J.L. Fowler, J.E. Brolley, Jr., Rev. Mod. Phys. 28 (1956)
/4/ P. Marmier and E. Sheldon, Physics of Nuclei and Particles (Academic, New York, 1969) Vol. 1, 156
/5/ H. Liskien, A. Paulsen, Nucl. Data Tabl. 11 (1973) 569

THE IMPLEMENTATION OF AN UNIVERSAL STOPPING POWER CODE TO THE ES 1055 COMPUTER

W. Enghardt
Zentralinstitut für Kernforschung Rossendorf, Bereich KF

J. Henniger
Technische Universität Dresden, Sektion Physik, WB Strahlenschutzphysik

Usually, in experimental setups that are aimed at studying the mechanism of heavy ion reactions (see e.g. [1]) the fragments emerging in the exit channel have to pass through some target material and possibly several thin foils before reaching the sensitive region of the detectors. For a precise data evaluation the knowledge of the stopping power values for a broad variety of ions in the substances penetrated is necessary.

The computer code STOPOW [2,3] meets these requirements. It is capable of calculating the stopping powers S and the ranges R of ions from hydrogen up to uranium having energies between 1 keV/amu and 1 GeV/amu. The calculations are also possible for mesons, however, radiation corrections have not been taken into account. Optionally the program can be used to compute further properties of the impinging ions, e.g. their effective charge (Z_{eff}), the time of flight (TOF) in a sufficiently thick target, the restricted energy loss (RSL) and linear energy transfers (LET). It is rather simple to include some more user-written routines which need stopping powers, ranges or the quantities mentioned above as input data. The stopping powers S can be transformed into mass stopping powers S/ϱ (ϱ - mass density of the target) or into stopping cross sections S/n (n - density of atoms or molecules in the target material). Solid and gaseous targets consisting of a pure chemical element, a compound or mixtures can be handled. The user has to provide only input data on the ions and the constituents of the target, since the program contains all other data necessary, e.g. the isotopic composition of all elements, the atomic masses and the ionization potentials.

Originally the FORTRAN program STOPOW has been intended to run on the CDC computers (types 6000 - 8000) of the JINR Dubna. We transferred it to the Rossendorf ES 1055. Minor modifications of the source had to be made due to the different FORTRAN versions implemented to CDC and ESER (or IBM) computers [4]. In order to obtain correct results on ESER computers the real variables have to be set to double precision. This can be simply done by switching on the AUTODBL option of the optimizing FORTRAN compiler [5]. The storage requirements of the load set does not exceed 300 kBytes, it takes about 10 s to calculate S, R and TOF of one ion at 183 different energies.

For illustration, we show in figs. 1 and 2 a comparison of calculated and measured stopping powers of some solids and gases for α-particles [6].

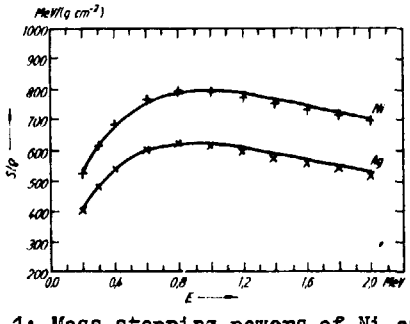

Fig. 1: Mass stopping powers of Ni and Ag for α-particles, the experimental data have been taken from [7].

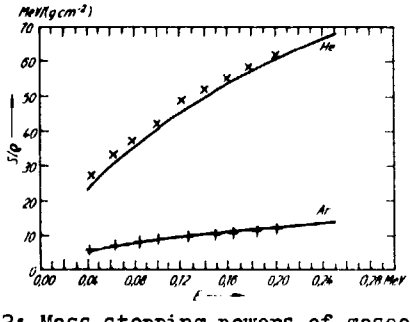

Fig. 2: Mass stopping powers of gaseous He and Ar for α-particles, the experimental data have been taken from [8].

References

[1] Gippner, P. et al.; Gemeinsamer Jahresbericht 1983, ZfK Rossendorf, ZfK-350 (1984) 115
[2] Henniger, J. and B. Horlbeck; Preprint JINR 10-83-366, Dubna 1983
[3] Krylov, A. and J. Henniger (to be published)
[4] Koren'ko, V.V. and G.A. Korobova; ES 1060 User Manual (russ.), Dubna, 1984, p. 49
[5] OC FORTRAN OE - Benutzungshinweise, VEB Robotron, Dresden, 1982, p. 112
[6] Henniger, J. et al.; Kernenergie 28 (1985) 272
[7] Santry, D.C., et al.; Nucl. Instr. Meth. 178 (1980) 531
[8] Fukuda, A.; J. Phys. B14 (1981) 4533

THE FORTRAN PROGRAMS KASSAMBA AND STRIDEM

H.-J. Keller
Zentralinstitut für Kernforschung Rossendorf, Bereich KF

The program KASSAMBA serves for data analysis of 256×256 channels matrices stored on digital cassettes or tapes. At the EC 1055 computer the following manipulations are carried out: (1) data transfer, (2) construction of selected singles spectra and (3) plot and print of singles as well as two-dimensional spectra. Fig. 1 shows an example of a 256×256 channels spectrum. For intensity representation lines are drawn of 1 channel length in x-direction and 0.1 channel distance in y-direction which enable 10 intensity graduations of e. g. 2^n, $1 \leq n \leq 10$.

For measured matrices of 64×64 channels the program STRIDEM calculates to each measured intensity value 8 further values by bicubic interpolation /1/ resulting in a 192×192 matrix giving in this way a more instructive picture, as shown in fig. 2. For intensity representation 14 lines are drawn of 1 channel (x) length and 0.0714 channel (y) distance in graduations of 2^n, $1 \leq n \leq 14$ (fig. 2a) or any other arbitrary sequence (fig. 2b).

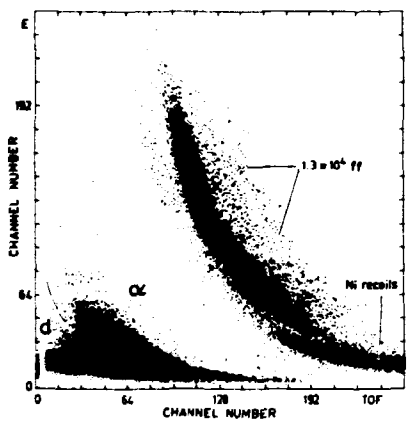

Fig. 1. TOF-E distribution of ternary fission events /2/.

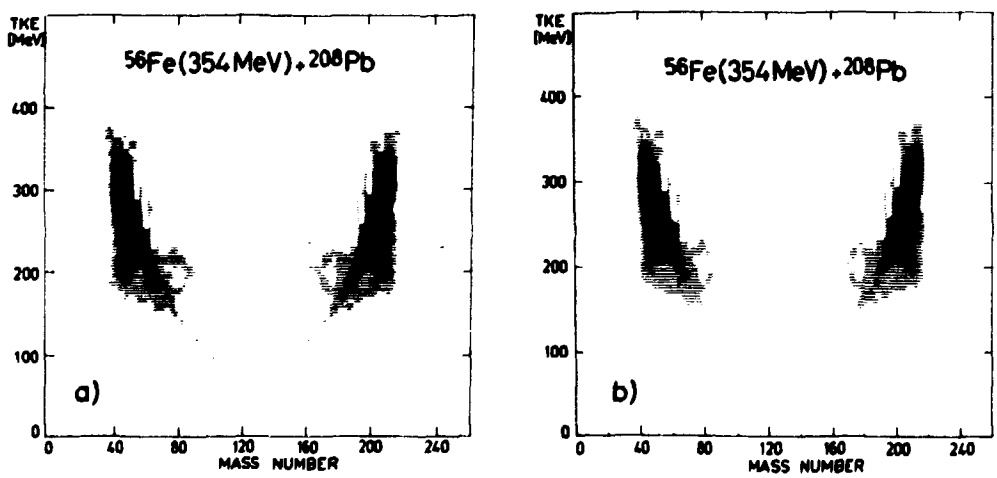

Fig. 2. TKE-A distribution of binary events of a heavy ion reaction /3/ in binary intensity code (a) and the arbitrary sequence (b) 4, 7, 10, 40, 70, 100, 300, 600, 900, 1200, 1800, 2400, 3000, 3600.

R e f e r e n c e s

/1/ H. Böttger, ZfK Rossendorf, ZfK-394 (1979) 32
/2/ R. Kotte et al., this annual report p. 3
/3/ P. Gippner et al., this annual report p. 2

ISOPLOT 2 - A PROGRAM FOR GRAPHIC REPRESENTATION OF FUNCTIONS Z = F(X,Y)

H. Böttger
Zentralinstitut für Kernforschung, Rossendorf, Bereich G
P. Gippner
Zentralinstitut für Kernforschung, Rossendorf, Bereich KF

Energy and mass distributions of binary fragments formed in collision systems with different projectile-target combinations were investigated using the double-arm time-of-flight spectrometer DEMAS /1-3/. The usual way to illustrate the obtained results is the graphic representation of three-dimensional structures or functions Z = F(X,Y) as isoline plots. The program ISOPLOT 2 allows to evaluate the isolines and to draw them on a digital plotter (type CALCOMP 565) by means of the software package ZFKPLOT /4/.
The functions F(X,Y) can be defined analytically or as points over a regular rectangular lattice. In the second case two methods of interpolation are available: the bi-linear and the bi-cubic interpolation, which use sliding HERMITE polynomials. The values to be represented can be given individually or by a set of DO-loops, each of which consisting of starting value, step and closing value. The isolines are calculated in discrete steps by the method of track tracing. This includes an automatic control of the step lengths in dependence on the local surface conditions like curvature and density of lines as well as the gradient values. The generated sets of points are collected in a file. Before the graphic output starts these sets are put in order with the aim to minimize the sum of raised-pen-motions of the plotter. The programm may generate scales, frames and line-numbers. If the function F(X,Y) shows high peaks a logarithmic transformation $F^* = \ln(1+F)$ can be performed to improve the quality of the interpolation. If F(X,Y) exhibits a strong statistical dispersion the measured values can be smoothed before processing. The different subroutines of the program are controlled by a set of functional parameters whose values have to be chosen by the user. These parameters allow an adaption to the special problem by the choice of the density of contour lines, boundaries of the step lengths, number of the values to be plotted, dimension of the graphic, resolving power of the line-recognizing algorithm and others.

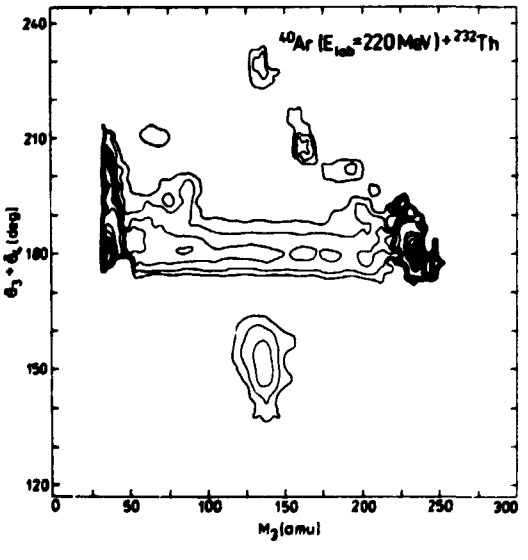

Fig. 1

Binary events observed in the reaction ^{40}Ar(220 MeV) + ^{232}Th drawn as contour-line plot in dependence of the parameters M_3 and $\bar{\Theta}_3 + \bar{\Theta}_4$.

As an example for a smoothed isoline plot the fig. 1 shows the binary events obtained by the investigation of the reaction ^{40}Ar(220 MeV) + ^{232}Th. The results are presented as a function of the parameters M_3 (mass of fragments measured in the ionization chamber 1 of the spectrometer DEMAS) and $\bar{\Theta}_3 + \bar{\Theta}_4$ (the sum of angles of both fragments in the center-of-mass system). The peaks are due to elastic scattering. The fragments in the mass region between 40 and 232 amu represent fission products. Only those events were accepted for further data processing, which satisfy the colinearity condition $\bar{\Theta}_3 + \bar{\Theta}_4 = 180^\circ \pm 3^\circ$ /2/.

References

/1/ Will, E. et al., Report JINR-13-85-754, Dubna 1985
Schilling, K.D. et al., to be published

/2/ Sodan, H. et al., JINR Rapid Communications, Dubna, N4-84 (1984) 15
Lukyanov, S.M. et al., Proc. Int. Worksh. on Gross Prop. of Nuclei and Nucl. Exc. XIII, Hirschegg (1985) 123

/3/ Gippner, P. et al., this report, p. 1

/4/ Böttger, H., ZfK-394 (1979)

THE EVALUATION OF $\gamma\gamma$-COINCIDENCE MATRICES

W. Enghardt
Zentralinstitut für Kernforschung Rossendorf, Bereich KF

After transforming experimental $\gamma\gamma$-coincidence data stored event by event on magnetic tapes to a 2048 x 2048 matrix [1], one has to deduce physically interesting information from these data. The FORTRAN program COSY is intended to meet the requirements that commonly arise during establishing a nuclear level scheme by evaluating $\gamma\gamma$-coincidences.

1. Background correction:
The background of an effect gate can be calculated from up to eight background gates by interpolation or extrapolation.

2. Peak search (optional):
Fast peak search and peak-area estimation can be performed for the background corrected spectra, a coincidence table containing the photopeak energies and relative intensities is printed.

3. Plotting (optional):
The background corrected coincidence spectra can be plotted by means of the CALCOMP 565 device [2]. The scale of the abscissa has been fixed at 0.2 mm per channel, the ordinate has been limited to 10 cm at maximum. Therefore, the appropriate scale of the ordinate has to be calculated for each spectrum. However, the user is allowed to choose this scale. In this case the drawing of a spectrum will be cut off, if its height exceeds 10 cm. The scaling factors are given on the picture.

4. Summation of background corrected spectra (optional):
In order to prove the existence of weak γ-ray transitions, sometimes it may be useful to enhance statistics by summing up all those gates where these lines appear or where they are expected. The spectra obtained can be handled in the same way as background corrected ones.

5. Dumping of background corrected spectra to magnetic tapes (optional):
The program described runs rather fast on the ES 1055 computer, e.g. it is capable of performing the construction, the background correction and the peak search for about ten coincidence spectra per minute of CPU-time. Therefore, the dumping option should only be applied to those spectra, for which a further processing, e.g. precise calculation of peak-areas or special drawings (for publications) are required.

References

[1] Enghardt, W. and U. Fromm; Gemeinsamer Jahresbericht 1984, ZfK Rossendorf, ZfK-559 (1985) 174

[2] Böttger, H.; Anwenderinformation ES 1055, 1. Fortsetzung, Rossendorf, 1983, p. 1

ON-LINE PROGRAMS FOR MULTI-PARAMETER MEASUREMENTS

W.D. Fromm
Zentralinstitut für Kernforschung, Rossendorf, Bereich KF

With the inclusion of particle identification the complexity of measurements at the Rossendorf accelerators rises continuously. In order to support such measurements in a more general manner programs for a user selectable number of parameters are supplied. Fast data-taking and sorting are handled by programs written in assembler language. The detailed physical analysis of the recorded data set is performed with FORTRAN-programs developed by the users.
With respect to the existing hardware (multiplex-interface /1/ and DMA-channel) two programs for recording and sorting multi-parameter events of up to seven parameters have been installed at the KRS 4201.
Program XPAR organizes the data-taking. The events are transferred by the multiplex-interface over the DMA-channel into the computer memory. Two alternating buffers of 252 words each are filled with raw data of 16 bit words. The 4 msb are used for labelling the start of an event and the number of the input channel. Therefore, the resolution of the measured parameters is 4096 channels. After inspection four control words are added and the data block is written to the magnetic disk which can store 4800 blocks. Singles spectra of the parameters are stored in main memory. A two-dimensional spectrum can be generated by means of an attached color display unit /2/. For the control of the CAMAC apparatus three user-defined subprograms for initialisation (CINI), start (CSTA) and stop (CSTP) of the data-taking can be linked.
For the interpretatinn of multi-dimensional measurements a flexible sorting program is essential. Its main purpose is a convenient reduction of the parameter space to facilitate human reception. The program XSOR is one attempt to solve this problem interactively. Using the magnetic disk as input device the sorting time can be kept small. Therefore, in one pass only one result spectrum (one- or two-dimensional) is produced and displayed. The user can improve the result in another pass changing the sorting conditions. Up to eight conditions can be imposed (logical AND). Conditions for one parameter (lower and upper limit) and two correlated ones (reference address to a table and scaling factor) can be formulated. The table is organized as linear array ordered after the first value with lower and upper limit of the second scaled value combined in 16 bit as content. In general such a table is the result of a preceding rtiirng and should be supplied by the user. In order to minimize the sorting time the most stringent condition should be the first entry in the sorting list.
The result can be presented as one- or two-dimensional spectrum. One-dimensional spectra are stored in main memory starting at a user-supplied address. Two-dimensional spectra depending on their size can be stored in main memory or are transmitted to external storage devices (see Table). The size of the matrix can be reduced by a user-supplied number of shifts. During the sorting process the correspondence of the data-set to the selected number of parameters is verified. Changes of the experiment number and the number of the last block sorted are protocolled.

Table 1: Presentation of two-dimensional results

mod=	1	2	3	4	5
storage	i n t e r n a l			external	
dimension	32*32	64*64	128*128	256*256	64*64
length(K)	1	4	16	64	4
device	KRS 4201	main	storage	color-display	4K-MCA

References

/1/ K. Heidel and E. Will; Gemeinsamer Jahresbericht 1981, ZfK-448(1982)p.202
/2/ W.D. Fromm and M. Kahlenbach; Gemeinsamer Jahresbericht 1983, ZfK-530(1984)p.131

BIT-MAP GRAPHICS WITH EC 1055 PROGRAMS

U. Fromm, W.D. Fromm, K.-H. Heinig and G. Otto
Zentralinstitut für Kernforschung, Rossendorf, Bereiche G und KF

At Rossendorf's main computing facility EC 1055 graphical output can be performed only by means of a slow drum-plotter. However, for a large variety of problems pattern generation does not mean "drawing lines" but rather "plotting single dots", possibly even plotting of consecutive dots in quite different regions of the image array. The dot-by-dot output of such an image with a plotter is very impractical, difficult and time-consuming. Devices like raster-scan displays or matrix-printers provide adequate means for the visualisation of these images, and due to their high resolution they can be used for drawings too.
At the measuring center of our department matrix-printers with graphic capability are available /1/. The maximum number of about half a million printed points per standard page is given by ca. 700 lines with 768 points each, which corresponds to a resolution of 24 points/cm. During one sweep of the carriage 10 rows of dots are printed in parallel.
Bit manipulations within the display array are very useful for computer simulations of physical processes /2/. For the generation of the image in the EC 1055 computer main memory must be reserved for an one-dimensional INTEGER*2 array NBIT of a length of at least 768*N elements, where 10*N is the number of pixels to be printed in y-direction. Every dot of the image is represented by one bit of this array. A set of FORTRAN and ASSEMBLER routines have been developed which perform address calculation and bit manipulations. For instance, the subroutine SET(I,J) sets a bit within the NBIT array which corresponds to a dot at coordinates x=I and y=J of the image produced later by the matrix-printer (I_{max}=768,J_{max}=10*N). The ASSEMBLER routines SBIT(INT,NR), RBIT(INT,NR), UBIT(INT,NR) and TBIT(INT,NR) set, reset, invert and test the NR^{th} bit of the INTEGER*2 array element INT, respectively. The result of the bit-test is of the type LOGICAL. The bit functions BITON and BITOFF available by the FORTRAN-OE-compiler /3/ are unsuited for this purpose because the number of the bit must be a constant.
The transfer of the huge amount of data from the EC 1055 to the microcomputer is accomplished by magnetic tape cassette /4/. The information for the 10 needles of the printer is stored in binary form in the array NBIT. In many applications large areas of the picture remain empty, i.e. no needle has to be activated. Therefore, before the output on cassette, consecutive zeroes are counted and written as negative number to the cassette. In this manner about a fourfold reduction of the data volume was achieved saving tape and time.

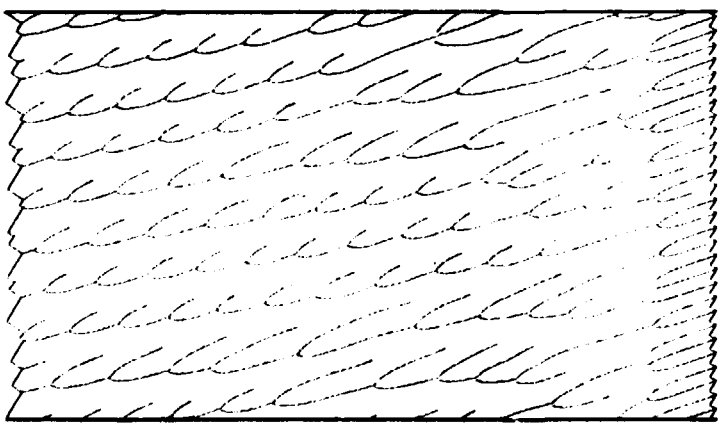

Fig. 1
Example of an image created by computer simulation with the EC 1055 (see also /5/)

References

/1/ W. Enghardt, W.D. Fromm; Gemeinsamer Jahresbericht 1984, ZfK-559(85)p.160
/2/ H.-J. Müller, K.-H. Heinig: this report p. 44
/3/ VEB Robotron; Optimierungscompiler FORTRAN OE, C 5463-0201-1, p.118
/4/ U. Fromm, W.D. Fromm, F. Schwarzenberg; Arbeitsbericht KFM-7/85, ZfK Rossendorf
/5/ K.-H. Heinig, G. Otto, H.-J. Müller; this report p. 42

LIST OF PUBLICATIONS, ACADEMIC PROMOTIONS, LECTURES AND CONFERENCE CONTRIBUTIONS, SCIENTIFIC MEETINGS AND AWARDS OF HONOUR

ZENTRALINSTITUT FÜR KERNFORSCHUNG, ROSSENDORF, BEREICH KF

VERÖFFENTLICHUNGEN

Andrejtscheff, W., L.K. Kostov, H. Rotter, H. Prade, F. Stary, M. Scuba, N. Tsoupas, Z.Z. Ding, P. Raghavan: Two-Quasiparticle Excitations and Collectivity in the Weakly deformed Transitional Isotopes ^{104,106,108}Cd. Nucl. Phys. A437 (1985) 167

Artemov, K.P., V.Z. Goldberg, M.S. Golovkov, I.P. Petrov, V.P. Rudakov, I.N. Serikov, V.A. Timofeev, H.U. Gersch, E. Hentschel: Observation of Direct ^{12}C Transfer in the ^{12}C(^{14}N,d)^{24}Mg Reaction. Phys. Lett. 149B (1984) 325

Bankwitz, P., M. Betzl, L.P. Drechsler, K. Feldmann, L. Fuentes, H. Kampf, K. Walther: Fabric Analysis of the Quartz Component in Granulite Rocks Using Neutron Time-of-Flight Diffraction. Gerlands Beitr. Geophysik 94 (1985) 507

Barz, H.W., J. Bondorf, R. Donangelo, H. Schulz: Statistical multifragmentation of nuclei(III) Decay of the fragments. NBI Preprint 85-15 (1985)

Barz, H.W., J. Bondorf, R. Donangelo, H. Schulz: Connection between the thermodynamical and percolation models for nuclear fragmentation. NBI Preprint 85-22 (1985)

Barz, H.W , L.P. Csernai, B. Kämpfer, B. Lukács: Stability of detonation waves leading to quark-gluon plasma. Phys. Rev. D32 (1985) 115

Barz, H.W., H. Iwe: Subthreshold antikaon production in relativistic nuclear collisions calculated in the cascade model. Phys. Lett. 153B (1985) 217

Barz, H.W., B. Kämpfer, B. Lukács, L.P. Csernai: Extra entropy production due to non-equilibrium phase transitions in relativistic heavy-ion collisions. Phys. Rev. C31 (1985) 268

Barz, H.W., B. Kämpfer, H. Schulz: Relativistic heavy ion collisions. ZfK-542 (1984)

Betzl, M.: Internationale Schule Neutronenstreuung '85. Kernenergie 10 (1985) 431

Betzl, M., L. Fuentes, J. Tobisch: Texture Study of Rolling Conditions for Zinc based Alloys. Preprint E14-85-473, JINR Dubna 1985

Bischoff, L.: Anwendung von neutronendotiertem Silicium für Halbleiterdetektoren. Fiz. Tekh. Polupr. 19 (1985) 12, 2118

Bischoff, L., K. Irmer, G. Zschornak: Detektoren aus neutronendotiertem Silicium als Kernstrahlungsdetektoren für Industrieroboter. Isotopenpraxis 21 (1985) 374

Blasek, G., A. Kahn, F.K. Naehring: Flüssigmetall-Ionenquellen zur Submikrometerstrukturierung und -analyse. vakuum-information 16 (1986)

Bondarenko, V.A., P.T. Prokof'ev, W. Enghardt, H. Prade, F. Stary, L. Käubler, H.-J. Keller: Protonenzustände in ^{149}Eu und triaxiale Kernform im Gebiet N=84-88 (in russ.). Preprint AdW Lett. SSR LAFI-070, Salaspils 1984

Bondorf, J., R. Donangelo, I.N. Mishustin, C.J. Pethick, H. Schulz, K. Sneppen: Statistical multifragmentation of nuclei (I) Formulation of the model. Nucl. Phys. A443 (1985) 321

Bondorf, J., R. Donangelo, I.N. Mishustin, H. Schulz: Statistical multifragmentation of nuclei (II). Application of the model to finite nuclei disassembly. NBI Preprint 85-15 (1985)

Bondorf, J., R. Donangelo, H. Schulz, K. Sneppen: Energy threshold for fragmentation and vaporization of the atomic nucleus. NBI Prepring 85-14 (1985)

Borany, J. von, B. Schmidt: Ionenimplantierte Si-Detektoren mit hohem Auflösungsvermögen. Fiz. Tekh. Polupr. 19 (1985) 12, 2122

Böttger, R., W.D. Fromm, H. Klein, H. Märten, D. Richter, D. Seeliger: The ^{252}Cf(SF) neutron spectrum in the high energy range. Proceedings of Int. Conf. on nuclear data for basic & applied science, Santa Fe, USA, Mai 1985

Brauer, G., E. Richter: Untersuchungen an Natriumalumosilikat- und Natriumkalziumsilikatgläsern nach Kalium/Natrium-Ionenaustausch mittels Positronenannihilation. Silikattechnik 35 (1984) 11, U2

Dienel, G., C. Jörren, E. Richter: Zum Verschleißverhalten ionenimplantierter Stahloberflächen. Schmierungstechnik 16 (1985) 118

Diener, G., M. Posselt: A self-consistent approach to the ideal magnetization in heterogeneous ferromagnetics. Phys. Status Solidi B129 (1985) 631

Dioszegi, i., A. Veres, W. Enghardt, H. Prade: Investigation of Low-Spin States of ^{140}Ce in the (n,n'γ) Reaction and within the Shell Model, J. Phys. G11 (1985) 853

Dioszegi, I., A. Veres, H. Prade, W. Enghardt: (n,n'γ) Reaction and Shell Model Study of ^{140}Ce. Proc. Int. Symp. on In-Beam Nuclear Spectroscopy, Debrecen, 14.-18.5.1984, p. 363

Dönau, F., H. Reinhardt: Spectroscopy of rotating quark bags. NBI Preprint 84-46 (1984)

Enghardt, W., H.U.Jäger, Proton $1h_{11/2}$ Excitations in Odd-Mass N=82 Nuclei. Nucl. Phys. A438 (1985) 141

Enghardt, W., H.U. Jäger, L. Käubler, H.-J. Keller, H. Prade, F. Stary: Description of Negative-Parity States in N=82 Isotones in Terms of $(\pi 1h_{11/2})^1$ Configurations. Proc. 19th Winter School on Physics, Selected Topics in Nuclear Structure, Zakopane, 3.-15.4.1984, p. 405

Feldmann, K.: Application of Neutron TOF-Diffraction to Texture Studies. Preprint E14-85-284, JINR Dubna 1985

Fromm, U., W.D. Fromm, F. Schwarzenberg: Hinweise zur Arbeit mit Magnetbandkassetten. Arbeitsbericht KFM-7/85, Rossendorf, Oktober 1985

Funke, L., P. Kemmnitz, J. Döring, G. Winter, A. Johnson, L. Hildingsson, Th. Lindblad: Transition probabilities in ^{81}Kr and ^{83}Kr. Proc. Int. Symp. on electromagnetic properties of high-spin states, Stockholm, 28.-31.5.1985, Friday 5

Geiler, H.-D., K.-H. Heinig: Theoretical Description of Explosive Crystallization Phenomena Induced by High-Temperature Pulses in thin Layers of Amorphous Semiconductors. ZfK-555 (1985) 451

Geiler, H.-D., K.-H. Heinig: Theoretical Investigation of the Stationary Lateral Movement of an Explosive Liquid-Phase Epitaxy Front (ELPE). ZfK-555 (1985) 466

Gippner, P., W. Enghardt, W.D. Fromm: Programm zur Bearbeitung experimenteller Daten des Zweiarm-Flugzeit-Spektrometers DEMAS (in russ.). Arbeitsberatung zu Experimenten am Strahl schwerer Ionen, Varna, 13.-19.9.1984, JINR D7-84-736 (1984) 77

Gippner, P., W. Seidel, P. Manfraß, F. Stary, K.D. Schilling, E. Will, H. Sodan, S.M. Luk'janov, Ju.E. Penionzkevic, G.G. Cubarjan: Das Zweiarm-Flugzeit-Spektrometer DEMAS (in russ.). Arbeitsberatung zu Experimenten am Strahl schwerer Ionen, Varna, 13.-19.9.1984, JINR D7-84-736 (1984) 75

Goncharova, N.G., A.N. Golzov, H.R. Kissener: Magnetische Hochspinanregungen des Kerns ^{14}C. 35. Allunionskonferenz "Kernspektroskopie und Struktur Atomkern", Leningrad, April 1985, p. 181

Goncharova, N.G., H.R. Kissener, R.A. Eramzhyan: Photospaltung von 1p-Schalenkernen (in russ.). Fiz. Ehlem. Chastits At. Yadra 16, 4 (1984) 773

Gudima, K.K., V.D. Toneev, G. Röpke, H. Schulz: Entropy evolution in heavy ion collisions. NBI Preprint 85-11 (1985)

Hähnert, M., A. Kolitsch, E. Richter: Ionentransport in Gläsern des Systems (1-y)Na O.yk O.0,4B O.4SiO. Glastechn. Ber. 58 (1985) 191

Heiner, E.: A dynamical theory for a disordered Hubbard chain far from equilibrium. I. Extended master equations. Phys. Status Solidi B127 (1985) 253

Heinig, K.-H.: Effect of Local Melting on Semiconductor Surfaces. Proc. Int. Conf. on Energy Pulse Modification of Semiconductors and Related Materials, Ed. K. Hennig, ZfK-555 (1985) 265

Heinig, K.-H., H.-D. Geiler: Phenomenological Theory of Explosive Solid Phase Crystallization in Amorphous Silicon. Part 1: Stationary Solutions. Phys. Status Solidi A92 (1985) 421

Heinig, k.-H., H.-D. Geiler, G. Otto: Theoretical Investigation of an Explosive Solid-Phase Nucleation (ESPN) Wave Front in a-Si. ZfK-555 (1985) 459

Heinig, K.-H., M. Voelskow, J. Matthäi, A. Zetzsche, C. Treutler: Local Melting by Nucleation on the Surface of Single Crystalline Silicon. ZfK-555 (1985) 280

Hensel, E., K. Wollschläger, D. Schulze, U. Kreißig, W. Skorupa, J. Finster: Si-O Compound Formation by Oxygen Ion Implantation into Silicon. Surf. Interf. Anal. 7 (1985) 207

Hensger, K.-E., A. Schubert, P. Klimanek, A. Mücklich: Werkstoffveredlungsverfahren für Federstähle. WP C21 D/269 512 5, 16.10.1985

Hohmuth, K., B. Rauschenbach: High Fluence Implantation of Nitrogen Ions into Titanium. Mater. Sci. Eng. 69 (1985) 489

Hohmuth, K., E. Richter, B. Rauschenbach, C. Blochwitz: Fatigue and Wear of Metalloid-ion-implanted Metals. Mater. Sci. Eng. 69 (1985) 191

Jäger, H.U., E. Hensel, U. Kreissig, W. Skorupa, E. Sobeslavsky: A model for the oxidation of silicon by high dose oxygen implantation. Thin Solid Films 127 (1985) 159

Just, G., W.D. Fromm, H. Zwanziger: Zur geochemischen Charakterisierung von Granitoiden mittels rechnergesteuerter INAA-Meßtechnik und multivarianter Statistik. 3. Tagung Computereinsatz in der Analytik COMPANA 85, Abstracts of Papers, Jena 1985, p. 18

Kachurin, G.A., N.P. Stepina, M. Voelskow, E. Wieser: Annealing behaviour of Low-Energy-Implanted Silicon. Phys. Status Solidi A90 (1985) 285

Kämpf, H., P. Bankwitz, M. Betzl, C. Legler: Results of Neutron Texture Analysis of Prevariscan and Variscan Magnetite Ores of the Erzgebirge Acticlinal Zone. Gerlands Beitr. Geophys. 94 (1985) 522

Kämpfer, B.: Phase transition in dense nuclear matter and explosive neutron star phenomena. Phys. Lett. 153B (1985) 121

Kämpfer, B., H.W. Barz, L.P. Csernai: Signatures of the Deconfinement Transition and the Double-Shock Phenomenon. UMTNP - 120/1985 (University of Minesota)

Kämpfer, B., H.W. Barz, B. Lukács: Quark-gluon-plasma formation in Relativistic Heavy Ion Collisions within the Hydrodynamical Description. KFKI-1985-77

Kämpfer, B., H.W. Barz, L. Münchow, B. Lukásc: Decay of the Baryon Rich Quark-Gluon-Plasma Produced in Heavy Ion Collisions. KFKI-1985-65

Kämpfer, B., H. Schulz, C.J. Horowitz: A two-phase description of hot nuclear matter and quark gluon plasma. Ann. Phys. (Leipzig) 41 (1985) 291

Kämpfer, B., H. Schulz, B. Lukács: Spherical hydrodynamical expansion of weakly excited blobs of nuclear matter. J. Phys. 11 (1985) L 47

Keller, H.-J., U. Hagemann, L. Käubler, H. Prade, F. Stary, S. Frauendorf: Configuration Dependent Triaxiality in ^{105}Ag and its Neighbours. Nucl. Phys. A444 (1985) 261

Kirchbach, M., H.U. Jäger: Shell-model studies of the one-pion exchange contribution to the chiral charge density in the mass-16 triad. 11th Europhysics Conference "Nuclear Physics with Electromagnetic Probes", Juli 1985, Paris

Kirchbach, M., H.-U. Jäger, M. Gmitro: Meson exchange corrections to the $0^+ \rightarrow 0^-$-beta decay of ^{16}C. Z. Physik A320 (1985) 689

Kirchbach, M., H.-U. Jäger, M. Gmitro: Meson exchange correction to the 0-decay of the C^{16} ground state. Z. Phys. A320 (1985) 689

Kirchbach, M., E. Truhlik: Der axiale Mesonaustauschstrom in der Kernphysik. Fiz. Ehlem. Chastits At. Yadra 16, 6 (1985) (in russ.)

Kirschbaum, D.: The Algebra of the Classical Hamiltonian Mechanics as the Closure of two Finite-dimensional Algebras. Preprint E2-84-739, JINR Dubna

Kleinwächter, P., I. Rotter: Spectroscopic properties of highly excited states. Phys. Rev. C32 (1985) 1742

Kolev, D., N. Nenov, Z. Petkova, N.G. Saiceva, K.D. Schilling: Untersuchung von Anregungsfunktionen und Isomerenverhältnissen in (Hl, αxn)-Reaktionen (in russ.) Arbeitsberatung zu Experimenten am Strahl schwerer Ionen, Varna, 13.-19.9.1984, JINR D7-84-736 (1984) 38

Kolitsch, A., E. Richter: Natrium/Kalium-Ionenaustausch an Silicatgläsern. Glastechn. Ber. 58 (1985) 40

Komarov, V.I., H. Müller, S. Tesch: Cluster excitation in hadron-nucleus collisions at medium and high energies. Fortschr. Phys. 33 (1985) 11

Kotte, R., G. Ortlepp, F. Stary, S.M. Luk'janov: Zeitnahme bei Detektoren mit Mikrokanalplaten (in russ.). Arbeitsberatung zu Experimenten am Strahl schwerer Ionen, Varna, 13.-19.9.1984, JINR D7-84-736 (1984) 90

Kudojarov, M.F., J.Ch. Lemberg, A.A. Pasternak, L.A. Rassadin, F. Dönau: Lebensdauer und Niveaustruktur in ^{83}Kr. Izv. Akad. Nauk Tadzh. 48 (1984) 1887

Lück, H.B.: Möglichkeiten und Grenzen bei der Herstellung von Mikrofiltern mit Hilfe der Kernspurtechnologie und Stand der Arbeiten im Zentralinstitut für Kernforschung Rossendorf. 2. Fachtagung "Theorie und Praxis der Membrantrennprozesse", Dresden, 3.-4.10.1985

Lück, H.B., B. Heinrich, R. Kirchbach, H. Matthes, W. Pfestorf, M. Seidel: Stand der Arbeiten zur Kernstellung von Kernspurmikrofiltern im ZfK Rossendorf. Arbeitstagung zur Anwendung von Kernspurmikrofiltern, Dubna, 16.-17.10.1985

Lukyanov, S.M., Ju.Ts. Oganessian, Yu.E. Penionzhkevich, H. Sodan, E. Will, G.G. Chubarian, P. Gippner, W. Seidel, K.-D. Schilling: Mass Distributions of Products in Reactions Leading to the Composite Systems with Z=108. Proc. Int. Workshop on Gross Properties of Nuclei and Nuclear Excitations XIII, Hirschegg, 14.-19.1.1985, ISNN 0720-8715, Darmstadt, 1985, p. 123

Lukyanov, S.M., Ju.Ts. Oganessian, Ju.E. Penionzhkevich, H. Sodan, E. Will, G.G. Chubarian, P. Gippner, K.-D. Schilling, W. Seidel, F. Stary: Fragment Mass Distributions in Heavy-Ion Reactions Leading to Composite Systems with Z=108. Proc. 2nd Int. Conf. on Nucleus-Nucleus Collisions, Visby, Sweden, 10.-14.6.1985, Vol. 1, Contributed Papers, p. 56

Märten, M., W. Neubert, D. Richter, D. Seeliger: Detailed investigations of fission neutron emission. Proc. Int. Conf. Neutron Physics, Santa Fe, USA, May 1985

Märten, M., W. Neubert, D. Richter, D. Seeliger: Measurement of fragment-neutron correlations in the spontaneous fission of ^{252}Cf. Proc. Int. Symp. on Reactions of fast neutrons, Smolenice, CSSR, June 1985

Matthies, S., H.R. Wenk: ODF-Reproduction with Conditional Ghost Correction. In: Preferred Orientation in Deformed Metals and Rocks", An Introduction to Modern Texture Analysis. Ed. by H.R. Wenk. San Diego: Academic Press 1985

Matz, W., U. Bärenwald, M. Dubiel: Neutron Diffraction Investigation of the Structure of Fluorophosphate Glasses. Phys. Status Solidi A90 (1985) 107

Matz, W., U. Hoppe: Untersuchung der Struktur amorpher Stoffe mit der Flugzeitneutronendiffraktion am NSWR. JINR P13-85-280, Dubna 1985

Medved, S.V., L. Prashakova, W.D. Fromm, F. Schwarzenberg: Ein Kontroller für die Kopplung eines grafischen Displays mit einem Zeichentisch. JINR-Preprint P11-85-469, Dubna 1985

Melzer, U., W. Matz, H. Mehner: ^{119}Sn Hyperfine fields in the ferromagnetic systems $Me_xSn_yFe_{3-x-y}O_y$ (Me:Zn^{2+}, Ga^{3+}, Ge^{4+}). Proc. Mössbauer Conf., Alma Ata, 26.9.-1.10.1983, "Application of the Mössbauer Effect" Plenum, vol. 3. New York 1985, p. 1187

Mende, G., J. von Borany, M. Deutscher, B. Schmidt, W. Skorupa, F. Fenske, W. Markgraf: Neuere Ergebnisse bei der Herstellung und Anwendung von anodischem SiO_2. Tagungsband 3. Symposium Physikalische Grundlagen zu Bauelementetechnologien der Mikrotechnik, Frankfurt/Oder 1984, S. 347

Mende, G., C. Bauer, C. Heiser, W. Rudolph, F. Fenske, A. Lehmann, W. Markgraf, U. Teschner: Über den Einfluß der Herstellungsbedingungen auf den Si-O-Si-Bindungswinkel, Wasserstoffgehalt und elektrophysikalische Eigenschaften von anodischen Oxidschichten auf Silicium. Tagungsband 16. Arbeitstagung Physik der Halbleiteroberfläche, Binz 1985, S. 253

Mende, G., F. Fenske, J. Finster, A. Lehmann, D. Schulz, U. Teschner, D. Treibmann: Über Struktur und Zusammensetzung von anodischem SiO_2. Tagungsband 15. Arbeitstagung Physik der Halbleiteroberfläche, Binz 1985, S. 293

Müller, H.-J.: Influence of local-environment on bound excitons and bound excitonic molecules in III-V alloys. I. The theory and numerical results for $GaAs_{1-x}P_x$:N. Phys. Status Solidi B132 (1985) 239
II. Numerical results for $Ga_xIn_{1-x}P$:N and the role of disorder topology for the optical spectrum. Phys. Status Solidi B132 (1985) 472

Müller, H.-J., H.-J. Wünsche, J. Röseler: What can DFF give for bound excitons to isoelectronic N-impurities in III-V-mixed crystals? Proc. Int. Conf. Excitons 84, Güstrow 1985, S. 247

Naehring, F.K., A. Kahn: Gallium Ion Micro Beam with Liquid Metal Ion Source for Ion Lithography. Proc. Int. Conf. on Electron Beam Technologies, Sofia 1985, p. 523

Naehring, F.K., G. Otto: Design of an Electrostatic Octupole for Micro-Beam Deflection. Phys. Status Solid A94 (1986) 2

Neumann, H., W. Matz, W. Hoyer, M. Wobst: Investigation on the Structure of Molten $Ge_{15}Te_{85}$ in Dependence on Temperature. Phys. Status Solidi A90 (1985) 489

Prade, H., W. Enghardt, H.U. Jäger, L. Käubler, H.-J. Keller, F. Stary, G. Winter: Excited States above the 6^+ Isomers in the Even-Mass N=82 Nuclei ^{138}Ba and ^{140}Ce. Proc. Int. Symp. on In-Beam Nuclear Spectroscopy, Debrecen, 14.-18.5.1984, p. 197

Prade, H., W. Enghardt, L. Käubler, H.-J. Keller, F. Stary, G. Winter: In-Beam Investigations and Structure Studies of the Even-Mass N=82 Nuclei ^{138}Ba and ^{140}Ce. Proc. 23. International Winter Meeting on Nuclear Physics, Bormio, Italy, 21-26.1.1985, p. 175

Prade, H., W. Enghardt, L. Käubler, H. Rotter, F. Stary, G. Winter, L.K. Kostov, W. Andrejtscheff, L.G. Kostova, P. Petkov: Lifetimes of Excited States in Even-Mass N=82 Nuclei. Proc. Symp. on Electromagnetic Properties of High Spin States, Stockholm, 28.-31.5.1985

Reinhardt, H.: Relativistic Pairing Field Theory. NBI-Preprint 84-12 (1984)

Reinhardt, H., B.V. Dang, H. Schulz: Deconfinement phase transition of hot and dense nuclear matter in the non-topological soliton bag model. Phys. Lett. 159B (1985) 161

Reinhardt, H., P.G. Reinhard, K. Goeke: Non-Markovian treatment of collective motion in extended time-dependent mean-field theories. Phys. Lett. 151B (1985) 177

Reinhardt, H., H. Schulz: Field theoretical treatment of the liquid-vapor phase transition in nuclear systems. Nucl. Phys. A432 (1985) 630

Richter, E.: Zur Natriumdiffusion in mit Titannitrid beschichtetem Natron-Kalk-Glas. Silikattechnik 35 (1934) 12, U2

Richter, E.: Sperrwirkung ionenimplantierter Glasoberflächen. Glastechn. Ber. 58 (1985) 59

Richter, E.: Verschleißschutz durch Ionenimplantation. Schmierungstechnik 16 (1985) 324

Roepke, G., H. Schulz, L.N. Andronenko, A.A. Kotov, W. Neubert, E.N. Volnin: Depletion of light cluster production in 1 GeV proton-nucleus collisions. Phys. Rev. C31 (1985) 1556

Rotter, H., J. Döring, L. Funke, L. Käubler, P. Kemnitz, P. Kleinwächter, L.O. Norlin, H. Prade, R. Schwengner, G. Winter, A.E. Sobov, A.P. Grinberg, I.Kh. Lemberg, A.S. Mishin, L.A. Rassadin, I.N. Chugunov: Evidence for a few-quasiparticle isomer in ^{84}Kr. Phys. Lett. 163B 323; Proc. Int. Symp. on electromagnetic properties of high-spin states, Stockholm, 28.-31.5.1985

Rotter, I.: Nuclear-structure investigations with inclusion of continuum states. Proc. Symp. "Nuclear Excited States", Lodz, Juni 1984, p. 183, ed. by L. Lason et al.

Rotter, I.: Many-body forces in finite nuclei and amplitude correlations in nuclear reaction cross sections. J. Phys. G11 (1985) L219

Rotter, I.: Spectroscopic investigation of isolated and overlapping resonance states. ZfK-537 (1985)

Rotter, I.: Nuclear structure investigations with inclusion of continuum states. Proc. Workshop "Coincident particle Emission from Continuum States in Nuclei", Bad Honnef, Juni 1984, p. 210, ed. by H. Machner and P. Jahn

Rüdenauer, F.G., W. Steiger, E. Wieser, R. Grötzschel, F. Naehring: Formation of droplets on Si surfaces bombarded by In from a capillary type liquid metal ion source. Vacuum 35/8 (1985) 315

Rudolph, W., C. Bauer, D. Grambole, C. Heiser, F. Herrmann, G. Mende, h. Flach, G. Jungnickel, G. Kelm: Messung von Wasserstoff-Tiefenprofilen mittels Kernreaktionen. Tagungsband 3. Symposium Physikalische Grundlagen zu Bauelementetechnologien der Mikroelektronik, Frankfurt/O. 1984 (1985) 613

Schulz, H., B. Kämpfer, H.W. Barz, G. Röpke, J. Bondorf: On the time-development of the liquid-vapor phase transition in an expanding nuclear system. Phys. Lett. 147B (1984) 17

Schulz, H., G. Röpke, V.D. Toneev, K.K. Gudima: Effective radii of light composites produced in relativistic heavy ion collisions. JINR Preprint E2-85-592, Dubna 1985

Schwarzenberg, F.: Hard- und Software-Ergänzungen für den Kleincomputer Z9001 als Voraussetzung für einen universellen Einsatz. Arbeitsbericht KFM-6/85, Rossendorf, Oktober 1985

Seidel, W., F. Stary: Herstellung dünner Polypropylenfolien (in russ.). Arbeitsberatung zu Experimenten am Strahl schwerer Ionen, Varna, 13.-19.9.1984, JINR D7-84-736 (1984) S. 82

Sodan, H., E. Will, S.M. Luk'janov, Ju.Z. Oganesjan, Ju.E. Penionzkevich, G.G. Cubarjan, P. Gippner, W. Seidel, K.D. Schilling: Study of Decay Product Mass Distributions in Reactions Leading to Composite Systems with Z=108 (in russ.). JINR Rapid Communications, No. 4-84, Dubna 1984, p. 15

Sobe, G., H. Schreiber, G. Weise, R. Voigtmann, G. Zies, J. Sonntag, W. Brückner, R. Grötzschel: Deposition of Cr-Si Thin Films by Reactive Plasmatron-Magnetron Sputtering. Thin Solid Films 128 (1985) 149

Stiehler, T., B. Kühn, K. Möller, J. Mösner, W. Neubert, W. Pilz, G. Schmidt: A measurement of the total cross section of the reaction $n + p \rightarrow d + \gamma$ at $E_n = 25$ MeV. Phys. Lett. 151B (1985) 185

Stiehler, T., J. Mösner, G. Schmidt, W. Pilz, J. Hutsch: A charged-particle spectrometer for measuring neutron-induced reaction products. Nucl. Instrum. Methods A236 (1985) 343

Tatarkiewicz, J., J. Krynicki, R. Grötzschel, K. Paprocki: Radiation damage distribution for 300 keV Sb ions implanted into silicon. Phys. Lett. 107A/1 (1985) 48

Uhlig, T., D. Schubert: Berechnung des π-Koeffizienten und des K-Faktors für polykristalline Siliziumschichten. ZfK-546 (1985)

Urwank, P., E. Wieser, A. Hässner, Ch. Kaufmann, H. Lippmann, I. Melzer: Formation of $MoSi_2$ by Light Pulse Irradiation. Phys. Status Solidi A90 (1985) 463

Weiß, L., A.Yu. Rumyantsev, A.S. Ivanov: Acoustic Phonon Dispersion of $CoSi_2$. Phys. Status Solidi B128 (1985) K 111

Wieser, E.: Lichtimpulsverfahren für Technologien der Mikroelektronik. Wissenschaft und Fortschritt 35 (1985) 94

Will, E.: Schneller Diskriminator für Flugzeitmessungen (in russ.). Arbeitsberatung zu Experimenten am Strahl schwerer Ionen, Varna, 13.-19.9.1984, JINR D7-84-736 (1984) 73

Will, E., H. Sodan, I.V. Kolesov, R. Kupczak, Ju.E. Penionzkevic, Ju.Z. Oganessjan, W. Seidel: 4π-Detektor für Reaktionsprodukte aus Schwerionenreaktionen (in russ.). Arbeitsberatung zu Experimenten am Strahl schwerer Ionen, Varna, 13.-19.9.1984, JINR D7-84-736 (1984) 70

Winter, G., F. Dubbers, J. Döring, L. Funke, P. Kemnitz, E. Will, D.S. Andreev, K.I. Erochina, I.Kh. Lemberg, A.A. Pasternak, L.A. Rassadin, I.N. Chugonov: On the irregularities in the band structures of ^{78}Kr. J. Phys. G11 (1985) 277

DIPLOMARBEITEN

Teichfuß, M.: Herstellung und Untersuchung von ortsempfindlichen Kernstrahlungsdetektoren aus neutronendotiertem Silizium. Juli 1985

PROMOTIONEN A (Dr. rer. nat.)

Rüdiger, J.: Experimentelle Untersuchung von Kerndrehmomenten in Schwerionenreaktionen, die von der Emission leichter geladener Teilchen begleitet werden. VIK Dubna, 1.11.1984

Dshemuchadse, S.: Einige Charakteristika der Bildungsprozesse neutraler seltsamer Teilchen und γ-Quanten bei 40 GeV/c. VIK Dubna, 17.11.1984

Enghardt, W.: Spektroskopie des Kernes ^{140}Ce und Erweiterung der Schalenmodellbeschreibung halbmagischer Kerne mit 82 Neutronen oder 50 Protonen. AdW der DDR, 22.3.1985

Borany, J. von: Hochauflösende ionenimplantierte Halbleiterdetektoren für die Teilchenspektrometrie. AdW der DDR, 2.5.1985

Helming, K.: Beiträge zu aktuellen Fragen der quantitativen Texturanalyse, insbesondere bezüglich der Reproduzierung von Orientierungsverteilungsfunktionen aus Polfiguren. AdW der DDR, 30.8.1985

Skorupa, W.: Zur Erzeugung von SiO_2 und Si_3N_4 durch Sauerstoff- bzw. Stickstoffimplantation in Silicium. AdW der DDR, 6.9.1985

Hensel, E.: Zur Erzeugung von SiO_2 und Si_3N_4 durch Sauerstoff- bzw. Stickstoffimplantation in Silicium. AdW der DDR, 6.9.1985

Voitus, W.: Untersuchungen an Nickelbasislegierungen mittels Neutronenkleinwinkelstreuung und Elektronenmikroskopie. TH Magdeburg, 17.9.1985

PROMOTIONEN B (Dr. sc. nat.)

Stiehler, T.: Die Bestimmung des totalen Wirkungsquerschnittes der Reaktion $n + p \rightarrow d + \gamma$ bei einer Neutronenenergie von E_n = 25 MeV. TU Dresden, 8.11.1985

Feldmann, K.: Anwendung der Neutronenflugzeitmethode zur quantitativen Texturanalyse. TU Dresden, 4.4.1985

VORTRÄGE, DIE AUSSERHALB DES EIGENEN KOLLEKTIVS GEHALTEN WURDEN

Aleksandrov, K.S., A.F. Bovina, V.N. Vornov, N.V. Gorev, I.M. Iskornev, S.V. Melnikova, S.V. Misjul, F. Prokert, I.N. Flerov: Ferroelastic Phase Transitions in Elpasolites. International Meeting on Ferroelectricity, Kobe, Aug. 1985

Andronenko, L.N., A.A. Kotov, W. Neubert, L.A. Vaishnene: Linear momentum transfer to residual nucleus leading to fission [h)]

Baither, D., R. Kögler, D. Panknin, E. Wieser: Residual defects in implanted silicon after annealing with incoherent ligth [c)]

Banisch, B., B. Tillack, R. Reinboth, M. Voelskow, J. Matthäi, E. Wieser: Recristallization of thick polycristalline silicon films on SiO_2 by CO_2-laser and lateral zone-melting technique [c)]

Bankwitz, P., K. Feldmann, L.P. Drechsler, K. Walther, L. Fuentes: Ergebnisse einer Neutronentexturuntersuchung in sächsischen Granuliten [a)]

Barkleit, G., K. Deutsch, N. Haase, C. Kunath, R. Häßler, H. Reuther: Mechanische und thermische Eigenschaften galvanisch abgeschiedener Nickelschichten und deren Veränderungen durch Ionenimplantation. 7. Symposium Verformung und Bruch, Magdeburg, 3.-5.9.1985

Barz, H.W.: Strangeness Production in Cascade Models [d)]

Barz, H.W.: Secondary Decay of Fragments. Workshop NBI Kopenhagen, April 1985

Barz, H.W.: Heavy-Ion Reactions at Relativistic Energies. V. Int. Arbeitsseminar Kerntheorie, Gjuletschitza, Juni 1985

Betzl, M.: Festkörperuntersuchungen mit Neutronen. Phys. Kolloquium der Sekt. Physik der TH "Carl Schorlemmer", Leuna-Merseburg, 2.4.1985

Betzl, M., K. Feldmann, K. Walther: Anwendung der Neutronen-Flugzeitmethode für die quantitative Texturanalyse [o)]

Betzl, M., K. Hennig, A. Mücklich, K. Feldmann, K. Walther, K.H. Kleinstück, J. Tobisch: Texture Investigation of Materials by Neutron Diffraction [l)]

Betzl, M., K. Hennig, A. Mücklich, K. Feldmann, K. Walther: Texture Investigations of Materials by Neutron Diffraction [k)]

Bischoff, L., K. Irmer: Einsatz von HLD aus ND-Si in einem B-Rückstreusensor [e)]

Borany, J. von, B. Schmidt: Entwicklung und Einsatz spezieller planarer Si-Detektorstrukturen [e)]

Deutscher, M., I. Beatus, G. Mende, H.-J. Döring, M. Elsner: Ionenimplantierte Silizium-Sperrschichtdetektoren für Elektronenstrahlgeräte [e)]

Deutscher, M., H.J. Döring: Structured silicon detectors for the registration of electrons in electron lithographic and measurement equipments. Int. Conf. on Electron Beam Technologies, Varna, Mai 1985

Dienel, G., A. Kolitsch, H. Reuther, E. Richter: Wear behaviour of ion implanted steel surfaces [c)]

Dienel, G., A. Kolitsch, E. Richter: Improvement of wear behaviour by surface alloying by ion implantation [l)]

Dienel, G., A. Kolitsch, E. Richter: Veränderung mechanischer Eigenschaften von Hartmetallen durch Ionenimplantation. 11. Int. Plansee Seminar B5, Reutte, 20.-24.5.1985

Dienel, G., A. Kolitsch, E. Richter: Modifizierung mechanischer Eigenschaften von Hartmetallen durch Ionenimplantation. VIII. Pulvermetallurgische Tagung, Dresden, 24.-26.9.1985

Döring, J.: Prolate-oblate shape transition in the odd-mass isotopes $^{75-83}Kr$ [f)]

Dvurechenskii, A.V., N.M. Igonina, R. Grötzschel: Upravlenie profilem primesi w kremnii w usloviyakh impulsnovo elektronovo otschiga, kharakteristiki p-n-perekhod [c)]

Eichhorn, F.: Some results of neutron diffraction on perfect crystals, University of Metz, 25.1.1985

Eichhorn, F., U. Schmidt, W. Voitus: Determination of material inhomogeneities by small-angle neutron scattering [l)]

Enghardt, W., H. Prade, H.U. Jäger, I. Käubler, H.-J. Keller, L.K. Kostov, F. Stary: Microscopic Structure of Semi-Magic Nuclei with 82 Neutrons or 50 Protons. 7th Int. Summer School on Nuclear Physics, Neutron Physics and Nuclear Energy, Varna, 22.-29.9.1985

Eschrig, H., R. Richter, L. Weiß, A.Yu. Rumyantsev, N.L. Mitrofanov, A.S. Ivanov, N.A. Chernoplekov: Phonon Anomalies in Copper-Base Alloys [r)]

Feldmann, K.: ICOTOM 7, Experimentelles zur Texturbestimmung [a)]

Feldmann, K.: Application of Neutron TOF-Diffraction to Texture Studies. Workshop on Experimental Technique of Texture Analysis, Clausthal-Zellerfeld, 25.-29.3.1985

Fromm, W.D.: Ein Vielkanalanalysator im CAMAC-Standard zur Steuerung eines Mikrostrahls für Strukturuntersuchungen. II. Int. Schule über Automatisierung der wissenschaftlichen Forschung, Puschtschino, 19.10.1985

Fromm, W.D.: Probleme des Einsatzes von Mikrorechnern und rechnergesteuerten Analysatorsystemen zur Steigerung der Effektivität der kernphysikalischen Routineanalytik. Lehrgang Anwendung kernphysikalischer Analysenverfahren in den geologischen Wissenschaften, KMU Leipzig, 4.11.1985

Fromm, W.D., H. Märten, W. Neubert, D. Richter, D. Seeliger: Experimental arrangement for the measurement of correlations between fission products and neutrons [h)]

Funke, L.: Few-particle excitations in Kr nuclei [f)]

Funke, L.: Transition probabilities in ^{81}Kr and ^{83}Kr. Int. Symp. on electromagnetic properties of high-spin states, Stockholm, 28.-31.5.1985

Geiler, H.-D., K.-H. Heinig: Theoretical Description of the Stationary Lateral Movement of an Explosive Liquid-Phase Epitaxy Front (ELPE) [j)]

Geiler, H.-D., D. Wolff, K.-H. Heinig, G. Otto: Ignition of explosive liquid phase epitaxy by solid phase nucleation [g)]

Geiler, H.-D., D. Wolff, K.-H. Heinig, G. Otto: Theoretical Study of the Ignition of ELPE-Waves by Autocatalytically Enhanced Solid-Phase Nucleation in a-Si [g)]

Gersch, H.U.: About the possibilities of measurement the K^+-K^+-interferences at the Synchrophasotron in Dubna. Arbeitstagung GIBS, VIK Dubna, 23.-25.4.1985

Gersch, H.-U.: Kaoneninterferometrie zur Untersuchung des frühen Stadiums von relativistischen Kernreaktionen - Vorschlag für ein Experiment am Dubnaer Synchrophasotron. Seminar des Laboratoriums für hohe Energien des VIK, Dubna, 27.11.1985

Gippner, P., K.-D. Schilling, W. Seidel, F. Stary, S.M. Lukyanov, Ju.Ts. Oganessian, Ju.E. Penionzhkevich, H. Sodan, E. Will, G.G. Chubarian: Fragment Mass Distributions in Heavy-Ion Reactions Leading to Composite Systems with Z=108 [m)]

Gippner, P., K.-D. Schilling, W. Seidel, F. Stary, E. Will, H. Sodan, S.M. Lukyanov, G.G. Chubarian, V.S. Salamatin, Ju.E. Penionzhkevich: Fragment Mass Distributions in Heavy-Ion Reactions Leading to Composite Systems with Z=108 [h)]

Grötzschel, R.: The Rossendorf activities in surface analytics by means of nuclear methods. Seminarvortrag im Institut für Mikroelektronik - Technologie Cernogolovka, Moskau, 13.3.1985

Grötzschel, R.: Nukleare Diagnostik von Festkörperoberflächen. 4. Tokamak-Schule des ZIE, Bad Stuer, Oktober 1985

Grötzschel, R., A.V. Dvurechenskii, V.P. Popov, B.P. Kaschnikov, M. Griepentrog: Rasuporyadochenie i amorfisatio pri obluchenii silno legirovannovo kremniya legkamu ionami (Poster) [c)]

Heera, V., B. Rauschenbach: A model of direct amorphisation of metals by high dose metalloid ion implantation [g)] and [c)]

Heinig, K.-H.: Melt Instability of Si During Pulse Heating [i)]

Heinig, K.-H.: The Modes of Explosive Crystallization of a-Si [i)]

Heinig, K.-H., H.D. Geiler, G. Otto: Theoretical Investigation of an explosive solid phase nucleation wave front in A-Si [j)]

Heinig, K.-H., G. Otto: Study of the Confinement of Subboundaries in SOI-Layers by Computer Simulation [c)] and [g)]

Heinig, K.-H., M. Voelskow, J. Matthäi, A. Zetzsche: Microscopic melt instabilities of laser or flash lamp irradiated silicon. Int. Conference "Trends in Quantum Electronics", Bukarest, 2.-6.9.1985

Heinig, K.-H., M. Voelskow, J. Matthäi, A. Zetzsche, C. Treutler: Local Melting by Nucleation on the Surface of Single Crystalline Semiconductors [j)]

Helming, K.: On the Reproduction of the ODF from incompletely measured pole figures [k)]

Hennig, K., M. Betzl, Characterization of Solids by Neutron Scattering [l)]

Hennig, K., E. Richter, A. Schmidt: Oberflächenveredlung mittels Ionenstrahlen. 5. Fachtagung Elektrotechnologie, Magdeburg, 28.-29.8.1985

Hoffmann, W., J. Hüller, M.T. Pham: Theorie und Anwendung von ionensensitiven Feldeffekttransistoren. TH Leuna-Merseburg, Juni 1985

Hoffmann, W., J. Hüller, M.T. Pham: pH-ISFET-Eigenschaften und Anwendungen. 7. Symposium Medizinische Physik, Greifswald, Oktober 1985

Hoffmann, W., j. Hüller, M.T. Pham: ISFET-Probleme und neue Entwicklungen. Symposium über spezielle Probleme der Elektrochemie, Meinsberg, November 1985

Iwe, H.: Strangeness-Erzeugung in der Reaktion C + Ta bei 4.2 GeV/c. VIK Dubna, Febr. 1985

Iwe, H.: Kaskadenmodell und rechentechnische Anforderungen [b)]

Iwe, H.: Kaskadenmodell zur Beschreibung von Reaktion mit relativistischen schwerer Ionen [b)]

Jäger, H.-U.: Model investigations of the oxidation of silicon by high dose implantation [q)] and [c)]

Jäger, H.-U.: Issledovanije formirovanija okisja pri oblutschenij kremnija bolschimi dozami kisleroda, Novosibirsk, 10.12.1985

Kämpf, H., P. Bankwitz, A. Frischbutter, M. Betzl: Neutronentexturuntersuchungen an Magnetitskarnen [a)]

Kämpfer, B.: Quarkmaterie und Phasenübergänge in Kernmaterie. Berliner Seminar für Theoretische Physik, Berlin, Oktober 1985

Kämpfer, B.: Confinement transition in the early universe. Copernicus-Centre Warschau, Mai 1985

Kirchbach, M.: Renormierung der chiralen Kernladungsdichte durch den Mesonaustauschstrom [b)]

Kirchbach, M.: Short-range and medium polarization effects on the two-body nuclear chiral charge density in the $0^+ \leftrightarrow 0^-, \Delta T = 1$ β-transitions in the mass - 16 triad [n)]

Kirchbach, M.: Introduction in the theory of the mesonic exchange currents. V. Int. Arbeitsseminar Kerntheorie in Gjoletschitza, Juni 1985

Kirchbach, M.: kernphysikalische Experimente zum Nachweis der Hypothese der spontanen Brechung der chiralen Symmetrie. V. Seminar "Statistische Physik", Güstrow, November 1985

Kirschbaum, D.: On a characterization of realizations for Lie algebras in canonical variables. Dubna, Nov. 1985, LIF Sektor 4 (Feldtheorie)

Kirschbaum, D.: A structure theorem for automorphism algebras in classical Hamiltonian Systems. Dubna, Nov. 1985, LIF Sektor 6 (Supergravitation)

Klimanek, P., A. Kühl, A. Mücklich: Texturentwicklung beim Kaltwalzen von α/β-Messing [t)]

Kolitsch, A., E. Richter: Alkaliionenaustausch an Glasoberflächen. IV. Arbeitstagung Ionentransportprozesse in Festkörpern, Jena 15.-18.10.1985

Kotte, R., H.-G. Ortlepp, F. Stary: Low-Mass Fragments from ^{252}Cf Spontaneous Fission [m)]

Kotte, R., H.-G. Ortlepp, F. Stary: Search for Superasymmetric Fission Products in ^{252}Cf [h)]

Kögler, R., E. Wieser: Influence of rapid isothermal annealing on the diffusion behaviour and the electrical activation of As and B implanted Si [c)]

Kögler, R., E. Wieser: Einfluß schneller isothermischer Ausheilung auf das Diffusionsverhalten und die elektrische Aktivierung von As- und B-implantiertem Si [g)]

Kögler, R., L. Zollfrank: Lichtimpulsanlagen im ZfK Rossendorf [v)]

Kreißig, U., W. Skorupa, E. Hengel, H. Bartsch: Buried insulating layers formed by high dose ion implantation into silicon [c)]

Küchler, R., E. Richter: Ultraschalluntersuchungen an chemisch verfestigten Gläsern. Symposium Mechanische Eigenschaften und Korrosion von Gläsern und glaskeramischen Werkstoffen, Berlin-Hessenwinkel, 11.-14.11.1985

Küchler, R., E. Richter: Heat production during ion implantation [s)]

Kühn, B.: Search for dibaryons in the deuteron breakup by pions [n)]

Lehmann, A., U. Teschner, G. Mende, H. Sobotta: Infrarotspektroskopische Bestimmung herstellungsbedingter Strukturgrößen von SiO_2-Schichten [g)]

Manfraß, P.: Positronentomographie (Positronenkamera und Vieldrahtproportionalzähler). Kolloquium der Sektion Physik der Bergakademie Freiberg, 24.10.1985

Manfraß, P., W.D. Fromm, D. Wohlfahrt: Entwicklung einer Positronenkamera auf der Grundlage von Vieldrahtproportionaldetektoren. Arbeitstagung Anwendung MWPC, Dubna, 18.-20.6.1985

Manfraß, P., W.D. Fromm, D. Wohlfahrt: Positronenkamera mit Gasdetektoren. Seminar der Radiologischen Klinik, Universität Rostock, 21.11.1985

Matthies, S.: Einführung in Auswertung von ICOTOM 7 [a)]

Matthies, S.: ICOTOM-7, Reproduktionsmethoden [a)]

Matthies, S.: Zu einigen speziellen Fragestellungen der Reproduktionsaufgabe [a)]

Matz, W.: Neutronendiffraktion zur Untersuchung der Struktur amorpher Festkörper. Glasseminar MLU Halle, Sektion Physik, 13.2.1985

Matz, W.: Bestimmung partieller Strukturfaktoren amorpher Metalle mit Neutronendiffraktion [o)]

Matz, W., Structure Investigations of Amorphous Materials by Neutron Diffraction [l)]

Matz, W., U. Bärenwald, M. Dubiel, D. Ebert, U. Hoppe: Neutronendiffraktion an Fluorophosphatgläsern [o)]

Mende, G., C. Bauer, R. Grötzschel, C. Heiser, A. Hofmann, J. Finster, W. Rudolph: Untersuchungen zum Mechanismus der anodischen Silicium-Oxydation [u)]

Mende, G., C. Bauer, C. Heiser, W. Rudolph, A. Lehmann, U. Teschner: Über den Einfluß der Herstellungsbedingungen auf die Zusammensetzung von anodischem Oxid auf Silicium. 10. Arbeitstagung der Arbeitsgemeinschaft Elektrochemie der Chemischen Gesellschaft der DDR, Garzau, 25.-27.2.1985

Morgenstern, H.: Erzeugung tiefer Niveaus im Zusammenhang mit der Bildung von Schottky-Barrieren für DLTS-Messungen [g)]

Möller, K.: Off shell sensitivity of the capture reaction $n + p \rightarrow d + \gamma$ [p)]

Mösner, J., K. Möller, W. Pilz, G. Schmidt, T. Stiehler: A measurement of the total cross section of the capture reaction $^2H(n,t)\gamma$ at $E_n = 25$ MeV [p)]

Mücklich, A., K. Hennig: Untersuchungen zur magnetischen Textur in Fe-Ni-Basislegierungen [a)]

Mücklich, A., K. Hennig: On the magnetic texture of an Fe-Ni-base alloy [k)]

Müller, H.-J., K.-H. Heinig: Computersimulation der Phasentransformation a-Si in poly-Si in quasi-zweidimensionalen Strukturen [g)]

Müller, H.: Cluster excitation in hadron-nucleus collisions [d)]

Münchow, L.: Skyrmionen in der Kernphysik. Dubna, August 1985, LTF

Naehring, F.K.: Design of an Electrostatic Octupole for Micro Beam Deflection [c)]

Naehring, F.K., A. Kahn, A. Hoffmann: A Gallium Ion Micro Beam [c)]

Neubert, W.: Gaszähler für geladene Teilchen, Entwicklungstendenzen [b)]

Neumann, H., W. Hoyer, W. Matz, M. Wobst: Temperaturabhängigkeit der Struktur schmelzflüssiger eutektischer Germanium-Legierungen [o)]

Ortlepp, H.-G.: Das 4π-Spektrometer PHOBOS (in russ.) [d)]

Ortlepp, H.-G., C.M. Herbach, K. Merla, G. Musiol, G. Pausch: Identification of Associated Particles in the TCAPM Fission Cross Section Measurements at the Tandem Accelerator of the CINR Rossendorf [h)]

Panknin, D., J. Hüller, Chr. Weise, E. Wieser, C. Döring: Influence of short time annealing on the electrical activation of implanted GaAs [c)]

Panknin, D., J. Hüller, Chr. Weise, E. Wieser, C. Döring: Einfluß der Kurzzeitausheilung auf die Ladungsträgerprofile in implantiertem GaAs [g)]

Panknin, D., Chr. Weise: Ausheilung und Aktivierung von implantiertem GaAs durch Kurzzeitausheilung im Festphasenregime. 13. Herbstschule "Physik und Chemie der A^{III}-B^{V}-Halbleiter" der KMU Leipzig, Breitenstein, 18.-23.11.1985

Pfitzner, A.: Collective fluctuations and intrinsic equilibration [d)]

Pfitzner, A.: Equilibration on the one-body level - a consequence of mean-field fluctuations[d)]

Polzer, G., R. Dietrich, W. Rudolph, D. Grambole: Erkenntnisse zur Ermittlung der Wasserstoffverteilung in Reibflächenbereichen von Zylindergleitbuchsen mit Hilfe der Kernresonanzspektroskopie. Tribotechnik-Tagung, Ingenieurhochschule Zwickau, Dezember 1985

Posselt, M.; Influence of recoil atoms on energy-loss and damage profiles [q)]

Posselt, M.: A short overview on Monte Carlo simulations of ion beam penetration into amorphous solids [c)]

Posselt, M.: Effect of subcascades on energy-loss and damage profiles [c)]

Prade, H.: In-beam Investigations and Structure Studies of the Even-Mass N=82 Nuclei ^{138}Ba and ^{140}Ce. 23. Int. Winter Meeting on Nuclear Physics, Bormio, 21.-26.1.1985

Prade, H.: In-beam Investigations and Structure Studies of Semi-Magic Nuclei with N=82 and Z=50. Institutsseminar AFI Stockholm, 21.3.1985

Prade, H.: In-beam Investigations and Structure Studies of Semi-Magic Nuclei with N=82 or Z=50. Institutsseminar, Institut für Isotope Budapest, 3.10.1985

Prade, H., W. Enghardt, L. Käubler, H.U. Jäger, H.-J. Keller, L.K. Kostov, F. Stary: Nuclear Structure Studies of N=82 Isotones and Tin Isotopes [m)]

Prokert, F.: Neutronenstreuung an inkommensurablen Strukturen. 13. Frühjahrsschule Ferroelektrizität '85, Güntersberge, 18.-22.3.1985

Prokert, F., S.V. Misjul: Anticrossing of Disperson Branches and Exchange of Eigenvectors in the Elpasolite Type Crystal $Cs_2NaBiCl_6$ [r)]

Rauschenbach, B.: Temperature influence during high-fluence nitrogen implantation [q)]

Rauschenbach, B., C. Blochwitz: Fatigue of metalloid ion implanted nickel [c)]

Rauschenbach, B., K. Hohmuth: Investigations of ion implanted metals by high-voltage electron microscopy. Höchstspannungs-Elektronenmikroskopie-Symposium, Halle, 16.-19.4.1985

Rauschenbach, B., K. Hohmuth: Synthesis of compounds by high-fluence nitrogen ion implantation in titanium [c)]

Rauschenbach, B., K. Hohmuth, E. Richter, R. Grötzschel: Ion beam mixing of copper/gold multilayers [q)]

Rauschenbach, B., E. Richter, V. Heera, H. Reuther, K. Hohmuth: Effects by ion implantation into metallic materials [c)]

Reinhardt, H.: Differentialgeometrischer Zugang zur Dissipation. Berliner Seminar Theoretische Physik, Berlin, November 1984

Reinhardt, H.: Deconfinement phase transition in the non-topological soliton bag model. GSI Darmstadt, Januar 1985

Reinhardt, H.: Rotating quark bags. International Workshop, Hirschegg, Januar 1985

Reinhardt, H.: Skyrmions [b)]

Reinhardt, H.: Liquid-vapor phase transition in hot nuclear matter: Microscopic approach to nucleation. Triest Meeting "Phase space approach to Nuclear Dynamics", Oktober 1985

Reuther, H.: Mößbaueruntersuchungen an stickstoff- und phosphorimplantiertem Eisen. Mößbauerkolloquium der Physikalischen Gesellschaft der DDR, Freiberg, 7.-8.2.1985

Reuther, H.: Conversion electron mössbauer spectroscopy of nitrogen and phosphorus implanted iron. XX. Winterschule für Physik, Zakopane, 20.-26.4.1984

Reuther, H., E. Richter: CEMS studies of ion implanted iron [c)]

Reuther, H., E. Richter. Conversion electron mössbauer spectroscopy studies of ion implanted iron [s)]

Rotter, H.: Untersuchung von ^{84}Kr am U-120 [d)]

Rotter, I.: Kernstrukturrechnungen bei großer Niveaudichte. Dubna LTF, Sektoren 1 und 2, 13.12.1985

Rotter, I.: Many-body effects in the nuclear structure of finite nuclei. NIIYaF der MGU, Moskau, 3.10.1985

Rotter, I.: Many-body effects in the nuclear structure of finite nuclei [n)]

Roß, R.: Automatic controlled facilities for irradiation of silicon crystals in the Rossendorf Research Reactor. IAEA Consultants Meeting on Silicon Transmutation Doping Techniques and Practices, Otwock-Swierck, 20÷22.11.1985

Rudolph, W.: Hydrogen detection and depth profiling by nuclear resonance reactions [d)]

Rudolph, W., C. Bauer, K. Brankoff, D. Grambole, R. Grötzschel, C. Heiser, F. Herrmann: Hydrogen content calibration using plastic foils (Poster) [c)]

Rudolph, W., C. Bauer, C. Döring, D. Grambole, R. Grötzschel, C. Heiser, F. Herrmann, P. Urwank: Analysis of boron doped silicon oxide layers by means of He backscattering and prompt nuclear reactions (Poster) [1), g)], Herbstschule "Mikrosonde", Fincken, November 1985 and [c)]

Rudolph, W., C. Bauer, C. Döring, D. Grambole, R. Grötzschel, C. Heiser, F. Herrmann, P. Urwank: Characterization of dielectric layers by means of Rutherford backscattering and prompt nuclear reactions [c)]

Rudolph, W., C. Bauer, D. Grambole, R. Grötzschel, C. Heiser, F. Herrmann: Hydrogen Content Calibration using Plastic Foils (Poster) [q)]

Rudolph, W., C. Bauer, D. Grambole, C. Heiser, F. Herrmann: Hydrogen Detection by Means of the $^{1}H(^{15}N,\alpha\gamma)^{12}C$ Resonance Reaction (Poster) [1), g), c)]

Rudolph, W., C. Bauer, D. Grambole, C. Heiser, F. Herrmann: Hydrogen depth profiling using nuclear resonance reactions [c)]

Rudolph, W., K. Hennig, S. Niese: Nukleare Analytik an metallischen Werkstoffen. 5. Fachtagung "Elektrotechnologie", Magdeburg, August 1985

Schmidt, B.: Halbleiter-Kernstrahlungsdetektoren. Frühjahrsschule der Abt. Strahlenschutz des ZfK, Langenhennersdorf, 15.-19.4.1985

Schmidt, B.: Moderne Methoden bei der Herstellung von Halbleiterkernstrahlungsdetektoren. Tagung Halbleiterdetektoren, Dubna, 24.-26.9.1985

Schmidt, U., F. Eichhorn: Nachweis der Änderung intermetallischer Phasen in AlCu während der Glühbehandlung mittels Neutronen-KWS [t)]

Schubert, D., U. Lorenz: Sensitive Resistor and Diode Structures of polycrystalline Silicon. 10. IMEKO-World-Congress, Praha, April 1985

Schubert, D., U. Lorenz: Sensitive Eigenschaften polykristalliner und kristallisierter Siliziumschichten [g)]

Schulz, H.: Fragmentierung von Kernmaterie [b)]

Schulz, H.: Liquid-gas phase transition in nuclear matter, Workshop NBI Kopenhagen, April 1985

Schulz, H.: Niels Bohr und seine Bedeutung für die Kernphysik. Zentrale Veranstaltung der AdW der DDR und der Urania, Berlin, September 1985

Seidel, W.: Moderne Schwerionenexperimente bei mittleren Energien [b)]

Skorupa, W., U. Kreißig, H. Oertel, H. Bartsch: Eigenschaften epitaktischer Siliciumschichten auf vergrabenem Si_3N_4, hergestellt durch Ionenimplantation [g)]

Skorupa, W., U. Kreißig, H. Oertel, H. Bartsch: Properties of epitaxial silicon layers on buried silicon nitride produced by ion implantation [c)]

Sobeslavsky, E.: Modelluntersuchungen zur Stickstoff-Implantation in Silizium [u)]

Stary, F.: Untersuchung der Fragmentation von Kernsystemen mit Z=108 mit dem Spektrometer DEMAS (in russ.) [d)]

Stary, F.: Erprobung des Modells einer Bragg-Ionisationskammer für das Spektrometer PHOBOS (in russ.). 25. Sitzung des Komitees für Schwerionenphysik, Dubna, 9.-11.4.1985

Stiehler, T., B. Kühn, K. Möller, J. Mösner, W. Neubert, W. Pilz, G. Schmidt: A measurement of the capture reaction $H(p,d)_\gamma$ at E_n = 25 MeV [d)]

Tesch, S.: Moderne Experimente in der Hochenergiephysik [b)]

Urwank, P., C. Bauer, C. Heiser, W. Rudolph: Boron depth profiling by the $^{11}B(d, \alpha_0)^9Be$ reaction [q)]

Vlad, C.M., G. Arndt, M. Betzl: Microstructures-mechanical Properties Trade-offs in Dual-phase Steels Processed directly off Rolling Mill [l)]

Voelskow, M., J. Matthäi, D. Schubert, T. Uhlig: Kurzzeittemperung und laterales Zonenschmelzen von LPCVD-Poly-Si-Schichten - Eigenschaften der Schichten und darin hergestellter Widerstandsstrukturen [v)]

Voelskow, M., J. Matthäi, A. Wolf, C. Höppner, K.H. Stegemann, D. Gerisch: Ein Verfahren zur Herstellung korngrenzenfreier Siliziumstreifen auf isolierendem Substrat [g)]

Voelskow, M.; J. Matthäi, A. Wolf, W. Scharff, K.H. Stegemann, D. Gerisch: Method of producing grain boundary free silicon stripes on insulating substrates [c)]

Voelskow, M., D. Schubert, S. Mutze, W. Jenschke: Structural and sensitive properties of piezoresistive elements prepared in silicon films recrystallized by zone melting [c)]

Voitus, W., F. Eichhorn: Neutronenkleinwinkelstreuung an Nickelbasislegierungen [o)]

Wieser, E.: Überblick über Grundlagen und Verfahren der Kurzzeittemperung und ihre Anwendung zur Silicidbildung [v)]

Winter, G.: Kernspektroskopie in Rossendorf [d)]

Wolf, A., K. Höppner, W. Scharff, M. Voelskow, J. Matthäi: Charakterisierung von mikrozonengeschmolzenem Silicium auf SiO_2 [g)]

Wünsch, R.: Decay of light hypernuclei by baryon emission [n)]

a) Internationale Winterschule Neutronenstreuung - Quantitative Texturanalyse, Stadt Wehlen, 28.1.-1.2.1985

b) Winterschule Kernphysik, Hörnitz bei Zittau, 1.-4.4.1985

c) Working Meeting on Ion Implantation in Semiconductors and Other Materials and Ion Beam Devices, Balatonaliga, 13.-18.10.1985

d) Kiev-Řez-Rossendorf-Krakov-Seminar, Kiev, 26.-30.3.1985

e) Int. Arbeitstagung Halbleiterdetektoren, Dubna, September 1985

f) 35. Allunionskonferenz über Kernspektroskopie und Struktur des Atomkerns, Leningrad, 15.-19.4.1985

g) 9. Tagung Physik und Elektronik, Berlin, 22.-25.10.1985

h) XV. Int. Symp. Fission and Nuclear Physics, Gaußig, 11.-15.11.1985

i) Int. Winter School on Laser Assisted Modification and Synthesis of Materials, Gyuletchitza, 10.-17.3.1985

j) 3. Tagung Irreversible Prozesse und dissipative Strukturen, Kühlungsborn, 18.-22.3.1985

k) 12. Hungarian Diffraction Conference, Sopron, 20.-24.8.1985

l) VI. Int. Symposium Hochreine Materialien in Wissenschaft und Technologie, Dresden, 6.-10.5.1985

m) 7th Europhysics Study Conference - Synthesis and Structure of Exotic Nuclei and Atoms, Albena, 15.-19.9.1985

n) III. Int. Symp. on Mesons an Light Nuclei, Bechyne, 27.5. - 1.6.1985

o) 19. Jahrestagung der VfK, Rostock, 23.-26.4.1985

p) X. European Symp. on the Dynamics of Few Body Systems, Balatonfüred, 3.-7.6.1985

q) 7th Int. Conf. Ion Beam Analysis, Berlin(West), 7.-12.7.1985

r) IUPAP-Conference "Phonon '85", Budapest, 26.-30.8.1985

s) IMJON 85, Jablonna, 28.-29.11.1985

t) Berg- und Hüttenmännischer Tag 1985, Freiberg, 11.-14.6.1985

u) 7. Herbstschule Isolatorphysik für die Mikro- und Optoelektronik, Ahrenshop, 7.-10.12.1985

v) Problemseminar "Passive elektronische Bauelemente", Karl Marx-Stadt, 3.-7.6.1985

VERANSTALTUNGEN

Internationale Winterschule Neutronenstreuung - Quantitative Texturanalyse, Stadt Wehlen, 28.1. - 1.2.1985

Winterschule Kernphysik, Hornitz bei Zittau, 1.4. - 4.4.1985

WISSENSCHAFTLICHE PREISE

Gustav-Hertz-Preis der Physikalischen Gesellschaft der DDR, Februar 1985
E. Wieser, R. Klabes, K.-H. Heinig, H. Woittennek

Magnus-Preis der Sektion Physik der Humboldt-Universität zu Berlin, November 1985
H.-J. Müller

Hervorragendes Neuererkollektiv der AdW für das Jahr 1985, Berlin, 13.9.1985
W. Boede, P. Reichel

Bereichspreis Kategorie I, 1. Preis 1985
H.W. Barz, B. Kämpfer: Theoretische Untersuchungen zur Anregung von Quarkfreiheitsgraden in relativistischen Schwerionenkollisionen

Bereichspreis Kategorie I, 2. Preis 1985
P. Gippner, K.D. Schilling, W. Seidel, F. Stary, E. Will, H. Sodan, G.G. Chubarian, S.M. Lukyanov und Yu.E. Penionzhkevich: Die Untersuchung der Fragmentierung schwerer Stoßsysteme mit Z_{SUM} = 108 mit Hilfe des Doppelarm-Flugzeitspektrometers DEMAS

Bereichspreis Kategorie I, 2. Preis 1985
J. Döring, L. Funke, P. Kemnitz, H. Rotter, G. Winter, E. Will, L. Käubler, P. Kleinwächter, H. Prade und R. Schwengner: Zwei- und Vierquasiteilchen-Anregungen im ^{82}Kr und ^{84}Kr

Bereichspreis Kategorie II, 1. Preis 1985
F. Schwarzenberg: Hard- und Software-Ergänzungen für den Heimcomputer Z 9001

Bereichspreis Kategorie II, 1. Preis 1985
B. Rauschenbach, E. Richter, C. Blochwitz: Ermüdung und Verschleiß implantierter Metalle mit Metallionen

Bereichspreis Kategorie III, 2. Preis 1985
W. Neubert: Bragg-Kurven-Spektroskopie von Spaltfragmenten mit Parallelplatten-Lawinenzählern

Bereichspreis Kategorie IV, 1985
M. Posselt: Der Einfluß der Rückstoßatome auf Energieverlust- und Schadensprofile

ZENTRALINSTITUT FÜR KERNFORSCHUNG, ROSSENDORF, BEREICH G

VERÖFFENTLICHUNGEN

Bogomolov, S.L., J. Dietrich, V.B. Kutner: Untersuchung des ionenoptischen Systems einer Zyklotronionenquelle, Preprint 9-85-432, VIK Dubna (1985)

Dietrich, J., G. Kerber, H. Odrich, W. Naumann:

A Multicharged Lithium Penning Ion Source for the Cyclotron. Nucl. Instrum. Methods A241 (1985) 596

Dietrich, J., G. Kerber, W. Naumann, H. Odrich: Ionenquelle für einen Beschleuniger. DDR-Patent, WP H05H/275 765 4

Dietrich, J., G. Kerber, W. Naumann, H. Odrich: Ionenquelle mit direkter Heizung für einen Beschleuniger. DDR-Patent, WP H05H/275 764 6

Friedrich, M., R. Günzel, A.Z. Kiss, E. Koltay, J. Felszervalvi: Bremsstrahlung Measurements with Collimated Thermoluminescent Dosimeters around a Tandem Accelerator. Nucl. Instrum. Methods A234 (1985) 1

Friedrich, M., W. Vogel: Verfahren zur Materialbestrahlung mit energiereichen Teilchen. DDR-Patent, WP G21K/274 032 4

Friedrich, M., S. Turuc: Extraktionssystem für eine Hochfrequenz-Ionenquelle. DDR-Patent, WP H01J/281 488 1

Hiekmann, S., R. Fülle: Anwendung der Displaytechnik bei der manuellen Prozeßführung. msr 9 (1985) 402

VORTRÄGE, DIE AUSSERHALB DES EIGENEN KOLLEKTIVS GEHALTEN WURDEN

Beyer, G.-J., M. Böttger, K. Eichhorn, H. Guratzsch, H. Kupsch, K. Regel, G. Winter: Die Anwendung des Rossendorfer Zyklotrons U-120 in Wissenschaft, Medizin und Technik (in russ.). Int. Conf. on Cyclotron and their Applications, Bechine, CSSR, 25. - 28.6.1985

Beyer, G.-J., R. Brückner, H. Guratzsch, K. Schomäcker, J. Steinbach: Die Produktion von Radionukliden mit dem Zyklotron U-120 des ZfK (in russ.). Int. Conf. on Cyclotron and their Applications, Bechine, CSSR, 25. - 28.6.1985

Beyer, G.-J., M. Böttger, K. Eichhorn, H. Guratzsch, H. Kupsch, K. Regel, G. Winter: Using of the Rossendorf Cyclotron U-120 in Science and Technology. Third Working Meeting on Radioisotopes Application and Radiation Processing in Industry. Leipzig, GDR, 23. - 27.9.1985

Dietrich, J., H. Odrich, G. Kerber, W. Naumann: Lithium Ion Sources for the Rossendorf Cyclotron U-120. Int. Conf. on Cyclotrons and their Applications, Bechine, CSSR, 25. - 28.6.1985

Friedrich, M.: Erfahrungen beim Einsatz verschiedener Fokussiersysteme an einer HF-Ionenquelle. Seminar des WB Angewandte Kernphysik, KMU Leipzig, 21.5.1985

Fülle, R., S. Hiekmann, W. Schmiedel: Lokaler Rechnerverband des ZfK. Arbeitsseminar der Kooperationsgemeinschaft EC 1055 der AdW, Silz, 12. - 15.3.1985

Hennig, K., H. Matthes, W. Pfestorf: Die Sputterquelle MISS-483. Konferenz "Energiereiche atomare Stöße", Oberstdorf, 1985

Linnemann, W.-J.: Rechnerkommunikation in einem verteilten Prozessrechnersystem. 18. Fachkolloqium Informationtechnik der TU Dresden, Dresden, 19. - 21.2.1985

Lück, H.B., G. Heinrich, R. Kirchbach, H. Matthes, W. Pfestorf, M. Seidel: Stand der Arbeiten zur Herstellung von Kernspurmikrofiltern im ZfK Rossendorf. Konferenz "Anwendung von Kernspurfiltern für die Lösung wissenschaftlich-technischer und volkswirtschaftlicher Aufgaben", Dubna, 16. - 18.10.1985

PROMOTIONEN A (Dr.-Ing.)

Hentschel, R.: Ionenoptische Berechnung des Niederenergiebereiches elektrostatischer Beschleuniger und seine zweckmäßige Gestaltung durch den Einsatz von Metallnetzen. AdW der DDR, Mai 1985

VERANSTALTUNGEN

XII. Frühjahrsschule für Beschleunigungstechnik, Neuschmölln, 4. - 8.3.1985

TECHNISCHE UNIVERSITÄT DRESDEN, SEKTION PHYSIK, WB THEORETISCHE PHYSIK

VERÖFFENTLICHUNGEN

Höhn, J., R. Reif: Ionenstrahlen in der Kernenergetik (Fortschrittsbericht) Kernenergie 28 (1985) 1

Milek, B., R. Reif, J. Revai: Three-body model for nucleon transfer and emission in heavy-ion collision. Phys. Lett. 150B (1985) 294

Guzman, F., R. Reif: Incomplete deep-inelastic heavy-ion collisions. Nucl. Phys. A436 (1985) 294

Schmidt, R.: Mass transport and energy equilibration in heavy-ion collisions. Z. Physik A320 (1985) 413

Milek, B., R. Reif: Nuclear Landau-Zener effect in $^{13}C + ^{17}O$? . Phys. Lett. 157B (1985) 134

Mädler, P.: Catapult mechanism for fast particle emission in fission and heavy-ion reactions. Z. Phys. A321 (1985) 343

Schmidt, R.: Nucleon exchange during a heavy-ion collision. Nucl. Phys. A445 (1985) 534

DIPLOMARBEITEN

Gleitsmann, T.: Mikroskopische und phänomenologische Untersuchungen zum Massentransfer in Schwerionenreaktionen

VORTRÄGE

Milek, B.: Zwei-Zentren-Schalenmodell, Frühjahrsschule des ZfK Rossendorf, Hörnitz, April 1985

Milek, B.: Elementary excitations in heavy-ion collisions, XVII. Masurische Sommerschule, Mikolajki, September 1985

Milek, B.: Landau-Zener effect and particle emission from Gamow states, VIK Dubna, Oktober 1985

Schmidt, R.: Energy and mass equilibration in heavy-ion collisions, XVII. Masurische Sommerschule, Mikolajki, September 1985

Schmidt, R.: "Fast fission" - the mass equilibration mode for very asymmetric heavy-ion collisions, VIK Dubna, Oktober 1985

Mädler, P.: Catapult mechanism for fast particle emission, XV. International Symposium on Nuclear Physics, Gaussig, November 1985

Reif, R.: Particle emission in large amplitude collective motion, XV. International Symposium on Nuclear Physics, Gaussig, November 1985

Mädler, P.: Schwerionenstöße bei mittleren Einschußenergien, Frühjahrsschule des ZfK Rossendorf, Hörnitz, April 1985

TECHNISCHE UNIVERSITÄT DRESDEN, SEKTION PHYSIK, WB KERNPHYSIK

VERÖFFENTLICHUNGEN

Adel-Fawzy, M., Förtsch, H., Schmidt, D., Seeliger, D. and Streil, T.: Tendency of direct excitation by neutron scattering at bombarding energies below 15 MeV on light nuclei, INDC(GDR)-34/GI, Vienna (1985) 23

Albert, A., Hansen, W., Reiche, Ch., Vogel, W., Elfruth, T., Seeliger, D., Seidel, K., Streubel, G., Unholzer, S.: Measurement of neutron leakage spectra from a lead sphere fed with 14 MeV neutrons, XIV-th Int. Symp. on the Interaction of Fast Neutrons with Nuclei - Neutron Generators and Application - Gaußig 1984, ZfK-562 (1985) 85

Dietrich, J., Jahn, U.: Extraction-process calculation for a duoplasmatron ion source XIV-th Int. Symp. on the Interaction of Fast Neutrons with Nuclei -Neutron Generators and Application-, Gaußig 1984, ZfK-562 (1985) 50

Eckstein, P., Gleisberg, F., Helfer, H., Krause, R., Jahn, U., Paffrath, E., Schmidt, D., Seeliger, D.: Design of a multi-purpose intense neutron generator, XIV-th Int. Symp. on the Interaction of Fast Neutrons with Nuclei -Neutron Generators and Application-, Gaußig 1984, ZfK-562 (1985) 24

Eckstein, P., Gleisberg, F., Krause, R., Schwierz, R., Schmidt, D., Seeliger, D., Computer control of the neutron generator INGE-1, XIV-th Int. Symp. on the Interaction of Fast Neutrons with Nuclei -Neutron Generators and Application-, Gaußig 1984, (1985) 63

Elfruth, T., Grimm, W., Loska, L., Pöthig, J., Seidel, K., Unholzer, S.: Data processing of differential neutron emission spectra from Pb and C, INDC(GDR)-34/GI, Vienna (1985) 15

Elfruth, T., Loska, L., Pöthig, J., Seeliger, D., Seidel, K., Unholzer, S.: A 14 MeV time-of-flight spectrometer for precise determination of angular dependences and measurement of neutron emission spectra from Pb and C, INDC(GDR)-34/GI, Vienna(1985)14

Elfruth, T., Hermsdorf, D., Kalka, H., Seeliger, D., Seidel, K., Unholzer, S.: Measurement of double-differential neutron emission cross sections from lead bombarded with 14 MeV neutrons, XIV-th Int. Symp. on the Interaction of Fast Neutrons with Nuclei -Neutron Generators and Application-, Gaußig 1984, ZfK-562 (1985) 110

Helfer, H., Hildebrandt, B., Seifert, A.: An evaluation of neutron yields from thick titanium-tritium-targets under deuteron bombardement, XIV-th Int. Symposium on the Interaction of Fast Neutrons with Nuclei -Neutron Generators and Application- Gaußig 1984, ZfK-562 (1985) 71

Helfer, H., Loska, L., Seidel, K., Unholzer, S.: Pulsing system of a 14 MeV neutron generator for time-of-flight spectroscopy, INDC(GDR)-34/GI, Vienna (1985) 13

Hermsdorf, D.,: Complexity of angular dependence of scattered fast neutrons - consequences and recommendations for measurement and application of data, XIV-th Int. Symp. on the Interaction of Fast Neutrons with Nuclei -Neutron Generators and Application- Gaußig 1984, ZfK-562 (1985) 113

Hermsdorf, D., Kalka, H., Seeliger, D.: On phenomenological calculations of continuous particle spectra by GEM and DI, INDC(GDR)-34/GI, Vienna (1985) 117

Jahn, U., Dietrich, J.: Ionoptical calculations of the intense neutron generator INGE-1 XIV-th Int. Symp. on the Interaction of Fast Neutrons with Nuclei -Neutron Generators and Application-, Gaußig 1984, ZfK-562 (1985) 46

Köhler, M., Meiling, W.: Einfacher mikrorechnergesteuerter Vielkanalysator, Materialien zum 18. Fachkolloquium Informationstechnik, TU Dresden, 19.-21.3.1985, (1985) 19

Märten, H., Neumann, D., Seeliger, D.: The use of a ^{252}Cf source for neutron detector calibration INDC(GDR)-34/GI, Vienna (1985) 21

Meiling, W.: Serielle Interfaces für Meßgerätekopplung, Mikroelektronik in Österreich, Berichte von der Informationstagung ME 85, Springer-Verlag, Wien, New York (1985) 256

Mittag, S., Pabst, D., Pikelner, L.B., Pilz, W., Tschammer, R., Meister, A., Seeliger, D. Seidel, K.: Chemically induced shifts of 235-U and 234-U neutron resonances, Nuclear Physics A 435 (1985) 97

Paffrath, E., Jahn, U., Schmidt, D.: The vacuum system of the intense neutron generator INGE-1, XIV-th Int. Symp. on the Interaction of Fast Neutrons with Nuclei -Neutron Generators and Application-, Gaußig 1984, ZfK-562 (1985) 59

Tunia, A., Jahn, U., Paffrath, E.: Experimental investigations of duoplasmatron ion source, XIV-th Int. Symp. on the Interaction of Fast Neutrons with Nuclei -Neutron Generators and Application-, Gaußig 1984, ZfK-562 (1985) 52

Jahn, U., Paffrath, E., Schmidt, D. and Seeliger, D.: Intensive Neutronengeneratoren auf der Basis der DT-Reaktion, Kernenergie 28 (1985) 433

DIPLOMARBEITEN

Boubakar, Barry: Kopplung des Mikrorechners MPS 4944 mit dem Vielkanalanalysator PHA 256 über ein serielles Interface

Birner, Henry: Theoretische Beschreibung und Darstellung der Energie- und Winkelabhängigkeit der inelastischen Streuung schneller Neutronen

Bookhagen, Jens: Beiträge zur Entwicklung einer gepulsten Penning-Hohlkathoden-Ionenquelle

Hartmann, Holger: Beiträge zur Übertragungstechnik von Meß- und Steuersignalen für die on-line Steuerung einer Ionenstrahlapparatur

Hehl, Torsten: Steuerprogramm für ein Flugzeitspektrometer zur Messung von Neutronenemissionsquerschnitten in der Interpretersprache BASIC

Seifert, Anne: Optimierung von Ionenquellen mit dem SLAC Electron Optics Program

Tiedt, A.: Entwicklung und Aufbau eines Gerätesystems zur Meßwerterfassung und Steuersignalausgabe mittels Mikrorechner

PROMOTIONEN A (Dr. rer. nat.)

Mittag, S.: Beiträge zur Untersuchung der chemischen und der temperaturbedingten Verschiebung von Neutronenresonanzen, TU Dresden, 13. 12. 1985

Randrianarisoa, Edmond: Programmsystem rechnergestützter Messungen von Neutronenstreuquerschnitten, TU Dresden, 13. 06. 1985

PROMOTIONEN B (Dr. sc. nat.)

Pilz, W.: Untersuchung der Ladungsverteilung hochangeregter spaltender Kernzustände und einiger Probleme der Wechselwirkung von Resonanzneutronen mit kristallinen Festkörpern und Gasen mit Hilfe der Neutronenresonanzspektroskopie, TU Dresden, 13. 12. 1985

Schmidt, D.: Spektrometrie schneller Neutronen zur Untersuchung des Reaktionsmechanismus bei Anregung von Kernzuständen unterschiedlicher Komplexität, TU Dresden, 21. 11. 1985

VORTRÄGE, DIE AUSSERHALB DES EIGENEN KOLLEKTIVS GEHALTEN WURDEN

Böttger, R., Fromm, W.D., Klein, H., Märten, H., Richter, D., Seeliger, D.: The Cf-252(sf) Neutron Spectrum in the High-Energy Range, Int. Conf. on Nucl. Data for Basic and Appl. Science, Santa Fe, 1985

Eckstein, P., Gleisberg, F., Jahn, U., Krause, R., Paffrath, E., Schmidt, D., Schwierz, R. Seeliger, D., Glotov, A.I., Romanov, V.A.: Intense Neutron Generator Project at the TUD, IV. Int. Symp. on Neutron Induced Reactions, Smolenice (CSSR), Juni 1985

Hermsdorf, D.: Einige neue Aspekte der Struktur und Nutzung von Kerndatenbibliotheken, Winterschule des Bereiches RP des ZfK Rossendorf, Hornitz, 21.-25.10.1985

Ignatovich, V.K., Meister, A., Mittag, S., Pilz, W., Seeliger, D., Seidel, K.: Temperature Shift of Neutron Resonances, IV. Int. Symp. on Neutron Induced Reactions, Smolenice (CSSR), Juni 1985

Ignatovich, V.K., Meister, A., Mittag, S., Pilz, W., Seeliger, D., Seidel, K.: Temperature Shift of Neutron Resonances, XV. Int. Symp. on Nuclear Physics - Nuclear Fission, Gaußig (1985)

Kalka, H., Hermsdorf, D., Seeliger, D.: Excitonmodel and Multistep-Compound Reactions, IV. Int. Symp. on Neutron Induced Reactions, Smolenice (CSSR) Juni 1985

Köhler, M., Meiling, W.: Einfacher mikrorechnergesteuerter Vielkanalanalysator, 18. Fachkolloquium Informationstechnik zu Problemen der Nachrichten- und Rechentechnik, TU Dresden, 19.-21.2.1985

Köhler, M. and Meiling, W.: A low-cost Multichannel Pulse-Height Analyzer PHA 256 Using Single-Chip Microcomputer, Int. Symp. für Kernelektronik, Dubna, Juli 1985

Märten, H., Seeliger, D.: Investigation of the 252 Cf spontaneous fission neutron spectrum, IV. Int. Symp. on Neutron Induced Reactions, Smolenice (CSSR), Juni 1985

Märten, H., Richter, D., Seeliger, D., Fromm, W.D., Neubert, D.: Differential Study of 252-Cf(sf) Neutron Emission, IV. Int. Conf. on Neutron Induced Reactions, Smolenice (CSSR) Juni 1985

Märten, H., Richter, D., Seeliger, D., Fromm, W.D., Neubert, W.: Experimental Arrangement for the Measurement of Correlations Between Fission Products and Neutrons, XV. Int. Symp. on Nuclear Physics - Nuclear Fission, Gaußig (1985)

Märten, H., Richter, D., Seeliger, D., Neubert, W.: On the Mechanism of Fission Neutron Emission, XV. Int. Symposium on Nuclear Physics - Nuclear Fission, Gaußig (1985)

Meiling, W.: Serielle Interfaces für Meßgerätekopplung, Mikroelektronik in Österreich, Berichte von der Informationstagung ME 85, 1985

Meiling, W., Krause, R.: Applicability of Serial Multi-Master Bus Systems to Scientific Instrumentation, Int. Symp. für Kernelektronik, Dubna, Juli 1985

Meiling, W., Krause, R.: Implementation of Serial Multi-Master Bus Controller Using Single-Chip Microcomputer, XV. Int. Symp. on Nuclear Physics - Nuclear Fission, Gaußig (1985)

Meister, A., Mittag, S., Pikelner, L.W., Pilz, W., Seeliger, D., Seidel, K.: Chemically Shifts of Uranium Neutron Resonances, IV. Int. Conf. on Neutron Induced Reactions, Smolenice (CSSR) Juni 1985

Meister, A., Mittag, S., Pikelner, L.B., Pilz, W., Seeliger, D., Seidel, K.: Measurement of the Mean-Square Charge Radii of Neutron Resonance States in Uranium Nuclei, XV. Int. Symp. on Nuclear Physics - Nuclear Fission, Gaußig (1985)

Meiling, W., Krause, R.: Multimasterfähige serielle Busse zur Kopplung von Moduln und Geräten, Votrag auf KDT-Jahrestagung "Mikrorechentechnik" Dresden, Dezember 1985

VERANSTALTUNGEN

XV. Intern. Symposium on Nuclear Physics - Nuclear Fission -, Gaußig, 11. - 15. November 1985

TECHNISCHE UNIVERSITÄT DRESDEN, SEKTION PHYSIK, WB ANGEWANDTE KERNPHYSIK

VERÖFFENTLICHUNGEN

Arlt,R.; Herbach,C.M.; Josch,M.; Musiol,G.; Ortlepp,H.-G.; Pausch,G.; Wagner,W.; Drapchinsky,L.V.; Ganza,E.A.; Kostochin,O.I.; Kovalenko,S.S.; Shpakov,V.I.: Absolute measurement of the U-235 fission cross-section at 4.45 MeV neutron energy using the TCPM, TU-Preprint 05-04-085

Arlt,R.; Bohne,H.; Herbach,C.M.; Josch,M.; Musiol,G.; Ortlepp,H.-G.; Pausch,G.; Wagner,W.; Alkhazov,L.D.; Drapchinsky,L.V.; Fomichev,A.V.; Kostochkin,O.I.; Shpakov,V.I.: Absolute fission cross-section at 14.7 MeV, 4.5 MeV and 18.8 MeV neutron energies, Techniques of measurements, analysis and instrumentation for 14 MeV neutron nuclear cross-sections INDC (GDR)-34/GI, p. 25

Arlt,R.; Herbach,C.M.; Josch,M.; Musiol,G.; Ortlepp,H.-G.; Pausch,G.; Wagner,W.; Drapchinsky,L.V.; Ganza,E.A.; Kostochkin,O.I.; Kovalenko,S.S.; Shpakov,V.I.: Absolute measurement of the U-235 fission cross-section at 4.45 MeV neutron energy using the TCAPM, Proc. of an Advisory Group Meeting on Nuclear Standard Reference Data, Geel, Belgium, 1984 IAEA-TECDOC-335 (1985), p. 174

Bischoff,L.; Irmer,K.; Zschornack,G.: Sensoren aus neutronendotierten Silizium als Kernstrahlungssensoren für Industrieroboter, Isotopenpraxis 21 (1985) 10, S. 347-351

Herbach,C.M.; Merla,K.; Musiol,G.; Ortlepp,H.-G.; Pausch,G.; Alkhazov,I.B.; Drapchinsky,L.V. Ganza,E.A.; Kovalenko,S.S.; Kostochkin,O.I.; Solovjev,S.M.; Shpakov,V.I.: Absolute measurements of the Pu-239 fission cross-section at 4.8, 8.65 and 18.8 MeV neutron energy using the TCPM, TU-Preprint 05-06-85

Herbach,C.M.; Josch,M.; Merla,K.; Musiol,G.; Ortlepp,H.-G.; Pausch,G.; Alkhazov,I.D.; Drapchinsky,L.V.; Ganza,E.A.; Kostochkin,O.I.; Kovalenko,S.S.; Shpakov,V.I.: Absolute fast neutron fission cross-section measurements of 235-U and 239-Pu using the time correlated associated method, TU-Preprint 05-05-85

Herbach,C.M.; Josch,M.; Merla,K.; Musiol,G.; Ortlepp,H.G.; Drapchinsky,L.V.; Ganza,E.A.; Kovalenko,S.S.; Kostochkin,O.I.; Shpakov,V.I.: Absolute measurements of the 235-U fission cross-section at 4.45 and 18.8 MeV neutron energy using the TCAPM, TU-Preprint 05-07-85

Irmer,K.; Musiol,G.; Kovalenko,S.S.; Petrazak,K.A.: Anwendung der Methode der zeitlich korrelierten assoziierten Teilchen (MEZKAT), Isotopenpraxis 21 (1985) 10, S. 344-346

Jugelt,P.; Bergter,J.; Heckel,J.; Kästner,D.; Klinger,P.; Musiol,G.; Ortlepp,H.-G.; Schiekel,M.; Scholz,W.; Zschornack,G.: Entwicklung eines Systems für die Stoffanalyse und Auflagendickenbestimmung, G4-Abschlußbericht TU Dresden, Sektion Physik (Oktober 1985)

Kreiseler,D.; Karrasch,G.; Wagner,W.; Musiol,G.; Zschornack,G.: Die Steuerung eines Farbdisplays mit Mikrorechner in der Konfiguration eines Kristalldiffraktionsspektrometers Preprint VIK, P10-85-244, Dubna, 1985

Karrasch,G.; Kreiseler,D.; Schulze,W.; Wagner,W.; Musiol,G.; Zschornack,G.: Ein rechnergestütztes fokussierendes Bragg-Kristalldiffraktionsspektrometer für die Röntgendiagnostik, EAS-6, Kassel, 1985 S. 189-190

Ortlepp,H.-G.; Pausch,G.: Application of the time-correlated associated particle method (TCAPM) to absolute fission cross-section measurements, Techniques of measurements, analysis and instrumentation for 14 MeV neutron nuclear cross-sections, INDC (GDR)-34/GI, p. 27

Reichmann,A.; Zschornack,G.; Wagner,W.: Wahrscheinlichkeitstheoretische Beschreibung von Geometrieeinflüssen auf die Parameter von Bragg-Kristalldiffraktionsspektrometern, EAS-6, Kassel, 1985 S. 191-194

Wagner,W.; Dunin,W.B.; Karrasch,G.; Kreiseler,D.; Nevskaya,N.A.; Zschornack,G.; Schulze,W.: Ein Kristalldiffraktionsspektrometer in Johansson-Geometrie, VIK-Kurzmitteilung, Nr. 6-85, S. 46-51

Zschornack,G.; Musiol,G.; Wagner,W.: Röntgenspektroskopie hochionisierter Schwerionen Teil I: Spektroskopie von Schwerionenquellen, TU-Preprint 05-01-85, Dresden 1985

Zschornack,G.; Karrasch,G.; Kreiseler,D.; Musiol,G.; Müller,G.; Schulze,W.; Wagner,W.: Röntgenspektroskopie hochionisierter Schwerionen Teil II: Apparative Entwicklungen, TU-Preprint 05-02-85, Dresden, 1985

VORTRÄGE, DIE AUSSERHALB DES EIGENEN KOLLEKTIVS GEHALTEN WURDEN

Autorenkollektiv, Mitglieder des Jugendobjektes, Seminargruppe 83/05/03: Sozialistische Rationalisierung - Beiträge der Studenten und jungen Wissenschaftler der TUD zur Durchsetzung der ökonomischen Strategie, Konferenzunterlagen der Zentralen Wissenschaftl. Studentenkonferenz Sozialistische Rationalisierung an der TUD, 10.-11.10.85 in Dresden, S. 4-11

Baumann,U.; Bischoff,L.; Kohlmetz,J.: Einfluß der Strahlungsfluenz auf die Eigenschaften von Halbleiterdetektoren, Konferenzunterlagen der Zentralen Wissenschaftl. Studentenkonferenz Sozialistische Rationalisierung an der TUD, 10.-11.10.85 in Dresden, S. 173

Bergter,J.: Computer-Controlled Colour Display for the Energy - Dispersive X-Ray Spectrometer EDR 183, Internationales Symposium "Kernphysikalische Meßtechnik", VIK Dubna 2.7.1985

Bergter,J.: Digitalteil des Spektrometers EDR 288, 4. Tagung d. Zentr. Arbeitstagung "Energiedispersive Röntgenspektrometrie" 11.-12.4.85 in Strausberg

Eggert,F.; Metz,A.; Mitzkat,G.; Scholz,W.: Die quantitative Software des energiedispersiven Röntgenspektrometers EDR-184 zur on-line-Auswertung der gemessenen Spektren für die Elektronenstrahl-Mikroanalyse (ESMA), COMPANA'85 3. Tagung "Computereinsatz in der Analytik", 9.-12. Sept. 85 in Jena, S. 38

Heinrich,B.; Irmer,K.; Pötschke,R.: Fast analysis of carbon content by inelastic scattering of neutrons, Tagung über Industrieanwendung von Isotopen-und Strahlenmethoden in Leipzig, Sept. 85

Herbach,C.M.; Merla,K.; Musiol,G.; Ortlepp,H.-G.; Pausch,G.; Alkhazov,I.L.; Drapchinsky, L.V.; Ganza,E.A.; Kovalenko,S.S.; Solovjev,S.M.; Shpakov,V.I.: Absolute fission cross-section measurement of Pu-239 at 4.8, 8.65 and 18.8 MeV and of U-235 at 4.45 and 18.8 MeV neutron energy, XV. Internat. Symposium on Nucl. Phys. "Nuclear Fission" Gaussig, GDR, Nov. 1985

Hartmann,F.; Zeuner,A.: Funktionale Auswertung radiometrischer Verweilzeitbestimmungen an Trommeltrocknern. 9. IBAUSIL 1985, Weimar 17.-21. Juni 1985, Weimar, Tagungsbericht

Herrmann,Ch.; Jugelt,P.; Kästner,D.; Scholz,W.: WIPHA - ein Programmsystem für die Analyse linienreicher Spektren in der Röntgendiffraktometrie, COMPANA'85, 3. Tagung "Computereinsatz in der Analytik", 9.-12. Sept. 85 in Jena, S. 29

Herzberg,H.; Jugelt,P.; Kästner,D.; Schiekel,M.: Dialogführung beim energiedispersiven Röntgenspektrometer EDR 183 und ihre arbeitspsychologische Bewertung COMPANA'85, 3. Tagung "Computereinsatz in der Analytik", 9.-12. Sept. 85 in Jena, S. 34

Jugelt,P.; Schiekel,M.: Einsatz energiedispersiver Röntgenspektrometer in der Stoff- und Strukturanalyse, Tagung über Industrieanwendungen von Isotopen- und Strahlenmethoden in Leipzig, Sept. 85

Jugelt,P.; Pohlers,A.; Streil,H.; Herms,G.: Experimentelle Trennung inkohärenter Streuanteile in der WDRD am Beispiel eines Kieselglases, XIX. Jahrestagung d. VFK, Rostock, 23.-26.4.85

John,D.; Kambach,Chr.; Langer,M.: Ein Programm zur quantitativen Röntgenanalyse an Stahlproben, COMPANA'85, 3. Tagung Computereinsatz in der Analytik 9.-12.Sept.85 in Jena, S. 35

Kreiseler,D.; Kerrasch,G.; Zschornack,G.: "Ein Programmsystem zur Darstellung und Bearbeitung von Diffraktionsspektren mit Hilfe eines Mikrorechners INTEL 8080 im on-line-Betrieb", COMPANA'85; 3. Tagung "Computereinsatz in der Analytik", 9.-12.Sept.1985, Jena, S. 30

Ortlepp,H.-G.; Herbach,C.M.; Merla,K.; Musiol,G.; Pausch,G.: Identification of associated particles in the TCAPM fission cross-section measurements at the tandem accelerator of the CINR Rossendorf, XV. Internat. Symposium on Nucl. Phys. "Nuclear Fission", Gaussig, GDR, Nov. 1985

Pausch,G.; Fromm,W.D.; Herbach,C.M.; Merla,K.; Musiol,G.; Ortlepp,H.-G.: CAMAC data acquisition system and data analysis in TCAPM fission cross-section measurements at the tandem accelerator of the CINR Rossendorf, XV. Internat. Symposium on Nucl.Phys. "Nuclear Fission", Gaussig, GDR, Nov. 1985

Pohlers,A.; Jugelt,P.; Oettel,H.: Experimentelle Untersuchung zur Leistungsfähigkeit von HLD in der WDRD an kristallinen Stoffen, XIX. Jahrestagung d. VFK, Rostock, 23.-26.4.85, Kurzreferate Berlin/85, S. 130

Pohlers,A.; Socher,W.; Jugelt,P.: Die Anwendung des HARTMANNschen Regressionsverfahrens in der winkel- und energiedispersiven Röntgenphasenanalyse, XIX. Jahrestagung d. VFK, Rostock, 23.-26.4.85, Kurzreferate Berlin/85, S. 80

Pohlers,A.; Jugelt,P.; Ziemann,M.; Kraft,A.: Aufbau und Erprobung eines energiedispersiven Hochdruckdiffraktometers, XIX. Jahrestagung d. VFK, Rostock, 23.-26.4.85, Kurzreferate Berlin 85, S. 131

Pohlers,A.; Försterling,G.: Die EDRD am Beispiel des Glasmetalls $Fe_{80}B_{20}$, XIX. Jahrestagung d. VFK, Rostock, 23.-26.4.85, Kurzreferate Berlin/85, S. 108

Steil,H.; Herms,G.; Pohlers,A.; Jugelt,P.: Experimentelle Trennung kohärenter und inkohärenter Strsuanteile in der WDRD an amphoren Stoffen, XIX. Jahrestagung d. VFK, Rostock, 23.-26.4.85, Kurzreferate Berlin/85, S. 92

Steil,H.; Herms,G.; Pohlers,A.; Jugelt,P.: Ergebnisse der experimentellen Comptonkorrektur an Gläsern, XIX. Jahrestagung d. VFK, Rostock, 23.-26.4.85, Kurzreferate Berlin/85, S. 120

Steil,H.; Riechmann,F.; Herms,G.; Pohlers,A.; Musiol,G.; Jugelt,P.: Trennung von kohärenter und inkohärenter Röntgenstrahlung mit Hilfe eines großflächigen Si(Li)-HLD bei Röntgengroßwinkelbeugung an Gläsern, Physikalische Manuskripte, Heft 7, Rostock, 1985

Scholz,W.: Analytischer Ausdruck zur Berechnung von Röntgenenergien in der energiedispersiven Röntgenspektrometrie, COMPANA'85, 3. Tagung "Computereinsatz in der Analytik", 9.-12.Sept. 85 in Jena, S. 34

Scholz,W.: Programm UNI-ZAF zur quantitativen energiedispersiven Röntgenmikroanalyse, 4. Tagung d. zentralen Arbeitsgruppe "Energiedispersive Röntgenspektrometrie" 11.-12.4.85, Strausberg

Socher,W.; John,D.; Kambach,Chr.; Otto,E.; Richter,O.; Pröhl,G.: Weiterentwicklung und Erprobung einer Meßeinrichtung zur zerstörungsfreien Qualitätskontrolle geschmiedeter Kaltwalzen, Konferenzunterlagen der Zentralen wissenschaftl. Studentenkonferenz Sozialistische Radionalisierung an der TUD, 10.-11.85 in Dresden, S. 167

Wagner,W.; Karrasch,G.; Musiol,G.; Zschornack,G.: "Die Analyse von charakteristischer Röntgenstrahlung von Ionen mit einem Kristalldiffraktionsspektrometer", Vortrag auf dem Komitee für Schwerionenphysik des VIK Dubna, 9.-11.April 1985

Wagner,W.; Dunin,W.B.; Karrasch,G.; Kreiseler,D.; Musiol,G.; Nevskaya,N.A.; Zschornack,G.; Schulze,W.: "Ein automatisiertes Kristalldiffraktionsspektrometer für Messungen der charakteristischen Röntgenstrahlung hochgeladener Ionen", XII. Internat. Kernelektroniksymp. 2.-6.Juni 1985, Dubna

Weber,Chr.; Weber,M.: Erprobung von Parametersuchverfahren zur Auswertung energiedispersiv gemessener Röntgenemissionsspektren, COMPANA'85, 3. Tagung "Computereinsatz in der Analytik", 9.-12.Sept.85 in Jena, S. 36

Zeuner,A.: Untersuchung der Bindemittelverteilung in Mineralwolleplatten mit Hilfe von radioaktiver Indikatoren, 9. IBAUSIL 1985, Weimar, Tagungsbericht Bd.

Zeuner,A.; Hartmann,F.: Residence Time Investigation and Material Balance for Fresh and Waste Water in a Rayon Plant by Radioisotope Application, 3rd Working Meeting on Radioisotope Application and Radiation Processing in Industry", Sept. 1985, Leipzig

Zeuner,A.; Henning,K.; Kiessling,M.: Investigation of the Material Transport Behavior of Tube- and Trough-Vibration Mills by Radioactive Indicators 3rd Working Meeting on Radioisotope Application and Radiation Processing in Industry, Sept. 1985, Leipzig

Zschornack,G.: "Röntgenspektroskopie hochionisierter Schwerionen", 6. Tagung "Energiereiche atomare Stöße" Oberstdorf/BRD, 27.01.-02.02.1985; 05-01-85, 05-02-85 TU-Preprint

Zschornack,G.: "Die Bestimmung der Ladungsdispersion hochgeladener Ionen im Elektronenring des Schwerionenkollektivbeschleunigers", Arbeitstagung Schwerionenkollektivbeschleuniger, Dubna, 4.-6. Juni 1985

Zschornack,G.; Musiol,G.; Reichmann,A.; Karrasch,G.; Kreiseler,D.; Schulze,W.; Tänzer,W.; Wagner,W.: "A Computer-Aided Bragg Crystal Diffraction Spectrometer for X-Ray Analysis", 3rd Working Meeting,"Radioisotope Application and Radiation Processing in Industry", 22.-27.Sept. 1985, Leipzig

DIPLOMARBEITEN

Eckardt, Frank: Methodische Untersuchungen zur Elementanalyse von Sedimenten

Khamsing: Aktivierungsanalyse von Elementen niedriger Ordnungszahl mit Hilfe von 14-MeV-Neutronen

Sprenger, Bernd: Berechnung von Spaltkammerspektren unter Berücksichtigung der realen Spaltkammergeometrie

Teichfuß, Marlon: Herstellung und Untersuchung von ortsempfindlichen Kernstrahlungsdetektoren aus neutronendotierten Silizium

Uhlenbrok, Jörg-Uwe: Untersuchungen zur Schaffung einer Methode zur eichprobenfreien Multielementanalyse mittels Röntgenfluoreszenz

PROMOTIONEN A (DR.RER.NAT)

Pohlers, Andreas: Methodische Untersuchungen zur Leistungsfähigkeit von Halbleiterdetektoren in der Röntgendiffraktometrie

WISSENSCHAFTLICHE PREISE

Dunin,W.P.; Karrasch,G.; Kreiseler,D.; Müller,G.; Musiol,G.; Nevskaya,N.A.; Schulze,W.; Wagner,W.; Zschornack,G.: III. Laborpreis des ONMU des VIK Dubna, "Entwicklung, Bau und Inbetriebnahme eines hocheuflösenden Bragg-Kristalldiffraktionsspektrometers"

Dunin,W.P.; Karrasch,G.; Kreiseler,D.; Müller,G.; Musiol,G.; Nevskaya,N.A.; Schulze,W.; Wagner,W.; Zschornack,G.: II. Institutspreis des VIK Dubna für wissenschaftlich-technische Arbeiten 1985, "Entwicklung, Bau und Inbetriebnahme eines hochauflösenden Bragg-Kristalldiffraktionsspektrometers"

PATENTE

Peter,D.; Schaal,J.; Müntel,J.; Schiekel,M.: Verfahren und Vorrichtung zur kontinuierlichen Brombestimmung in Betriebslösungen. WPG 01 N/ 2642572

Zschornack,G.; Musiol,G.; Müller,G.; Oertner,H.-J.; Pohlers,A.; Schulze,W.: Fokussierendes Bragg-Kristalldiffraktionsspektrometer, WPG 01 N/ 2734037

KARL-MARX-UNIVERSITÄT LEIPZIG, SEKTION PHYSIK, WB ANGEWANDTE KERNPHYSIK

VERÖFFENTLICHUNGEN

Stephan, D., V. Geist: Investigation of Lattice Strain in Proton-Irradiated GaP by a Modified Auleytner Technique. phys. stat. sol. (a) 87 (1985) 589

Pickenhain, R., V. Geist, W. Seifert, K. Jacobs, St. Brehme: Green and yellow light emitting diodes produced from vapour phase epitaxial GaP : N II. Defects produced by 1 Me V proton irradiation. phys. stat. sol. (a) 88 (1985) 721

Ascheron, C., C. Bauer, H. Sobotta, V. Riede: Investigations of Hydrogen Implanted GaP Single Crystals by Means of Particle Induced γ - Spectroscopy, Infrared Spectroscopy, and Rutherford Backscattering Channelling Technique. phys. stat. sol. (a) 89 (1985) 549

Ascheron, C., A. Schindler, G. Otto: A Study of Proton Bombardment Induced Swelling of GaP Single Crystals. phys. stat. sol. (a) 92 (1985) 169

DIPLOMARBEITEN

Kasper, Stefan: Aufbau einer Interfaceeinheit zur direkten Datenübertragung zwischen EDR 184 und EMG 666, KMU Leipzig, Juli 1985

PROMOTION B (Dr.sc.nat.)

Geist, Volker: Untersuchung und Anwendung des protoneninduzierten Kosseleffekts, KMU Leipzig, 28.10.1985

VORTRÄGE

Pechner, R., A. Schindler, R. Flagmeyer, F. Bigl, J. Flachowsky: ^{64}Cu-Adsorption und RBS-Untersuchungen an ionenstrahlgeätztem GaAs. 13. Herbstschule Physik und Chemie der A III B V - Halbleiter, Breitenstein, November 1985

Flagmeyer, R.: Rutherford backscattering channeling (RBC) - eine Methode zur Analyse dünner Schichten. 13. Herbstschule Physik und Chemie der A III B V - Halbleiter, Breitenstein, November 1985

Flagmeyer, R., G. Kühn, B. Schumann, W. Gasch: $Ca_{1-x}Sr_xF_2$ - Epitaxie - Schichten auf (100) GaAs - Substraten. 13. Herbstschule Physik und Chemie der A III B V - Halbleiter, Breitenstein, November 1985

Flagmeyer, R., B. Schumann: RBC - Analyse von flash-aufgedampften Erdalkalifluoridschichten auf GaAs. 13. Herbstschule Physik und Chemie der A III B V - Halbleiter, Breitenstein, November 1985

Frey, H., J. Vogt, G. Otto: Simulation of thick target x-ray yield for PIXE analysis. COMPANA'85, Jena, September 1985

Geist, V., D. Stephan: Röntgenbeugungsuntersuchungen an protonenbestrahlten GaP-Kristallen. 14. Jahrestagung VfK, Rostock, April 1985

Geist, V., D. Stephan: X-ray investigations by a modified Auleytner-method. 6th Int. Symp. High purity materials in science and technology, Dresden, Mai 1985

Hörig, W., C. Ascheron, G. Nocke: Einfluß von protonenstrahlinduzierten Defekten auf die optische Absorption von GaP im Energiebereich der Bandkante. 13. Herbstschule Physik und Chemie der A III B V - Halbleiter, Breitenstein, November 1985

Kasper, St.: Stoffanalytik am Teilchenbeschleuniger - Meßprozeßautomatisierung. 10. Zentrale Studentenkonferenz Physik, Magdeburg, Februar 1985

Kasper, St: Inteface - Erweiterung IFE 1 für Rechner - Systeme des Typs EMG 666. 18. Leistungsschau der KMU, Leipzig, Mai 1985

Lehmann, D.: Interaktive Computeranalyse von Rückstoßspektren zur Bestimmung des Wasserstoffgehaltes in Oberflächenschichten von Proben. COMPAMA'85, Jena, September 1985

Otto, G., U. Wolf, H.-E. Zschau: Tiefenprofilierung von Fluor mittels Resonanzreaktionen. COMPAMA'85, Jena, September 1985

Otto, G.: Stoffnachweis mittels kernphysikal. Anregungsverfahren. Lehrgang Geophysik, Leipzig, November 1985

Schumann, B. G. Kühn, W. Gasch, G. Wagner, R. Flagmeyer, W. Hauffe, O. Müller: Lattice matched (Ca, Sr) F_2 - mixed crystal films on (100) GaAs. 9. Tagung Physik und Elektronik, Berlin, Oktober 1985

Sobotta, H., V. Riede, C. Ascheron: Infrarotspektroskopische Charakterisierung von protonen - und deuteronen implantiertem GaP und InP. 13. Herbstschule Physik und Chemie der A III B V - Halbleiter, Breitenstein, November 1985

Vogt, J., St. Kasper, W. Hofmann, D. Lehmann, G. Otto: Rechnergestütztes Meßsystem zur ortsaufgelösten quantitativen Elementanalyse mittels Spektroskopie ioneninduzierter Gamma- u. Röntgenstrahlung. COMPAMA'85, Jena, September 1985

Vogt, J.: The use of proton beams for light element analysis of biological and geological samples. Institutskolloquium, Debrecen, September 1985

Vogt, J., G. Otto: Einige Ergebnisse der Untersuchung von geologischen Proben mittels Spektrometrie protoneninduzierter Röntgen- u. Gammastrahlung. Lehrgang Geophysik, Leipzig, November 1985

Zschau, E., C. Ascheron: Rechnerauswertung von Strahlenschadenprofilen in zweikomponentigen Halbleitereinkristallen. Seminar, VIK Dubna, Oktober 1985

HUMBOLDT-UNIVERSITÄT ZU BERLIN, SEKTION PHYSIK, BEREICH 06 - ATOMSTOSSPROZESSE DER FESTKÖRPERPHYSIK

VERÖFFENTLICHUNGEN

A. Mertens, H. A. Klose, and Mg. Tang: Ion beam contacting of Silicon, II. Antimony in n-Silicon. phys. stat. sol. (a) 88 (1965) 1, 369 - 374

K. Maass, K. Irmscher, and H. A. Klose: On the determination of deep level concentration profiles by DLTS measurements. phys. stat. sol. (a) 91, 904 (1985)

H. A. Klose: Aspekte der niederenergetischen Ioneninplantation. Wiss. Zs. der HUB, Math.-Naturwiss. Reihe, Heft 9 (1985), 808 - 818

J. Bollmann, K. Appelfeller, H. A. Klose und B. Lukasch: Bestimmung von Ladungsträgerprofilen - Probleme und Grenzen der Methoden bei geringen Reichweiten. Wiss. Zs. der HUB, Math.-Naturwiss. Reihe Heft 9 (1985), 838 - 851

K. Irmscher, K. Maass und H. A. Klose: DLTS-Analyse von Konzentrationsprofilen tiefer Störstellen in ioneninplantiertem Silizium. Wiss. Zs. der HUB, Math.-Naturwiss. Reihe, Heft 9 (1985), 861 - 869

R. Wedell: Reichweiten und Sputtering bei niedrigen Energien. Wiss. Zs. der HUB, Math.-Naturwiss. Reihe, Heft 9 (1985), 819 - 826

B. Lukasch und J. Bollmann: Vorstellungen zu Ausheilmechanismen bei konventioneller Langzeittemperung. Wiss. Zs. der HUB, Math.-Naturwiss. Reihe, Heft 9 (1985), 827 - 837

M. Griepentrog, A. Mertens und U. Müller-Jahreis: Möglichkeiten und Probleme bei der Analyse flacher Fremdatomverteilungen in Halbleitern mittels SIMS. Wiss. Zs. der HUB, Math.-Naturwiss. Reihe, Heft 9 (1985), 852 - 860

H. Kerkow, G. Kreysch und R. Wedell: Mechanische Spannungen in Si nach Ioneninplantation. Wiss. Zs. der HUB, Math.-Naturwiss. Reihe, Heft 9 (1985), 870 - 879

W. Frentrup und M. Griepentrog: Ionenstrahlgetterung in $A_{III}B_{V}$-Verbindungen. Wiss. Zs. der HUB, Math.-Naturwiss. Reihe, Heft 9 (1985), 887 - 896

J. Bollmann, H. A. Klose und A. Mertens: Oberflächennahe tiefe Zentren in ioneninplantiertem Silizium. Proc. der 16. Tagung "Physik der Halbleiteroberfläche" des ZIE der AdW, 16, 267 (1985)

H. A. Klose: Recent developments in ion beam technology. Proc. 1st Int. Autumn School "Gettering and Defect Engineering in the Semiconductor Technology" IHP der AdW der DDR 1985, 120 - 125

W. Frentrup and M. Griepentrog: Ion beam gettering of Copper and Nickel in A^3B^5-compounds. Proc. 1st Int. Autumn School "Gettering and Defect Engineering in the Semiconductor Technology", IHP der AdW der DDR 1985, 329 - 335

D. Hildebrandt, W. Frentrup, and C. E. Richter: Depth profiling of low energy implanted H isotopes in Si by SIMS. ZIE der AdW der DDR, Preprint 85-4

W. Frentrup, M. Griepentrog, and U. Müller-Jahreis: Negative secondary ion emission influenced by alkali atoms. phys. stat. sol. (a) 91, 447 (1985)

G. Vizhelethy, G. Mezey, E. Kotai, A. Mannaba, D. Hildebrandt, W. Frentrup: Erosion and Deposition Investigations on Special Probes in T-10. Fusion and Plasma Physics, Budapest, Sept. 1985, part. II, p. 603 - 606

H. Düsterhöft, M. Griepentrog, A. Mertens, U. Müller-Jahreis: SIMS-Untersuchungen in oberflächennahen Bereichen. Proc. der 16. Tagung "Physik der Halbleiteroberfläche" des ZIE der AdW der DDR, 16, 273 (1985)

R. Wedell: Scaling Laws for Radiation Energies of Axial Channeled Electrons in simple Single String Potentials. Nucl. Instr. and Methods in Physics, Research B (Konferenzmaterialien der 11th (CACS), zur Veröffentlichung angenommen

M. Riedel und H. Düsterhöft: Energy Distribution of positive secondary ions by bombardment of pure elements and amorphous alloys with O_2-ions. Reinstofftagung 6.-10.5.85 in Dresden

H. Düsterhöft und R. Pippig: Eine einfache Ionenquelle zur Erzeugung von Edelgas- und Alkaliionen. Exp. Techn. Phys., angenommen

M. Riedel und H. Düsterhöft: Energy distribution of positive secondary ions by bombardment of pure elements and amorphous alloys with Ar-ions. 3rd Joint Vacuum Conference, 7.-9.10.85 Debrecen/Ungarn

P. G. Rüdenauer, M. Riedel, H. E. Beske, H. Düsterhöft u.v.a.: Intern. Laboratory Cross Calibration Experiment for SIMS Quantification. Anal. Chemistry, 57, 1636 (1985)

H. Düsterhöft, R. Daugs und R. Pippig: A New Method for the Interpretation of Energy Distribution Measured on Secondary Ions. phys. stat. sol. (a) 87, 499 (1985)

M. Riedel, H. Düsterhöft und A. Honig: Energy Distribution of Positive Secondary Ions by Bombardment of Pure Elements and Amorphous Alloys with O_2- and Ar-Ions. SIMS V 29.9.-4.10.85 Washington/USA

R. Wedell: Solution of the Nonlinear Equation of Motion of Relativistic Positrons under Planar Channeling Conditions. Annalen der Physik, zur Veröffentlichung angenommen

P. Gehrmann, K. Lenkeit, and R. Stolle: Measurements of Proton Channeling Energy Losses in Silicon in the Intermediate Energy Region. phys. stat. sol., zur Veröffentlichung angenommen

P. Gehrmann and R. Wedell: Calculation of Helium Stopping Powers in the Intermediate Energy Region. Rad. Eff. Lett., 8[5] 205 (1985)

DIPLOMARBEITEN

K. Holldack: Diffusionsanomalien von B in Si infolge Ionenbeschusses.

M. Klein: Untersuchungen zur Temperaturabhängigkeit der Strahlenschadensentstehung und in-situ-Ausheilung bei der Ionenimplantation in einkristallinem Silizium.

K. Appelfeller: Zur Bestimmung von oberflächennahen, durch niederenergetische Ionenimplantation erzeugten Dotierungsprofilen.

T. Wagner: Messung der Zerstäubungsausbeute an Halbleiter- und Metallproben beim Beschuß mit Alkali- und Edelgasionen.

U. Schade: SIMS-Untersuchungen an Mehrschichtstrukturen.

DISSERTATIONEN A

M. Griepentrog, W. Frentrup: Untersuchungen zur Ionenstrahlgetterung in GaP und GaAs. Diss. A, Febr. 1985.

K. Irmscher: Kapazitätsspektroskopische Analyse tiefer Störstellen in ionenbestrahltem Si. Diss. A, Mai 1985.

VORTRÄGE

M. Riedel, H. Düsterhöft: Energy Distribution of Positive Secondary Ions by Bombardment of Pure Elements and Amorphous Alloys with O_2 Ions. 6. Int. Symp. High-Purity Materials in Science and Technol., Mai 1985, Dresden (DDR)

H. Düsterhöft: Theoretische und empirische Modelle zur Berechnung der Sekundärionenausbeute. ebenda

M. Riedel, H. Düsterhöft: Energy Distribution of Positive Secondary Ions by Bombardment of Pure Elements and Amorphous Alloys with Ar-Ions. 3. Joint Vacuum Conf., Okt. 1985, Debrecen (Ungarn)

M. Riedel, H. Düsterhöft: Energy Distribution of Positive Secondary Ions by Bombardment of Pure Elements and Amorphous Alloys with Ar- and O_2-Ions. SIMS-V-Conf., Okt. 1985, Washington, D.C. (USA)

M. Riedel, H. Düsterhöft: Energy Distribution of Positive Secondary Ions by Bombardment of Pure Elements and Amorphous Alloys with O_2-Ions. Analysentagung, Juni 1985, Berlin-West

R. Wedell: Theorie der Strahlung bei Kanalleitung und damit verbundene Probleme. XV. Allunionskonf. Physik der Wechselwirkung geladener Teilchen mit Einkristallen, Mai/Juni 1985, Moskau (UdSSR)

H. A. Klose: Recent developments in ion beam technology. 1st Int. Autumn School "Gettering and Defect Engineering", Garzau 10.10.85, IMP der AdW der DDR

G. Vizhelethy, G. Mezey, E. Kotai, A. Mannaba, D. Hildebrandt, W. Frentrup: Erosion and Deposition Investigation on Special Probes in T-10. 12. European Conf. on Controlled Fusion and Plasmaphysics, Sept. 1985, Budapest (Ungarn)

G. Lehmann, S. Mechahougui, U. Müller-Jahreis: Quelques aspects d' application du SIMS Comune methode de microanalyse pour étude d' un acier a dispersoide. 2. Int. Sem. zur Materialphysik, Okt. 1985, Algerien

R. Wedell: Scaling Laws for Radiation of Axial Channeled Electrons in Simple Single String Potentials. 11. Int. Conf. on Atomic Collisions in Solids, August 1985, Washington D.C., USA

K. Holldack, H. Kerkow, W. Frentrup: Anomalous diffusion of B in Si due to heavy ion bombardment. Working Meeting on Ion Implantation in Semiconductors and other Materials and Ion Beam Devices, Okt. 1985, Balatonaliga (Ungarn)

H. Kerkow, G. Kreysch, G. Wolf, K. Holldack: Ion beam assisted annealing of amorphized Silicon. ebenda

I. Gehrmann, K. Lenkeit, R. Stolle: Bremsquerschnitte kanalisierter Protonen in Silizium im Bereich ihrer extremsten Werte. XV. Allunionskonferenz Physik der Wechselwirkung geladener Teilchen mit Einkristallen, Mai/Juni 1985, Moskau (UdSSR)

K. Lenkeit: Ladungszustand kanalisierter Protonen in Silizium. ebenda

J. Bollmann, H. A. Klose, and A. Mertens: Electrical properties and spatial distribution of surface-near defects. Int. Conf. "Ion Implantation", Balatonaliga 1985

J. Bollmann, and H. A. Klose: Surface-Near distributions of deep levels caused by low-energy high-dose Sb implantations. ebenda

J. Bollmann, H. A. Klose und A. Mertens: Oberflächennahe tiefe Zentren in ionenimplantiertem Silizium. 16. Tagg. "Physik der HL-OF", Binz, 8.4.1985

J. Bollmann, H. A. Klose und A. Mertens: Oberflächennahe Implantationsdefekte in Silizium. 9. Tagg. "Physik und Elektronik", 24. 10. 1985

K. Irmscher, H. A. Klose und K. Maass: Zur Feldabhängigkeit der Emissionsraten tiefer Zentren in Silizium. ebenda, 22./23.10.1985

H. Kerkow, G. Kreysch, G. Wolf: Ionenstrahl-gestützte Ausheilung amorphisierter Si-Schichten. ebenda

A. Ende, W. Henrion, H. Kerkow: Charakterisierung von TiN-Schichten. ebenda

W. Frentrup, M. Griepentrog, U. Müller-Jahreis: Einfluß von Alkalimetallen auf die Sekundärionenemission. ebenda

H. Düsterhöft, A. Mertens, M. Griepentrog, U. Müller-Jahreis: SIMS als Festkörperanalysenmethode. 16. Arbeitstagung ZIE "Physik der HL-Oberfläche", Binz, April 1985

R. Wedell: Channeling and Channeling Radiation. Catholic University of America, Washington D.C. (USA) August 1985

R. Wedell: Radiation of Relativistic Positrons and Electrons in Single Crystals. State University of New York at Albany, New York (USA) August 1985

R. Wedell: Channeling of Ions and Channeling Radiation of Light Particles. Argonne National Laboratory, Argonne (USA) August 1985

R. Wedell: Theoretical Description of Energy Losses in the Intermediate Energy Region. Atomic Energy of Canada limited Research Company, Chalk River, Canada, August 1985

U. Müller-Jahreis: Sekundärionen-Massenspektrometrie - Mikroanalyse und -Mikroskopie an Halbleitermaterialien. 7. Weiterbildungslehrgang der Sektion Physik, Berlin, Oktober 1985

B. Gruska, R. Wolf, W. Frentrup, K. Jacobs: Physikalische Eigenschaften Be-implantierter GaAs-Schichten. Physik und Elektronik, Berlin, Oktober 1985

B. Gruska, W. Frentrup, F. Koch, R. Wolf, J. Gerlach: Kurzzeittemperung Be-implantierter GaAs-Schichten. ebenda

K. Holldack, W. Frentrup, H. Kerkow: Implantationsprofile nach einer strahleninduzierten Diffusion. ebenda

B. Klose und H. A. Klose: Optische Erscheinungen in der Atmosphäre. Experimentalsonntagsvorlesung der URANIA am 9.6.1985

H. A. Klose: Kapazitätsspektroskopie von Störstellen in Halbleitern. 7. Weiterbildungsveranstaltung der Sektion Physik, Berlin, 29. 10. 1985

H. Kerkow: Oberflächenanalyse mit PIXE. ebenda

FRIEDRICH-SCHILLER-UNIVERSITÄT JENA, SEKTION PHYSIK, WISSENSCHAFTSBEREICH IONOMETRIE

VERÖFFENTLICHUNGEN

André, G., E. Glaser, G. Götz, H. Bartsch;
Explosive crystallisation of silicon layers influenced by modification of the layer parameters; Proc. Int. Conf. Energy Pulse Modification of Semiconductors and Related Materials (EPM), ed. K. Hennig, Dresden 1985, p. 492.

André, W., K. Herre, D. Stook, H.-D. Geiler;
Selective energy deposition into silicon films; Proc. EPM, p. 82.

Dvurechenskii, A. V., W. M. Igonina, H.-D. Geiler, U. Jahn, A. Mertens;
Impurity profiles produced by the variation of the crystallization velocity during pulse annealing; Proc. EPM, p. 48.

Dittmar, A., K. Gärtner, G. Götz;
Formation of homogeneous films of Ni-silicide by ms-pulse laser and furnace annealing of sandwich structures; Proc. EPM, p. 571.

Fuschini, E., A. Ugguzzoni, K. Gärtner, K. Hehl;
Axial blocking in a master equation approach; Nucl. Instr. and Methods in Physics Research B 12 (1985) 334.

Geiler, H.-D., K.-H. Heinig;
Theoretical investigation of the stationary lateral movement of an explosive liquid-phase epitaxy front; Proc. EPM, p. 466.

Geiler, H.-D., K.-H. Heinig;
Theoretical description of explosive crystallization phenomena induced by high temperature pulses in thin layers of amorphous semiconductors; Proc. EPM, p. 451.

Glaser, E., J. Böhme, G. Götz, M. Wagner, H. Bartsch;
Crystallization of indium implanted amorphous silicon layers induced by millisecond laser pulses; Proc. EPM, p. 318.

Gärtner, K., K. Hehl;
Axial dechanneling. IV Stacking faults; Nucl. Instr. and Meth. in Physics Research B 12 (1985) 205.

Götz, G.;
Laser beam induced explosive crystallization in silicon; Proc. EPM, p. 423.

Götz, G.;
Explosive crystallization in silicon; Proc. Int. Winterschool on Laser Assisted Modification and Synthesis of Materials, ed. S. Metev, Sofia 1985, p. 7.

Herre, K., W. André, G. Götz;
Surface smoothing and increase of conductivity in polycrystalline silicon films by laser irradiation; Proc. EPM, p. 152.

Heinig, K.-H., G. Otto, H.-D. Geiler;
Theoretical investigation of lateral explosive solid phase nucleation (ESPN) wave fronts in amorphous silicon films; Proc. EPM, p. 459.

Heinig, K.-H., H.-D. Geiler;
Phenomenological theory of explosive solid phase crystallization of amorphous silicon. Part I: Stationary solutions; phys. stat. sol. (a) 92 (1985) 421.

Jetschke, S., K. Hehl;
Diffusion and recrystallization processes during annealing of N^+- and P^+-implanted $LiNbO_3$; phys. stat. sol. (a) 88 (1985) 193.

Reinsperger, G.K., F. Schwabe, B. Selle;
Nondestructive analysis of thin $Zn_xCd_{1-x}S$ films by Rutherford backscattering and optical measurements; phys. stat. sol. (a) 88 (1985) 745.

Stock, D., H.-D. Geiler, K. Hehl;
A model of crystallisation processes controlled by temperature pulses in amorphous semiconductors. I. Steplike temperature pulse; phys. stat. sol. (a) 89 (1985) 57.

Stock, D., H.-D. Geiler, K. Hehl;
Theoretical investigation of laser induced ultrafast melting and solidification processes of c-Si layers in the regime of kinetic interface control (KIC); Proc. EPM, p. 30.

Stock, D., H.-D. Geiler, K. Hehl;
Theoretical evidence for opposite moving phase fronts during ultrafast solidification processes; phys. stat. sol. (a) 87 (1985) K 115.

Wagner, M., H.-D. Geiler, G. Götz;
Time-resolved investigation of large-areas explosive crystallization of amorphous silicon layers; phys. stat. sol. (a) 92 (1985) 413.

Wagner, M., E. Glaser, G. Andrä, G. Götz;
In situ investigation of controlled explosive crystallization processes in amorphous silicon layers; Proc. EPM, p. 485.

Wendler, E., W. Wesch;
Investigation of residual defects in laser annealed GaAs with optical methods; Proc. EPM, p. 535.

Wendler, E., W. Wesch, G. Götz;
Near-edge optical absorption behaviour in weakly damaged ion-implanted GaAs; phys. stat. sol. (a) 93 (1986) 207.

Wesch, W., G. Götz, P. Ressel, A. Unkroth;
Laser annealing of ion implanted $A_{III}B_V$-compound semiconductors; in: Ionnaja implantazija v poluprovodnikach i drugich materialach, Vilnius 1985, p. 342.

Wesch, W., G. Götz, P. Ressel, D. Stock, A. Unkroth;
Pulse laser induced recrystallization and dopant incorporation in ion implanted GaAs layers; Proc. EPM, p. 527.

Wesch, W., E. Wendler, G. Götz, K. Unger, H. Röppischer, Chr. Resagk;
Laser induced defects in GaAs layers; phys. stat. sol. (b) 130 (1985) 539.

Wesch, W., G. Götz, N. P. Kekelidze, G. P. Kekelidze;
Radiation defects in argon implanted InAs; Bull. Academy of Sciences of Georgian SSR 118 (1985) no. 3.

DIPLOMARBEITEN

Dranda, K.: Experimentelle Untersuchungen zum Einfluß von Fremdatomen und einer einkristallinen Matrix auf die Explosivkristallisation in dünnen amorphen Si-Schichten.

Sebastian, J.: Echtzeituntersuchungen zur Kinetik explosiver Flüssigphasenkristallisationsprozesse amorpher Siliciumschichten.

Winter, S.: Untersuchungen zur Zündung und Ausbreitung von Explosivkristallisationsprozessen durch gezielte Energiedeponierung an lateral strukturierten Schichten.

Wolff, D.: Stationäre Lösung des eindimensionalen Problems der explosiven Flüssigphasenepitaxie in SOI-Strukturen.

PROMOTIONEN A (DR. RER. NAT.)

Schastak, S. I.: Ausnutzung nichtlinearer optischer Effekte zur Verbesserung der Homogenität der räumlichen Intensitätsverteilung von Hochleistungslaserimpulsen und deren Anwendung bei der Laserausheilung, 3.12.1985.

VORTRÄGE

Andrä, W., G. Götz: Eigenschaften ionenimplantierter und laserausgeheilter flacher n^+p-Übergänge in Silicium. 9. Tagung Physik und Elektronik, Berlin, Okt. 1985.

Andrä, W.: Eigenschaften ionenimplantierter und laserausgeheilter flacher pn-Übergänge. 9. Tagung Physik und Elektronik, Berlin, Okt. 1985.

Bartsch, H., G. Andrä, E. Glaser: TEM cross sectional imaging of laser-induced crystallization after ion implantation. Working Meeting Ion Implantation, Balatonaliga, Okt. 1985.

Däweritz, I., E. Krause, F. Schwabs, B. Selle: RBS applied to the analysis of thin polycrystalline II-VI compound films. Working Meeting Ion Implantation, Balatonaliga, Okt. 1985.

Dittmar, A., K. Gärtner, G. Götz: Bildung von Ni-Silizid durch ms-Laserbestrahlung. Tagung "Silizide in der Mikroelektronik", Ahrenshoop, Okt. 1985.

Däweritz, I., E. Krause, F. Schwabe, B. Selle: Charakterisierung dünner polykristalliner $A_{II}B_{VI}$-Schichten durch Rutherford-Rückstreuung. 9. Tagung Physik und Elektronik, Berlin, Okt. 1985.

Geiler, H.-D., D. Wolff, K.-H. Heinig: Prozeßmodellierung lateraler explosiver Kristallwachstumsprozesse für SOI-Technologien. 9. Tagung Physik und Elektronik, Berlin, Okt. 1985.

Glaser, E., G. Andrä, H. Bartsch, K. Drenda, G. Götz: Formation of monocrystalline layers by explosive crystallization of ion implanted amorphous silicon. Working Meeting Ion Implantation, Balatonaliga, Okt. 1985.

Gärtner, K., E. Glaser, G. Götz, K. Hehl: Defect analysis by dechanneling. Int. Conf. Ion Beam Analysis, Berlin-West, Juli 1985.

Götz, G., K. Gärtner: Nichtkonventionelle Silizierungsverfahren. Tagung "Silizide in der Mikroelektronik", Ahrenshoop, Okt. 1985.

Kaschner, C., A. Witzmann, K. Gärtner, G. Götz: Epitaktisches Wachstum von $NiSi_2$ durch Laserbestrahlung. Tagung "Silizide in der Mikroelektronik", Ahrenshoop, Okt. 1985.

Kahlert, V., D. Gehrisch, G. Götz, E. Glaser, M. Wagner, G. Andrä: Explosivkristallisation von amorphen Siliciumschichten und deren Anwendung für mikroelektronische Bauelemente. 9. Tagung Physik und Elektronik, Berlin, Okt. 1985.

Kaschner, C., A. Witzmann, K. Gärtner, G. Götz: Epitaxial growth of $NiSi_2$ by laser annealing. V. Int. Conf. Lasers and their Application, Dresden, Okt. 1985.

Wesch, W., K. Gärtner, E. Wendler, G. Götz: Investigation of defects in weakly damaged GaAs layers. Int. Conf. Radiation Effects in Insulators, Guildford/England, Juli 1985.

Wesch, W., K. Gärtner, E. Wendler, G. Götz: RBS and optical investigations of defects in weakly damaged GaAs layers. Int. Conf. Ion Beam Analysis, Berlin-West, Juli 1985.

Wesch, W., G. Götz: Rapid annealing of ion implanted GaAs. Working Meeting Ion Implantation, Balatonaliga, Okt. 1985.

Wesch, W., P. Ressel, T. Bachmann, D. Stock, G. Götz: Laserinduzierte Rekristallisation von ionenimplantiertem GaAs. 9. Tagung Physik und Elektronik, Berlin, Okt. 1985.

Wendler, E., W. Wesch, P. Ressel, K. Gärtner: Flüssigphasenepitaxie von ionenimplantiertem GaAs. XIII. Herbstschule KMU "Physik und Chemie der $A_{III}B_{V}$-Halbleiter", Breitenstein, Nov. 1985.

Witzmann, A., A. Dittmar, K. Gärtner, G. Götz: Bildung von Ni_2Si und NiSi auf As-dotiertem Silicium. 9. Tagung Physik und Elektronik, Berlin, Okt. 1985.

BERGAKADEMIE FREIBERG, SEKTION PHYSIK, WB ANGEWANDTE PHYSIK

VERÖFFENTLICHUNGEN

Herforth, L., K. Hübner, W. Stolz: Thermolumineszenz in Dosimetrie und Geowissenschaften. Ann. Physik 42 (1985) 461

Stolz, W.: Messung ionisierender Strahlung. Akademie-Verlag, Berlin 1985 und Verlag Physik-Chemie, Weinheim 1985

Unterricker, S.: Quadrupole coupling constants of $A^{II}B^{VI}$-compounds with wurtzite structure. Proceedings of the XXth Winter School on Physics 13. - 26. April 1985, Zakopane - Poland, p. 437

Degering, D., S. Unterricker: Determination of small yttrium concentrations in geological samples by charged particle activation analysis. Poster and Proceedings of the 3rd Working Meeting "Radioisotope Application and Radiation Processing in Industry", ZfI Leipzig, 23. - 27. 9. 1985

Pietzsch, C., J. Rotsche, K. Reichelt, R. Schröder: Untersuchungen an Farbkörpern auf der Basis von SnO_2 für die keramische Industrie. Silikattechnik 36 (1985) 316

DIPLOMARBEITEN

Wendebau, G.: Paragenetische, geochemische und thermobarometrische Untersuchungen an ausgewählten Bereichen der Fluoritlagerstätten Ilmenau - Gehren. Bergakademie Freiberg, 10. 6. 1985

VORTRÄGE, DIE AUSSERHALB DES EIGENEN KOLLEKTIVES GEHALTEN WURDEN

Stolz, W., H. Kubsch: Untersuchungen zur natürlichen Radioaktivität an der Bergakademie Freiberg in den Jahren 1908 - 1921. Physikhistorisches Kolloquium der Phys. Gesellschaft in der DDR, Leipzig, 14. 2. 1985

Leeder, O., W. Stolz, G. Wendebaum: Thermolumineszenz-Untersuchungen an Fluoriten. Isotopenkolloquium, Freiberg, 5. 9. 1985

Gast, H., W. Stolz: Langzeitmessungen der ^{220}Rn- und ^{222}Rn-Aktivität der Bodenluft nahe der Erdoberfläche. Isotopenkolloquium, Freiberg, 5. 9. 1985

Stolz, W.: Radon - Anwendungen in den Geowissenschaften und Quelle der natürlichen Strahlenbelastung. Bereichsseminar, TU Dresden, 8. 11. 1985

Pietzsch, C.: Mößbaueruntersuchungen zum zweiphasigen Zerfall des Martensits. Mößbauer-Kolloquium, 7. - 8.2.1985, Freiberg

Pietzsch, C.: Mößbauerspektroskopie - Einführung und Anwendung für die Silikattechnik. KDT-Veranstaltung, Freiberg, 18. 9. 1985

Gellermann, R., H. Kubsch: Mößbauer- und Pb-210-Untersuchungen an Ostseesedimenten. Mößbauerkolloquium, 7. - 8. 2. 1985, Freiberg

Unterricker, S.: ME- und TDPAC-Ergebnisse zur Struktur amorphisierter Sondenumgebungen in tetraedrisch koordinierten Halbleitern. Mößbauer-Kolloquium, 7. - 8. 2. 1985, Freiberg

Unterricker, S.: Anwendung der Methode der gestörten γ-γ-Winkelkorrelationen in der Festkörperphysik. "Seminar Metallimplantation" im ZfK Rossendorf, 1. 10. 1985

Unterricker, S.: TDPAC investigation of radiation damaged semiconductors. Institut für Metallurgie, Abteilung Festkörperphysik der AGH Krakow, VR Polen, 18. 12. 1985

Degering, D.: Yttriumbestimmung in geologischen Proben mittels (α,2n)-Reaktion. Lehrgang "Anwendung kernphysikalischer Analysenverfahren in den geologischen Wissenschaften". KMU Leipzig, 4. - 8. 11. 1985

Hebert, D., K. Fröhlich, T. Franke, R. Gellermann, S. Unterricker, J. H. Kim: Preliminary results of the underground laboratory in Freiberg,GDR. The Third International Conference on Low-Level Counting, Bratislava, CSSR, 21. - 25. 10. 1985. Erscheint in Nucl. Instr. Meth. Phys. Res.

VERANSTALTUNGEN

Mößbauerkolloquium, 7. - 8. 2. 1985 in Freiberg. Bergakademie Freiberg, Sektion Physik